Bulletin of the
Geological Society
of Denmark

DGF

Chief editor

Lotte Melchior Larsen, Geological Survey of Denmark and Greenland (GEUS), Øster Voldgade 10, DK-1350 Copenhagen K, Denmark. Tel: +45 38142252; Fax: +45 38142250; E-mail: lml@geus.dk

Scientific editors

Lars Clemmensen, Department of Geography and Geology, University of Copenhagen, Øster Voldgade 10, DK-1350 Copenhagen K, Denmark. Tel: +45 3532 2476; E-mail: larsc@geo.ku.dk (clastic sedimentology)

Ole Graversen, Department of Geography and Geology, University of Copenhagen, Øster Voldgade 10, DK-1350 Copenhagen K, Denmark. Tel: +45 3532 2447; E-mail: oleg@geo.ku.dk (sedimentary basins and structural geology)

Claus Heinberg, Institute of Environment, Technology and Society, University of Roskilde, P.O. Box 260, DK 4000 Roskilde, Denmark, Tel. +45 4674 2299; E-mail: heinberg@ruc.dk (palaeontology)

Michael Houmark-Nielsen, Natural History Museum of Denmark, University of Copenhagen, Øster Voldgade 5-7, DK-1350 Copenhagen K, Denmark. Tel: +45 3532 4344; E-mail: michaelhn@snm.ku.dk (Quaternary geology)

Jesper Milàn, Geomuseum Faxe, Østsjællands Museum, Østervej 2, DK-4640 Faxe, Denmark. Tel: +45 24636348; E-mail: jesperm@oesm.dk (palaeontology)

Lars Nielsen, Department of Geography and Geology, University of Copenhagen, Øster Voldgade 10, DK-1350 Copenhagen K, Denmark. Tel: +45 3532 2454; E-mail: ln@geo.ku.dk (geophysics)

Erik Thomsen, Department of Earth Sciences, University of Aarhus, C.F. Møllers Allé, DK-8000 Aarhus C, Denmark. Tel: +45 8942 2627; E-mail: erik.thomsen@geo.au.dk (palaeontology and stratigraphy)

Henrik Tirsgaard, Mærsk Olie og Gas AS, Esplanaden 50, DK-1263 Copenhagen K, Denmark. Tel: +45 3363 40 00; E-mail: het@maerskoil.dk (carbonate sedimentology and petroleum geology)

J. Richard Wilson, Department of Earth Sciences, University of Aarhus, C.F. Møllers Allé, DK-8000 Aarhus C, Denmark. Tel: +45 8942 2526; E-mail: jrw@geo.au.dk (igneous petrology and geochemistry)

Instructions to authors:

See inside the back cover and also:
http://2dgf.dk/publikationer/bulletin/vejledning.html

Cover: Danmarks Geologipris 2010 was in 2011 awarded to Troels Nielsen for his research on the kimberlites of West Greenland. An important paper is concerned with the Majuagaa kimberlite dyke in the Maniitsoq region (cover photo). The dark brown kimberlite dyke is 2 m thick and vertical with repeated en echelon offsets as seen in the foreground. It is dated at 564 Ma and intrudes the Archaean Finnefjeld gneiss complex. (Nielsen, T.F.D. & Sand, K.K. 2008: The Majuagaa kimberlite dike, Maniitsoq region, West Greenland: constraints for an Mg-rich silicocarbonatite melt composition from groundmass mineralogy and bulk compositions. Canadian Mineralogist 46, 1043–1061).

Glauconitic deposits at Julegård on the south coast of Bornholm, Denmark dated to the Cambrian

LARS B. CLEMMENSEN, RICHARD G. BROMLEY & PAUL MARTIN HOLM

Bioturbated, glauconitic siltstones and sandstones are overlain by presumed Upper Triassic deposits at coastal exposures at Julegård on the south coast of Bornholm. These glauconitic deposits have not previously been dated. A ^{40}Ar-^{39}Ar dating of the glaucony gives an age of 493 ± 2 Ma suggesting the deposits belong to the Lower Cambrian Norretorp Member of the Læså Formation. The shallow marine deposits are strongly bioturbated, but only a single ichnoassociation is represented. The ichnogenus is referable to either *Trichophycus* Miller and Dyer, 1878 or *Teichichnus* Seilacher, 1955. Rare examples of *Rusophycus* Hall, 1852, probably trilobite trace fossils, are also represented.

Lars B. Clemmensen (larsc@geo.ku.dk), Department of Geography and Geology, University of Copenhagen, Øster Voldgade 10, DK-1350 Copenhagen K, Denmark. Richard G. Bromley, Geological Museum, University of Copenhagen, Øster Voldgade 5-7, DK-1350 Copenhagen K, Denmark. Paul Martin Holm, Department of Geography and Geology, University of Copenhagen, Øster Voldgade 10, DK-1350 Copenhagen K, Denmark

The age and stratigraphy of the sediments on the landward edge of the down-faulted Arnager Block on the south coast of Bornholm at Julegård (Figs 1 and 2) have been open for more than one interpretation. Grönwall and Milthers (1916) and Gry (1969) mapped all the sediments cropping out between a point approximately 200 m east of Risebæk and a point aproximately 400 m west of Julegård, a coastal section of about 1.5 km, as Upper Triassic. Gravesen *et al.* (1982) mentioned that the stratigraphic position of the beds near Julegård is uncertain and that they may belong to the Lower Cretaceous Rabekke Formation. Hamann (1987), Jensen and Hamann (1989), and Graversen (2004a; 2004b; 2009) also placed these sediments in the Lower Cretaceous.

In most years the coastal exposures between Risebæk and Julegård are poor and only show minor outcrops of various white and greenish grey sandstones to a large degree covered by displaced red and green Triassic clay, or by down-wasted Quaternary deposits. In 2008 several storms, however, had removed large parts of the slope deposits and formed relatively large and well exposed coastal sections at Julegård (Figs 2 and 3). The newly exposed sections show glauconitic marine sediments at their base. These sediments, which are rich in trace fossils, are overlain by red and green clay of typical Late Triassic appearance and by light greyish to whitish fluvial sand and conglomerates.

None of these sediments have previously been described in detail and a first description of the glauconitic marine deposits at the base of the Julegård section is presented here. Their contact to overlying terrestrial deposits of presumed Triassic age appears gradational but as the trace fossil content in the shallow marine, glauconitic sediments is of Cambrian affinity, it was decided to carry out a ^{40}Ar-^{39}Ar dating of the glaucony to support the sedimentological studies.

Geological setting

The study area on the south coast of Bornholm is situated in the Fenno-Scandian Border Zone at the boundary between the Northwest European Craton and the Baltic Shield-East European Platform (Fig. 1; EUGENO-S 1987; Graversen 2004a; 2004b; 2009).

The studied section lies at the northeastern (land-
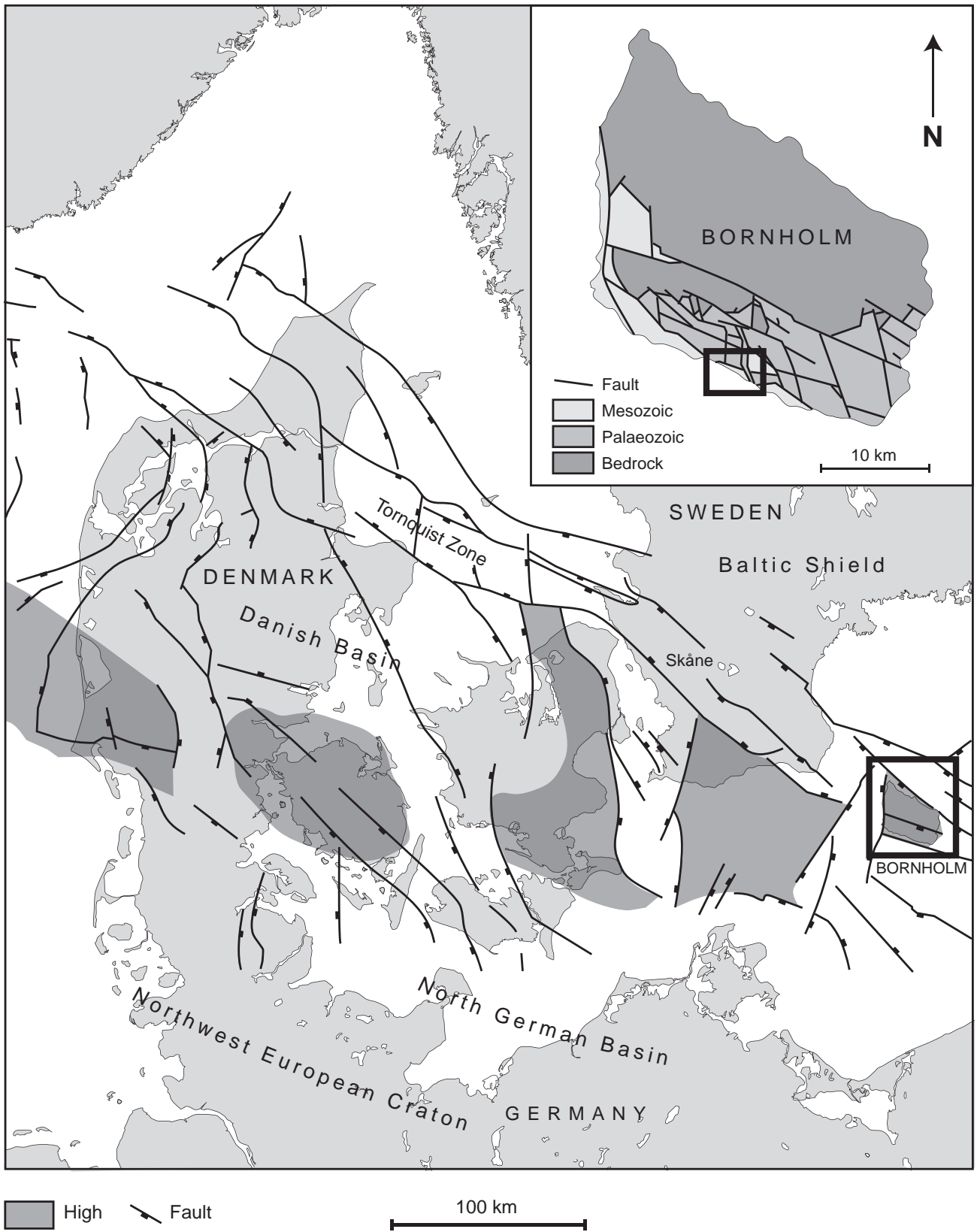
Fig. 1. Location map showing the position of Bornholm in a structural framework. Map based on Surlyk *et al.* (2008). Bornholm is composed of a Precambrian crystalline basement overlain by Palaeozoic and Mesozoic sediments that are broken down into a number of small fault blocks (Graversen 2009). The study site occurs in the down-faulted Arnager Block on the south coast of Bornholm (Fig. 2).

ward) edge of the Arnager Block and forms part of a small coastal strip of sediments between Julegård and Risebæk (Fig. 2; Gry 1969; Gravesen *et al.* 1982). The exposed sediments were mapped as Upper Triassic by Gry (1969). At Julegård these sediments are delineated shortly inland by a fault zone running WNW–ESE and separating the presumed Triassic deposits from uplifted Palaeozoic deposits of the Bornholm Block (Fig. 2; Gry 1969). This fault zone is well displayed some 300 m west of the Julegård section and Lower Cambrian deposits ("Green Shales") are exposed here in the steep cliff of the Bornholm Block (Fig. 2; Grönwall and Milthers 1916; Hansen 1936). The deposits, which belong to the Norretorp Member of the Læså Formation (Surlyk 1980; Nielsen & Schovsbo 2007) are glauconitic and relatively strongly lithified, contain numerous phosphorite nodules, and are strongly bioturbated. In contrast to the view of Gry (1969), Hamann (1987) and Jensen and Hamann (1989) placed a fault-bounded block of Lower Cretaceous sediments at Julegård. According to their view the Upper Triassic sediments are seen only in coastal outcrops near Risebæk and again in coastal outcrops west of
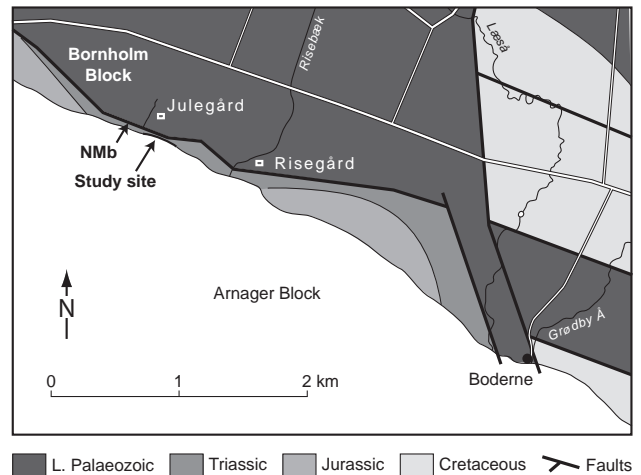
Fig. 2. Detailed location map of the south coast of Bornholm around Julegård. Based on Gry (1969). Glauconitic sediments of the Norretorp Member are exposed in the uplifted Bornholm Block at NMb (Grönwall and Milthers 1916; Hansen 1936). At the study site in the down-faulted block, sediments of the Norretorp Member also occur and are here overlain by sediments of presumed Upper Triassic age.
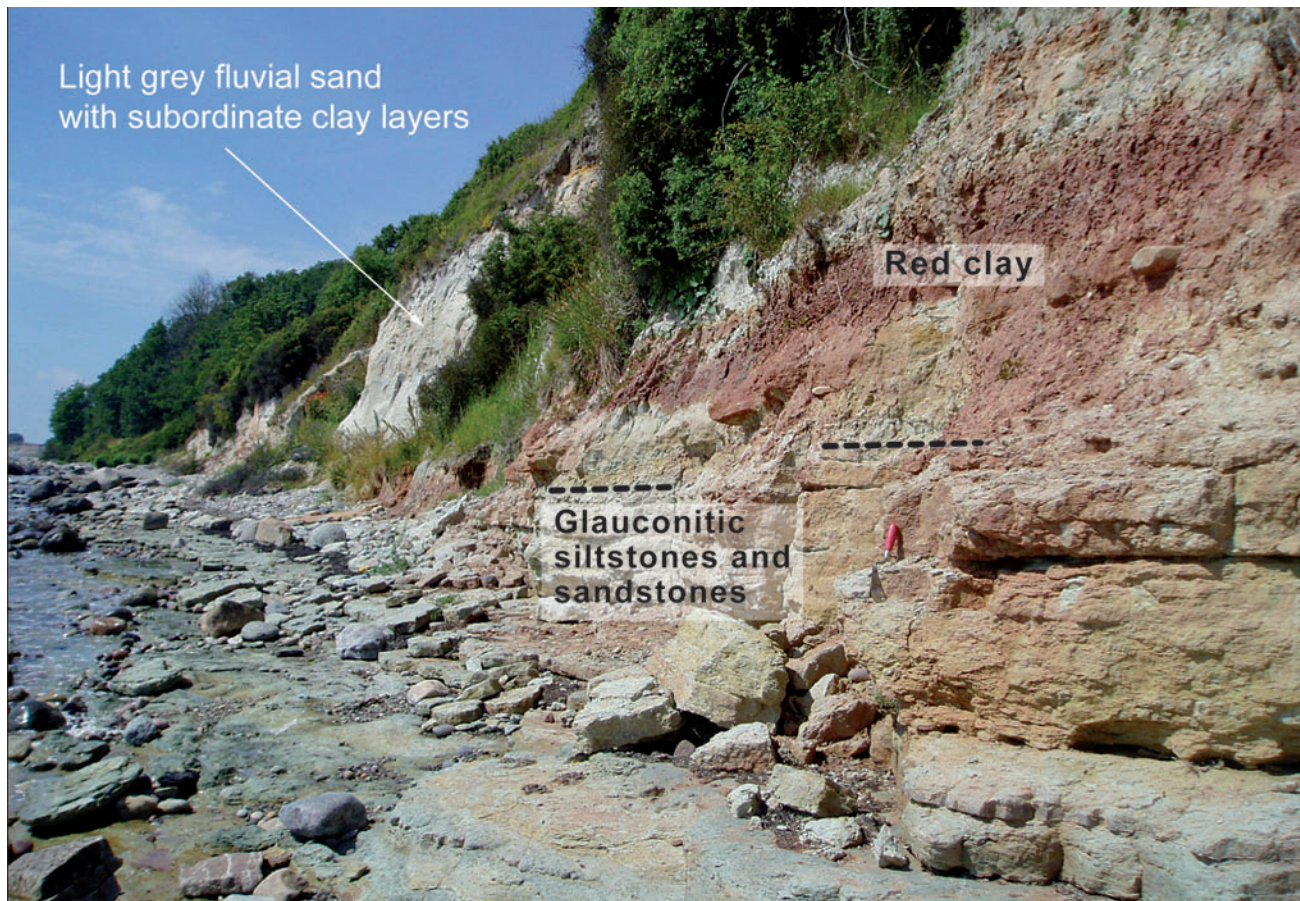
Fig. 3. General view of the studied outcrops at Julegård. Glauconitic, marine deposits of Cambrian age are overlain by red and green lacustrine clay and light greyish to whitish fluviatile sand and conglomerate of presumed Late Triassic age. The boundary between the two units is given by the discontinuous line. View is towards the west.
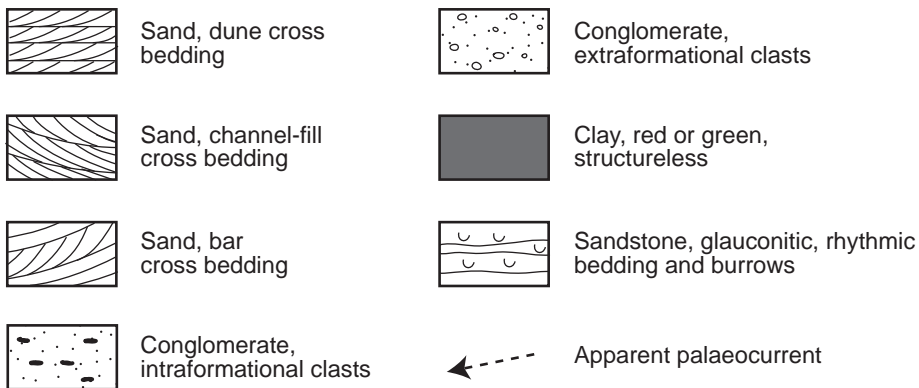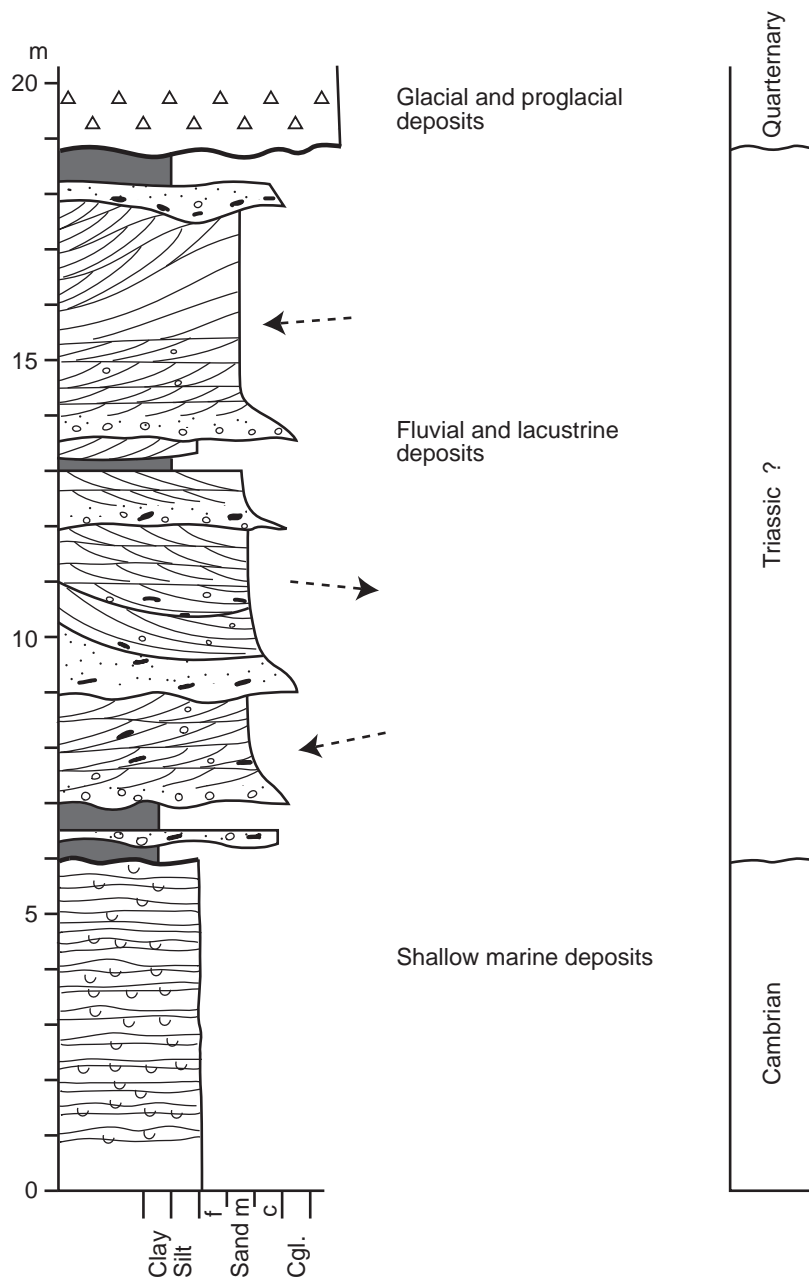
Fig. 4. The sedimentary succession at Julegård on the south coast of Bornholm.

Legend:

Sand, dune cross bedding

Sand, channel-fill cross bedding

Sand, bar cross bedding

Conglomerate, intraformational clasts

Conglomerate, extraformational clasts

Clay, red or green, structureless

Sandstone, glauconitic, rhythmic bedding and burrows

Apparent palaeocurrent

Julegård. According to Hamann (1987) the lithology of the Mesozoic sediments at Julegård was similar to that of the Lower Cretaceous Rabekke Formation, but he also mentioned that the demarcation of the block was somewhat uncertain. Graversen (2004a; 2004b; 2009) followed the interpretation of Jensen and Hamann (1989) and also indicated the presence of Lower Cretaceous sediments at Julegård.

The Julegård section

The Julegård section described here belongs to the down-faulted Arnager Block and is composed of two different sedimentary units covered by Quaternary deposits (Figs 3 and 4). Glauconitic, greenish grey sandstone and siltstone with numerous trace fossils at the base are overlain by red or green clay and silt, and light greyish, kaolinitic fluvial sand and conglomerate. The glauconitic sediments, which have an exposed thickness of about 6 m, are exposed in the beach zone and in low coastal cliffs. In an eastward direction, towards Risebæk, the glauconitic sediments are replaced by well-stratified, greyish sandstones and multicoloured clay of presumed Triassic age. The contact between the two types of sediments is covered by Quaternary deposits and modern dune sand. The glauconitic sediments at Julegård dip gently towards the west and are overlain, without any major erosional surface, by multicoloured clay and light greyish sand and conglomerates also dipping towards the west. The glauconitic sediments described here at the base of the Julegård section are rich in trace fossils. These trace fossils have only received sporadic description in the literature. Gry (1969) noted the appearance of *Skolithos*-like burrows in some sandstones, and Gravesen *et al.* (1982) also noted the occurrence of bioturbated sandstones.

The age of the sediments at Julegård has not previously been examined and the existence of two different sedimentary units has not previously been reported.

Fig. 5. General view of the glauconitic deposits extensively bioturbated with *Trichophycus/Teichichnus.*

0   5 cm

Sparse ostracods in red clay facies at Risebæk, 0.8 km east of Julegård, indicate an Early to Middle Keuper (Late Ladinian – Carnian) age for these sediments (Christensen 1972; Gravesen *et al.* 1982). The uppermost unit at Julegård is dominated by light greyish to whitish fluvial sands and conglomerates but also contains thin red or green clay layers (Figs 3 and 4). The light greyish to whitish colour of the sand is most likely due to a content of kaolinitic clay. The clasts in the conglomerates are composed of intraformational clay lumps as well as extraformational pebbles and cobbles. The characteristic red and green colours of the thin clay layers suggest that the uppermost unit is of Late Triassic age (Figs 3 and 4). A red clay near the base of the terrestrial succession at Julegård was screened for pollen and spores, but proved to be barren. A dark grey mud layer in overlying terrestrial sediments was also barren (S. Piasecki, personal communication 2010). A definite proof of the age of this unit has to await further palynological investigation.

The glauconitic marine deposits at the base of the Julegård section have apparently been assigned Late Triassic as well as Early Cretaceous ages by previous authors, although the sediments have not been described in any detail. The marine deposits were sceened for microfossils and palynomorphs, but proved to be barren (S. Piasecki, personal communication 2009). It was decided therefore to carry out a ^{40}Ar-^{39}Ar age determination on the glaucony contained in the shallow marine deposits. This analysis, as discussed below, suggests that the deposits are of Cambrian age and belong to the Lower Cambrian Norretorp Member of the Læså Formation (Surlyk 1980; Nielsen & Schovsbo 2007).

The glauconitic deposits
Lithology

These sediments have an exposed thickness of about 6 m (Fig. 4). They are composed of a number of lightly cemented, greenish grey siltstones and fine-grained sandstones having a totally bioturbated ichnofabric (Figs 5 and 6). Physical sedimentary stuctures are very poorly preserved due to the extensive biotur-

0   5 cm

Fig. 6. Closer view of longitudinal section of the spreite structure attributable to *Trichophycus/Teichichnus*.

Fig. 7. Bedding plane exposure of *Trichophycus/Teichichnus.*

bation, ichnofabric index 4–5, but at some horizons, small-scale wave-generated structures are seen. This succesion is broken by a number of relatively well cemented sandstones with typical thicknesses between 5 and 20 cm. Some of these sandstones are well stratified, but most are massive and/or show evidence of bioturbation. One sample from the lightly cemented deposits had a carbonate content of 14%, but most of the carbonate probably originates from secondary fracture fillings. A thin section reveals that the sediment is composed of quartz (about 80–85 %), feldspars (10%), and bright green glaucony (5–10%). We follow Huggett and Gale (1997) and use the term glaucony and not glauconite for these green grains since the exact mineralogy of the grains is unknown. The glaucony grains are rounded to subangular and have almost the same grain-size distributions as the detrital grains with which they are mixed. An XRD-analysis indicates the presence of illite and kaolinite. There is a complete lack of phoshorite nodules.

The sediments are interpreted as a shallow marine deposit. The lithology suggests that the sediments were deposited between fair weather and storm wave base in the transition zone between the lower shoreface and the shelf. The presence of glaucony grains supports this interpretation as ideal conditions for glaucony formation are fully marine conditions, 10–30 m water depth, low sedimentation rate, and periodic winnowing (Huggett & Gale 1997).

Trace fossils

The trace fossils in the Norretorp Member have previously been described by Clausen and Vilhjálmsson (1986) from outcrops southwards from Snogebæk harbour to Broens Odde on the east coast of Bornholm. A diverse assemblage of trace fossils was described, representing seven ichnogenera, occurring in four ichnoassociations.

The trace fossils at the Julegård locality have a very different signature. Diversity is much reduced, and only a single ichnoassociation is represented. The ichnofabric is dominated by a spreite structure, possibly attributable to *Teichichnus* Seilacher, 1955, but

0   5 cm

Fig. 8. *Rusophycus* isp., probably the resting trace of a trilobite.

possibly to *Trichophycus* Miller & Dyer, 1878 (Figs 5 and 6). Both of these cover more or less horizontal spreite structures. However, as Osgood (1970) indicated, the distinction between these two ichnogenera is not completely understood. Schlirf & Bromley (2007) applied *Teichichnus duplex* to spreite structures in Cambrian sandstones of nearby southern Sweden. This ichnospecies cannot be applied to the spreite structures at Julegård. However, A. Rindsberg, G. Mángano and L. A. Buatois have briefly visited the Julegård locality and all preferred to name the spreite structures as *Trichophycus* isp. This ichnotaxonomic problem will be addressed in the near future.

The density of bioturbation is so great that details of the morphology are hard to make out, despite the high-quality preservation (Fig. 7). This form may be the same as that called *Buthotrephis palmata* Hall, 1852 by Clausen & Vilhjálmsson (1986) at Broens Odde. Together with the spreite structure are seldom specimens of *Rusophycus* Hall, 1852, probably the resting traces of trilobites (Fig. 8).

Argon analysis of glaucony

Method

Jaw crushed material was sieved to a fraction of 200–300 μm. Bright green round glaucony grains were separated using a combination of heavy liquids and magnetic separation, and subsequently purified under an optical microscope by hand picking. The sample was irradiated in the TRIGA reactor at Oregon State University, Corvallis, USA. FCT-3 biotite was used as monitor assuming an age of 28.03 ± 0.01 Ma (2). The sample was dated using the incremental heating technique. Argon was released from the samples using a CO_2 integrated laser. The incremental heating was performed in 10 steps from 300°C to 1200°C and the released argon gas was introduced into a MAP 215-50 mass spectrometer after purification. Each measurement series includes 10 steps of measurements of the isotopes ^{36}Ar, ^{37}Ar, ^{38}Ar, ^{39}Ar and ^{40}Ar. After every 3 or 4 steps, blanks were measured and corrections were made along with calculations of decay and corrections for mass fractionation and interference reactions between neutrons and isotopes of Ca, K and Cl (Mc-Dougall & Harrison 1988). Data were treated in the program ArArCALC (Koppers 2002) and an age from each step was calculated assuming an initial ^{40}Ar-^{36}Ar ratio of 295.5. All ages are reported with an uncertainty of 2σ. Further analytical and instrumental details are published by Duncan & Hogan (1994).
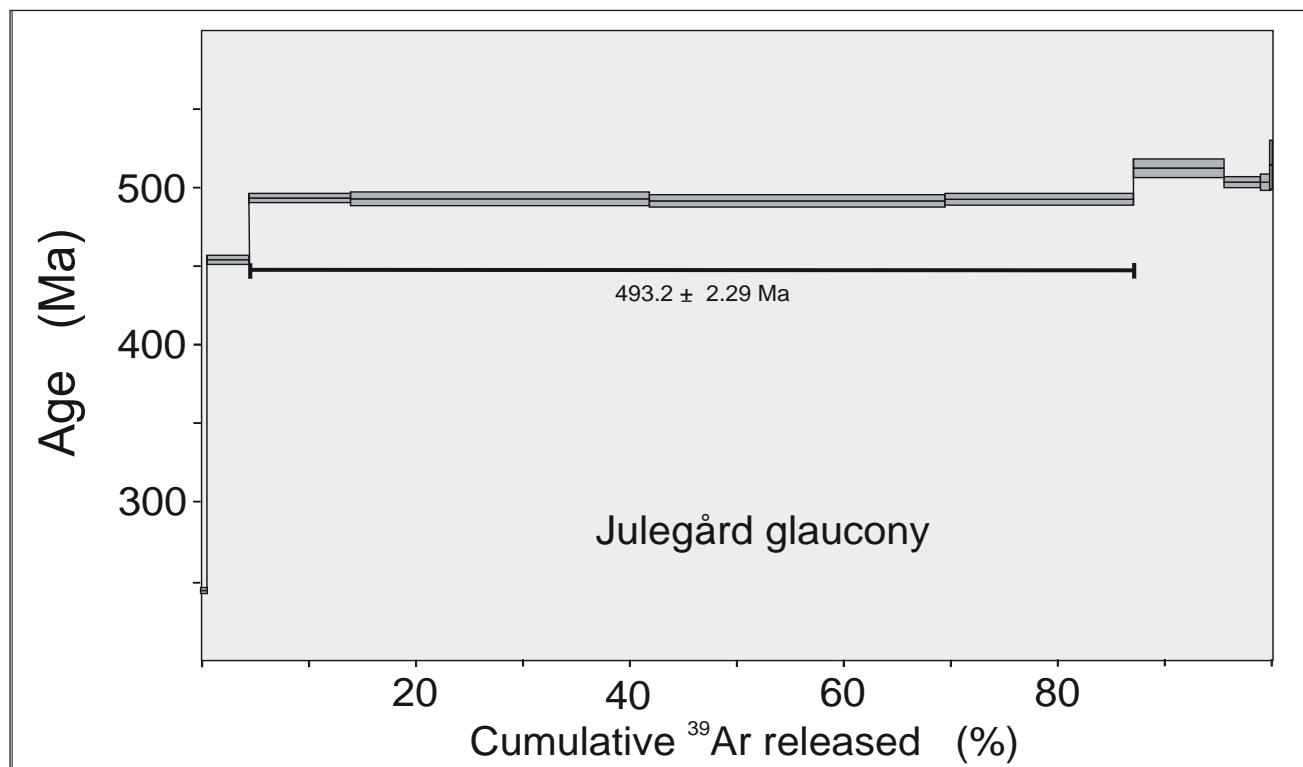
Fig. 9. Age spectrum for stepwise ^{40}Ar-^{39}Ar analysis of glaucony from the marine deposits at Julegård, south coast of Bornholm.

Results

Most of the released argon is present in four successive increments of the analysis (steps 3–6 representing 83% ^{39}Ar), Table 1. With their consistent calculated ages they constitute an age plateau of 493.2 ± 2.2 Ma (2) with an MSWD of 0.3 (Fig. 9). The two low-temperature increments yield lower ages, and the four steps at the highest temperatures yield increasing ages with a maximum of 515 ±15 Ma. The total of the released argon results in a calculated age of 492. 4 ± 2.2 Ma (2). An isochron for the same four increments 3–6 results in an age of 494.0 ± 3.1 Ma (2) statistically identical to the plateau age. The small non-radiogenic component of the argon (0.3 – 4.3 % of the ^{40}Ar) is indistinguishable from atmospheric argon, and no excess Ar is indicated. The plateau age result, which analytically is a highly significant age of 493 ± 2 Ma (2), is preferred.

Interpretation

The glaucony of the Julegård sample is considered to have retained the radiogenic argon that accumulated from at least the time of its maturation some few million years after its formation as an authigenic mineral (Odin 1982). However, glaucony has been shown to lose argon during irradiation in the sample prepara-

tion for ^{40}Ar-^{39}Ar isotope analysis (Foland *et al.* 1984; Smith *et al.* 1993). This is due to the habit of glaucony to crystallize as laminae thinner than the recoil distance of ^{39}Ar formed during irradiation. Therefore the calculated age would be expected to be higher than the geological age if recoil took place. Detected ^{39}Ar losses may amount to 27–64% (Smith *et al.* 1993) or 17–29% (Foland *et al.* 1984), resulting in correspondingly too high calculated ages. The release of Ar from glaucony during heating is probably related to dehydration of the crystals. For the Julegård sample this occurred over a considerable temperature interval of 275°C and this could indicate that recoil either was extremely uniform or did not occur. In case of the latter, the calculated age of 493 ± 2 Ma is also the geological age. However, if recoil occurred, the formation age may be between Carboniferous and Jurassic.

It is interesting to note that ^{40}Ar-^{39}Ar analysis of glaucony from the Middle Cambrian Kalby Clay (Poulsen 1966) which formed from the erosion of the Exsulans Limestone Bed resting on the Læså Formation yielded three high-temperature steps constituting 42% of the ^{39}Ar with Middle Cambrian ages of 491–513 Ma (Fig. 10; Holm 1984). If indeed these two argon analyses both have age significance, the Julegård deposit is indicated to be Cambrian.

We note that the age calculated for the Julegård
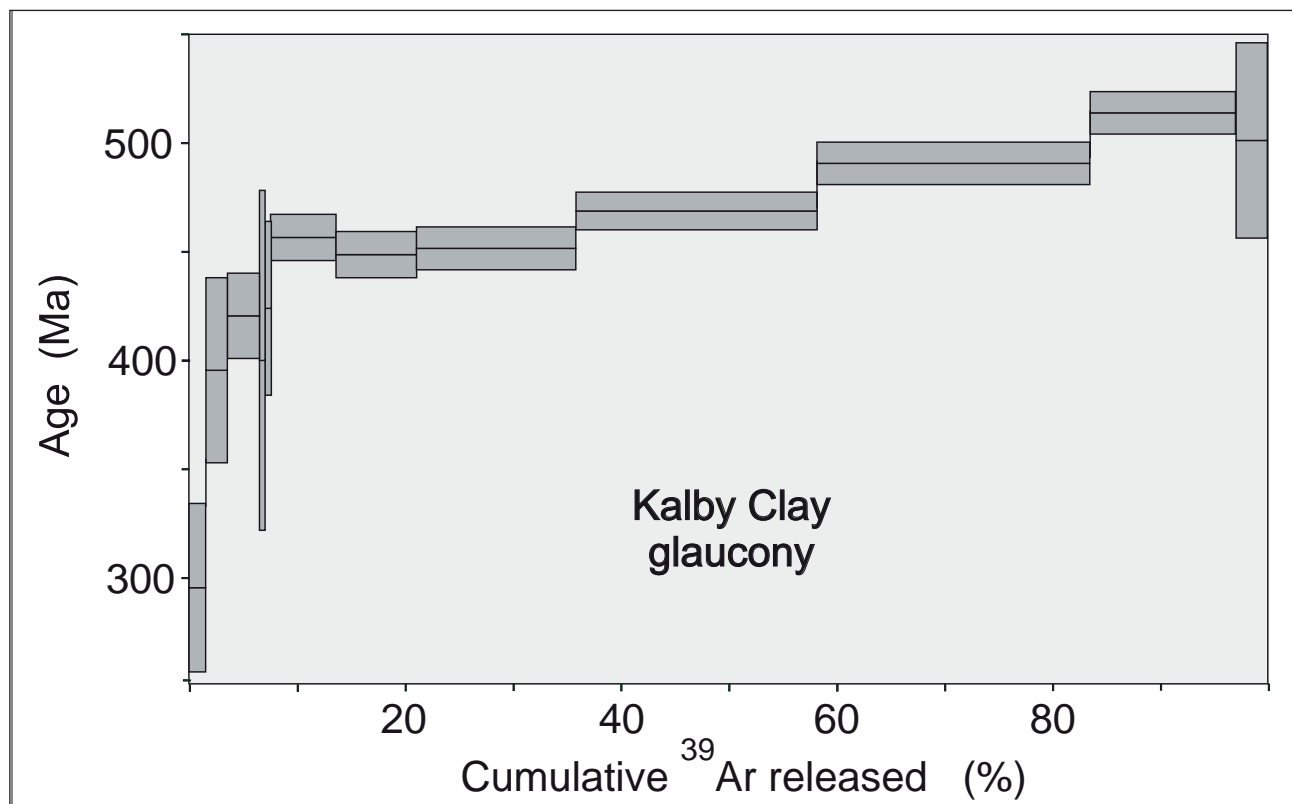
Fig. 10. Age spectrum for stepwise ^{40}Ar-^{39}Ar analysis of glaucony from the Kalby Clay (Exsulans Limestone Bed) of the Middle Cambrian of Bornholm (from Holm 1984).

glaucony is both younger than the previously reported age of 510 ± 5 Ma for calcite concretions in Middle Cambrian black shales in southern Sweden (Israelson *et al.* 1996) and biostratigraphic information that indicates an Early Cambrian age for the Norrretorp Member (Poulsen 1967). Therefore, the glaucony may have suffered an Ar loss. The considerable indicated systematic error on the Ar analysis thus precludes a more precise interpretation of the age.

Discussion and conclusions

Coastal exposures at Julegård on the south coast of Bornholm have so far only received little attention. The outcrops described here belong to the Arnager Block. They are formed by two very different lithological units, shallow marine siltstone and sandstone at the base and fluvial sand and conglomerates with subordinate multicoloured clay layers at the top.

The shallow marine deposits in the lower unit are densely bioturbated. Most trace fossils are attributed to the ichnogenus *Teichichnus* or possibly to *Trichophycus* but the sediments also contain rare specimens of *Rusophycus* probably the resting traces of trilobites. The shallow marine deposits contain glaucony, and a [40]Ar-[39]Ar dating of the glaucony yields a calculated age of 493 ± 2 Ma, which is a Late Cambrian (Furongian) age (cf. Israelson *et al.* 1996), but because of the lithology of the studied unit, it most likely belongs to the Early Cambrian Norretorp Member of the Læså Formation (Surlyk 1980; Nielsen & Schovsbo 2007). The lithology of the studied unit suggests that it may belong to the upper, more sand-rich, part of the Norretorp Member (cf. Nielsen and Schovsbo 2007). The fluvial sand and conglomerates with subordinate multicoloured

clay layers in the upper unit have been interpreted to belong to the Lower Cretaceous Rabekke Formation (Jensen and Hamann 1989), but these sediments are here considered to be of Upper Triassic age in agreements with the descriptions of Grönwall and Milthers (1916) and Gry (1969).

The recognition of Cambrian deposits of the Norretorp Member below presumed Upper Triassic sediments in the down-faulted block at Julegård is new and suggests that the displacement along the main fault zone that runs a little inland is less than the thickness of the Norretorp Member or less than 100 m (cf. Nielsen and Schovsbo 2007).

During the winter of 2009–2010, violent storms largely covered the Cambrian exposure at Julegård with off-shore sand and also caused extensive burial by collapse of the overlying Triassic sediments. These conditions may represent the normal situation, thereby explaining the lacking report of Cambrian exposure at the Julegård study site by previous stratigraphers.

Acknowledgements

Table 1.
Results of [40]Ar-[39]Ar analysis of Julegård glaucony.

Incremental Heating		36Ar(a)	37Ar(ca)	38Ar(cl)	39Ar(k)	40Ar(r)	Age ± 2σ (Ma)	40Ar(r) (%)	39Ar(k) (%)	39(k)/40(a+r) ± 2σ	36(a)/40(a+r) ± 2σ
1	300 °C	0.000021	0.000118	0.000002	0.003279	0.243317	244.23 ± 1.88	97.49	0.49	0.013137 ± 0.000071	0.000085 ± 0.000020
2	400 °C	0.000056	0.000997	0.000067	0.026575	3.898078	454.53 ± 1.96	99.58	3.98	0.006789 ± 0.000033	0.000014 ± 0.000002
3	500 °C	0.000116	0.001964	0.000123	0.063170	10.186094	494.00 ± 2.49	99.66	9.47	0.006181 ± 0.000036	0.000011 ± 0.000001
4	600 °C	0.003169	0.007112	0.000000	0.186282	30.002479	493.49 ± 3.56	96.97	27.93	0.006021 ± 0.000049	0.000102 ± 0.000002
5	700 °C	0.003141	0.008633	0.000214	0.184080	29.549727	492.06 ± 3.16	96.95	27.60	0.006040 ± 0.000043	0.000103 ± 0.000003
6	775 °C	0.002882	0.012251	0.000059	0.118050	18.987092	492.90 ± 3.50	95.71	17.70	0.005951 ± 0.000048	0.000145 ± 0.000004
7	850 °C	0.000201	0.005776	0.000230	0.055918	9.403260	512.43 ± 5.39	99.37	8.38	0.005909 ± 0.000071	0.000021 ± 0.000001
8	925 °C	0.000115	0.003292	0.000111	0.023417	3.859033	503.48 ± 2.99	99.13	3.51	0.006015 ± 0.000041	0.000030 ± 0.000002
9	1050 °C	0.000041	0.001789	0.000032	0.005688	0.937941	503.72 ± 5.04	98.73	0.85	0.005988 ± 0.000066	0.000043 ± 0.000010
10	1200 °C	0.000004	0.000623	0.000004	0.000569	0.096303	515.26 ± 14.83	98.91	0.09	0.005845 ± 0.000125	0.000037 ± 0.000085
Total fusion (total of 10 increments)							492.41 ± 2.19				
								MSWD			
Weighted plateau of 4 increments 3-6							493.23 ± 2.19	0.33	82.69		
										40/36 ± 2σ	
Isochron (inverted) of 4 increments 3-6							494.02 ± 3.09	0.23		Non-radiogenic Ar:	272 ± 64

a = atmospheric, ca = calcium, cl = chlorine, k = potassium, r = radiogenic

References

Christensen, O.B. 1972: Det danske sænkningsområdes udvikling i det mellemste Mesozoikum. Dansk Geologisk Forenings Årsskrift for 1971, 55–62.

Clausen, C.K. & Vilhjálmson, M. 1986: Substrate control of Lower Cambrian trace fossils from Bornholm, Denmark. Palaeogeography, Palaeoclimatology, Palaeoecology 56, 51–68.

Duncan, R.A.& Hogan, L.G. 1994: Radiometric dating of young MORB using the $^{40}Ar/^{39}Ar$ Incremental Heating method. Geophysical Research Letters 21 (18), 1927–1930.

EUGENO-S Working Group 1987: Crustal structure and tectonic evolution of the transition between the Baltic Shield and the North German Caledonides (The EUGENO-S Project). Tectonophysics 150, 253–348.

Foland K. A., Linder, J. S., Laskowski, T.E. & Grant, N.K. 1984: $^{40}Ar/^{39}Ar$ dating of glauconites: measured ^{39}Ar recoil loss from well-crystallized specimens. Chemical Geology 46, 241–264.

Graversen, O. 2004a: Upper Triassic – Cretaceous stratigraphy and structural inversion offshore SW Bornholm, Tornquist Zone, Denmark. Bulletin of the Geological Society of Denmark 51, 111–136.

Graversen, O. 2004b: Upper Triassic – Lower Cretaceous seismic sequence stratigraphy and basin tectonics at Bornholm, Denmark, Tornquist Zone, NW Europe. Marine and Petroleum Geology 21, 579–612.

Graversen, O. 2009: Structural analysis of superimposed fault systems of the Bornholm horst block, Tornquist Zone, Denmark. Bulletin of the Geological Society of Denmark 57, 25–49.

Gravesen, P., Rolle, F. & Surlyk, F. 1982: Lithostratigraphy and sedimentary evolution of the Triassic, Jurassic and Lower Cretaceous of Bornholm, Denmark. Danmarks Geologiske Undersøgelse, Serie B, Nr. 7, 49 pp.

Gry, H. 1969: Megaspores from the Jurassic of the Island of Bornholm, Denmark. Meddelelser fra Dansk Geologisk Forening 19, 69–89.

Grönwall, K.A. & Milthers, V. 1916: Beskrivelse til Geologisk Kort over Danmark (i Maalestok 1 : 100,000). Kortbladet Bornholm. Danmarks Geologiske Undersøgelse, I. række Nr. 13, 281 pp.

Hall, J. 1852: Palaeontology of New York 2, 362 pp. Albany, New York.

Hamann, N.E. 1987: Den mesozoiske bassinudvikling ved Bornholm. MSc. thesis, Københavns Universitet, 101 pp.

Hansen, K. 1936: Die Gesteine des Unterkambriums von Bornholm. Danmarks Geologiske Undersøgelse, II. Række Nr. 62, 1–194.

Holm, P.M. 1984: Analysis by the $^{40}Ar/^{39}Ar$ method of glauconite from the Kalby clay, Bornholm. In: Exploitation of Oil and Gas Resources. Energiministeriet.

Huggett, J.M. & Gale, A.S. 1997: Petrology and palaeoenvironmental significance of glaucony in the Eocene succession at Whitecliff Bay, Hampshire basin, UK. Journal of the Geological Society, London, 154, 897–912.

Israelson, C., Halliday, A.N. & Buchardt, B. 1996: U-Pb dating of calcite concretions from Cambrian black shales and the Phanerozoic time scale. Earth and Planetary Science Letters 141, 153–159.

Jensen, J.B. & Hamann, N.E. 1989: Geological mapping of Mesozoic deposits along the eastern margin of the Rønne Graben, offshore Bornholm, Denmark. Bulletin of the Geological Society of Denmark 37, 237–260.

Koppers, A.A.P. 2002. ArARCALC – software for $^{40}Ar/^{39}Ar$ age calculations. Computers & Geosciences 28, 605–619.

McDougall, I. & Harrison, T.M. 1988. Geochronology and Thermochronology by the $^{40}Ar/^{39}Ar$ Method. Oxford University Press, 212 pp.

Miller, S.A. & Dyer, C.B. 1878: Contributions to paleontology, no. 1. Cincinnati Society of Natural History 1, 24–39.

Nielsen, A.T. & Schovsbo, N.H. 2007: Cambrian to basal Ordovician lithostratigraphy in southern Scandinavia. Bulletin of the Geological Society of Denmark 53, 47–92.

Odin, G.S.1982. Numerical Dating in Stratigraphy. Wiley-Interscience, New York, 454 pp.

Osgood, Jr, R.G. 1970: Trace fossils of the Cincinnati area. Paleontographica Americana 6 (41), 281–444.

Poulsen, C. 1967: Fossils from the Lower Cambrian of Bornholm. Det Kongelige Danske Videnskabernes Selskab. Matematisk-Fysiske Meddelelser 36, 2, 1–48.

Poulsen, V. 1966: Cambro-Silurian Stratigraphy of Bornholm. Bulletin of the Geological Society of Denmark 16, 117–137.

Schlirf, M. & Bromley, R.G. 2007: *Teichichnus duplex* n. isp., new trace fossil from the Cambrian and the Triassic. Beringeria 37, 133–141.

Seilacher, A. 1955: Spuren und Facies im Unterkambrium. In: Schindewolf, O.H. and Seilacher, A. (eds): Beiträge zur Kenntnis des Kambriums in der Salt Range (Pakistan). Akademie der Wissenschaften und der Litteratur, Abhandlungen der matematisch-naturwissenschaftlichen Klasse 10, 117–143.

Smith, P.E., Evensen, N.M. & York, D. 1993: First successful $^{40}Ar-^{39}Ar$ dating of glauconies: Argon recoil in single grains of cryptocrystalline material. Geology 21, 41–44.

Surlyk, F. 1980: Denmark. In: geology of the European countries, Denmark, Finland, Iceland, Norway, Sweden, 1–50. Dunod (Published in cooperation with the Comité National Francais de Géologie (C.N.F.G.) on the occasion of the 26th International Geological Congress).

Surlyk, F. Milàn, J. & Noe-Nygaard, N. 2008: Dinosaur-tracks and possible lungfish aestivation burrows in a shallow coastal lake; lowermost Cretaceous, Bornholm, Denmark. Palaeogeography, Palaeoclimatology, Palaeoecology 267, 292–304.

Mineral X, a new thalcusite homologue from the Ilímaussaq complex, South Greenland

Contribution to the mineralogy of Ilímaussaq, no. 144

S. KARUP-MØLLER & E. MAKOVICKY

Mineral X is assumed to be a new member of the thalcusite homologous series with the structural formula $TlCu_{2N}S_{2N+1}$ with N=1.5. It was found in loose ussingite-analcime boulders on the Taseq slope towards the Narsaq Elv in the northern part of the Ilímaussaq complex in South Greenland in association with chalcothallite, cuprostibite, galena, sphalerite, bornite, antimonian silver and seinäjokite. Supergene alteration has resulted in a number of secondary Cu-Sb-minerals. The primary ore minerals appear to have crystallized contemporaneously under low S-fugacities.

Sven Karup-Møller (svka@byg.dtu.dk) Department of Civil Engineering, Technical University of Denmark; Emil Makovicky (Emilm@geo.ku.dk), Institute of Geography and Geology, University of Copenhagen, Denmark.

At present three primary thallium bearing minerals have been discovered at the Ilímaussaq complex in South Greenland: chalcothallite, rohaite and thalcusite (Semenov *et al.* 1967; Karup-Møller 1978a; Kovalenker *et al.* 1978; Makovicky *et al.* 1980; Karup-Møller and Makovicky 2001). All minerals referred to in this paper are listed in Table 1. Chalcothallite and rohaite are known only from their type localities within the Ilímaussaq complex. Chalcothallite occurs in ussingite veins in naujaite on the Taseq slope towards Narsaq Elv in the northern part of the complex. Associated ore minerals are cuprostibite, native silver, chalcosite, gudmundite and thalcusite. Rohaite was found in an analcime-sodalite vein in lujavrite at Kvanefjeld. Associated primary ore minerals here are cuprostibite, chalcosite, sphalerite, loellingite and antimonian silver. Rohaite is partly altered to secondary digenite-senarmontite aggregates. The thalcusite type locality is Talnakh in the Norilsk region, Siberia, Russia (Kovalenker *et al.* 1978). The mineral has also been found at the Murun massif, Aldan Shield, Yakutia, Russia (Dobrovol'skaya *et al.* 1984); Dobrovol'skaya & Nekrasov 1994), at Rajapura-Dariba, Rajasthan, India (Mookherjee *et al.* 1984) and at Mont Saint-Hilaire, Quebec, Canada (Mandarino & Anderson 1989). Within the Ilímaussaq massif thalcusite has

been found at three localities: at Taseq associated with chalcothallite, as minor inclusions in naujaite at the head of Kangerluarsuk fjord in the southern part of the complex and in coarse ussingite associated with cuprostibite at Nakkaalaaq mountain in the north-eastern part of the complex.

Mineral locations and sample material

In 2006 Tom Weidner found additional chalcothallite in two erratic ussingite-analcime boulders some 200 m. apart on the Taseq slope towards the Narsaq Elv. The total amount of material collected was about 5 kg. We assume that these boulders come from the same mineral vein system that hosts the chalcothallite type material. They are referred to as boulder 1 and 2 below. They contain an estimated 1–2% disseminated sulphides in random distribution. A total of 10 polished sections with ore minerals have been studied. In boulder 1 chalcothallite is associated with a new Tl-sulphide described below as mineral X. Additional ore minerals present are cuprostibite, sphalerite, bornite, galena, antimonian silver and chalcosite-like phases.

The mineral relationships observed suggest that the ore minerals crystallized contemporaneously. In boulder 2 the only Tl-phase present is chalcothallite. Additional ore minerals identified are galena, sphalerite and seinäjokite. Supergene alteration has resulted in a number of secondary Cu-Sb minerals.

Table 1. Minerals identified or referred to in the present study

Mineral X	$Tl_2(Cu,Fe)_6S_5$
Chalcothallite	$Tl(K)_2Cu(Fe,Ag)_{6.35}SbS_4$
Rohaite	$Tl(Pb,K)_2Cu_{8.67}Sb_2S_4$
Thalcusite	$TlCu_3FeS_4$
Cuprostibite	Cu_2Sb
Gudmundite	$FeSbS$
Seinäjokite	$FeSb_2$
Loellingite	$FeAs_2$
Native silver	Ag
Allargentum	(Ag,Sb)
Antimonian silver	$(\sim Ag_{0.954}Sb_{0.037}Cu_{0.004})$
Chalcosite	$Cu_{2-x}S$
Digenite	Cu_9S_5
Bornite	Cu_5FeS_4
Spalerite	ZnS
Galena	PbS
Senarmontite or valentinite	Sb_2O_3 (b, Fig.5; b, Fig.6; d, Fig.10)
Cuprostibite alteration mineral (c, Fig.5)	$PbCu_2(OH)_5 \cdot nH_2O$
Cuprostibite alteration mineral (b Fig.7)	$(Cu,Fe)Pb_2Sb_{12}(OH)_{24} \cdot nH_2O$
Supergene alteration phase after unknown mineral (e, Fig. 6)	$Cu_2Sb_5(OH)_8 \cdot nH_2O$
Unidentified Fe-As-mineral (c, Fig.9). Vivianite variety?	$Fe_3(AsO_4)_2 \cdot H_2O.$
Ussingite	$Na_2AlSi_3O_8(OH)$
Analcime	$NaAlSi_2O_6 \cdot H_2O$
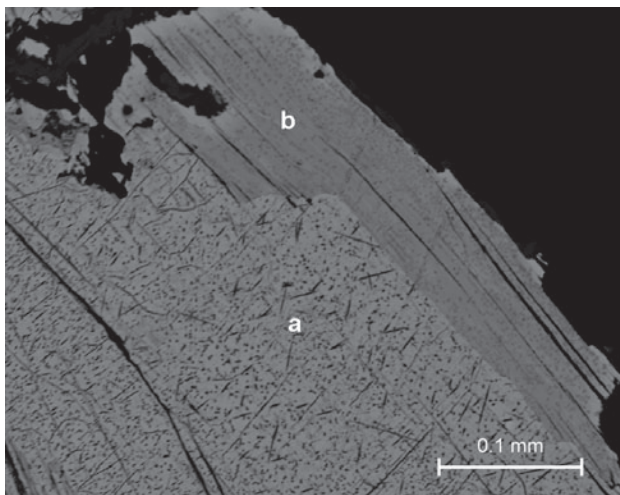
Fig. 1. Grain boundary between chalcothallite (a, composition in Table 3-2) and mineral X (b, Table 2-1). Both minerals show lamellar cleavage. Chalcothallite is dotted by an exsolved phase (Table 3-4) which appears to be oriented after several crystallographic directions in the host. A secondary mineral occurs along cleavage planes in the two Tl-minerals (black lamellae, Table 3-5).
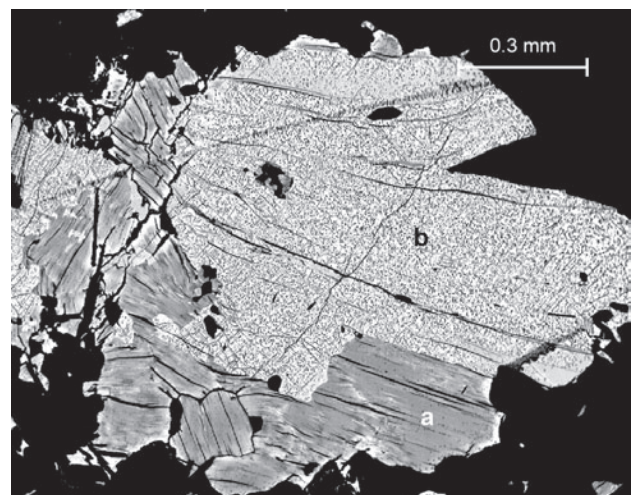
Fig. 2. An aggregate of grains of mineral X (a, Table 2-2) in contact with a large chalcothallite grain (b, Table 4-3) that contains the exsolved phase.

Microprobe analyses

Electron microprobe analyses were carried out at the Institute of Geography and Geology, University of Copenhagen, using a JEOL 733 superprobe in wavelength dispersive mode, JEOL Pax-11 for instrumental control, and using an on-line ZAF correction program. The excitation voltage was 15 kV and beam current 15 nA. The beam diameter was 1 micron. Wavelengths and standards used were CuK, SbL, SK (synthetic Cu$_3$SbS$_4$), AsL (synthetic Cu$_3$AsS$_4$), AgL (Ag), ZnK (synthetic ZnS), KK (KAlSi$_3$O$_8$), FeK (Fe$_2$O$_3$), ClK (sodalite), PbL (PbS), Se SeL (SeS) and TlL (TlAsS$_2$). The detection limit is estimated to be 0.02 wt.% for all elements. All figures 1–11 are backscattered electron (BSE) images.

Mineral descriptions

Mineral X

Due to its softness and fine grain size it was not possible to isolate crystal fragments of this apparently new mineral for single crystal studies. A new mineral name has therefore not been proposed, and it is referred to below as mineral X. In reflected light it is not possible to distinguish mineral X from chalcothallite. In backscattered electron images it is slightly darker than the associated chalcothallite (Figs. 1–3). Mineral X forms lamellar grains with one pronounced cleavage. Cleavage fractures are filled with unidentified secondary products. The mineral occurs either in aggregates with random orientation (bottom part of Fig. 2) or in parallel intergrowths with chalcothallite (Figs. 1–3). It appears to be chemically homogeneous and does not contain inclusions of other minerals. Microprobe analyses carried out on the mineral in two polished sections are listed in Table 2.

Although a crystal structure determination could not be carried out, a model structure for mineral X can be calculated using structural formulae of the known homologues of thalcusite (Kovalenker *et al.*

Table 2. Microprobe analyses of the new thallium phase – mineral X

	1	2	3
No of analyses	5 (Fig. 1)	6 (Fig. 2)	15
Ag	0.09 (11)	0.10 (12)	0.09 (10)
Cu	30.63 (59)	29.35 (91)	28.82 (57)
Fe	10.48 (16)	10.50 (30)	11.39 (43)
Sb	0.12 (9)	0.43 (14)	0.13 (12)
Tl	39.21 (137)	38.05 (130)	40.74 (115)
K	0.97 (42)	n.a.	n.a.
S	18.46 (31)	18.77 (20)	19.30 (35)
Total	99.96	97.2	100.34
Molar ratios			
Ag	0.05	0.06	0.06
Cu	32.93	32.39	31.06
Fe	12.82	13.18	13.96
Sb	0.07	0.25	0.07
Tl	13.11	13.06	13.65
K	1.7	–	–
S	39.33	41.05	41.21

Average analytical values, wt% (standard deviations in brackets)
n.a.: not analysed; –: not detected

Fig. 3. A relatively large chalcothallite grain with the exsolved unidentified phase (a) in contact with chalcosite (c). On the extreme right a fragment of mineral X (b) lies in contact with chalcothallite and morphologically resembles the associated secondary 'chalcosite'.

Fig. 4. Aggregate of chalcothallite / mineral X grains (a) partly decomposed to secondary phases (b, Tables 4-1 and 4-2).

1976; Klepp *et al.* 1980; Berger & Eriksson 1990; all summarized in Makovicky 2005). The known homologues are N = 1, with the model formula $TlCu_2S_2$ with a single-tetrahedron layer; N = 2 with the model formula $TlCu_4S_3$ with a double-tetrahedron layer; and N = 3 with the model formula $TlCu_6S_4$ with a triple-tetrahedron layer. The resulting general formula of the series is $TlCu_{2N}S_{N+1}$ where 'Tl' denotes Tl and K, 'Cu' denotes Cu, Fe and minor Ag, and 'S' stands for S and Se.

There are two ways to calculate the order number N from the results of chemical analyses:

the ratio of the atomic proportions of the tetrahedral cations, Cu, Fe and Ag to the eight-coordinated cations Tl and K gives: $N_1 = (Cu+Fe+Ag)/2(Tl+K)$;

the ratio of anions to the tetrahedral cations: $(S+Se)/(Cu+Fe+Ag) = (N+1)/2N$, simplified hereafter as 'S/Cu', yields: $N_2 = 1/(2S/Cu-1) = Cu/(2S-Cu)$. All these expressions are derived from the general formula given above.

These formulae are structure-based and deal with (presumed) structure sites, i.e., they are not concerned with the valency of individual elements. Application of these formulae to the results in Table 2 gives $N_1 = 1.55$ and $N_2 = 1.39$ for analysis 1, and $N_1 = 1.65$ with $N_2 = 1.21$ for analysis 3. It gives $N_1 = 1.75$ and $N_2 = 1.25$ for analysis 2 that contains elevated contents of Sb that are foreign to the structural model applied. The first two analyses are fairly close to the model with N = 1.5 although the second of these might have somewhat elevated S values, which is reflected in the N_2-value.

For comparison, thalcusite from the head of the Kangerluarsuk fjord, published by Makovicky *et al.* (1980), has $N_1 = 1.06$ and $N_2 = 1.03$, in agreement with the theoretical value N=1.

Parallel to the thalcusite homologous series just described there is a series of Tl-containing channel structures with Cu-S(Se) based channel walls (partitions). They have been summarized in Makovicky (2005, Table 7; 2008, Table 21). Applying the above formulae to this series, $TlCu_3Se_2$ (Berger, 1987) results in $N_1 = 1.5$ and $N_2 = 3.0$, $TlCu_5Se_3$ (Berger *et al.*, 1990) gives $N_1 = 2.5$ and $N_2 = 5$, and $TlCu_7S_4$ (Berger & Sobott, 1987) yields $N_1 = 3.5$ and $N_2 = 7.0$. All these structures show large systematic discrepancies between the N_1 and N_2 values, very different from our case. Closest to the layer-like results is the structure of $Rb_3Cu_8Se_6$ (Schils & Bronger, 1979) with $N_1 = 1.33$ and $N_2 = 2.0$ since this structure is transitional between a channel and a layer type.

The results indicate that, in full agreement with its appearance, mineral X has a layer structure with, presumably, alternating single- and double-tetrahedron layers, which give the resulting N = 1.5. When we take a single (Cu,Fe)-Tl sandwich, with a thickness equal to the ½c parameter of bukovite (Johan & Kvaček, 1971),
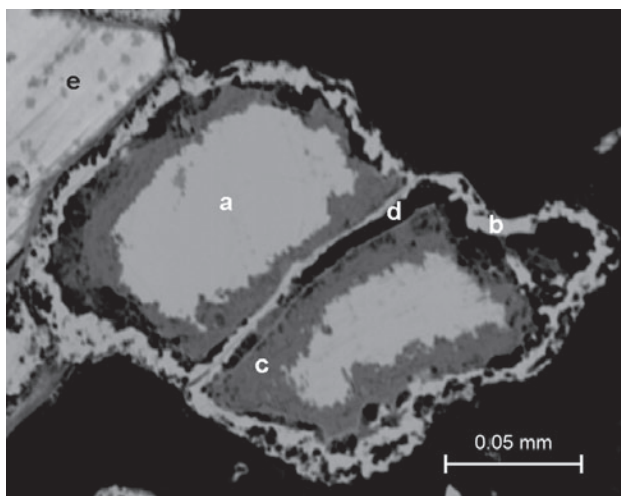
Fig. 5. Two partly decomposed cuprostibite grains (a). The shapes of the original cuprostibite grains are marked by narrow layers of antimony oxide (b, Table 5-2). Remnants of cuprostibite are separated from the antimony oxide by a dark gray layer of a secondary unidentified Cu-Sb-mineral (c, Table 5-1) and unidentified gangue (d). The surrounding gangue mineral (e) is either analcime or ussingite.
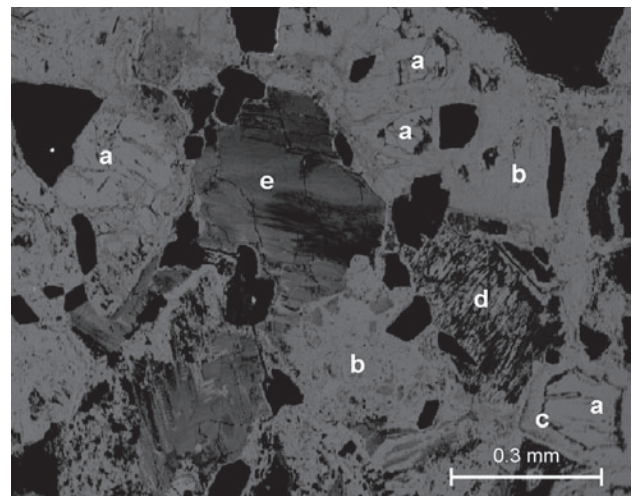
Fig. 6. Extensively decomposed cuprostibite (a). The major part of the alteration area is dominated by antimony oxide (b), very close in composition to that of antimonian oxide in Fig. 5 (Table 5-2). The shape of a cuprostibite crystal is vaguely preserved at the bottom right. The central remnants of the crystal are separated from marginal antimony oxide by a narrow layer of a dark grey Cu-Sb-phase (c). In other places cuprostibite grains are thoroughly penetrated by this phase (d). In the central to left area there is a chemically rather homogeneous mineral (e, Table 5-3) that forms a pseudomorph after an unidentified primary mineral.

i.e. equal to 6.85Å, and a sandwich with a thickness (9.33Å) corresponding to the $\underline{c}$ parameter of synthetic $TlCu_4Se_3$ (Klepp *et al.*, 1980), the resulting $\underline{c}$ parameter of the 1:1 intergrowth will be 16.18Å. Using the $\underline{c}$ (thalcusite)/$\underline{c}$(bukovite) ratio to recalculate selenide to sulfide, the expected $\underline{c}$ parameter of mineral X is 15.8Å. The ideal formula for N = 1.5 is $Tl_2(Cu,Fe)_6S_5$.

The valency of Tl (and K) is M^+ in these structures, and with the divalent anion $(S,Se)^{2-}$, the average valency of the tetrahedrally coordinated cations has to be $v = (2N+1)/2N$ that for N = 1.5 gives v = 1.33. Valency balance for analyses 1 and 3 in Table 2 gives the average valency of iron as $Fe^{2.39+}$ and $Fe^{2.68+}$, respectively, close to $Fe^{2.5+}$.

The ideal formula with $Fe^{2.5+}$ is $Tl_2Cu_{4.67}Fe_{1.33}S_5$, i.e. a Cu/Fe ratio of 3.5. The observed ratios are lower, indicating more iron than in the ideal formula, probably because of the deviation of analytical atomic ratios in Table 2 from the ideal value of 15.38 at.% 'Tl', 46.15 at.% 'Cu' and 38.46 at.% S.

Chalcothallite

In boulder 1 chalcothallite is always characterized by the presence of an exsolved phase that occurs as minute grains evenly distributed throughout the host (Figs. 1–3). A tendency for these to be aligned after several crystallographic directions can sometimes be recognized (Fig. 1). Numerous microprobe analyses were completed on chalcothallite in several polished sections. Selected analyses are listed in Table 3-2 and 3-3. In boulder 2 chalcothallite is homogeneous with no signs of an exsolved phase or inclusions of other minerals. Microprobe analyses of the mineral in two polished sections are listed in Table 3-6 and 3-7.
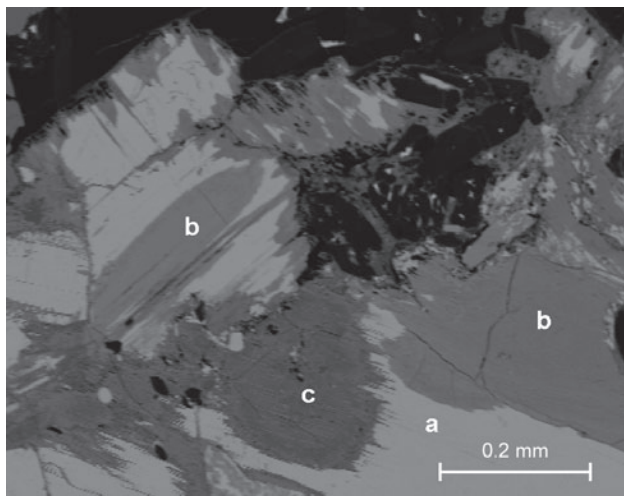
The fine grain size of the exsolved phase renders quantitative microprobe analysis impossible. A semi-quantitative analysis (Table 3-4) indicates that it is enriched in Ag, Fe, Sb, As, K and S and impoverished in Cu and Tl. Semi-quantitative analyses were also completed on the phase developed along cleavage fractures in chalcothallite grains, such as the grain shown in Fig. 1 (Table 3-5). This phase appears to be a Cu-Sb-Fe-rich oxide/hydroxide, possibly with small amounts of Tl and S. However, due to its fine grain size it cannot be excluded that the low Tl and S-values recorded are due to overlap of the microbeam with the adjacent chalcothallite host.

Supergene alteration of chalcothallite and mineral X has rarely taken place (Fig. 4). Microprobe analyses of the alteration product gave a broad range in compositions, from Cu-rich and Fe-poor (Table 4-1) to Cu-poor and Fe-rich (Table 4-2), with small amounts of Zn and Pb. Nearly all Tl, and most of the Sb, present in the original phase appears to have been removed during the alteration process. The low totals indicate that we are dealing with strongly hydrated products.

Cuprostibite

Cuprostibite (Cu_2Sb) has close to ideal composition with only trace amounts of other elements. It is quite common and has been either partly or completely replaced by at least three secondary minerals. In Fig. 5 it is possible to distinguish between two alteration products, a dark phase (c) surrounding remnants of cuprositbite (Table 5-1) with a composition close to $PbCu_2(OH)_5 \cdot nH_2O$, and a light grey marginal phase

Fig. 7. Cuprostibite grains (a) partly replaced by two secondary Cu-Sb minerals; a dark grey phase (c) (not analyzed, but presumably identical with the dark grey phase in Fig. 5) and a slightly lighter grey phase (b) forming two homogeneous replacement bodies (Table 6-4).
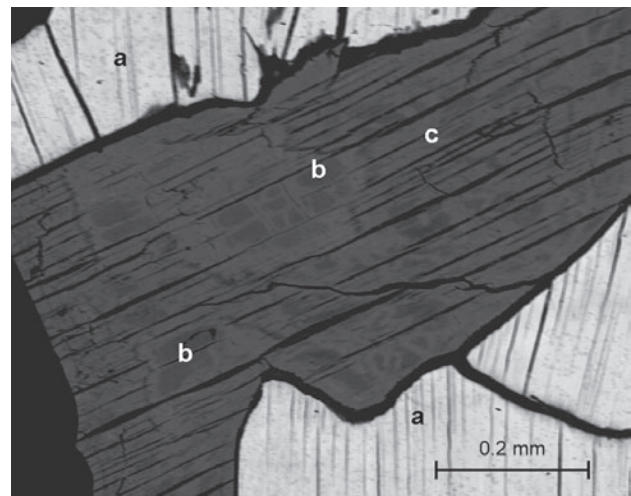
Fig. 8. Mineral X (a) associated with bornite that has almost completely decomposed to a secondary member of the chalcosite group of minerals. Remnants of original bornite (b, Table 6-2) lie embedded in the secondary 'chalcosite' (c, Table 6-1).

(b, Table 5-2), which may be either senarmontite or valentinite (Sb$_2$O$_3$ with about 1.8 wt% Cu). The shape of the original cuprostibite grains is marked by a thin rim of this phase. Some areas of strongly decomposed cuprostibite are characterized by relatively large heterogeneous replacement products (Fig. 6) char-

Table 3. Microprobe analyses of chalcothallite and associated Tl-phases

	1	2	3	4	5	6	7
No. of analyses		12	7	1	4	9	13
Ag	1.32	0.50 (15)	0.26 (23)	1.25	0.53 (41)	0.03 (7)	0.04 (7)
Cu	34.26	35.85 (35)	37.80 (70)	30.87	24.16 (507)	38.93 (52)	35.77 (100)
Fe	3.88	3.63 (16)	3.92 (9)	8.06	7.71 (290)	3.81 (6)	3.92 (28)
Pb	–	–	–	–	1.98 (118)	–	–
Sb	12.15	12.27 (36)	12.67 (34)	19.33	21.20 (178)	12.69 (17)	11.92 (28)
As	–	0.08 (5)	0.09 (7)	1.3	0.09 (11)	0.08 (4)	0.13 (5)
Tl	33.94	34.95 (70)	30.01 (53)	13.37	5.16 (376)	30.05 (89)	35.62 (83)
K	0.78	0.23 (4)	1.58 (10)	1.93	n.a.	1.65 (10)	0.51 (3)
Te	–	0.05 (4)	0.05 (6)	0.17	0.04 (4)	0.03 (4)	0.03 (5)
S	12.54	12.78 (24)	13.02 (15)	18.74	3.74 (111)	13.10 (21)	12.44 (24)
Total	98.87	100.34	99.4	95.02	64.48	101.37	100.38
Molar ratios to S=4.00							
Ag	–	0.05	0.02	0.08	0.17	0	0
Cu	5.51	5.5	5.86	3.33	13.04	6	5.8
Fe	0.71	0.65	0.69	0.99	4.73	0.67	0.72
Pb	–	–	–	–	0.33	–	–
Sb	1.02	1.01	1.03	1.08	5.97	1.02	1.01
As	–	0.01	0.01	0.12	–	0.01	0.02
Tl	1.7	1.72	1.45	0.45	0.86	1.49	1.8
K	–	0.06	0.4	0.34	–	0.41	0.13
S	4	4	4	4	4	4	4

Average analytical values, wt% (standard deviations in brackets). –: not detected.
Notes. 1: Chalcothallite (type specimen) kept at the Geological Museum in Copenhagen. The analysis is reproduced from Makovicky *et al.* (1980). 2 and 3: Composition of chalcothallite in two aggregates in boulder 1 (Figs. 1 and 2 respectively). 4: Semi-quantitative analysis of the exsolved phase in chalcothallite in Fig. 1. 5: Analyses of fracture-filling in Fig. 1. 6 and 7: Composition of chalcothallite in two aggregates from boulder 2.
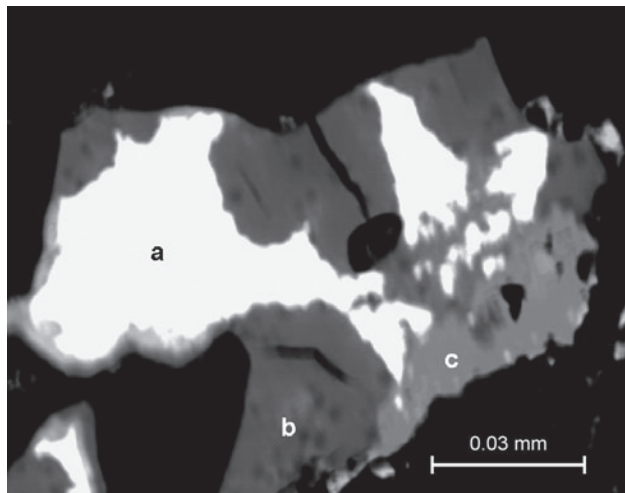
Fig. 9. Galena grain (a) partly replaced by an unidentified member of the chalcosite group of minerals (b, Table 6-4) and an As-rich mineral, possibly a member of the vivianite series (c, Table 6-5).
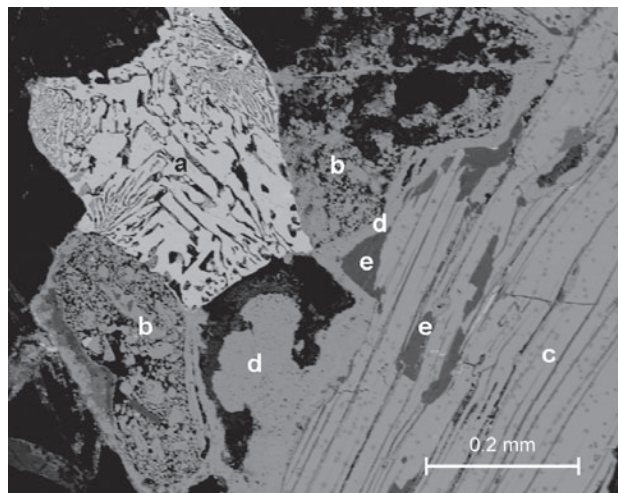
Fig. 10. Exsolution aggregate of antimonian silver (a) enclosed in decomposed cuprostibite grains (b) in contact with chalcothallite (c). The outline of the original cuprostibite grains is marked by a narrow layer of grains of antimony oxide (d). A primary phase (e) of the chalcosite group lies interstitial to chalcothallite.

acterized by a mixture of, apparently, the same two phases which are nicely separated in Fig. 5. In such material there are, in addition to strongly decomposed cuprostibite, well defined patchy dark grains of an unknown mineral of presumably supergene origin (e, Fig. 6; Table 5-3). It is quite homogeneous with a composition close to $Cu_2Sb_5(OH)_8 \cdot nH_2O$. The identity of the product and of the original mineral remains unknown. Homogeneous replacement patches of a secondary Pb-Sb-oxide/hydroxide into cuprostibite have also been identified (b, Fig. 7, Table 5-4). The simplified empirical composition of this phase may be written as $(Cu,Fe)Pb_2Sb_{12}(OH)_{24} \cdot nH_2O$.

Bornite-chalcosite group

Relatively coarse bornite crystallized simultaneously with chalcothallite and mineral X. Later, presumably supergene alteration of this bornite resulted in the formation of a phase of the chalcosite group with the composition $Cu_{1.81}S$ with small contents of Fe and Sb (Table 6-1). Without X-ray diffraction, unambiguous identification of this phase is not possible due to the small amounts present. In Fig. 8 isolated islands (b) of the original bornite with composition $Cu_{1.22}Fe_{0.29}S_{1.00}$ (Table 6-2) lie as remnants enclosed in the replacing 'chalcosite'. Areas dominated by this secondary phase are characterized by strong basal cleavage and the cleavage fractures are filled with unidentified products.

Another phase of the chalcosite group with the composition $Cu_{2.31}S$ and with small amounts of Ag, Pb, Sb and Se (Table 6-3) is situated interstitially to chalcothallite (Fig. 10) and appears to have crystallized at the same time. Again, identification of this compositionally unusual phase is not possible without X-ray diffraction.
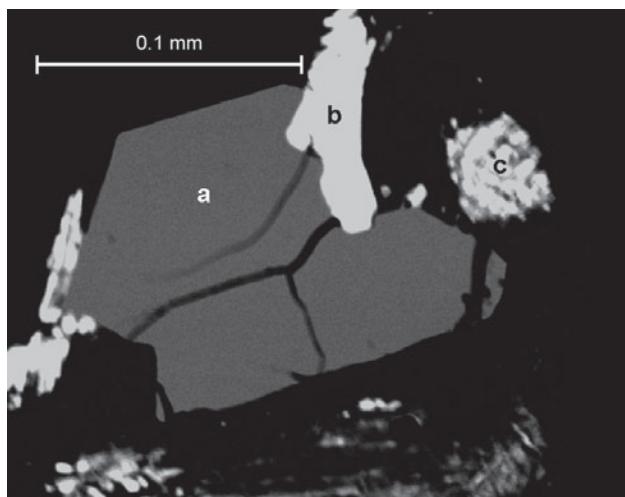
Fig. 11. Crystals of seinäjokite (a) associated with galena (b) and an exsolution aggregate of antimonian silver (c).

Galena

Galena, in association with both chalcothallite-mineral X and cuprostibite, has sometimes been partly replaced by a phase of the chalcosite group with the composition $Cu_{1.82}S$ (b, Fig. 9; Table 6-4). Very rarely this secondary phase is intergrown with an Fe-As-mineral (c, Fig. 9; Table 6-5). The simplified composition of this mineral may be written as $Fe_3(AsO_4)_2 \cdot H_2O$ with a minor Cu-content. It is possibly a member of the vivianite series. Galena intergrown with chalcothallite in another mineral association has been partly replaced by a chalcosite-like phase with the composition $Cu_{2.08}S$ that contains small amounts of Ag, Pb, Sb and Se (Table 6-6). Small amounts of Cu (0.69(30) wt.%) and Se (0.34(2)wt %) (average of 5 analyses, standard deviation in brackets) was recorded in the galena. The content of Sb is less than 0.04 wt.% and that of Ag is below the detection limit. Galena in two other mineral associations contained smaller amounts of these four elements.

Sphalerite

Sphalerite is the most common of the ore minerals. It lies isolated in gangue minerals but also occurs as intergrowths with other ore minerals. Small amounts of Cu (0.17(7)wt.%) and Fe (1.25(4) wt.%) (average of 5 analyses) were recorded.

Table 4. Microprobe analyses of decomposition products of chalcothallite/mineral X in Fig. 4.

	1	2
No. of analyses	2	2
Ag	0.04	0
Cu	51.25	17.95
Fe	7.44	30.51
Zn	0.33	0.87
Pb	0.33	2.54
Sb	0.76	1.6
Tl	0.01	0.35
S	4.27	1.53
Total	64.1	55.35
Molar ratios		
Ag	0.04	–
Cu	74.57	30.82
Fe	11.99	59.57
Zn	0.45	1.45
Pb	0.33	1.33
Sb	0.64	1.43
Tl	–	0.19
S	11.98	5.22

Average analytical values, wt%
–: not detected

Antimonian silver

Rare myrmekite-like aggregates of antimonian silver and an apparently 'decomposed' allargentum phase are associated with both cuprostibite and chalcothallite-mineral X (Fig. 10). The antimonian silver has 94.3 wt.% Ag, 4.2 wt.% Sb and 0.26 wt.% Cu ($\sim Ag_{0.954}Sb_{0.037}Cu_{0.004}$), whereas the composition of the intergrown 'decomposed phase' could not be determined due to its small grain size. The chemical composition, texture and optical properties in reflected light of these aggregates suggest that they represent a decomposed high-temperature antimonian silver phase. On cooling this phase dropped into the two-component phase region between antimonian silver and allargentum and thus decomposed into these two phases (see Ag-Sb phase diagram in Somanchi 1966). Alteration of the allargentum variety took place later. Antimonian silver, allargentum and dyscrasite associated with cuprostibite from Ilímaussaq have been described by Karup-Møller (1978a).

Seinäjokite

Euhedral crystals of seinäjokite ($FeSb_2$ with 0.49(4) wt.% Cu) are associated with chalcothallite and galena (Fig. 11). Seinäjokite is known from Ilímaussaq as disseminated grains in lujavrite-MC at Kvanefjeld (Karup-Møller 1978b).

Discussion

Higher homologues of the thalcusite series ($TlCu_{2N}S_{N+1}$) are expected to indicate sulphur fugacity in the ore-forming environment that is reduced in comparison to thalcusite-forming solutions. Formation of mineral X therefore parallels the crystallization of chalcothallite which is a complex sulphide-antimonide with a rare combination of anions, again made possible by low sulphur fugacity. Further indication of these conditions are cuprostibite, antimonian silver and seinäjokite.

The high content of Fe in mineral X is caused by cation-valency requirements, contrasted by the low Fe-contents of the associated chalcothallite, in which the valency requirements are different. The former also contrasts with low Fe-contents in the associated sphalerite, indicating that mineral X and bornite are the principal concentrators of Fe from the solutions generally poor in iron, which also produced the two major gangue minerals ussingite and analcime. Bornite, galena and sphalerite tolerate very varied sulphur

Table 5. Secondary Sb-Cu oxide/hydroxide phases after cuprostibite

	1		2		3		4	
No. of analyses	8		3		10		10	
Ag	0.11 (10)		0.01 (2)		0.06 (1)		–	
Cu	35.65 (549)		1.77 (35)		12.43 (30)		2.24 (17)	
Fe	0.14 (2)		0.08 (3)		0.03 (3)		0.54 (13)	
Zn	0.01 (2)		–		1.40 (11)		–	
Pb	0.31 (32)		–		0.09 (9)		15.28 (104)	
Sb	39.25 (430)		83.19 (70)		62.59 (92)		54.94 (83)	
Te	–		0.15 (16)		–		–	
S	–		0.08 (7)		0.18 (15)		–	
Total	75.47		85.28		76.78		73.00	
Molar ratios*								
Ag	0.12[a]	–	0.02[a]	–[b]	0.07[a]	–[c]	–[a]	–[d]
Cu	63.03	1.74	3.90	0.04	26.72	1.90	6.17	0.78
Fe	0.28	0.01	0.19	–	0.07	–	1.68	0.21
Zn	0.01	–	0.01	–	2.92	0.20	–	–
Pb	0.17	–	–	–	–	–	12.95	1.96
Sb	36.22	1.00	95.52	1.00	70.22	5.00	79.20	12.00
Te	0.02	–	0.36	–	–	–	–	–
S	0.15	–	–	–	–	–	–	–

Average analytical values, wt% (standard deviations in brackets). –: not detected.
*Molar ratios: [a] to sum of elements = 100; [b] to Sb = 1.00, [c] to Sb = 5.00, [d] to Sb = 12.00
Notes. 1 and 2: Dark- and light-grey replacement phases after cuprostibite (c and b, Fig. 5). 3: Relatively large mineral grain e, Fig. 6, in matrix of light grey replacement material after cuprostibite (b, Fig. 6). 4: Homogeneous replacement bodies in cuprostibite (b, Fig. 7).

fugacity regimes and do not contradict the above conclusions about low S-fugacity.

The various primary and secondary 'chalcosites' cover a broad compositional range from $Cu_{2.32}S$ to $Cu_{1.81}S$, and several of them contain small but significant amounts of Fe, Pb and Sb. Without X-ray diffraction data the true identification of these phases is not currently possible.

Acknowledgements

References

Berger, R. 1987: A phase-analytical study of the Tl-Cu-Se system. Journal of Solid State Chemistry 70, 65–70.

Berger, R. & Ericksson, L. 1990: Crystal structure refinement of monoclinic $TlCu_6Se_4$. Journal of Less-Common Metals 161, 165–173.

Berger, R. & Sobott, R.J. 1987: Characterization of $TlCu_7S_4$, a crookesite analogue. Monatsheft Chemische Wissenschaft 118, 967–972.

Berger, R., Ericksson, L. & Meerschaut, A. 1990: The crystal structure of $TlCu_5Se_3$. Journal of Solid State Chemistry 87, 283–288.

Dobrovol'skaya, M.G.& Nekrasov, I.Ya. 1994: The sulfides of alkali metals and their phase relations in K-Fe-Cu-S system. Abstracts of the 16th international General Meeting of the International Mineralogical Association, Pisa, Italy, 99.

Dobrovol'skaya, M.G., Malov, V.S., Rogova, V.P. & Vyal'sov, L.N. 1984: New find of potassium-bearing thalcusite in charoitic rocks of the Murunskiy pluton. Doklady Earth Science Section 267, 171–174.

Johan, Z. and Kvaček, M. 1971: La bukovite $Cu_{3+x}TlFeSe_{3-x}$, une nouvelle espèce minérale. Bulletin Societé France Mineralogie 94, 529–533.

Karup-Møller, S. 1978a: Primary and secondary ore minerals associated with cuprostibite. Bulletin Grønlands Geologiske Undersøgelse 126, 23–47.

Table 6. Primary and secondary Cu-Fe-S phases

	1	2	3	4	5	6
No. of analyses	7	5	7	11	6	5
Ag	0.10 (10)	0.15 (11)	0.27 (16)	0.36 (32)	0.08 (9)	0.24 (13)
Cu	77.90 (202)	62.13 (131)	81.45 (75)	71.40 (145)	1.36 (37)	76.92 (34)
Fe	1.91 (109)	13.15 (74)	0.02 (3)	–	28.83 (57)	–
Pb	–	–	1.09 (37)	4.94 (120)	0.07 (9)	2.22 (36)
Sb	0.52 (30)	0.19 (21)	1.37 (20)	3.27 (45)	0.79 (33)	3.42 (29)
As	–	–	–	–	27.40 (35)	0.43 (6)
Se	–	–	0.30 (6)	0.73 (6)	0.29 (5)	0.43 (6)
S	21.74 (21)	25.58 (43)	17.82 (32)	19.84 (52)	0.50 (24)	18.63 (21)
Total	102.24	101.24	102.32	100.54	59.32	101.86
Molar ratios*						
Ag	0.05[a]	0.07[a]	–[a]	0.19[a] 0.01[b]	–[a]	0.12[a]
Cu	63.06 1.81[b]	48.62 1.22[b]	68.99 2.31[b]	62.22 1.81	0.12	65.86 2.08[b]
Fe	1.75 0.05	11.68 0.29	–	–	2.82	–
Pb	–	–	0.28 0.01	1.32 0.04	–	0.58 0.02
Sb	0.22	0.08	0.60 0.02	1.49 0.04	0.04	1.53 0.05
As	–	–	–	–	2	–
Se	0.05	–	0.21 0.01	0.51 0.01	0.02	0.30 0.01
S	34.87 1.00	39.55 1.00	29.92 1.00	34.26 1.00	0.09	31.61 1.00

Average analytical values, wt% (standard deviations in brackets). –: not detected.
* Molar ratios: [a] to sum of elements = 100.0; [b] to S = 1.00
Notes. 1: Chalcosite group phase (c, grey, Fig. 8) partly replacing 2; 2: Bornite (b, dark grey, Fig. 8); 3: Primary Cu-S phase interstitial to chalcothallite; 4: Secondary chalcosite group phase; 5: As-rich mineral of the vivianite group of minerals partly replacing galena (b, c and a respectively in Fig. 9); 6: Secondary chalcosite group phase partly replacing galena enclosed in chalcothallite.

Karup-Møller, S. 1978b: The ore minerals of the Ilímaussaq intrusion: their mode of occurrence and their conditions of formation. Bulletin Grønlands Geologiske Undersøgelse 127, 51 pp.

Karup-Møller, S. & Makovicky, E. 2001: Thalcusite from Nakkaalaaq, the Illímuassaq alkaline complex, South Greenland. Geology of Greenland Survey Bulletin 190, 127–130.

Klepp, K.O., Boller, H. & Völlenkle, H. 1980: Neue Verbindungen mit KCu_4S_3 Struktur. Monatshefte für Chemie 111, 727–733.

Kovalenker, V.A., Laputina, I.P. Yevstigneyeva, T.L. & Izoitko, V.M. 1976: Thalcusite $Cu_{3-x}Tl_2Fe_{1-x}S_4$; a new sulfide of thallium from copper-nickel ores of the Talnakh Deposit. Zapiski Vsesoyuznogo Mineralogicheskogo Obshchestva 105(2), 202–206 (in Russian).

Kovalenker, V.A. Laputina, I.P., Semenov, E.I. & Yevstigneyeva, T.L. 1978: Potassium-bearing thalcusite from the Ilímaussaq pluton and new data on chalcothallite. Doklady Akademii Nauk SSSR 239, 1203–1206 (in Russian). (Translation: Doklady Earth Science Sections 239, 159–162).

Makovicky, E. 2005: Micro and mesoporous sulfide and selenide structures. Reviews in Mineralogy and Geochemistry 57, 403–434.

Makovicky, E. 2008: Crystal structures of sulfides and other chalcogenides. Reviews in Mineralogy and Geochemistry 61, 7–125.

Makovicky, E., Johan, Z. & Karup-Møller, S. 1980: New data on bukovite, thalcusite, chalcothallite and rohaite. Neues Jahrbuch für Mineralogie Abhandlungen 138, 122–146.

Mandarino, J.A. & Anderson, V. 1989: Monteregian Treasures, the Minerals of Mont Saint–Hilaire, Quebec 281 pp. Cambridge: Cambridge University Press.

Mookherjee, A., Mozgova, N.N., Golovanova, T.I. & Mishra, B. 1984: Rare minerals from Rajapura-Dariba, Rajasthan, India VI: Thalcusite, its geochemical significance. Neues Jahrbuch für Mineralogie Monatshefte 10, 444–454.

Schils, H. & Bronger, W. 1979: Ternäre Selenide des Kupfers. Zeitschrift Anorganishe Allgemeine Chemie 456, 187–193.

Semenov, E.I, Sørensen, H., Bessmertnaja, M.S. & Novorossova, L.E. 1967: Chalcothallite – a new sulphide of copper and thallium from the Ilímaussaq alkaline intrusion, South Greenland. Bulletin Grønlands Geologiske Undersøgelse 68, 13–26 (also Meddelelser om Grønland 181(5)).

Somanchi, S. 1966: Subsolidus phase relations in the system Ag–Sb. Canadian Journal of Earth Sciences 3, 211–272.

On the osteology and phylogenetic affinities of *Morsoravis sedilis* (Aves) from the early Eocene Fur Formation of Denmark

GERALD MAYR

Morsoravis sedilis is a small bird from the early Eocene Fur Formation of Denmark, which in the original description was considered to be most closely related to Charadriiformes. Because *Morsoravis* has subsequently been likened to *Pumiliornis tesselatus*, an equally enigmatic bird from the middle Eocene of Messel in Germany, I perform here the first phylogenetic analysis including the two taxa. This analysis supports a sister group relationship between *Morsoravis* and *Pumiliornis*, and the clade including the two taxa is recovered as the sister taxon of the late Eocene/early Oligocene *Eocuculus*. I report a possible, albeit lost, second specimen of *Morsoravis*, and identify derived characters in support of a sister group relationship between *Morsoravis* and *Pumiliornis*. The analysis did not resolve the higher-level affinities of the clade including *Morsoravis*, *Pumiliornis*, and *Eocuculus*, and did not confirm charadriiform affinities of *Morsoravis*. More data on the osteology of the fossils, as well as an improved understanding of the interrelationships of extant birds, are needed for a well-established phylogenetic assignment of these fossil taxa.

Gerald Mayr [Gerald.Mayr@senckenberg.de], Forschungsinstitut Senckenberg, Sektion Ornithologie, Senckenberganlage 25, 60325 Frankfurt am Main, Germany.

Morsoravis sedilis Bertelli *et al.,* 2010 is a small bird from the early Eocene Fur Formation of the island of Mors in Denmark (Fig. 1), which is based on an exceptionally well-preserved partial skeleton lacking both wings and the pectoral girdle (Fig. 2A). This fossil was studied by Kristoffersen (2002) and Lindow (2007) in unpublished PhD theses and formally described by Bertelli *et al.* (2010). These authors considered *M. sedilis* to be most closely related to charadriiform birds, and the species also resulted as sister taxon of Charadriiformes in a phylogenetic analysis performed by Bertelli *et al.* (2010). This placement received, however, only weak support, and *Morsoravis* differs distinctly from charadriiform birds in features of the hind limb, whose osteology indicates perching capabilities and an arboreal way of living (Kristoffersen 2002; Lindow 2007; Bertelli *et al.* 2010). If it was indeed on the stem lineage of Charadriiformes, it would indicate an unexpected ecomorphological diversity of these birds.

Mayr (2009) questioned charadriiform affinities of *Morsoravis* and assumed that it is most closely related to *Pumiliornis tesselatus* from the middle Eocene of

Fig. 1. Map of Central Europe showing the localities mentioned in the text.

Messel in Germany (Fig. 2 B, C). This species is known from two partial skeletons and was compared with "gruiform", charadriiform, and "ciconiiform" birds in the original description (Mayr 1999). In a later study (Mayr 2008), it was hypothesized that *Pumiliornis* is more closely related to the equally enigmatic taxon *Eocuculus*, which is represented by postcranial skeletons from the late Eocene of North America and the early Oligocene of Céreste in France (Chandler 1999; Mayr 2006, 2008).

Here I perform the first phylogenetic analysis including *Morsoravis*, *Pumiliornis*, and *Eocuculus*. I further comment on some osteological features of *Morsoravis* and discuss new character evidence for close affinities between this taxon and *Pumiliornis*.

Material and methods

Osteological terminology follows Baumel & Witmer (1993). Phylogenetic analyses were conducted with the
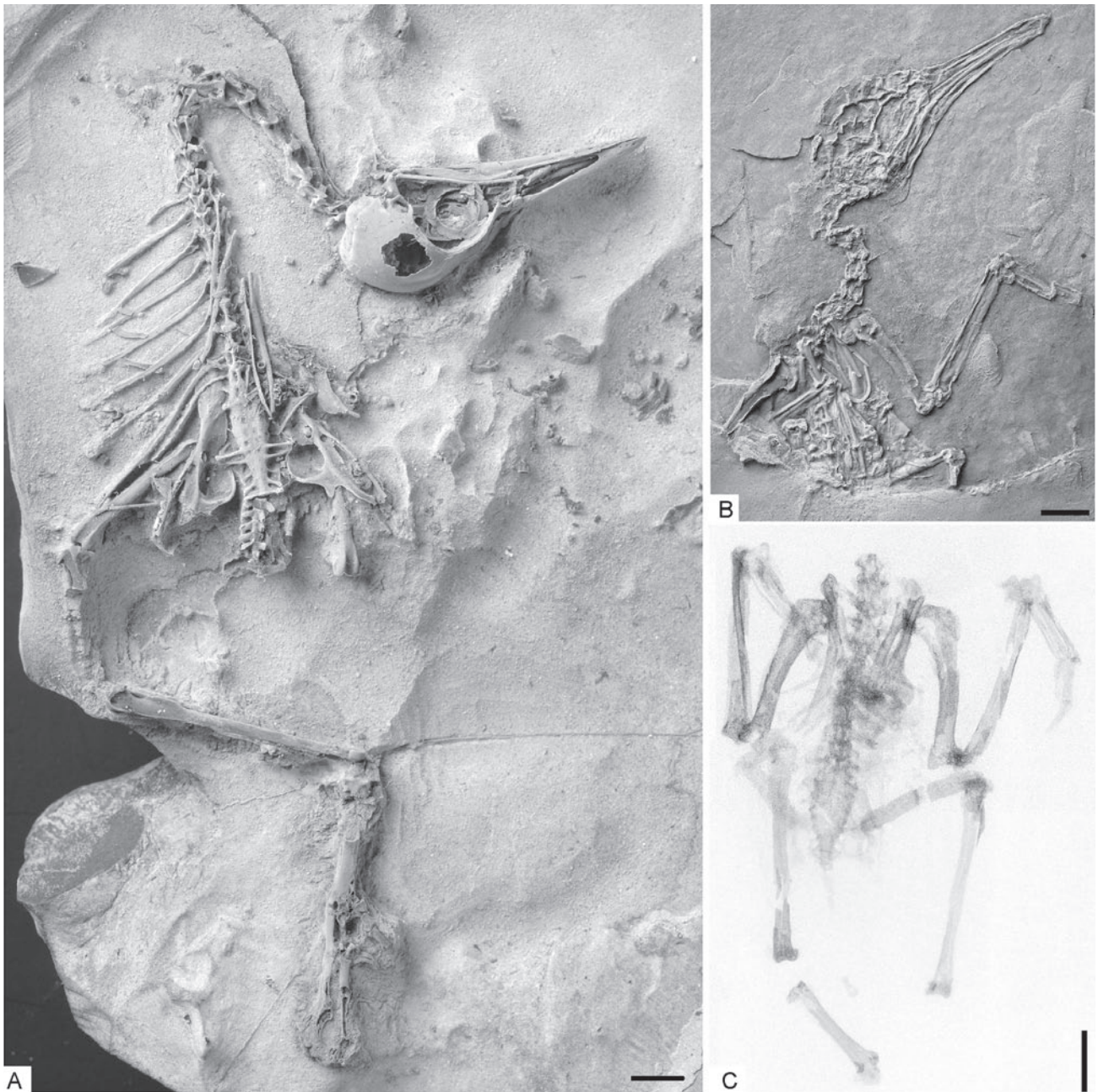
Fig. 2. **A**, *Morsoravis sedilis* from the early Eocene of Denmark (holotype, MGUH 28930); note that the fragile specimen has been damaged after Bertelli *et al.*'s (2010) description, so that the skull roof and most of the right tibiotarsus are now broken. **B**, *Pumiliornis tessellatus* from the middle Eocene of Germany (holotype, SMF-ME 2092A). **C**, *Pumiliornis tessellatus*, x-ray photograph of specimen SMF-ME 2475A+B. The specimens in A and B were coated with ammonium chloride. Scale bars equal 5 mm.

heuristic search modus of NONA 2.0 (Goloboff 1993) through the WINCLADA 1.00.08 interface (Nixon 2002), using the commands hold 10000, hold/10, mult*1000, and max*. The character matrix (see Appendices) is based on the data set of Mayr & Clarke (2003), which was also used in the analysis of Bertelli *et al.* (2010). Five additional characters and coding modifications are incorporated (Appendix 1). The emended matrix comprised 47 ingroup taxa and 153 characters. Following Mayr & Clarke (2003), three characters (55, 71, 91) were coded as ordered. In addition to the fossil taxa *Morsoravis*, *Pumiliornis*, and *Eocuculus*, I also added extant Mesitornithidae (*Monias benschi*) to the analysis as mesites exhibit schizorhinal nostrils and also resemble *Morsoravis* in other osteological features. The Mesozoic non-neornithine taxa *Apsaravis*, *Hesperornis*, and *Ichthyornis* were used as outgroups. Consistency index (CI) and retention index (RI) were calculated, as well as bootstrap support values with 1000 replicates, three searches holding one tree per replicate, and TBR branch swapping without max*.
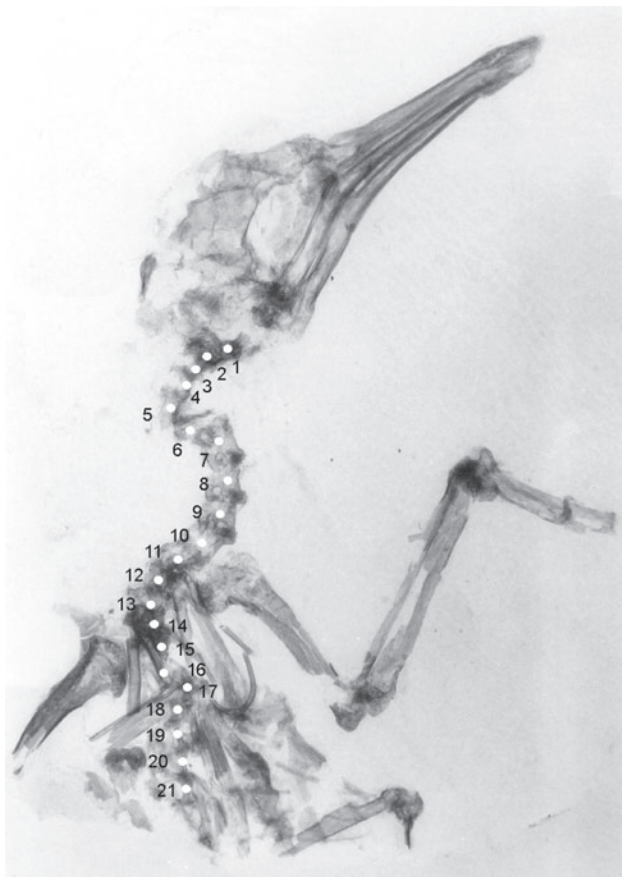
Fig. 3. *Pumiliornis tessellatus* Mayr, 1999 from the middle Eocene of Germany (holotype, SMF-ME 2092A), x-ray photograph. The white dots indicate the position of the presacral vertebrae. Vertebrae 14–16 can not be directly observed and their positions were estimated from the average distance between the vertebral bodies.

For *Eocuculus* I scored only data obtained from the two reliably identified skeletons (Chandler 1999; Mayr 2006), but not from the tentatively referred wings described by Mayr (2008).

Institutional abbreviations: MGUH - Geological Museum of the University of Copenhagen, Denmark; MNHN - Muséum National d'Histoire Naturelle, Paris, France; SMF - Forschungsinstitut Senckenberg, Frankfurt am Main, Germany.

Comparison between *Morsoravis*, *Pumiliornis*, and *Eocuculus*

Morsoravis sedilis is about 1.3 times larger than *Pumiliornis tessellatus*, but as far as comparisons are possible, the two species exhibit a very similar osteology. Detailed comparisons between *Pumiliornis* and *Eocuculus* were already made by Mayr (2008), so that I here focus on comparisons between these two taxa and *Morsoravis*.

The only known skull of *Pumiliornis* is badly crushed and does not allow the recognition of osteological details, but accounting for the bad preservation it corresponds well with the skull of *Morsoravis* in overall proportions (Fig. 2). Bertelli *et al.* (2010) noted that the nostrils of *Morsoravis* are schizorhinal, and schizorhinal nostrils were also reported for *Pumiliornis* (Mayr 2008).

Morsoravis has a high number of 21 presacral vertebrae (the cranial portion of the synsacrum was erroneously marked as 22nd vertebra in Bertelli *et al.* 2010: text-fig. 8). In previous descriptions of *Pumiliornis* (Mayr 1999, 2008), the vertebral count was not given. The number of presacral vertebrae can, however, be ascertained on the x-ray photograph of the holotype, which substantiates the presence of 21 presacral vertebrae in *P. tessellatus* (Fig. 3).

Bertelli *et al.* (2010) stated that the thoracic vertebrae of *Morsoravis* lack the heterocoelous condition (based on the morphology of vertebra 15 and the contact between the thoracic vertebrae). However, after a re-evaluation of the holotype I note that they actually are heterocoelous, as the ventral sections of the rims of the corpora vertebrarum are curved and do not form straight lines as in opisthocoelous birds (Fig. 4). The thoracic vertebrae of *Morsoravis* further are pleurocoelous, i.e., with deep lateral depressions, as are those of *Pumiliornis* and *Eocuculus* (Fig. 4; Mayr 2008).

The pelvis of the *Pumiliornis* specimens is poorly preserved, but the *Eocuculus* pelvis matches well with that of *Morsoravis* in overall proportions (Fig. 5).

The tibiotarsus of *Morsoravis* differs from that of *Pumiliornis* in that it exhibits an ossified pons supratendineus, which is absent in *Pumiliornis* (Mayr 2008). Unlike *Pumiliornis*, there is further an ossified retinacu-

lum musculi fibularis (Fig. 6C). Otherwise, however, the bones show a close resemblance. Most notably, the tibiotarsus of *Morsoravis* also exhibits a marked crest along the medial surface of its proximal end, which was described by Mayr (2008) for *Pumiliornis* (Fig. 6). This feature has not been mentioned for *Morsoravis* by previous authors and is here reported for the first time. The known specimens of *Eocuculus* do not allow recognition of this crest, but the distal end of the tibiotarsus of *Eocuculus* resembles that of *Morsoravis* (compare Figs. 6C and 7C).

The tarsometatarsus of *Morsoravis* corresponds with that of *Pumiliornis* in overall proportions, but close comparisons are hindered by the fact that the bone is damaged or poorly preserved in all fossils. Both taxa agree in that the foramina vascularia proximalia are widely separated, the shaft is dorsoplantarly flattened, and exhibits an intermuscular line along the lateral portion of its dorsal surface. As detailed by Mayr (2008), the wide proximal phalanx of the fourth toe, together with the plantarly deflected tarsometatarsal trochlea for this toe, suggest the presence of semizygodactyl feet in *Pumiliornis* (i.e., the fourth toe was spread laterally but not completely reversed as in fully zygodactyl birds). Owing to the preservation of the holotype, presence of this condition can not be established for *Morsoravis*, but seems likely because of the very wide proximal phalanx of the fourth toe.

The orientation of the slightly laterally spread fourth toe of the *Morsoravis* holotype, which exhibits its dorsomedial rather than dorsal surface, is also indicative of semizygodactyl feet. The trochlea metatarsi II of *Morsoravis* has a characteristic morphology in that its medial surface bears a marked groove and is bilobed (Fig. 7D). This condition is very unlike that of Charadriiformes and most other birds but resembles that found in Coliiformes, especially the Eocene Sandcoleidae (Fig. 7E). The trochlea metatarsi II is not well enough preserved in *Pumiliornis* to safely establish presence or absence of this trait; in *Eocuculus* it is absent. The trochlea metatarsi III appears proportionally larger in *Pumiliornis*, but as this trochlea is damaged in the *Morsoravis* holotype, close comparisons are not possible. As noted by Bertelli *et al.* (2010), the incisura intertrochlearis medialis of *Morsoravis* is wider than in *Pumiliornis*, but this impression may be caused by the fact that the damaged trochlea metatarsi III lacks its dorsal portion.

Morsoravis and *Pumiliornis* show a close resemblance in the proportions and morphology of the pedal phalanges. *Pumiliornis* is characterized by a very wide proximal phalanx of the fourth toe (Mayr 2008), which is also present in *Morsoravis* (Fig. 7).

Elements of the wing and pectoral girdle are not preserved in the *Morsoravis sedilis* holotype. However, Kristoffersen (2002: pl. 11) assigned a partial postcrani-
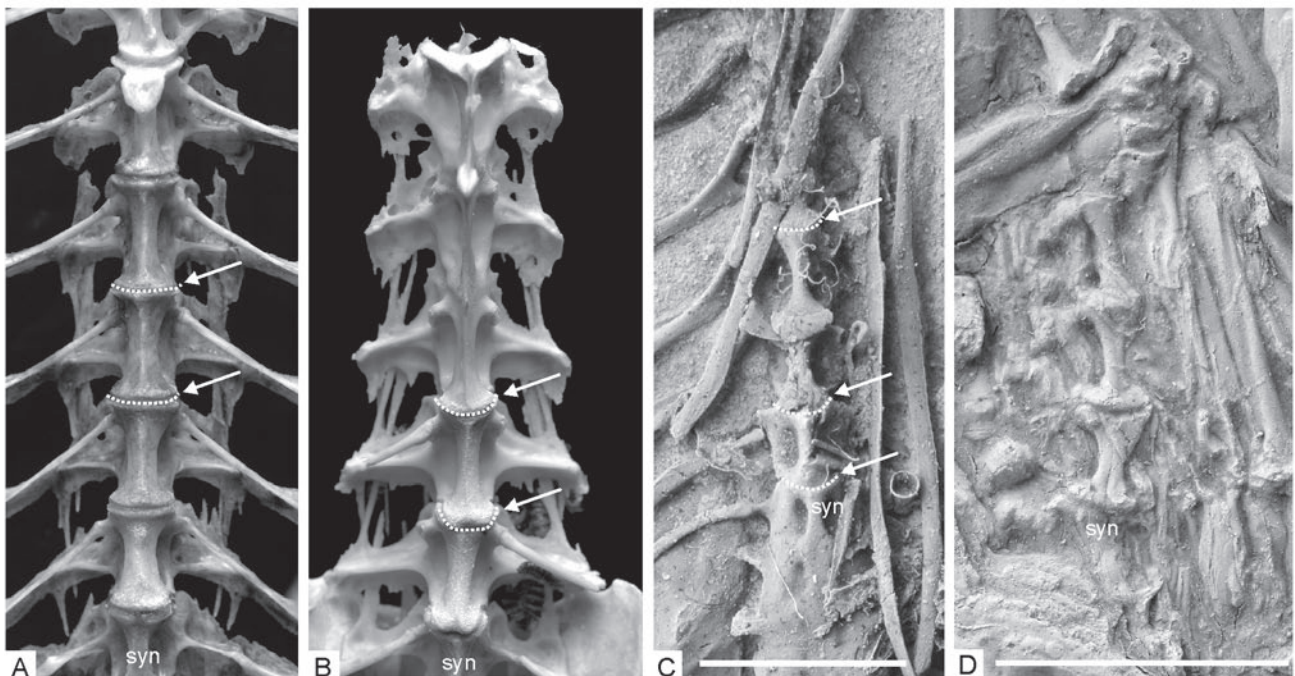
Fig. 4. Caudalmost thoracic vertebrae (ventral views) for comparison. **A**, opisthocoelous vertebrae of *Larosterna inca* (Charadriiformes, Sternidae). **B**, heterocoelous vertebrae of *Scolopax rusticola* (Charadriiformes, Scolopacidae). **C**, *Morsoravis sedilis* (holotype, MGUH 28930). **D**, *Pumiliornis tessellatus* (holotype, SMF-ME 2092A). Dotted lines (arrows) indicate the curvature of the rims of the corpora vertebrarum. Note the presence of pleurocoelous vertebrae in all four species. Abbreviation: syn – synsacrum. The fossil specimens were coated with ammonium chloride. Scale bars equal 5 mm; the pictures of the two extant taxa are not to scale.

al skeleton from the Fur Formation to the Zygodactylidae ("Primoscenidae"), which actually matches well with the osteology of *Morsoravis*. Unfortunately, this specimen (Fig. 5A, B), which has the collection number MGUH VP 1289 and which was also figured by Bonde *et al.* (2008: 113), seems to be lost now (S. L. Jakobsen, pers. comm.). With femur and tibiotarsus lengths of ~13.9 and ~23.5 mm respectively (Kristoffersen 2002), it corresponds well with the *M. sedilis* holotype in size, in which these bones measure 14.8/15.2 and 25.6 mm

Fig. 5. **A**, partial postcranial skeleton from the Fur Formation (MGUH VP 1289), which may belong to *Morsoravis sedilis* (see text; the specimen is now lost, photo by S. L. Jakobsen). **B**, detail of the sternum of MGUH VP 1289 for comparison to that in C. **C,** *Eocuculus* cf. *cherpinae* from the early Oligocene of France (SMF Av 425). **D**, pelvis (ventral view) of *M. sedilis* (holotype, MGUH 28930). **E**, *E.* cf. *cherpinae* from the early Oligocene of France (SMF Av 425). The specimens in A, B, and D were coated with ammonium chloride. Scale bars equal 5 mm.

(Bertelli *et al.* 2010). As in *Morsoravis* the synsacrum bears two pairs of marked fossae on the ventral surface of its cranial end, and the thoracic vertebrae are pleurocoelous (Fig. 5A). According to Kristoffersen (2002), MGUH VP 1289 exhibits a small processus intermetacarpalis on the carpometacarpus, which was, however, only visible before acid preparation of the fossil, after which the carpometacarpus was hidden by the sternum. The short and broad sternum bears two pairs of deep incisions in its caudal margin and is very different from the sternum of charadriiform birds, but corresponds well with that of *Eocuculus* (Fig. 5).
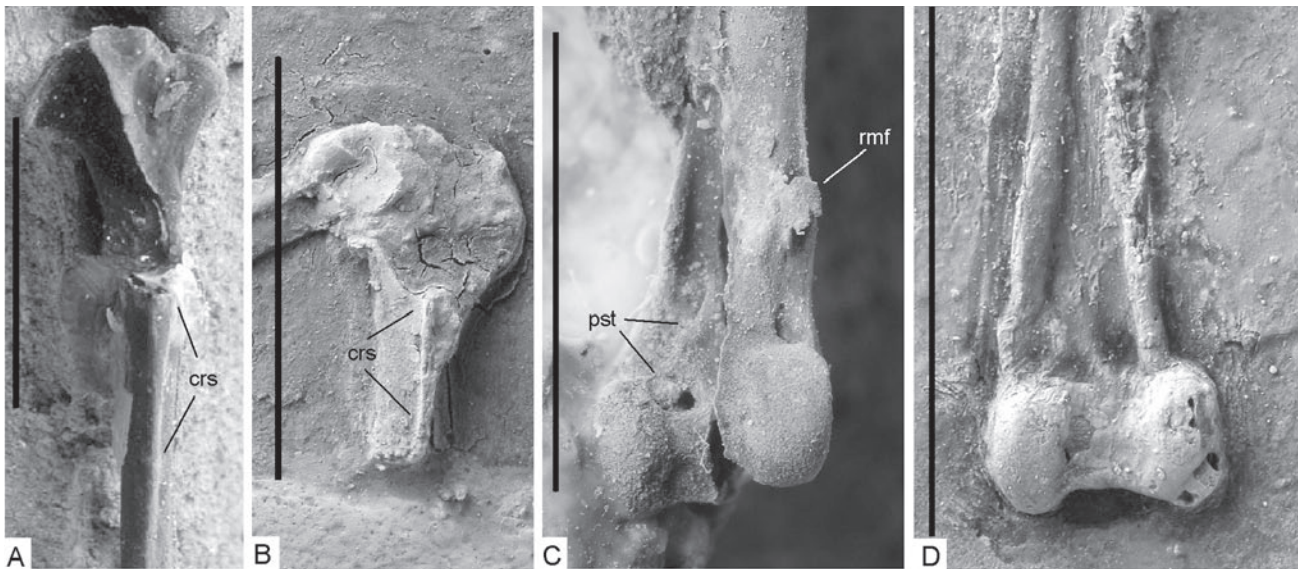
Fig. 6. Tibiotarsus of *Morsoravis sedilis* and *Pumiliornis tessellatus* for comparison. **A**, *M. sedilis* (holotype, MGUH 28930), proximal end of right tibiotarsus in medial view. **B**, *P. tessellatus* (holotype, SMF-ME 2092A), proximal end of left tibiotarsus in medial view. **C**, *M. sedilis* (MGUH 28930), distal end of left tibiotarsus in cranial view. **D**, *P. tessellatus* (SMF-ME 2475B), distal end of right tibiotarsus in cranial view. Abbreviations: crs – crest along medial side of proximal tibiotarsus; pst – pons supratendineus; rmf – ossified retinaculum musculi fibularis. All specimens were coated with ammonium chloride. Scale bars equal 5 mm.
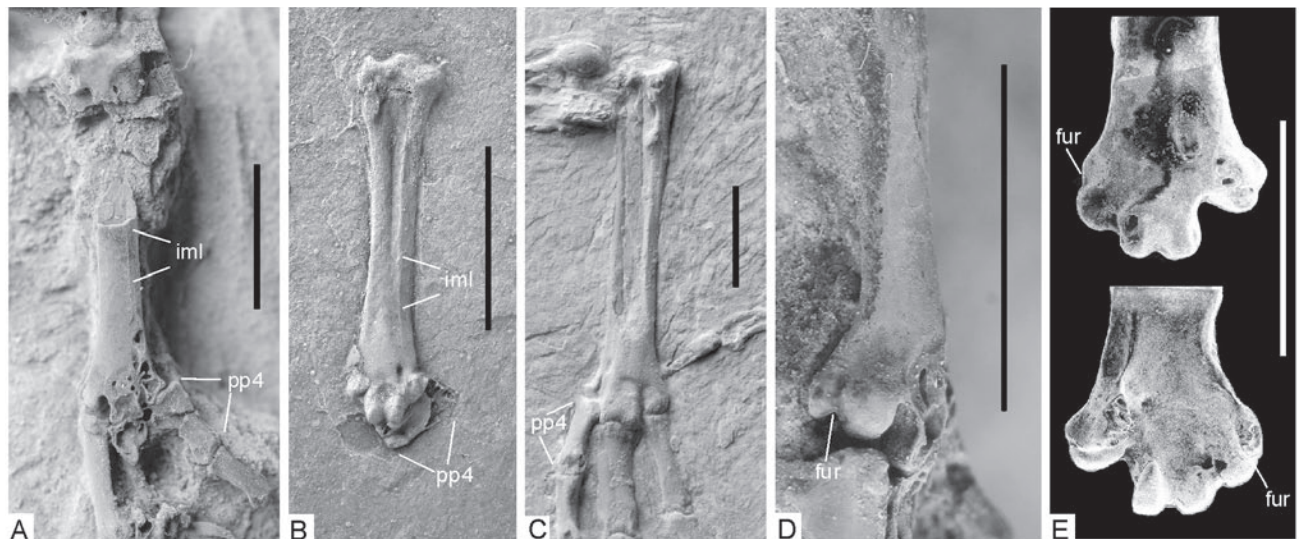
Fig. 7. Tarsometatarsus for comparison. **A**, *Morsoravis sedilis* (holotype, MGUH 28930), left tarsometatarsus in dorsal view. **B**, *Pumiliornis tessellatus* (SMF-ME 2475B), left tarsometatarsus in dorsal view. **C**, *Eocuculus* cf. *cherpinae* (SMF Av 425), right tarsometatarsus in dorsal view. **D**, *Morsoravis sedilis* (holotype, MGUH 28930), distal end of left tarsometatarsus in medial view. **E**. undetermined species of the coliiform Sandcoleidae from the early Eocene of France (MNHN CB-17347; from Mayr & Mourer-Chauviré 2004), distal end of left tarsometatarsus in dorsal (above) and plantar (below) view. Abbreviations: fur – furrow on medial surface of trochlea metatarsi II, iml – intermuscular line, pp4 – proximal phalanx of fourth toe. The specimens in A–D were coated with ammonium chloride; E is a SEM picture. Scale bars equal 5 mm.

Results of phylogenetic analysis

Analysis of the character matrix resulted in eight most parsimonious trees (Length = 769, CI = 0.21, RI = 0.47), the strict consensus tree of which is shown in Figure 8. The analysis supports a clade including *Morsoravis*, *Pumiliornis*, and *Eocuculus*, which, however, received only a low bootstrap support of 59%. The following characters were optimized as apomorphies of this clade (numbers refer to the character list): (6) nostrils schizorhinal; (58) caudalmost presacral vertebrae with deep lateral excavations; (74) processus uncinati not fused to ribs; (82) ulna distinctly exceeding humerus in length; (151) tibiotarsus with crest along medial side of proximal end, opposite crista fibularis; (152) tarsometatarsus, foramina vascularia proximalia widely separated; (153) proximal phalanx of fourth toe short and very wide.

Concerning the extant taxa, some clades obtained in the present and Bertelli *et al.*'s (2010) analysis are not in agreement with well-supported clades based on molecular data, which, for example, recover sister group relationship between Phoenicopteridae and Podicipedidae (Ericson *et al.* 2006; Hackett *et al.* 2008; Mayr 2011b). In the present analysis, Podicipedidae were shown to be the sister taxon of Gaviidae, but grouping of these foot propelled diving birds is an artefact of the data set, which includes many characters pertaining to hind limb myology (see discussion in Mayr & Clarke 2003). Likewise, sister group relationship between Steatornithidae and Trogonidae is not supported by all current molecular analyses (Ericson *et al.* 2006; Hackett *et al.* 2008).

Discussion

The analysis supports a close relationship between *Morsoravis* and *Pumiliornis*, and also suggests that these early/middle Eocene taxa form a clade together with the late Eocene/early Oligocene *Eocuculus*. *Morsoravis* and *Pumiliornis* are distinguished from all other avian taxa by the unique combination of the following features: (1) beak with schizorhinal nostrils; (2) presence of 21 presacral vertebrae; (3) the thoracic vertebrae are pleurocoelous, i.e., with deep lateral excavations; (4) tibiotarsus with crest along medial side of proximal end; and (5) the proximal phalanx of fourth toe is short and very wide. The clade including *Morsoravis*, *Pumiliornis*, and *Eocuculus* received, however, only low bootstrap support and three of the above features (1, 2, 4) are unknown for *Eocuculus*.
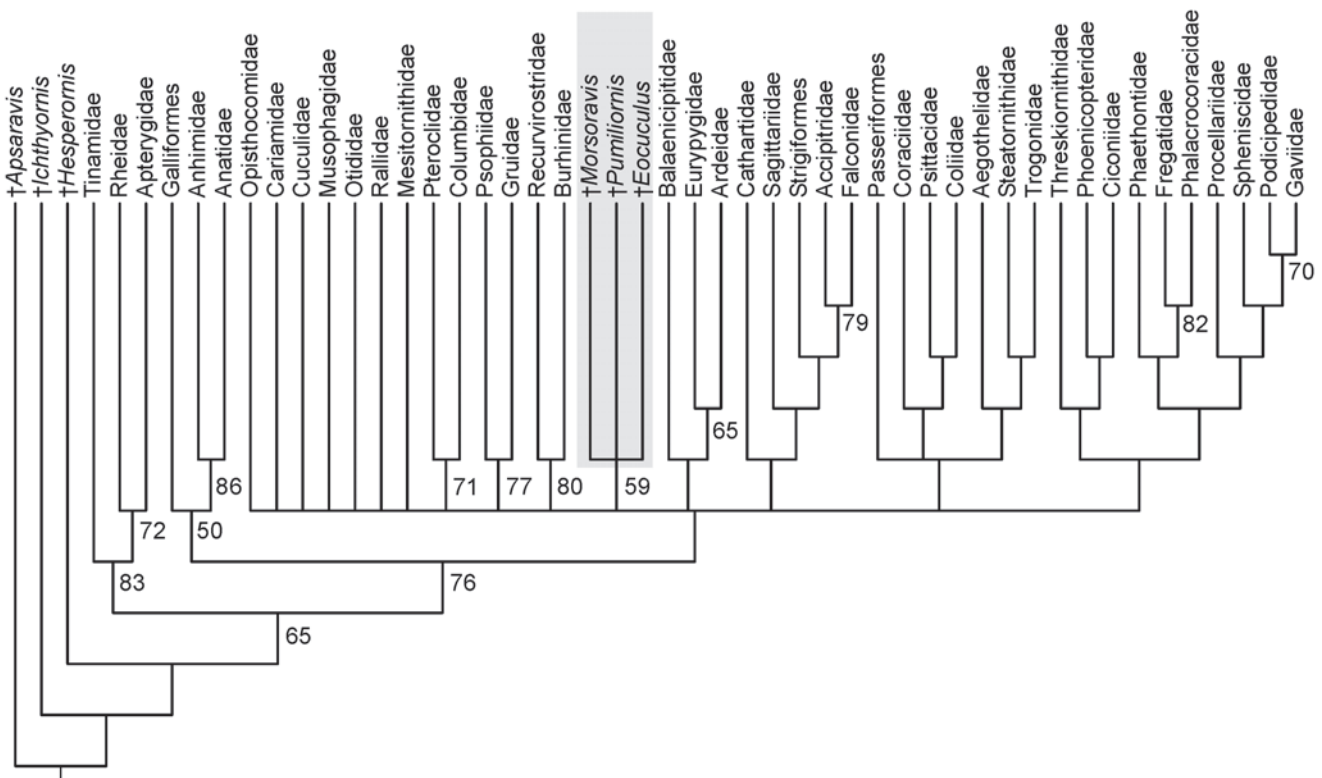
Fig. 8. Strict consensus tree of eight most parsimonious trees (Length = 769, CI = 0.21, RI = 0.47) resulting from analysis of the character matrix in Appendix 2. Unsupported nodes are collapsed, bootstrap support values are indicated next to the nodes. The clade including *Morsoravis*, *Pumiliornis*, and *Eocuculus* is highlighted in gray.

Three characters were optimized as apomorphies of a clade including *Morsoravis* and Charadriiformes in the analysis of Bertelli *et al.* (2010), that is, the presence of (1) opisthocoelous and (2) pleurocoelous thoracic vertebrae, as well as (3) the absence of a foramen in the caudoventral portion of the pygostyle. None of these features is restricted to Charadriiformes, and the last occurs in many unrelated taxa (e.g., Mayr & Clarke 2003). Based on a re-evaluation of the *Morsoravis* holotype I am confident that the thoracic vertebrae of this taxon actually are heterocoelous (see above; Fig. 4). Moreover, opisthocoelous vertebrae evolved independently within Charadrii and Lari and were probably absent in the stem species of Charadriiformes (Mayr 2011a). Pleurocoelous vertebrae belong to the stem species pattern of charadriiform birds (Mayr 2011a) and have a restricted distribution among extant birds (e.g., Mayr & Clarke 2003). They are, however, present in *Ichthyornis*, a stem lineage representative of Neornithes (Clarke 2004) and the palaeognathous Lithornithidae (Leonard *et al.* 2005), and were also reported in a number of fossil taxa whose closest extant relatives lack depressions on the vertebral bodies, such as stem group Galliformes (Dyke & Gulas 2002), Piciformes (Mayr & Knopf 2005), and the putatively psittaciform Halcyornithidae ("Pseudasturidae") (Mayr 2002: fig. 2D).

Kristoffersen (2002) and Lindow (2007) further listed the presence of schizorhinal nostrils as evidence for charadriiform affinities of *Morsoravis*. However, although schizorhinal nostrils probably do belong to the stem species pattern of Charadriiformes (Mayr 2011a), they occur in many other unrelated taxa, such as Threskiornithidae, Mesitornithidae, Columbidae, Gruidae, Trochilidae, and Furnariidae. The same is true for the dorsally curved retroarticular processes of the mandible, which, albeit present in many Charadriiformes, are also found in Galliformes, Threskiornithidae, Mesitornithidae, Rallidae, and some Gruidae (*Balearica*) and Picidae (*Jynx*).

The present analysis does not resolve the higher-level affinities of the clade including *Morsoravis*, *Pumiliornis*, and *Eocuculus*, but charadriiform affinities of *Morsoravis* are not supported by the morphology of the fossil. *Morsoravis* has an unusually low number of only 12 scleral plates (Bertelli *et al.* 2010). Most birds, including Palaeognathae and Galloanseres, exhibit a scleral ring with a modal number of 14 or 15 plates, which is likely to be the plesiomorphic condition for Neoaves. In Charadriiformes, the modal number of scleral plates is variable, and whereas 12 or 13 are present in some taxa (Turnicidae, Rostratulidae, Jacanidae, Alcidae), the majority has 15 (Livezey & Zusi 2006). Among extant birds a modal number of 12 plates is otherwise present in Cuculidae, Opisthocomidae, Trochilidae,

Coliiformes, and Psittaciformes, whereas Suloidea and Columbiformes have only 11 plates (Lemmrich 1931; Livezey & Zusi 2006).

Morsoravis and *Pumiliornis* further share with coliiform and psittaciform birds a crest on the medial surface of the proximal tibiotarsus; as noted above, the peculiar bilobed trochlea metatarsi II of the tarsometatarsus of *Morsoravis* resembles that of the Eocene Sandcoleidae, which are stem group representatives of Coliiformes (Fig. 4). *Morsoravis* and *Pumiliornis* are, however, distinguished from all "higher land bird" taxa by a high number of 21 presacral vertebrae, which may represent a plesiomorphic feature, because 20 or more presacral vertebrae are present in Mesozoic birds outside Neornithes as well as in palaeognathous birds and Galloanseres (by contrast, "higher land bird" taxa invariably have 19 or fewer presacral vertebrae). I thus note that, although recognition of close affinities between *Morsoravis* and *Pumiliornis* sets into a phylogenetic context two enigmatic avian taxa with a distinctive morphology, more data on the osteology of the fossils as well as an improved understanding of the interrelationships of extant birds are needed for a well-established phylogenetic assignment of these fossil taxa.

Acknowledgements

References

Baumel, J.J. & Witmer, L.M. 1993: Osteologia. In: Baumel, J.J., King, A.S., Breazile, J.E., Evans, H.E. & Vanden Berge, J.C. (eds), Handbook of Avian Anatomy: Nomina Anatomica Avium. Publications of the Nuttall Ornithological Club 23, 45–132.

Bertelli, S., Lindow, B.E.K., Dyke, G.J. & Chiappe, L.M. 2010: A well-preserved 'charadriiform-like' fossil bird from the Early Eocene Fur Formation of Denmark. Palaeontology 53, 507–531.

Bonde, N., Andersen, S., Hald, N. & Jakobsen, S.L. 2008: Danekræ - Danmarks bedste fossiler. Gyldendal, Copenhagen, 224 pp.

Chandler, R.M. 1999: Fossil birds of Florissant, Colorado: with a description of a new genus and species of cuckoo. In: Santucci, V.L. and McClelland, L. (eds): National Park Service Paleontological Research, Volume 4. Geologic Resources Division Technical Report NPS/NRGRD/GRDTR-99, 49–53.

Clarke, J.A. 2004: Morphology, phylogenetic taxonomy, and systematics of Ichthyornis and Apatornis (Avialae: Ornithurae). Bulletin of the American Museum of Natural History 286, 1–179.

Dyke, G.J. & Gulas, B.E. 2002: The fossil galliform bird Paraortygoides from the Lower Eocene of the United Kingdom. American Museum Novitates 3360, 1–14.

Ericson, P.G.P., Anderson, C L., Britton, T., Elzanowski, A., Johansson, U.S., Källersjö, M., Ohlson, J.I., Parsons, T.J., Zuccon, D. & Mayr, G. 2006: Diversification of Neoaves: integration of molecular sequence data and fossils. Biology Letters 2, 543–547.

Goloboff, P.A. 1993: NONA version 2.0. S.M. de Tucumán, Argentina. http://www.cladistics.com/Software.html

Hackett, S.J., Kimball, R.T., Reddy, S., Bowie, R.C.K., Braun, E.L., Braun, M.J., Chojnowski, J.L., Cox, W.A., Han, K.-L., Harshman, J., Huddleston, C.J., Marks, B.D., Miglia, K J., Moore, W.S., Sheldon, F.H., Steadman, D.W., Witt, C.C. & Yuri, T. 2008: A phylogenomic study of birds reveals their evolutionary history. Science 320, 1763–1767.

Kristoffersen, A.V. 2002: The avian diversity in the latest Paleocene – earliest Eocene Fur Formation, Denmark. A synopsis. Ph.D. dissertation, University of Copenhagen, Geological Institute, Copenhagen.

Lemmrich, W. 1931: Der Skleralring der Vögel. Jenaische Zeitschrift für Naturwissenschaften 65, 513–586.

Leonard, L., Dyke, G.J. & van Tuinen, M. 2005: A new specimen of the fossil palaeognath Lithornis from the earliest Palaeogene of Denmark. American Museum Novitates 3491, 1–11.

Lindow, B.E.K. 2007: The early evolution of modern birds: Fossil evidence from the Lower Eocene Fur Formation of Denmark. Ph.D. dissertation, National University of Ireland, University College Dublin.

Livezey, B.C. & Zusi, R.L. 2006: Higher-order phylogeny of modern birds (Theropoda, Aves: Neornithes) based on comparative anatomy: I. – Methods and characters. Bulletin of Carnegie Museum of Natural History 37, 1–544.

Mayr, G. 1999: Pumiliornis tessellatus n. gen. n. sp., a new enigmatic bird from the Middle Eocene of Grube Messel (Hessen, Germany). Courier Forschungsinstitut Senckenberg 216, 75–83.

Mayr, G. 2002: On the osteology and phylogenetic affinities of the Pseudasturidae - Lower Eocene stem-group representatives of parrots (Aves, Psittaciformes). Zoological Journal of the Linnean Society 136, 715–729.

Mayr, G. 2006: A specimen of Eocuculus Chandler, 1999 (Aves, ?Cuculidae) from the early Oligocene of France. Geobios 39, 865–872.

Mayr, G. 2008: Pumiliornis tessellatus Mayr, 1999 revisited – new data on the osteology and possible phylogenetic affinities of an enigmatic Middle Eocene bird. Paläontologische Zeitschrift 82, 247–253.

Mayr, G. 2009: Paleogene fossil birds. Springer, Heidelberg, 262 pp.

Mayr, G. 2011a: The phylogeny of charadriiform birds (shorebirds and allies) – reassessing the conflict between morphology and molecules. Zoological Journal of the Linnean Society 161, 916–943.

Mayr, G. 2011b: Metaves, Mirandornithes, Strisores, and other novelties – a critical review of the higher-level phylogeny of neornithine birds. Journal of Zoological Systematics and Evolutionary Research 49, 58–76.

Mayr, G. & Clarke, J. 2003: The deep divergences of neornithine birds: a phylogenetic analysis of morphological characters. Cladistics 19, 527–553.

Mayr, G. & Knopf, C. 2005: A tiny barbet-like bird from the Lower Oligocene of Germany: the smallest species and earliest substantial fossil record of the Pici (woodpeckers and allies). The Auk 122, 1055–1063.

Mayr, G. & Mourer-Chauviré, C. 2004: Unusual tarsometatarsus of a mousebird from the Paleogene of France and the relationships of Selmes Peters, 1999. Journal of Vertebrate Paleontology 24, 366–372.

Nixon, K.C. 2002: WinClada, version 1.00.08. published by the author, Ithaca, NY. http://www.cladistics.com/Software.html

Appendices

Appendix 1. Character descriptions. Character list follows Mayr & Clarke (2003), with five characters (149-153) newly added and the description of three (15, 44, 94) modified. Concerning *Morsoravis*, scorings of six characters differ from Bertelli *et al.* 2010 (who also followed Mayr and Clarke 2003): I completed codings for characters with uncertain scores (10, 11, 36 and 113), and modified the scoring of two characters (3 and 57). Below is a list of characters, whose descriptions or scorings were modified or that were newly added. See Mayr & Clarke (2003) for a complete list of characters and further comments concerning the scoring of the extant taxa.

3   Upper beak, lamellae for filter feeding: absent (0), vestigial (1), well developed (2). Because the keratinous parts of the beak are not preserved in the fossil, I scored this character as unknown for *Morsoravis* (contrary to Bertelli *et al.* 2010, who coded it as absent).

6   Nostrils: schizorhinal, i.e., caudal margin slit-like and extending caudally to naso-frontal hinge; cranial kinesis rhynchokinetic: no (0), yes (1). I corrected the erroneous scoring of this character by Mayr & Clarke (2003) for Gruidae, and coded it as present (1) for this taxon.

10 Os mesethmoidale reaching rostrally markedly beyond naso-frontal hinge: no (0), yes (1). Bertelli *et al.* (2010) coded this character as unknown. However, I consider it unlikely that a rostral portion of this structure is broken, which is as fragile as any other portion of the septum orbitale (which is mostly preserved).

11 Palate, processus maxillopalatini of ossa maxillaria fused along their midline: absent (0), present (1). Remains of one unfused processus maxillopalatinus are preserved in the holotype, therefore I scored this character as absent for *Morsoravis* (Bertelli *et al.* 2010 coded it as unknown).

15 Os palatinum, crista ventralis: absent (0), present (1). Character description was modified from Mayr & Clarke (2003), where only a well-developed crista ventralis was scored. Accordingly, this character was scored present in Cariamidae, Gaviidae, Phaethontidae, and Fregatidae, in addition to the taxa coded "1" by Mayr & Clarke (2003).

22 Os palatinum and os pterygoideum fused: yes (0), no (1). I corrected the erroneous scoring of this character by Mayr & Clarke (2003) for Hesperornithidae and coded it as absent (1) for this taxon.

31 Os opisthoticum/prooticum, pila otica with cluster of small pneumatic openings: no (0), yes (1). I corrected the erroneous scoring of this character by Mayr & Clarke (2003) for Phoenicopteridae, and coded it as present (1) for this taxon.

32 Fronto-parietal suture in adult birds: open (0), closed (1). I corrected the erroneous scoring of this character by Mayr & Clarke (2003) for Apterygidae, and coded it as closed (1) for this taxon.

36 Quadratum, processus oticus, pneumatic foramina on dorsal end of caudal surface: absent (0), present (1). The dorsal margin of the caudal surface of the quadrate, which is exposed in the fossil, is not pierced by these foramina; therefore I scored this character as absent for *Morsoravis* (Bertelli *et al.* 2010 coded it as unknown).

44 Mandible: not as follows (0), with long and strongly mediolaterally compressed processus retroarticularis (1), with narrow, dorsally upcurved processus retroarticularis (2).

Character description was modified from Mayr & Clarke (2003), where only the presence of a retroarticular process was scored. Character state 1 was coded present in Anatidae, Anhimidae, Phoenicopteridae, and Pteroclidae. Character state 2 was scored for Galliformes, Threskiornithidae, Recurvirostridae, Rallidae, Gruidae, and *Morsoravis*

57 Thoracic vertebrae: at least part of series amphicoelous or opisthocoelous, i.e., with subround, central articular surfaces that lack the dorsoventral compression and saddle-shaped articular surface seen in heterocoelous vertebrae (0), series completely heterocoelous (1). Scoring of this character differs from Bertelli *et al.* (2010) concerning *Morsoravis*, which has heterocoelous thoracic vertebrae. I further corrected the erroneous scoring of this character by Mayr & Clarke (2003) for Phalacrocoracidae, and coded it as absent (0) for this taxon.

58 Caudalmost presacral vertebrae pleurocoelous, i.e., with deep lateral excavations: no (0), yes (1). I coded Psittaciformes as polymorphic for this character, as pleurocoelous vertebrae occur in some stem group representatives (Halcyornithidae, see Mayr 2002).

65 Coracoid, foramen nervi supracoracoidei: present (0), absent (1). I corrected the erroneous scoring of this character by Mayr & Clarke (2003) for Rheidae, and coded it as absent (1) for this taxon.

85 Carpometacarpus, os metacarpale minus strongly bowed, delimiting a large spatium intermetacarpale: no (0), yes (1). I corrected the erroneous scoring of this character by Mayr & Clarke (2003) for Anatidae and Opisthocomidae, and coded it as absent (0) for Anatidae and present (1) for Opisthocomidae.

94 Pelvis, foramen ilioischiadicum caudally closed: no (0), yes (1). Character description was modified from Mayr & Clarke (2003), where Rheidae were assigned a separate state.

100 Tibiotarsus, distal end, ossified pons supratendineus: absent (0), present (1). I corrected the erroneous scoring of this character by Mayr & Clarke (2003) for Apterygidae and coded it as absent (0).

105 Tarsometatarsus, hypotarsus, tendon of musculus flexor digitorum longus enclosed in bony canal: no (0), yes (1). I corrected the erroneous scoring of this character by Mayr & Clarke (2003) for Coliidae.

106 Tarsometatarsus, hypotarsus, tendon of musculus flexor hallucis longus enclosed in bony canal: no (0), yes (1). I corrected the erroneous scoring of this character by Mayr & Clarke (2003) for Coliidae.

113 Osseous claws, pair of canals lateral and medial to tuberculum extensorium: absent (0), present (1). The ungual phalanx bears an open sulcus neurovascularis, therefore I scored this character as absent for *Morsoravis* (Bertelli *et al.* 2010 coded it as unknown).

149 Phallus: present (0), absent (1). Newly added character.

150 Modal number of plates in scleral ring: 14 or more (0), 13 or less (1). Scoring after Lemmrich (1931) and Livezey & Zusi (2006). Newly added character.

151 Tibiotarsus, well-developed crest along medial side of proximal end, opposite crista fibularis: absent (0), present (1). Newly added character.

152 Tarsometatarsus, foramina vascularia proximalia widely separated: no (0), yes (1). Extant Coliidae exhibit only a single foramen vasculare proximale. Newly added character.

153 Fourth toe, proximal phalanx short and very wide: no (0), yes (1). Newly added character.

Appendix 2. Character scorings. Newly added characters and scorings that differ from Mayr & Clarke (2003) or Bertelli *et al.* (2010) are highlighted. Multistate characters are denoted by "a" (0&1), "b" (1&2), "c" (2&3), and "d" (3&4), unknown character states by "?". These data are also contained in the supplementary data file Morsoravis.winc which can be imported by the phylogenetic analysis program Winclada. This program is freely available at http://www.cladistics.com/about_winc.htm

Apsaravis
??????????????????????0???????00??????1?0??????????b?00000??0000000????000000001?000?000010000??0010000100???0?????????
??????????????????????????**???0**

Hesperornis
00?00000?0000000000001000000?0100100000?0?0000000??00002011000000000000010200?00???0???????12000010000000000001000?????
??????????????????????????????????**??000**

Ichthyornis
00?00000?0???????????000?a00??00000??000000010?00?0b?01?0000000001010??000000001000000
0a010000000000000100??????????????????????????????????????**??0??**

Rheidae
100100000100100000000000000000011000100?1111000000000001010000??0**1**0010000200?00???0??00???0?10**1**000000000000001010000??
?0010???0??????1?14??????0010000**00000**

Apterygidae
100100010100000000000000000000111000000011110001100100101000??00001000100?00???0??00???0c10000000**0**00000011010000000
0000000000000010a120100??001?000**00000**

Tinamidae
1001000001000000000000000000001000010001111000010a0001100000001100000011011000000000000004000001001000000000010000
001000000000000000100a0100000000**a0000**

Galliformes
100000000001000000111010100100100100100110**2**1000a10100111a00100010000100010110101000000003101101a01001010000000a0
00000000000000000100100001000010000**a0000**

Anhimidae
1010000000110?011011110101001001111001001101101 0a10
0a1001010101000001000201200101010110000004111010101001000010000000???00????00??00??????????00000?000**00000**

Anatidae
1020000000110?00101111010110100111100100110110aa0001001010101000100000ab011001010101a**0**00000d1010a0001001000000110000
0110001000ba?00a00a2000000000100000**00000**

Opisthocomidae
100010000000000000110110000010110101000011000011011100111010010011110??11110010111010**1**1000031111000000010100100000000
0000000100000011001000010000100??00**11000**

Podicipedidae
100000000001001100011110000011010100100011000100 0a000121101010001000001010000110101100001140110100
1a01111?0001000011110100001?100110014001?01000100**11000**

Phoenicopteridae
1021000000100?11001011000101**1**1010010001101010111000121101000000000111111001110101100001021110111111111100001100100
00100000000100001 4001001000?001**10000**

Threskiornithidae
10010100001100110011011000101101010010001102 0a011001001110100000000011100100101011000000031110010010110001000000?00
00001000000001000001000000000100010**10000**

Cariamidae
10000000001110**1**1001111100000101101010000110000010101000010100000100001101100101010001100021110100100000001010000?
????1????0?????????????10001?00**10000**

Strigiformes
110010010000101101???1000000100101000000110010001101000010100a00000
0a0100100101011100000021111000000010000100001000011010001?0000101011000000111000**10001**

Recurvirostridae
100001000001001100000100101010010100100011102000011010000011010010000110010000101110000100201100101101100000010a000?
?????0???0?????????????00000110 0**10000**

Burhinidae
1000000000000?11000101100000100101011000110000000001100001101001000001100100001011100001003011001001011000010100 00?
????1????0?????????????00000110 0**10000**

Accipitridae
110000010000a011001111100000100101000000110010 00100a00a0101001000000
aa1011001010111000000211100010100100001000010001110110000000010103100000010?000**10000**

Falconidae
110000010000101100101100000100101 00a0001100100011010 0a11010010000001110110010101111 00000
0b111001101001000010000100011101100000000010003100000010100**10011**

Sagittariidae
1100000100a0100101???1000000100111010000110011100111000010100010000000112100101110100000002111101101000000010000000000010100000000001031000000010??00**10000**

Cuculidae
100000010010011101???110000010a1010a000011001000a001a000101010001a000100a10010101010aa10001aa1a0000100101101100000001100a1011010000110010000100010000100a0**11000**

Musophagidae
10000001000000000000101100000101111000000011000000a10110001011010000001
1a0010010101010111000200110010100101001000000?0?00?0?1101????0???????????10000100**11000**

Cathartidae
11000000000000011101???100001110101001000110010000a101001010100000001000100100100101111100000002111001101000000010000000000100a11000000000100510000001110000**10000**

Gaviidae
1000000000000?**1**10001111010001101010010001100010011000010101010000000002010000010101000000140110100110011?0001100000110000000110010101401?000001000**10000**

Spheniscidae
10010000000000010001110100011011110100011000001100001000100000000000110100000???0??0000001011000011000000110110??0000a10000000100001101200101??000?010**10010**

Phaethontidae
10001000000000**1**000100110000011011100000011000101110100201011??010000011102100101011100000001011000001001100010011100??
?00?1??????0???????????000001000**10000**

Fregatidae
1101001?10000?**1**110110110000111011100000011000100110100001011010?10100000112100101011100000102011010001001010010001010000111111000?0000001000500000010000?10**10000**

Phalacrocoracidae
1101101?10100?11a1???110000011011100100011001100100000020**0**0110110100010101100001011100000010311100001100101101001101000011001?00000000?000210000010001?10**11000**

Balaenicipitidae
1101101?00100?1111???1100011011010010001100000101000010101011100000101111001010111000000003111?0000100101101000000000000110001000000100100000000000??10**10000**

Eurypygidae
10000100000100?110001011000001011110010001100000101000021101010001000111011001010111000000002011000001001000010000000?
???????????0???????????000011?00**10000**

Ardeidae
1000000000a000110001111000001001111a01000110000010100002010101000100011001100101011100000002111000001001011a010000010000001110010?0001100100000000110a0**10000**

Ciconiidae
1000000000110?1101???110000a11010101100011000010001001010100010a000a01111001010111a000a003111011101
1a1100010000001000011000000001000001000001000?000**10000**

Procellariidae
11010000000000110000010010011101110a10001100010011000010111000000000011
1a010000110010000102011000011011000000011?0000011000000100010004001?00000?000**10000**

Otididae
1000000000000011001111100000101101000000110000010100100010001100001001001010100000003011?1110100101001010000?
??001????0?????????????0000?1000**10000**

Pteroclidae
10000000000000100001???10000001001010000001101100011010011101010001000001001110101110100000020110010010010100001000?
?????0???0???0?0?1?????000011000**11000**

Columbidae
100001000000010101???10000001011110000001100000011000011010100010000a00a11110101110100100201100100100101011000000010000000000000000010001a0011000**11000**

Rallidae
1000000000010110001111000001011010100011002000011000000a00b010101000a001101100001010000000004111101001a01
0a00000000000000001000200000001000000001000**11000**

Psophiidae
10000000000000010001111000001001010110001100000001000021100010000010002121001010100010000031111010011110001000000?
????1????0???????????????100000?00**10000**

Gruidae
10000**1**00000a1011000111000101011110110001102000100000021100010000010a021210010101110000003111010011110100001000000000?000000000000100000000000000**10000**

Steatornithidae
11001001001100011???100000100111000010110000000100000100111000100000001100101111110000001011000000010000100000001
00011?001?0?0?0000?0100000011?00**10000**

Psittaciformes
110010010010a00101???110000010011100000011000100110aa0001**a**101000a00011101100101011110000000211100000a00100011100
0a010000011000?010111109010100010100**11a11**
Coliiformes
100000010011010101???1100000101111010000110001001101100010110000a000010001001010
1a10100000101100011001000**01**01000000100000110010?0101101051101100001?00**111?0**
Trogonidae
10001001000000001011010000001001110000101100100011000000101110001000010001001011111010000010110000010010111100000001
1?1?????01??0?0??008?1??10001100**11010**
Aegothelidae
11000000000??0010000010000001001110100001100010011000000101110000000000000010010101110000000000110000010010101100000000
10??01?001?0?0?1000?0100000011?00**10010**
Coraciidae
100000010010001110110110000010010100000011000000a1a111000101110001000011001001010111000000001011000001001010110000000
0a1000010001?000110005100?00001100**11010**
Passeriformes
1000000000000000000000110000010a1010000001100100011010000101110001000011011001010111000a0001011000001001011110000a0a
1000011001??0000100070b1a0100010000**10a00**
Morsoravis
10**?**00100?**00**?00??????????0?0???010100**0**?0?01102???????10010**1**1000???????????0???????????????01?110010010??????100??**0**?????????
????????????????????????????**1111**
Pumiliornis
10???10?????0?????????????????1?????0?1???????????01011????0010?0????0?00????111?00??00?011?0??000010???100??0?0?????????
????????????????????????????111
Eocuculus
???11?01?0???????0?000??????1??00??001?1100??010010??1100??0????????????
?????????????????????????????11
Mesitornithidae
10000100?00001110011011000001011010000001102000010011011100010?0100001101011101010100010002001101001001011010000000?
?????????????????????????????????????10110

Coastal evolution of a cuspate foreland (Flakket, Anholt, Denmark) between 2006 and 2010

LARS B. CLEMMENSEN, METTE BENDIXEN, LARS NIELSEN, SABRINA JENSEN
& LOUISE SCHRØDER

Flakket is a cuspate marine foreland on the north coast of Anholt in the Kattegat sea. It is composed of a number of gravel-rich beach ridges typically covered by aeolian sand and intervening swales and wetlands including a relatively large lagoon. The most recent evolution of the coastline of this marine foreland between May 2006 and September 2010 is documented in this paper. Flakket is under erosion on its northwestern side, which has retreated up to 40 m during the observation period. The shoreline of the northeastern side of the beach-ridge plain moved up to 70 m in a seaward direction during the same period.

Many coastal areas in northern Denmark possess well-developed marine forelands (Jessen 1897; Schou 1945; Hansen 1995; Clemmensen *et al.* 2001; Nielsen *et al.* 2006; Bjørnsen *et al.* 2008). The overall morphology of the marine foreland can take various shapes with the most common types being beach-ridge plains, spits and cuspate forelands. The marine forelands are typically characterized by closely situated beach ridges separated by swales (Jessen 1897; Hansen 1995; Nielsen *et al.* 2006; Clemmensen & Nielsen 2010). The marine forelands have developed over the past 7000–8000 years and their long-term development was controlled by isostatic uplift, sea-level change, sediment supply, and wind and wave climate (e.g. Brun 1993; Clemmensen *et al.* 2001, Bjørnsen *et al.* 2008). While some marine forelands such as the northernmost part of the Skagen Odde spit system (Clemmensen *et al.* 2001; Nielsen & Johannessen 2009) and the major part of the Anholt beach-ridge system (Bjørnsen *et al.* 2008; Clemmensen & Nielsen 2010) have been characterized by uninterrupted and simple growth during most of their evolution, other systems such as many of the spit systems on Læsø (Hansen 1995) experienced growth punctuated by erosion phases and associated reorganization of the spit structures. Little is known, however,

on the processes that caused these major changes in coastal evolution in the past, and we also have little knowledge of the rates of coastal change that took place during these events of coastal reorganization. Studies of modern evolution of foreland systems may thus add to a better understanding of past evolution of these complex coastal systems.

Flakket

Anholt is a small island in the middle of the Kattegat sea (Fig. 1). The island is composed of a glacial highland towards the west, a raised beach-ridge plain towards the east, and a lower-lying marine foreland, Flakket, towards the north (Fig. 2; Larsen & Kronborg 1994; Bjørnsen *et al.* 2008; Nielsen & Clemmensen 2009; Clemmensen & Nielsen 2010). Formation and preservation of the beach-ridge deposits are partly due to isostatic land rise which amounts to around 9 m during the past 6600 years (Bjørnsen *et al.* 2008). Flakket forms a rounded protrusion on the north coast of Anholt and can be classified as a cuspate foreland (Gulliver 1896; Johnson 1919; Moslow *et al.* 1981; Semeniuk *et al.* 1988;

Park & Wells 2007). Flakket is composed of a number of NW–SE trending gravel-rich beach ridges. The berm and the outermost beach ridge are devoid of aeolian sand cover while most inland ridges are covered by aeolian sand forming typical dune ridges. Intervening depressions, swales, are developed as wetlands with a rich swamp vegetation. One of these wetlands comprises a relatively large coastal lagoon (Figs 3–4). Flakket faces the medium-energy Kattegat sea. Tidal variation is insignificant, with the tidal range reaching no more than 0.4 m; sea-level change related to meteorological conditions, however, is significant and short-term variation may reach 2 m or more (Nielsen & Clemmensen 2009; Clemmensen & Nielsen 2010). Nearshore processes are controlled by wave action and by longshore currents transporting sediment towards the east under the influence of the dominating westerly winds (Cappelen & Jørgensen 1999; Jönsson & Holmquist 1995). Wave energy has been modelled on the basis of measurements from 1979–2007 in an area around 20 km southwest of Anholt. From these analyses the significant wave height is estimated to be 3.0 m and the maximum wave height 5.6 m based on the extreme values for a 5 year return period (Grode & Hansen 2010).

Flakket started to develop around AD 1000 as indicated by optically stimulated luminescence dating of one of the oldest beach ridges on the marine foreland

(Andrew Murray, personal communication 2010). The early stages of foreland evolution are not known from map information, but topographical maps from 1792 to 1991 supplemented by an aerial photo from 2005 indicate that Flakket is a highly dynamic coastal system (Fig. 2; Larsen & Kronborg 1994). Until 1887 Flakket had a linear shoreline over most of its length. Reorganization of the foreland started after 1887 and is most likely linked to construction of the harbour at the northwest corner of the island in 1902. The construction of the habour seems to have modified the local littoral currents and caused the formation of a cuspate foreland. Sediment from distant sources and sediment released by erosion of deposits at the westernmost part of the foreland was transported northeastward by longshore currents and deposited in shallow water under the influence of constructive wave action from different directions. After 1934, erosion on the western side of the foreland continued and the cuspate foreland was shifted eastward and grew wider (Fig. 2). This shift in coastal dynamics was probably supported by an enhanced influence of westerly winds after 1920 (Jönsson & Holmquist 1995). Evolution of Flakket after 1934 was linked to continued beach-ridge formation. Beach ridges were fed by material from the eastward moving longshore currents and sand and gravel were deposited high on the beachface during extreme events with elevated sea
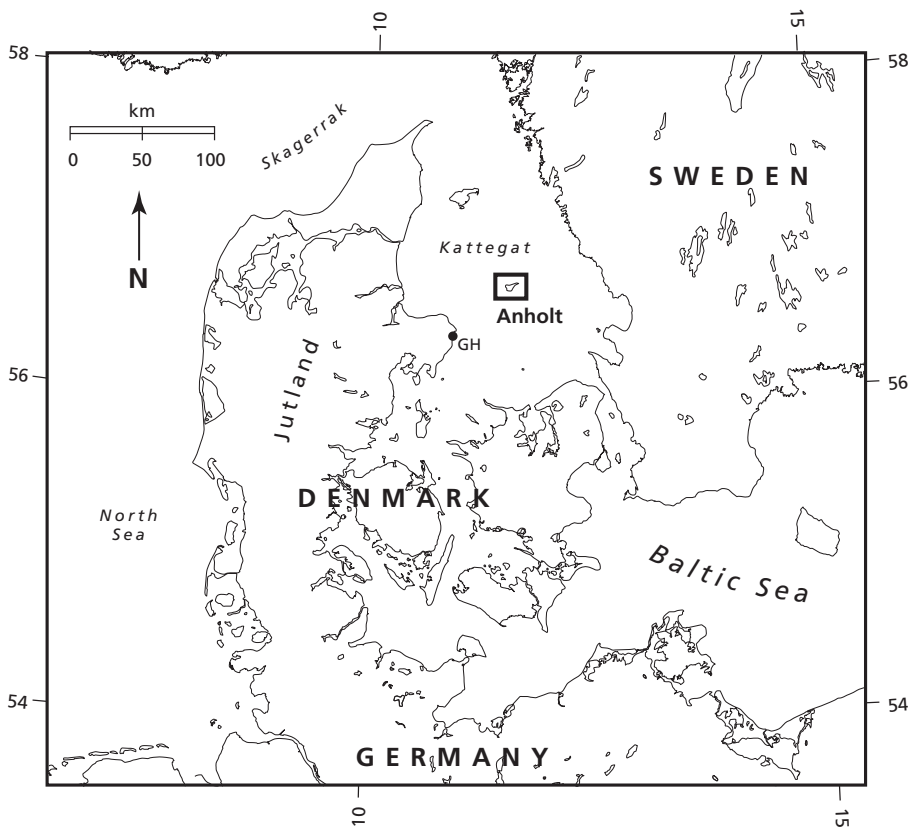
Figure 1. Location map of Anholt. The location of Grenå Havn is given by GH.
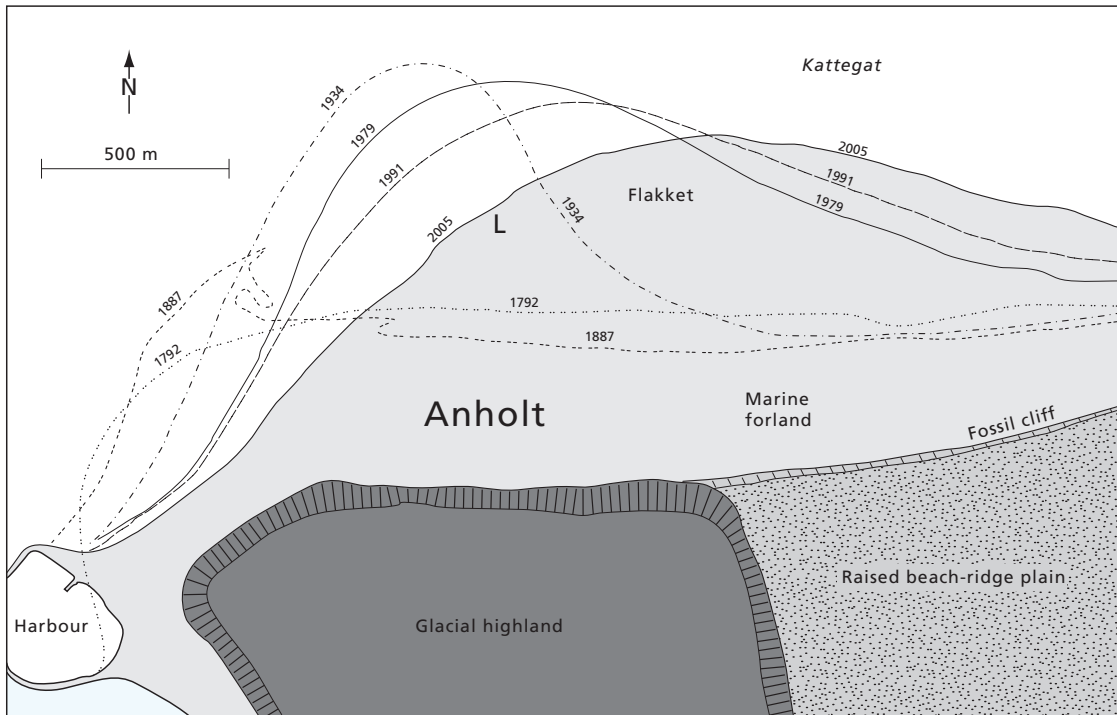
Figure 2. Evolution of the cuspate foreland Flakket on the north coast of Anholt. The reconstruction is based on topographical maps measured in AD 1792, 1887, 1934 and 1979/80 and 1991 supplemented by an aerial photo from 2005. The maps were first digitized and later georeferenced in order to integrate the maps in ARCGIS software. The location of the lagoon is given by L.
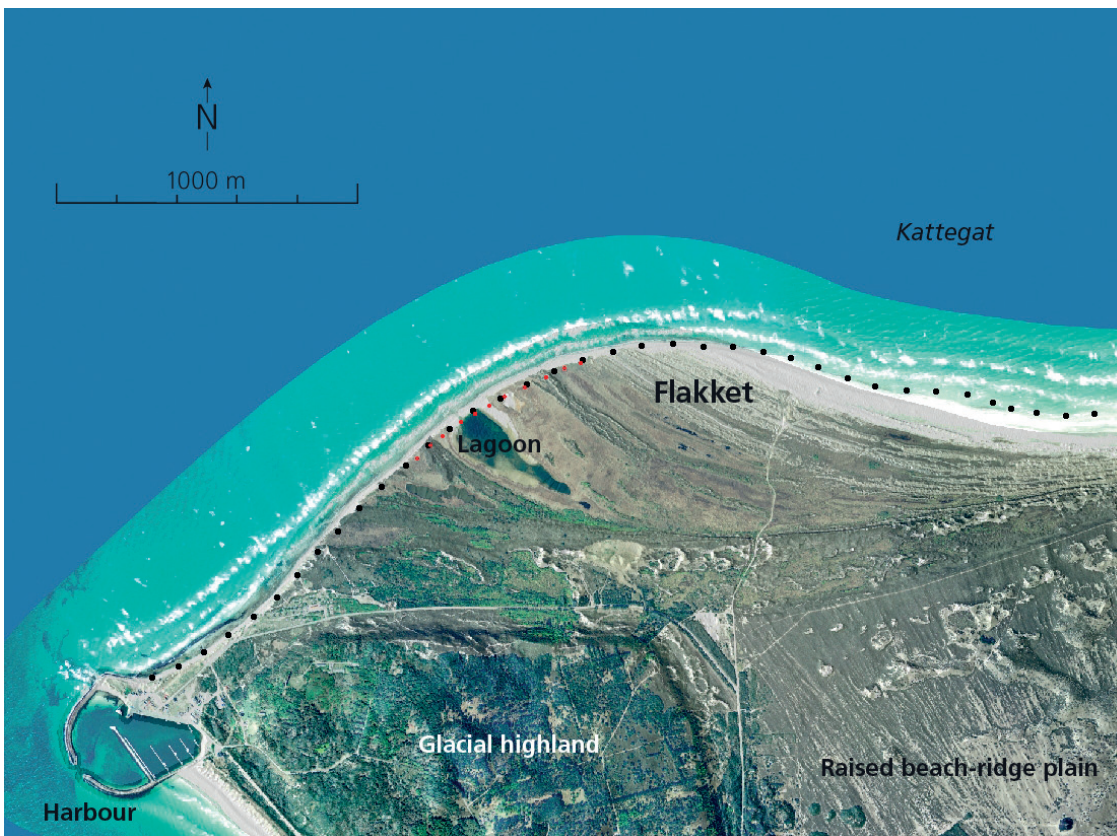
Figure 3. Orthophotograph of Flakket (May 14, 2006) with shoreline positions measured on September 2, 2010 (black dots) and on November 11, 2010 (red dots).

level and strong wave run-up (Nielsen & Clemmensen 2009). Simultaneously with beach-ridge formation and progradation of the northeastern side of the marine foreland, the northwestern side of Flakket was eroded leading to a truncation of the oldest beach ridges (Figs 3–4). This wave erosion has led to rapid coastal retreat, and in the area immediately east of the harbour a short stretch of the shoreline is now not more than about 25 m from the main road on the island (Fig. 3).

We here present new data that documents the most recent shoreline changes on Flakket between May 2006 and September 2010 with supplementary data from November 2010. Our data makes it possible to quantify the rates of coastal change with special emphasis on the scale of erosion that has taken place on the northwestern side of Flakket since May 2006.

Methods and results

Our analysis is based on an aerial photo from May 2006 supplemented by field measurements of shoreline positions in September 2010 and November 2010. Beach morphology was studied in August 2007, June 2008, August 2009, September 2010 and November 2010.

The aerial photo from May 2006 shows the curved shoreline of Flakket (Fig. 3). The beach is relatively narrow and featureless on the northwestern and retreating side of Flakket, and the beach is here commonly backed by eroded swales and beach/dune ridges. The beach on the northeastern and prograding side of Flakket is relatively wide and in August 2007 the beach was here composed of a seaward dipping beachface of sand with a few scattered stones backed by an up to 1.8 m high gravel-rich berm with relatively steep sides. Inland of the gravel-rich berm followed a flat-based swale covered by sand and a few scattered stones, an inactive, gravel-rich beach ridge, a second flat-based swale, and most inland a dune-covered beach ridge (Nielsen & Clemmensen 2009). Due to coastal progradation, however, the characteristics of this system change rapidly and in November 2010 a new, incipient berm had developed in front of the large berm which had become inactive. At the same time, the two swales that were practically devoid of aeolian sand in August 2007 had now been partly covered by low aeolian dunes and vegetation had invaded the swales and the outermost beach ridge.

On May 14, 2006, when the aerial photo was taken, sea level at the nearby Kattegat station Grenå Havn varied between 0.20 m at 08.30 and -0.07 m at 15.40

Figure 4. Orthophotograph of the retreating part of Flakket (May 14, 2006) with shoreline positions on September 2, 2010 (black dots) and on November 11, 2010 (red dots). The diameter of a black dot is around 5 m.

(Farvandsvæsenet, Danish Maritime Safety Administration). With beachface gradients around 6° this means that the observed shoreline changed from 3.0 m landward to 1.0 m seaward of the DVR90 (Danish Vertical Reference 1990) shoreline during the above mentioned period. The aerial photo portrays nicely the beach-ridge plain at Flakket with beach ridges that are curved and roughly trending NW–SE; the truncated nature of the first formed beach ridges is clearly seen (Fig. 3). It can be observed that the lagoon at Flakket is separated from the Kattegat sea by a narrow beach barrier.

During fieldwork in September 2010 the position of the shoreline at Flakket was measured with traditional GPS. The shoreline (here defined as the water's edge, which equals the upper limit of wave uprush; Hughes & Turner, 1999) was tracked from a point near the harbour towards the east for a distance of approximately 3500 m. A total of 37 points with an average distance of 175 m were measured (Figs 3–4). The lateral accuracy of the measured positions provided by this standard GPS system was typically around ±5 m. The measurements were carried out on September 2 between 11.30 and 12.35. Water levels at the nearby Kattegat station at Grenå Havn rose from 0.01 m to 0.12 m above mean sea level in this time interval (Farvandsvæsenet); it ap-

peared that wave run-up was of minor importance on Anholt in this interval. Thus the measured shoreline was only about 0.15 to 1.7 m more landward than the DVR90 shoreline.

During fieldwork in November 2010 the shoreline position of the central part of Flakket was remeasured with a Trimble R8 DGPS. This was done to acquire supplementary data on the shoreline position near the lagoon. The shoreline (water's edge) was tracked for a distance of approximately 600 m and 11 points were measured (Figs 3–4). These measurements are significantly more accurate than the data from the standard GPS, and points are given with an accuracy of ±0.03 m. The data were collected between 10.00 and 10.30 on November 11, 2010 and the sea level (at Grenå Havn) was elevated around 0.20 m in this time interval (Farvandsvæsenet); wave runup on Anholt caused the water level at the water's edge to be elevated by an additional 0.30 m. Thus the measured shoreline was about 7 m more landward than the DVR90 shoreline.

We also carried out a DGPS survey of the beach barrier which separates the lagoon at Flakket from the sea. The barrier, which is gravel-rich, consists of two spit segments cut by a narrow inlet (Fig. 5). The western and longest of these spit segments has a length of 140 m and reaches heights of around 1.20 m above
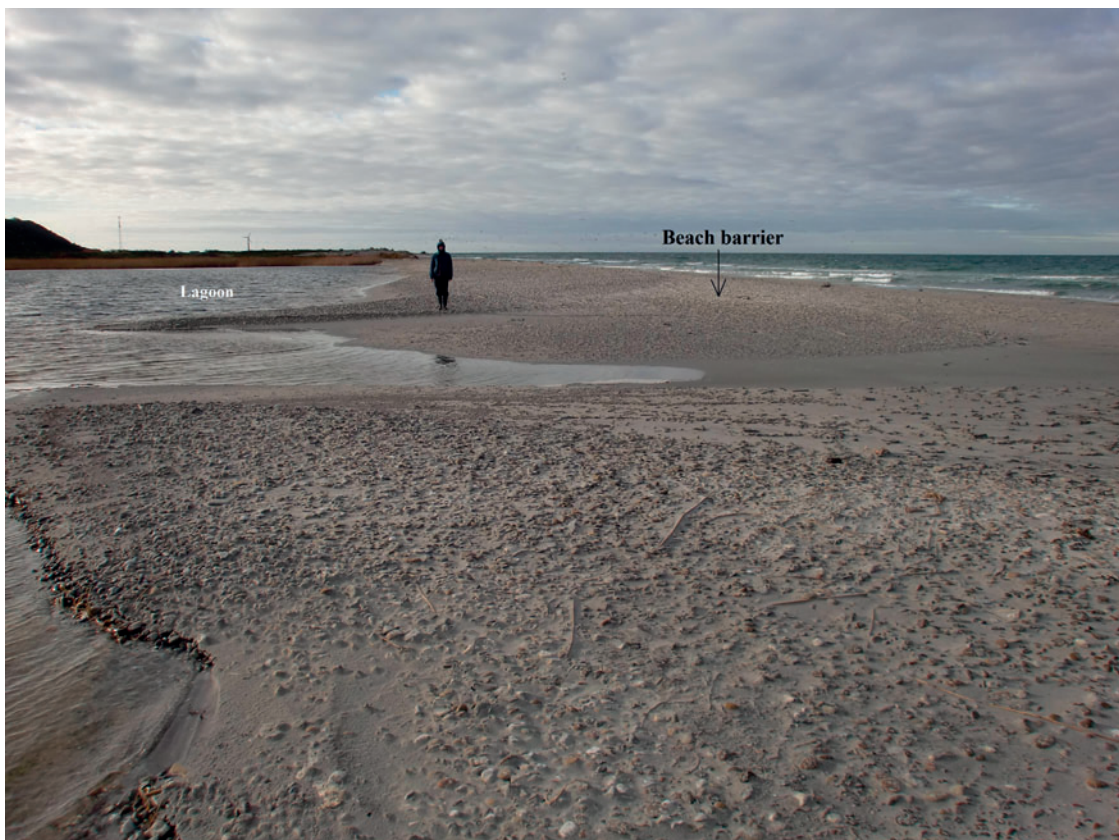
Figure 5. A narrow beach barrier separates the lagoon on Flakket from the Kattegat sea. A partly sand-filled inlet cuts the beach barrier in the foreground of the photo and recurved spits have developed along along both sides of the inlet. View towards the southwest.

mean sea level, while the inlet has a threshold value of around 0.50 m above mean sea level. Wash-over tongues of beach material are seen at the back side of the barrier spit.

Discussion and conclusions

The accuracy of the traditional GPS is around ±5 m under ideal conditions and defining the shoreline from these data may therefore involve a small inaccuracy. When the points as here form a smooth curved line it is believed, however, that our GPS measurements yield a reasonably accurate estimate of the shoreline position in early September 2010 (Fig. 3).

In early September 2010, Flakket formed a rounded cuspate marine foreland with its northernmost point approximately 500 m northeast of the lagoon (Fig. 3). The results presented here clearly indicate that the northwestern side of Flakket has retreated between May 2006 and September 2010, while the northeastern side of Flakket has prograded. Coastal retreat appears to have been been particularly pronounced close to the lagoon on Flakket, and shoreline retreat here is up to 40 m or almost 10 m per year assuming a constant retreat over the study period (Fig. 4). Shoreline retreat is linked to a deficit in sediment supply at this side of the foreland. Simultaneously with coastal retreat on the northwestern side of Flakket the northeastern side of the foreland has prograded and the shoreline has here advanced up to 70 m in response to a surplus in sediment supply (Fig. 3).

The shoreline of the northwestern part of Flakkket of November 11, 2010 agrees well with that observed on September 2, 2010, although the November shoreline is situated 1 to 9 m more inland than the September shoreline (Fig. 4); these differences in shoreline position can primarily be accounted for by the higher water level in the Kattegat sea during the observation period on November 11.

According to Sørensen *et al.* (2007), water levels of 1.02 m above mean sea level are statistically reached once a year (at Grenå Havn), while levels of 1.63 m above mean sea level are reached every 20 years indicating that the lagoon, which is separated from the sea by a beach barrier reaching heights up to 1.20 m above mean sea level, is likely to be flooded during extreme events with elevated sea level (Fig. 5). The presence of newly formed wash-over tongues at the back side of the beach barrier also indicates that waves frequently overtop the barrier and that sea water during these episodes enters the lagoon.

Figure 6. The retreating coast on the northwest side of Flakket is backed by eroded dune ridges; the dune ridge shown is situated immediately southwest of the lagoon. View towards the northeast.

The northwestern side of Flakket is backed by eroded dune ridges and peat-bearing swales, also indicating that coastal retreat has taken place here in recent years (Fig. 6). Sand from the eroded dune ridges and the uppermost part of the beach is becoming available for aeolian transport and a large part of the old beach-ridge plain at the westernmost edge of Flakket is now being covered by inland transported aeolian sand. Aeolian sand also frequently covers the main road leading to the harbour.

The central part of Flakket including the lagoon is part of an EU habitat on Anholt (Natura 2000), and is of particular interest because of its well-developed wetlands and swales that separate the dune ridges. Our new data indicate that the lagoon at Flakket and the surrounding wetlands are likely to be flooded frequently in coming years. Coastal retreat not only diminishes the area of the beach-ridge plain and the lagoon, but it also leads to an increased inland transport of aeolian sand. Coastal retreat of the northwest side of Flakket may also impact the infrastructure on the island as the main road leading to the harbour is running on a narrow beach-ridge plain between a high inland cliff and the retreating shoreline.

The documented coastal evolution of Flakket between 2006 and 2010 demonstrates that the eastward shift of the cuspate foreland that began around 1934 continues. It most likely records a dominance of westerly winds and a related eastward directed longshore drift on the north coast of Anholt. This study of coastal evolution of a cuspate foreland shows that coastal changes can be very rapid, and although the changes seen on Flakket probably started due to man-induced processes (habour construction) they document that local rates of erosion can be very high, and that significant parts of a beach-ridge plain can disappear rapidly. Between 1934 and the present a wedge of beach-ridge sediments up to 500 m wide has disappeared on the northwest side of Flakket amounting to an erosion rate of up to 6.5 m/year; between 2006 and 2010 erosion rates up to 10 m/year are measured. These rates of erosion are indeed high when compared to other Danish coastal systems, where erosion rates along the Danish North Sea coast are up to 3–5 m/year (e.g. Christiansen & Møller 1979–1980; Aagaard *et al.* 2004) and erosion rates along shores in the Kattegat sea are up to 2m/year (e.g. Binderup 1997).

The eastward shift of the cuspate foreland leads to the formation of an erosion surface cutting into older beach-ridge and swale deposits along the western part of the system. This erosion surface related to local beach retreat would share many of its characteristics with a transgressive ravinement surface (e.g. Goy *et al.* 2003; Storms & Kroonenberg 2007; Johnston *et al.* 2007). Care should be taken therefore in the analysis of ancient beach-ridge systems to distinguish between areal extensive erosion surfaces formed during sea-level rise, and erosion surfaces of more local distribution formed during morphodynamic reorganization of the system.

Acknowledgements

References

Aagaard, T., Nielsen, J., Jensen, S.G., & Friderichsen, J. 2004: Longshore sediment transport and coastal erosion at Skallingen, Denmark. Geografisk Tidsskrift-Danish Journal of Geography 104, 5–14.

Binderup, M. 1997: Recent changes of the coastline and nearshore zone, Vejrø Island, Denmark: Posssible consequences for future development. Journal of Coastal Research 13, 417–428.

Bjørnsen, M., Clemmensen, L.B., Murray, A. & Pedersen, K. 2008: New evidence of the Littorina transgressions in the Kattegat – optically stimulated luminescence dating of a beach ridge system on Anholt, Denmark. Boreas 37, 157–168.

Brun, P. 1993: Relation between growth of a marine foreland and sea level rise case: The Skagen Spit, North Jutland, Denmark. Journal of Coastal Research 9, 1125–1128.

Cappelen, J. & Jørgensen, B. 1999: Observed wind speed and directions in Denmark – with climatological standard normals, 1931–90. Danish Meteorological Institute, Technical Report 99-13, 295 pp.

Christiansen, C. & Møller, J.T. 1979–1980: Beach erosion at Klim, Denmark. A ten-year record. Coastal Engineering 3, 283–296.

Clemmensen, L.B. & Nielsen, L. 2010: Internal architecture of a raised beach ridge system (Anholt, Denmark) resolved by ground-penetrating radar investigations. Sedimentary Geology 223, 281–290.

Clemmensen L.B., Richardt, N. & Andersen, C. 2001: Holocene sea-level variation and spit development: data from Skagen Odde, Denmark. The Holocene 11, 323–331.

Farvandsvæsenet, Danish Maritime Safety Administration (http://www.frv.dk)

Goy, J.L., Zazo, C. & Dabrio, C.J. 2003: A beach-ridge progradation complex reflecting periodical sea-level and climate variability during the Holocene (Gulf of Almeria, Western Mediterranean). Geomorphology 50, 251–268.

Grode, P.D. & Hansen, H.F. 2010: Anholt offshore wind farm - Supplementary metocean analyses for transformer platform. Energinet.dk. Final Report. January 2010, 36 pp (http://www.dhigroup.com).

Gulliver, F.D. 1896: Cuspate forelands. Geological Society of America, Bulletin 7, 399–422.

Hansen, J.M. 1995: En ø's opståen, kystdannelse og vegetationsudvikling: Naturlige og menneskeskabte landskaber på Læsø. Geologisk Tidskrift 2, 1–74.

Hughes, M. & Turner, I. 1999: The Beachface. In: Short, A.D. (ed.), Handbook of Beach and Shoreface Morphodynamics. John Wiley & Sons, Chichester, 119–144.

Jessen, A. 1897: Beskrivelse til Geologisk Kort over Danmark. Kortbladene Læsø og Anholt. Danmarks Geologiske Undersøgelse, Series I, No. 4, 48 pp.

Johnson, D.W. 1919: Shore processes and shoreline development. Wiley, New York, 584 pp.

Johnston, J.W. Thompson, T.A. & Baedke, S.J. 2007: Systematic pattern of beach-ridge development and preservation: Conceptual model and evidence from ground-penetrating radar. Geological Society of America, Special Paper 432, 47–58.

Jönsson, P. & Holmquist, B. 1995: Wind direction in southern Sweden 1740-1992: Variation and correlation with temperature and zonality. Theoretical and Applied Climatology 51, 183–198.

Larsen, G. & Kronborg, C. 1994: Geologisk Set: Det mellemste Jylland. Anholt. Geografforlaget, Brenderup, Denmark, 57–61.

Moslow, T.F. & Heron Jr., S.D. 1981: Holocene depositional history of a microtidal cuspate foreland: Cape Lookout, North Carolina. Marine Geology 41, 251–270.

Nielsen, L. & Clemmensen, L.B. 2009: Sea-level markers identified in ground penetrating radar data collected across a modern beach ridge system. Terra Nova 21, 474–479.

Nielsen, L.H. & Johannessen, P. 2009: Facies architecture and depositional processes of the Holocene-Recent accetionary forced regressive Skagen spit system. Sedimentology 56, 935–968.

Nielsen, A., Murray, A.S., Pejrup, M. & Elberling, B. 2006: Optically stimulated luminescence dating of a Holocene beach ridge plain in northern Jutland, Denmark. Quaternary Geochronology 1, 305–312.

Park, J.-Y. & Wells, J.T. 2007: Spit growth and downdrift erosion: Results of longshore transport modelling and morphological analysis of the Cape Lookout cuspate foreland. Journal of Coastal Research 23, 553-568.

Schou, A. 1945: Det marine Forland. H. Hagerups Forlag, 236 pp.

Semeniuk, V., Searle, D.J. & Woods, P.J. 1988: The sedimentology and stratigraphy of a cuspate foreland, Southwestern Australia. Journal of Coastal Research 4, 551–564.

Storms, J.E.A. & Kroonenberg, S.B. 2007: The impact of rapid sea level changes on recent Azerbaijan beach ridges. Journal of Coastal Research 23, 521–527.

Sørensen, P., Sørensen, C., Ingvardsen, S.M., Andersen, I. & Kloster, B.B. 2007: Højvandsstatistikker 2007 – Extreme sea level statistics for Denmark, 2007. Danish Coastal Authority (http://www.kyst.dk).

A new species of *Rhysocaryoxylon* (Juglandaceae) from the Lower Eocene Fur Formation of Mors island (northwest Jutland, Denmark)

JAKUB SAKALA & VLADIMÍR GRYC

A new species of the morphogenus *Rhysocaryoxylon* Dupéron (*Rhysocaryoxylon madsenii* Sakala & Gryc sp. nov.) is described from the Lower Eocene of the Fur Formation, Mors island, Denmark. This permineralized fossil angiosperm wood is semi-ring-porous with distinct growth ring boundaries, vessels solitary or in radial multiples of 2–5, perforation plates exclusively simple, and tyloses abundant. Rays are 1–5-seriate and heterocellular with a body composed of procumbent cells and 1–4 rows of upright marginal cells. Axial parenchyma is reticulate with numerous prismatic crystals both in chambered cells and idioblasts, forming long chains up to 12 cells high. Its equivocal botanical affinities within the family Juglandaceae are discussed.

Jakub Sakala [rade@natur.cuni.cz], Charles University in Prague, Faculty of Science, Institute of Geology and Palaeontology, Albertov 6, 128 43 Praha, Czech Republic.
Vladimír Gryc [gryc@mendelu.cz], Mendel University in Brno, Faculty of Forestry and Wood Technology, Department of Wood Science, Zemědělská 3, 613 00 Brno, Czech Republic.
Corresponding author: Jakub Sakala

The Fur Formation with interbedded argillaceous diatomites and ash layers has an extensive history in the Danish geological literature (see Pedersen & Surlyk 1983 for geological overview and historical background). Although its age has been a matter of controversy, it is today generally considered to be Early Eocene in age (Pedersen *et al.* 2004). The sediments are often fossiliferous. Manchester & Wheeler (2006) noted several taxa of fossil plants from quarries on the island of Mors, including the remains of fruits, leaves and wood. The present paper provides a detailed wood anatomical study of one part (2 × 2 × 3 cm) of a bigger fragment (11.5 × 10 × 5.5 cm) of a stem which was originally at least 30 cm in diameter (estimate by Manchester & Wheeler (2006) based on growth ring curvature). The specimen was found in 2005 by Henrik Madsen in the Ejerslev Moler open pit mine (see Pedersen *et al.* 2004, Fig. 1B) on the east coast of Mors (Fig. 1) and preliminary studies of this fossil were undertaken by Manchester & Wheeler (2006). They presented two hypotheses for the fossil wood: it either represents a relatively early occurrence of *Juglans* or belongs to an extinct juglandaceous type. The aim of our study is to indicate which one of these two hypotheses is more likely.

Fig. 1. Map of Denmark showing the position of the island of Mors (dark grey) and the fossiliferous site of the Ejerslev Moler open pit mine (white star in inset).

Material and methods

Three thin sections currently housed in the palaeobotanical collections in the Florida Museum of Natural History, Gainesville, USA, were studied. They had been prepared following standard techniques and were observed under optical microscopes Olympus BX–51 and Leica DM2000 in normal transmitted light. The anatomical description is in accordance with the IAWA Hardwood List (IAWA Committee 1989).

Systematic Palaeobotany

Juglandaceae DC. ex Perleb, nom. cons.
Rhysocaryoxylon Dupéron
Rhysocaryoxylon madsenii Sakala & Gryc, sp. nov. (Figs 2, 3)

Diagnosis: Heteroxylous semi-ring-porous wood with distinct growth ring boundaries. Vessels are solitary or in radial multiples of 2–5, and can exceed 300 μm in tangential diameter, perforation plates are exclusively simple, tyloses abundant. Rays are 1–5-seriate and heterocellular with body composed of procumbent cells and 1–4 marginal rows of upright cells. Axial parenchyma is reticulate with numerous prismatic crystals both in chambered cells and idioblasts, forming long (up to 12 cells high) vertical chains.

Holotype designated here: One piece of wood (No. UF 19079 – 49102) and three thin sections (49102tr, 49102tg, 49102rd), all housed in the palaeobotanical collections of the Florida Museum of Natural History, Gainesville, USA.
Locus typicus: Ejerslev Moler Pit, Mors island, northwest Jutland, Denmark.
Stratum typicum: Lower Eocene of the Fur Formation.
Etymology: Named for the finder Henrik Madsen.
Occurrence: Known from the type locality only.

Macroscopic description: One silicified piece of fossil wood, dimensions of the analyzed sample 2 × 2 × 3 cm, colour brown-black, interpreted as a fragment of a trunk.

Microscopic description: Growth rings: present. Wood: semi-ring-porous (Fig. 3A). Vessels: 4–6 per square mm, solitary (36 %) or in radial multiples of 2–5 (generally 2–3, Fig. 2A); tangential diameter of early vessels 160–240–365 μm (minimum–mean–maximum), latewood vessels 80–140–280 μm, vessels in the earlywood are distinctly larger than those in the latewood (gradual change), outline of solitary vessels round to radially elongated (oval) in transverse section; vessel element length 426–642 μm (mean 522 μm); vessels walls are thick (about 5 μm); perforation plates are exclusively simple, end walls oblique; tyloses are abundant (Fig. 3F); intervessel pits alternate, polygonal in shape (Fig. 3C), medium in size (7–10 μm). Rays: heterocellular up to 5 cells wide (18–98, mean 54 μm), commonly 2–5 seriate (Figs 2B, 3G) and 128–573 μm high (mean 281 μm), uniseriate rays are rare, body of multiseriate rays is composed of procumbent and square cells with 1–4 rows of upright marginal cells (Fig. 3E); no crystalliferous elements observed; vessel-ray pits not observed. Axial parenchyma: reticulate with numerous prismatic crystals both in chambered cells and idioblasts forming long (up to 12 cells high) vertical chains (Fig. 3D), rarely paratracheal vasicentric (Fig. 3B). Fibres: undistinguishable pits, non-septate; walls medium-thick.

Discussion

The anatomy of this fossil wood was originally described by Manchester & Wheeler (2006) in Prague where they clearly showed its juglandaceous affinity and resemblance to the genus *Juglans*. The wood of Juglandaceae, both extant and extinct, has been reviewed several times (e.g., Kribs 1927; Heimsch
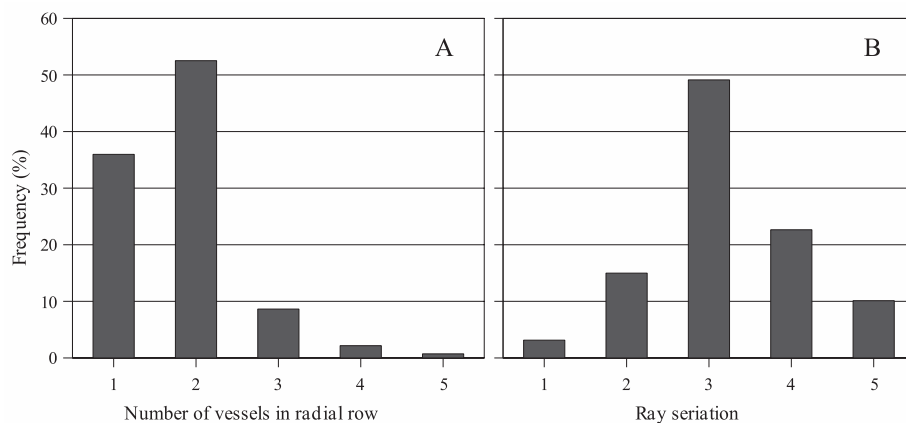
Fig. 2. **A**, frequency of solitary vessels and vessels in radial multiples of 2, 3, 4, and 5. **B**, ray seriation (ray width in cell numbers) in the holotype sample of *Rhysocaryoxylon madsenii*.

& Wetmore 1939; Stark 1953; Müller-Stoll & Mädel 1960; Manchester 1987; Dupéron 1988; Manchester & Wheeler 1993; Blokhina 2007; Cao 2008; InsideWood 2004–onwards) so the botanical affinities of our fossil wood can be ascertained with a good degree of certainty. As already stated by Manchester & Wheeler (2006), the lack of scalariform perforations distinguishes our fossil sample from wood of the subfamily Engelhardioideae Iljinskaya *sensu* Manos & Stone (2001), both modern (genera *Engelhardia*, *Oreomunnea*, *Alfaroa* and ?*Alfaropsis*) and fossil (morphogenus *Engelhardioxylon* defined by Manchester 1983). The lack of crystals in idioblasts in ray parenchyma sets our wood apart from the extant *Platycarya* and fossil *Clarnoxylon* defined by Manchester & Wheeler (1993); *Platycarya* also exhibits ring-porous wood with vasicentric tracheids and spiral thickening in vasicentric tracheids and small vessels (Heimsch & Wetmore 1939). The long mostly

1–3-seriate tangential lines of axial parenchyma with crystals differentiate our wood from *Pterocarya* and the sections *Cardiocaryon*, *Trachycaryon* and *Juglans* of the genus *Juglans* (Dupéron 1988 p. 274). *Carya* generally has very thick-walled smaller vessels, and if crystalliferous, crystals are solitary (or only a few) and placed in the significantly enlarged axial parenchyma cells (idioblasts). Our wood with long (up to 8–10 cells high) crystalliferous chains in axial parenchyma most closely resembles that of the section *Rhysocaryon* of *Juglans*, i.e., the so-called 'black walnuts'. Its features point to a particular position different from both wood anatomical groups in the section *Rhysocaryon*, i.e., north temperate black walnuts (semi-ring porous wood, enlarged axial parenchyma cells with crystals) and tropical black walnuts (absence of reticulate thickening, long crystalliferous chains in axial parenchyma with > 5 crystals), as distinguished by Miller (1976 p.
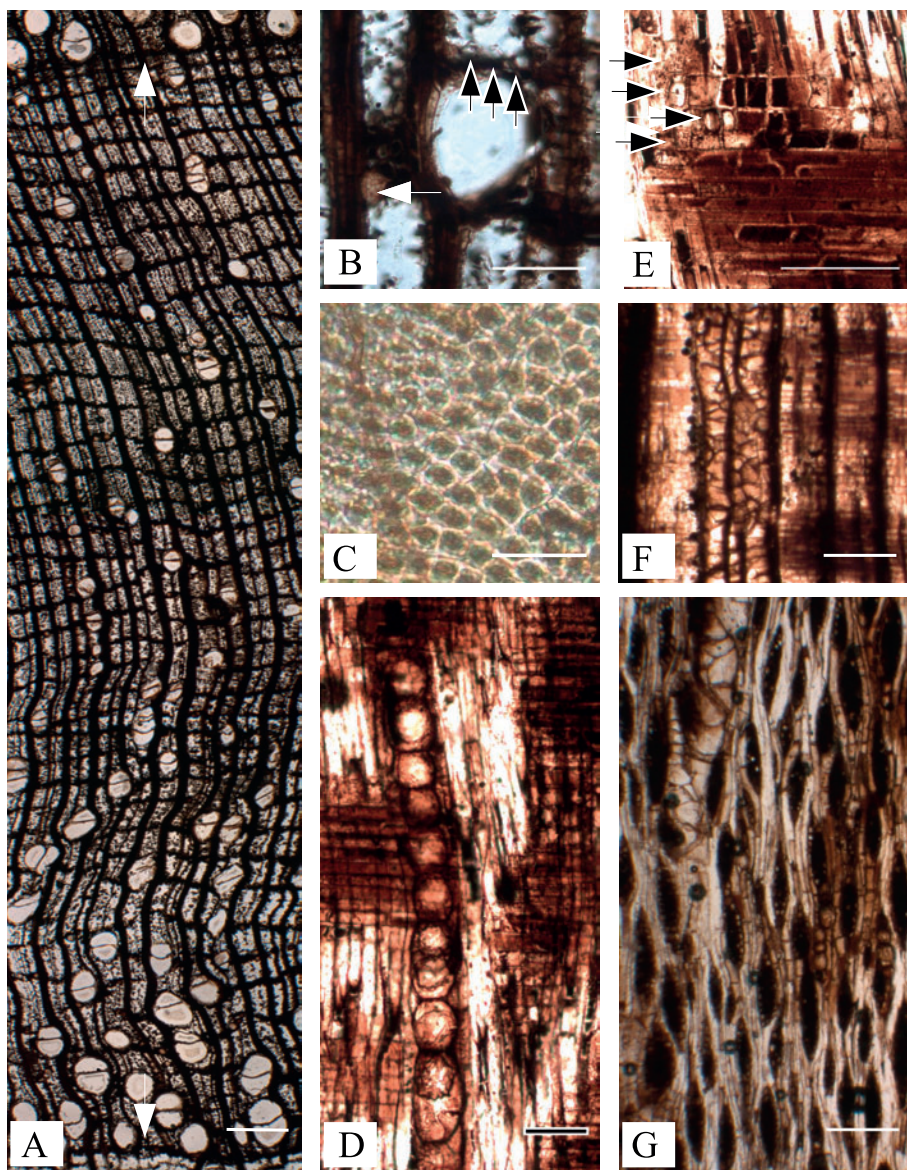
Fig. 3. *Rhysocaryoxylon madsenii*. **A**, semi-ring-porous wood with distinct growth ring boundaries (white arrows), TS. **B**, vessel surrounded by paratracheal vasicentric parenchyma (black arrows) and crystals in reticulate axial parenchyma (white arrow), TS. **C**, alternate intervessel pits, TLS. **D**, part of a 12 cell high crystalliferous chain in axial parenchyma with both chambered cells and idioblasts (at the bottom), RLS. **E**, heterocellular ray with four marginal rows of upright cells (black arrows), RLS. **F**, general view with abundant tyloses within vessels, RLS. **G**, general view with rays, TLS. Scale bars = 25 μm in C; 150 μm in B, D, E; 250 μm in F, G; 500 μm in A. RLS = radial longitudinal section; TLS = tangential longitudinal section; TS = transverse section.

375) based on extant material. In fact, it seems that our wood belongs to an extinct type, not really attributable to a living group, mainly with respect to its unique crystalliferous axial parenchyma with long vertical chains of both chambered cells (shorter, slightly enlarged, rather typical of *Juglans*) and idioblasts (as long as normal axial parenchyma cells but significantly larger, rather typical of *Carya*). It must be stressed that a uniqueness of the crystalliferous parenchyma that we observed in our wood has already been recorded by Selmeier (1995) in *Eucaryoxylon castellanii* from the Eocene of France. However, Selmeier's (1995) climatically induced explanation, i.e. more frequent crystals occur in tropical species (see Miller 1976 p. 375) cannot be completely adopted for our wood which in contrast to *Eucaryoxylon castellanii* is semi-ring-porous with distinct growth ring boundaries.

Despite the presence of idioblasts, our wood is attributable to the morphogenus *Rhysocaryoxylon* which was defined by Dupéron (1988 p. 263) to accommodate fossil woods close to the section *Rhysocaryon* of *Juglans*. *Rhysocaryoxylon* was nomenclaturally superfluous when published and therefore illegitimate from the nomenclatural point of view, so either a proposal must be prepared for Taxon to conserve the name *Rhysocaryoxylon* against *Caryojuglandoxylon*, or new combinations must be published in the future. Nine species have so far been assigned to *Rhysocaryoxylon* (Gregory *et al.* 2009): type species *R. schenkii* (Felix) Dupéron, *R. triebelli* (Caspary) Dupéron, *R. tertiarum* (Prakash & Barghoorn) Dupéron, *R. fryxellii* (Prakash & Barghoorn) Dupéron, *R. caucasicum* (Gaivoronsky) Dupéron, *R. pilinyense* (Greguss) Dupéron, *R. pravalense* S. Iamandei & E. Iamandei, *R. ocii* S. Iamandei & E. Iamandei and *R. transylvanicum* S. Iamandei & E. Iamandei. The type species was originally described by Felix (1884) and later reinvestigated in more detail by Müller-Stoll & Mädel (1960). This wood is however very different from our new species in having only very narrow 1–2(3)-seriate rays. Similarly, *R. triebelli* also has very narrow rays and, moreover, presents smaller vessels (up to 200 μm) and very long chains (up to 20 cells) of crystalliferous parenchyma (Müller-Stoll & Mädel 1960; Van der Burgh 1973). Wheeler & Dillhoff (2009) recently reviewed the type species of both *R. tertiarum* and *R. fryxellii*, which had originally been described by Prakash & Barghoorn (1961a, b) from the Middle Miocene Vantage Flora (Washington, USA). Although *R. tertiarum* is quite similar to our wood, both *R. tertiarum* and *R. fryxellii* have narrower homocellular rays which differentiate them from *R. madsenii*. *Rhysocaryoxylon caucasicum* is also very different in that its rays are only 1–2-seriate (Gaivoronsky 1962). Another species *R. pilinyense* was originally described by Greguss (1969). Thin sections of the type

species are deposited in the Botanical Department of the Hungarian Natural History Museum in Budapest under No. 2008.222.3., and they were recently studied by the first author. This species differs from ours by diffuse-porous wood with thinner rays and generally smaller vessels with thicker walls. Finally, there are three species of *Rhysocaryoxylon* described by Iamandei & Iamandei (2002, 2003) which can also be differentiated by their significantly smaller vessels with a tangential diameter up to 126 μm, narrower 2–3-seriate rays and not very obvious tangential bands of axial parenchyma in *R. ocii* and *R. transylvanicum*. A unique combination of three anatomical features in our wood sample, namely, relatively big vessels (which can exceed 300 μm), heterocellular rays 1–5 cells wide, and long chains (up to 12 cells) of crystalliferous parenchyma with chambered and significantly enlarged cells (idioblasts), allows its recognition as a new species within the morphogenus *Rhysocaryoxylon*: *R. madsenii* Sakala & Gryc, sp. nov.

Conclusions

Manchester & Wheeler (2006) preliminarily described this fossil wood and proposed that it might either represent a relatively early occurrence of *Juglans* or an extinct type related to juglandaceous fruit genera such as *Juglandicarya* or *Cruciptera*. Our detailed microscopical description clearly shows that the later hypothesis is the more plausible. The particularity of crystalliferous axial parenchyma does not allow us to conclude a direct similarity between our fossil wood and the genus *Juglans* as we know it today. It rather points to an extinct type, which is not in contradiction with its Early Eocene age. In support of this conclusion is the observation by S. R. Manchester that nuts of the section *Rhysocaryon* of *Juglans* (black walnuts), although morphologically distinctive and thick-walled (likely to be preserved), seem to be missing from the European fossil record (Manchester, personal communication 2011).

Acknowledgments

References

Blokhina, N.I. 2007: Fossil wood of the Juglandaceae: Some questions of taxonomy, evolution, and phylogeny in the family based on wood anatomy. Paleontological Journal 41, 1040–1053.

Cao, N. 2008: Analyse à trois éléments et anatomie du bois des Fagales Engl., PhD Thesis, 239 pp. Paris: Muséum national d'Histoire naturelle.

Dupéron, J. 1988: Les bois fossiles de Juglandaceae: inventaire et révision. Review of Palaeobotany and Palynology 53, 251–282.

Felix, J. 1884: Die Holzopale Ungarns in palaeophytologischer Hinsicht. Mitteilungen aus dem Jahrbuch der königlichen ungarischen geologischen Anstalt 7, 1–44.

Gaivoronsky, V.G. 1962: A wood of walnut from the Middle Oligocene of the Western Caucasus. Palaeontological Journal 1962 (2), 170–173 (in Russian).

Gregory, M., Poole, I. & Wheeler, E.A. 2009: Fossil dicot wood names – an annotated list with full bibliography. IAWA Journal, Supplement 6, 1–220.

Greguss, P. 1969: Tertiary angiosperm woods in Hungary, 151 pp. Budapest: Akadémiai Kiadó.

Heimsch, C. & Wetmore, R.H. 1939: The significance of wood anatomy in the taxonomy of the Juglandaceae. American Journal of Botany 26, 651–660.

Iamandei, S. & Iamandei, E. 2002: New Juglandaceous fossil wood in the Middle Miocene lignoflora of Prăvăleni-Ociu (South Apuseni). Acta Palaeontologica Romaniae 3, 185–198.

Iamandei, S. & Iamandei, E. 2003: A new Juglandaceous fossil wood from the Badenian of Prăvăleni-Ociu (South Apuseni). Studii şi Cercetări de Geologie 48, 91–98.

IAWA Committee 1989: IAWA list of microscopic features for hardwood identification. IAWA Bulletin new series 10, 219–232.

InsideWood 2004–onwards. Published on the Internet. http://insidewood.lib.ncsu.edu/search [May 27, 2011].

Kribs, D.A. 1927: Comparative anatomy of the woods of the Juglandaceae. Tropical Woods 12, 16–21.

Manchester, S.R. 1983: Fossil wood of the Engelhardieae (Juglandaceae) from the Eocene of North-America: *Engelhardioxylon* gen. nov. Botanical Gazette 114, 157–163.

Manchester, S.R. 1987: The fossil history of the Juglandaceae. Monographs in Systematic Botany from the Missouri Botanical Garden 21, 1–137.

Manchester, S.R. & Wheeler, E.A. 1993: Extinct juglandaceous wood from the Eocene of Oregon and its implications for xylem evolution in the Juglandaceae. IAWA Journal 14, 103–111.

Manchester, S.R. & Wheeler, E.A. 2006: Wood of Juglandaceae from the Early Eocene of Mors Island, Denmark. Abstracts of the 7th European palaeobotany-palynology conference at Prague, Czech Republic, 6–12 September 2006, 87. (http://www.conference.cz/eppc2006/final_programme.pdf)

Manos, P.S. & Stone, D.E. 2001: Evolution, Phylogeny, and Systematics of the Juglandaceae. Annals of the Missouri Botanical Garden 88, 231–269.

Miller, R.B. 1976: Wood Anatomy and Identification of Species of *Juglans*. Botanical Gazette 137, 368–377.

Müller-Stoll, W.R. & Mädel, E. 1960: Juglandaceen-Hölzer aus dem Tertiär des pannonischen Beckens. Senckenbergiana lethaea 41, 255–295.

Pedersen, G.K. & Surlyk, F. 1983: The Fur Formation, a late Paleocene ash-bearing diatomite from northern Denmark. Bulletin of the Geological Society of Denmark 32, 43–65.

Pedersen, G.K., Pedersen, S.A.S., Steffensen, J. & Pedersen, C.S. 2004: Clay content of a clayey diatomite, the Early Eocene Fur Formation, Denmark. Bulletin of the Geological Society of Denmark 51, 159–177.

Prakash, U. & Barghoorn, E.S. 1961a: Miocene fossil woods from the Columbia basalts of Central Washington. Journal of the Arnold Arboretum 42, 165–203.

Prakash, U. & Barghoorn, E.S. 1961b: Miocene fossil woods from the Columbia basalts of Central Washington, II. Journal of the Arnold Arboretum 42, 347–362.

Selmeier, A. 1995: *Eucaryoxylon castellanii* n. sp., (Juglandaceae), a silicified wood from the Eocene of Castellane, France. Mitteilungen der Bayerischen Staatssammlung für Paläontologie und historische Geologie 35, 169–192.

Stark, E.W. 1953: Wood anatomy of the Juglandaceae indigenous to the United States. Purdue Agricultural Experiment Station Bulletin 595, 1–42.

Van der Burgh, J. 1973: Hölzer der niederrheinischen Braunkohlenformation, 2. Hölzer der Braunkohlengruben „Maria Theresia" zu Herzogenrath, „Zukunft West" zu Eschweiler und „Victor" (Zülpich Mitte) zu Zülpich. Nebst einer systematisch-anatomischen Bearbeitung der Gattung *Pinus* L. Review of Palaeobotany and Palynology 15, 73–275.

Wheeler, E.A. & Dillhoff, T.A. 2009: The Middle Miocene Wood Flora of Vantage, Washington, USA. IAWA Journal, Supplement 7, 1–101.

New theropod, thyreophoran, and small sauropod tracks from the Middle Jurassic Bagå Formation, Bornholm, Denmark

JESPER MILÀN

Three new dinosaur tracks are described from the Middle Jurassic Bagå Formation of Bornholm, Denmark. The tracks are all preserved as natural casts on the underside of fluvial sandstone blocks originating from the old Hasle Klinkefabrik's clay pit, now called Pyritsøen. The new tracks are from a medium-sized theropod, a thyreophoran, and a small sauropod. Together with a thyreophoran track and large sauropod tracks described in 2005, the Middle Jurassic dinosaur fauna of Bornholm now comprises theropods, two sizes of sauropods and at least one type of thyreophoran dinosaur. This is important additional data for the very scarce Middle Jurassic dinosaurian skeletal record of Europe.

Jesper Milàn [jesperm@oesm.dk], GeomuseumFaxe, Østsjællands Museum, Østervej 2, DK-4640 Faxe, Denmark. Also Department of Geography and Geology, University of Copenhagen, Øster Voldgade 10, DK-1350 Copenhagen K, Denmark.

Remains of Mesozoic terrestrial vertebrates are scarce in Denmark and have so far only been found in the few Mesozoic outcrops along the west and southwest coast of the Baltic island of Bornholm (Fig. 1). Loose teeth of small and large dromaeosaurs (Bonde & Christiansen 2003; Lindgren *et al*. 2008), and a possible sauropod tooth (Christiansen & Bonde 2003) have been found in the Lower Cretaceous (Berriasian) Rabekke, Robbedale and Jydegaard Formations together with a rich microvertebrate fauna comprising remains of turtles, crocodilians, amphibians, primitive lizards, and a tooth from a multituberculate mammal (Bonde 2004; Lindgren *et al*. 2004, 2008; Rees *et al*. 2005; Schwarz-Wings *et al*. 2009). Turtle fragments together with fish remains are known from the Berriasian Jydegård Formation (Noe-Nygaard *et al*. 1987; Noe-Nygaard & Surlyk 1988).

Tracks of a large sauropod and a small thyreophoran dinosaur were found in the Middle Jurassic Bagå Formation in 2004 (Milàn & Bromley 2005) and recently a dinosaur trampleground and possible lungfish aestivation burrows were described from the lowermost Cretaceous Rabekke Formation (Surlyk *et al*. 2008).

Dinosaur remains are more commonly encountered in the southern part of Sweden, where numerous dinosaur tracks and trackways of theropod dinosaurs, a single thyreophoran dinosaur track, and a few skeletal remains are known from the Rhaetian – Hettangian Höganäs Formation (Bölau 1952, 1954; Pleijel 1975; Ahlberg & Siverson 1991; Gierlinski & Ahlberg 1994; Milàn & Gierlinski 2004). The Campanian Åsen locality in the Kristianstad Basin has yielded remains of neoceratopsian dinosaurs (Lindgren *et al*. 2007).

After the initial discovery of dinosaur tracks in the Bagå Formation in 2004 (Milàn & Bromley 2005), the area has on several occasions been thoroughly searched for more track material. A large block with three distorted, superimposed tracks was originally found together with the other tracks in 2004 but was not described at that time. During 2005–2006 two new partially preserved tracks were found, and in 2010 a third new track was found. This paper describes the new track material from the Middle Jurassic Bagå Formation, which adds important new information about the composition of the Middle Jurassic dinosaur fauna of Bornholm and Scania.

Geological setting

The type section of the Bagå Formation is the Bagå Graven of the Hasle Klinkefabrik at Sorthat (Gravesen *et al.* 1982; Michelsen *et al.* 2003; Nielsen *et al.* 2010) (Fig. 1), and includes the coal-bearing clays and sands in the Rønne-Hasle Fault Block of southwest Bornholm. These beds had been traditionally named the Levka, Sorthat and Bagå beds (Gry 1969). During a revision partly based on well-core material (Michelsen *et al.* 2003), the lower part of the Bagå Formation, showing evidence of marine influence, was separated as the Sorthat Formation, thereby leaving the revised Bagå Formation entirely composed of non-marine sediments.

The Bagå Formation comprises thick grey clay, dark to black coaly clays with rootlets, coal beds, and medium- to fine-grained, cross-bedded or laminated sandstone. In the upper part, poorly sorted, muddy and pebbly sandstone beds locally contain boulders of weathered granite, and deposition is interpreted to have taken place in lakes and swamps, small crevasse channels, lacustrine deltas and fluvial channels (Gravesen *et al.* 1982; Koppelhus & Nielsen 1994; Michelsen *et al.* 2003; Nielsen *et al.* 2010). The age of the Bagå Formation is Middle Jurassic, Bajocian–Bathonian (Gry 1969; Koppelhus & Nielsen 1994).

The dinosaur tracks described by Milàn & Bromley (2005) and the new tracks described here were found as natural casts (sensu Lockley 1991) on the underside of slabs of coarse-grained sandstone beds that were broken up and dumped on the adjacent beach during quarrying for clay. Today quarrying has ceased and the clay pit, now known as Pyritsøen, has become water-filled hindering in situ studies of the track-bearing layers.

New dinosaur tracks from the Bagå Formation

In the following, the institutional abbreviation MGUH means the Natural History Museum of Denmark.

Theropod tracks

The specimens are preserved as natural casts on the underside of a sandstone slab measuring 40×43 cm, with an average thickness of 11 cm (MGUH 29290). The slab was found by Stig Peberholm in 2010 and was lying loose on the beach at Pyritsøen (Fig. 1). The cast of the track is 25 cm long, 19 cm wide and about 3 cm deep. The track is mesaxonic, tridactyl and almost complete except for the tip of one toe (Fig. 2). The casts of the digits are long and terminate in impressions of sharp claws. A faint indication of digital pads is visible on the digits. The divarication angles between the middle and outer digits are 19° and 17°, giving at total divarication angle of 36° (Fig. 2B). The middle digit protrudes forward relative to the outer digits, and the
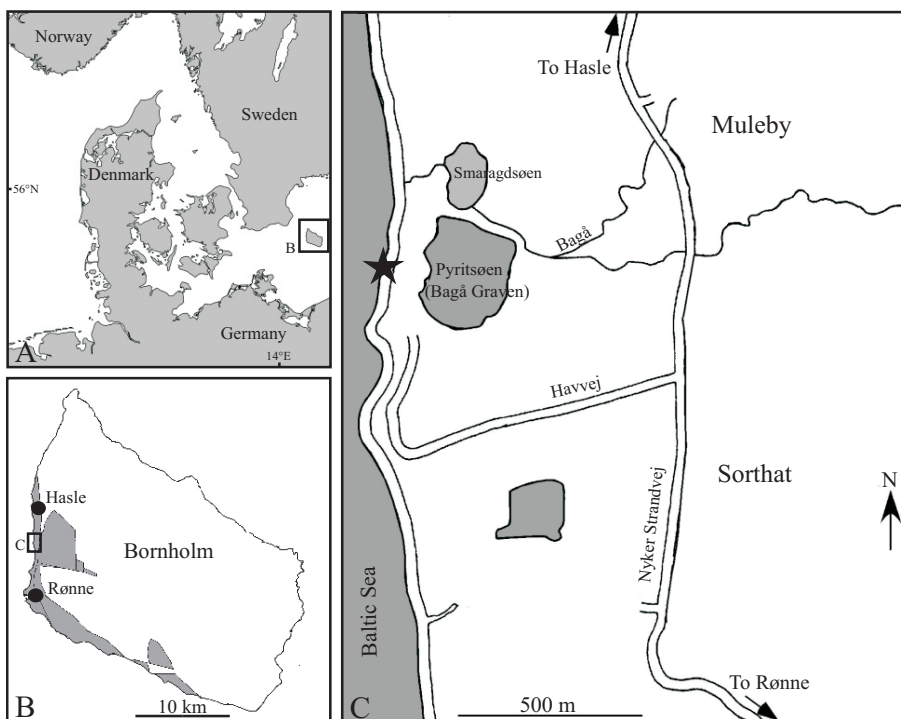
Fig. 1. Location maps. **A**, Bornholm is situated in the Baltic Sea south of Sweden. **B**, map of Bornholm with Mesozoic outcrops indicated in grey, based on Jensen & Hamann (1989). Rectangle marks the location of the Bagå Formation by Pyritsøen, between Hasle and Rønne. **C**, dinosaur track locality at Pyritsøen, sited near the villages of Muleby and Sorthat. Asterisk marks the position on the beach where the specimens were collected. After Milàn & Bromley (2005).

cast of its claw is slightly directed to the left. One of the outer digits extends further backwards than the middle digit and the outer digit on the opposite side (Fig. 2B). The track walls of the digit casts are sharply defined relative to the tracking surface. A second vaguely defined tridactyl track is present beside it, but due to its shallowness and poorly defined outline it is hard to get exact measurements from it.

Interpretation. Theropod tracks are generally longer than wide, with elongated narrow digits terminating in sharp claw impressions and a low divarication angle between the outer digits. The proximal pad impressions of digit IV extend further back than those of digits III and II, giving the tracks a distinct asymmetric 'heel' area. The claw impression of the middle digit III is in many cases directed inward toward the midline of the trackway (Moratalla *et al.* 1988; Thulborn 1990; Lockley 1991; Farlow *et al.* 2000). This identifies the new-found track as the cast of a left foot of a theropod dinosaur.

The hip height of the track maker can be estimated from the foot length. Thulborn (1990) estimated the hip height of theropods with a foot length less than 25 cm to be 4.5 times the foot length and for theropods
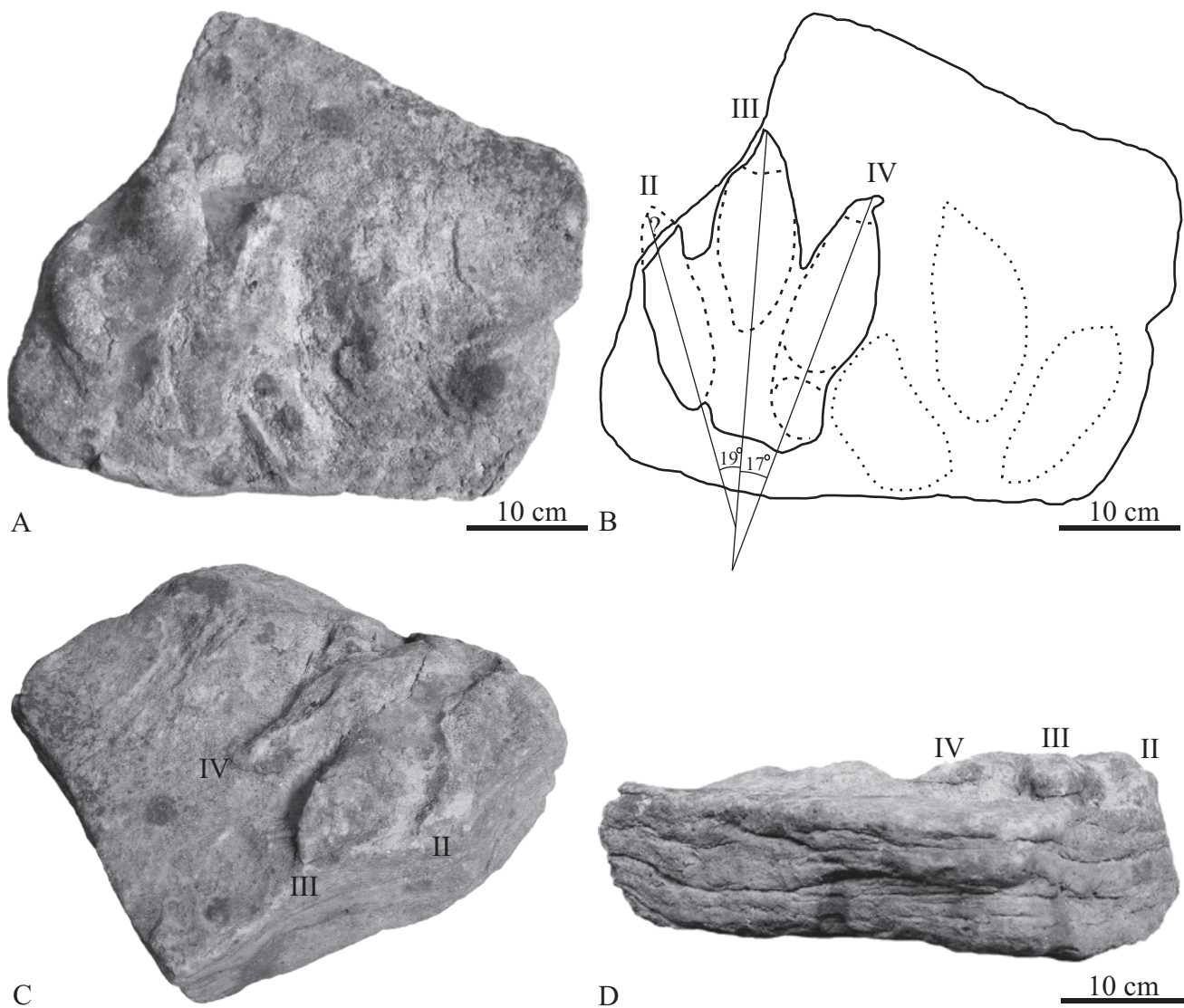
Fig. 2. Sandstone slab containing the natural cast of a well-preserved theropod track and a second poorly preserved track (MGUH 29290). **A**, the well-preserved track is complete except for the termination of digit II; the less well-preserved track is situated beside it. **B**, interpretative drawing of the block. Digital pads and the interpreted extension of digit II are indicated by broken lines. The second poorly defined track is indicated by dotted lines. **C**, oblique frontal view of the slab, with good view of the sharp claws of the digits. **D**, frontal view of the slab through the long axis of digit III. Notice the well-defined track walls of the digits, and that the cast of digit III is slightly deformed towards digit IV. The second less well-preserved track to the left has a much lower and poorly defined relief.

New theropod, thyreophoran, and small sauropod tracks from the Middle Jurassic Bagå Formation · 53
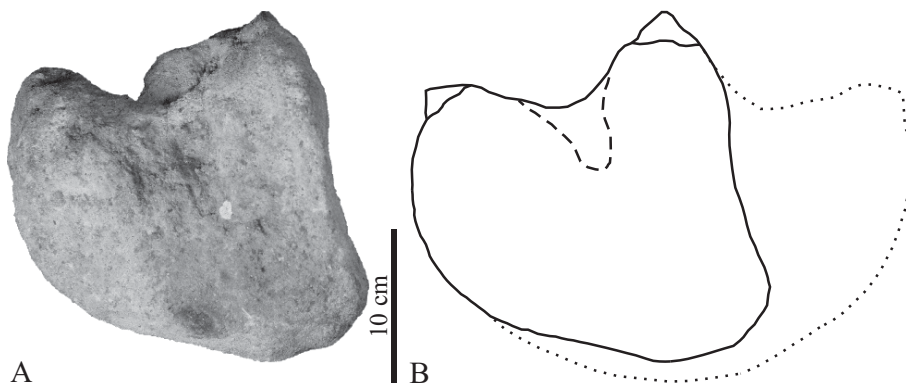
Fig. 3. Partial natural cast of a thyreophoran pes track (MGUH 29291). **A**, the preserved part comprises casts of two well-preserved digit impressions with short triangular claws. **B**, interpretative drawing of the specimen, where the missing digit is indicated by a broken line. The reconstruction is based on the shape of the thyreophoran ichnogenus *Stegopodus* (Gierlinski & Sabath 2008).

with a foot length in excess of 25 cm to be 4.9 times the foot length. As the specimen from Bornholm is 25 cm long, the estimated hip height of the animal is between 112 and 122 cm, and the estimated total body length is around 4 m. The cast of digit III is sideways deformed towards the right and the cast of digit II is deformed towards the left, as if the digits have diverged from the tracking surface to the bottom to the track. The outward deformation of digit III is similar to that found in Late Triassic, Early and Late Jurassic theropod tracks (Milàn *et al.* 2006), while the outward deformation of digit II is not typical of fossil tracks. However, this is observed in tracks of an extant emu, *Dromaius novaehollandiae*, when accelerating from a walk to a run. Here digits II and III diverge as the foot is pressed down through the sediment (Milàn 2006).

The second vaguely defined track on the slab is also tridactyl, and the general dimensions also suggest a theropod origin. However, the low relief and undefined digit impressions of the track, plus the fact that one of the digit impressions disappear below the other track, suggest the second track to be an under-track (Milan & Bromley 2006, 2008) originating from a stratigraphically higher level.

Thyreophoran track

The specimen was found by Gunver Krarup Pedersen in 2005 and consists of an isolated, partial natural cast consisting of two well-preserved digit impressions (MGUH 29291). The cast is 19 cm wide and 21.5 cm long. A fresh break limits the cast along the outer edge of the right digit. The casts of the digits are well-defined, very short and broad and have preserved evidence of short triangular claws (Fig. 3). Between the two digits casts is preserved a sandstone cast of a part of the original tracking surface. Here the angle
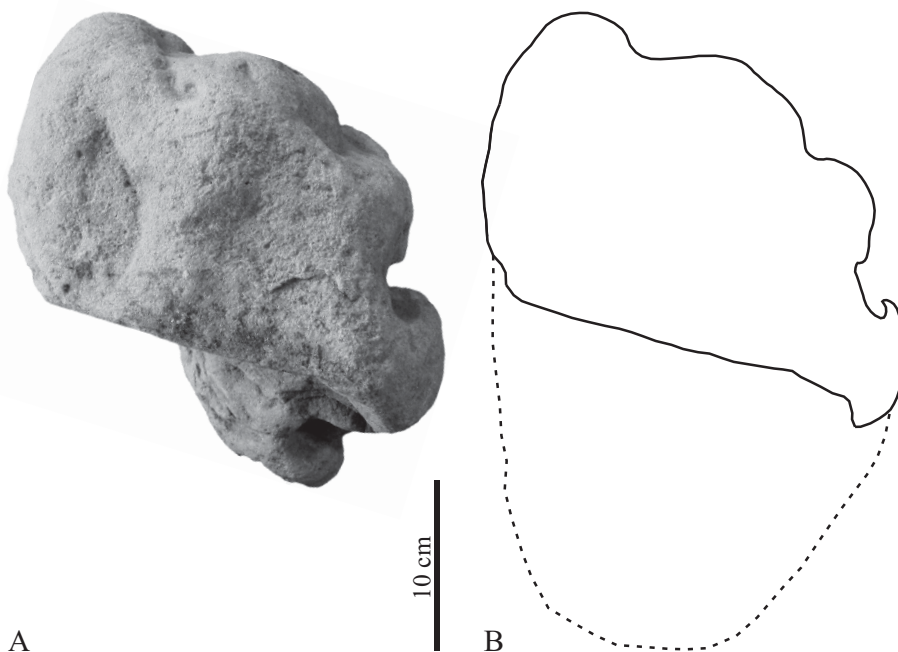
Fig. 4. Natural cast of a small sauropod track (MGUH 29292). **A**, only the front half with the casts of four short, blunt digits is preserved. **B**, interpretative drawing of the track, with the extent of the missing part indicated by a broken line. The reconstruction is based on an average of the two sauropod pes tracks from the same locality previously described by Milàn & Bromley (2005).

between the original tracking surface and the track walls is sharply defined.

Interpretation. The morphology of the two complete, broad digits with short triangular claws (Fig. 3) fits the morphology of the thyreophoran ichnogenus *Stegopodus* from the Middle Jurassic of Morocco and Upper Jurassic of Utah (Lockley & Hunt 1998; Gierlinski & Sabath 2008; Gierlinski *et al.* 2009). *Stegopodus* is tridactyl, with very short, broad and rounded digits, and assuming the cast is broken and the missing part represents another digit, the track can be interpreted as a *Stegopodus* specimen and thus represents a pes from a thyreophoran dinosaur. The sharply defined outline of the track and the well-defined casts of the claws demonstrate that it is a cast of a true track, and not an undertrack (Milàn & Bromley 2006, 2008).

Sauropod track

The specimen is a natural cast representing the front half of a track which is entaxonic and displays four short, blunt casts of digits (MGUH 29292). Without the missing part, the cast measures 17.5 cm in length and 31 cm at the widest across the digit impressions (Fig. 4). The impressions of the digits are outward rotated relative to the orientation of the foot. The cast has an average depth of 11 cm, deepest at the digit impressions.

Interpretation. The short blunt digits, and the shape of the cast, with the interpreted missing heel part added, are consistent with the morphology of a sauropod pes track, which is characterized by being elongated, entaxonic, and can display from three to five short
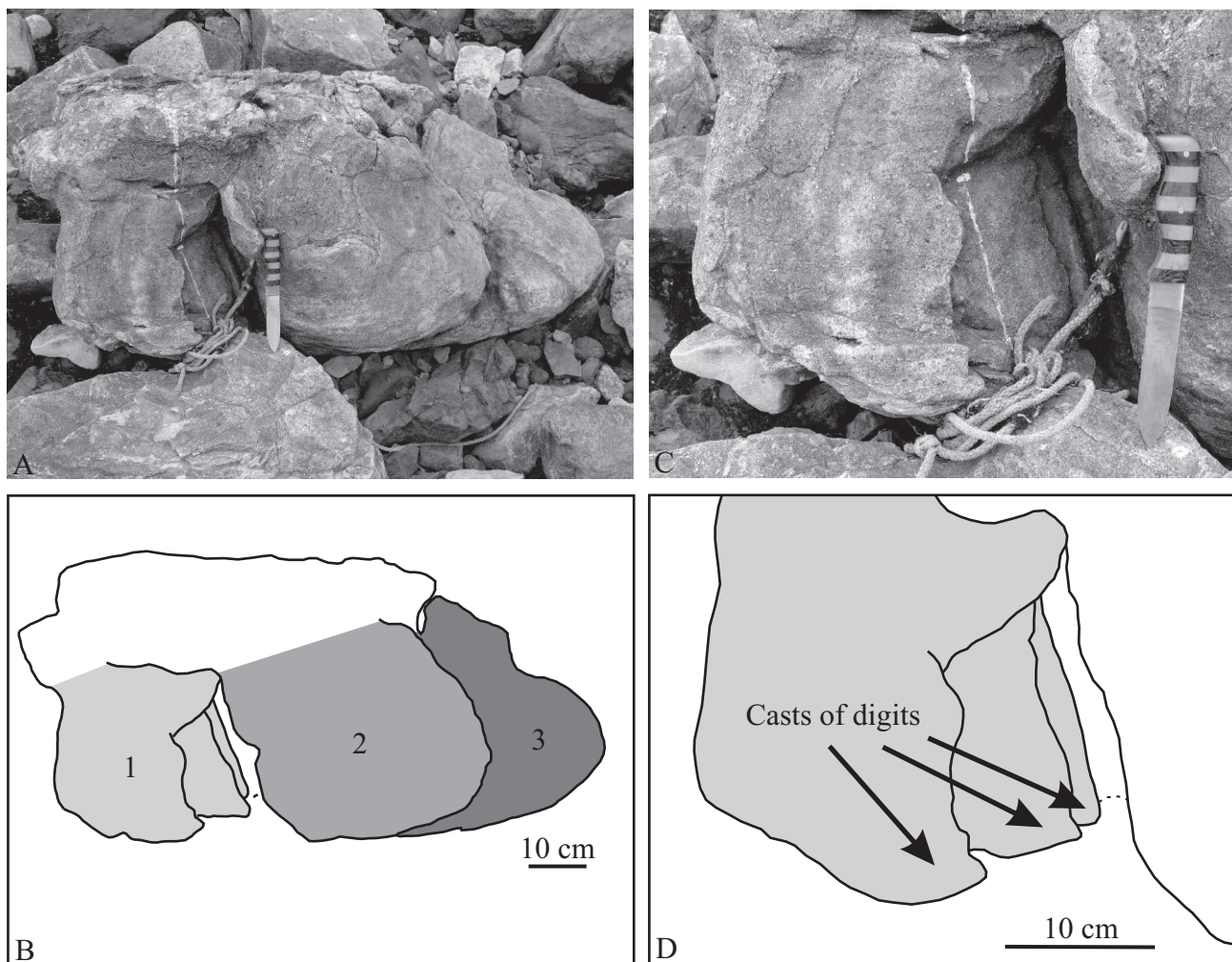
Fig. 5. Block with the natural casts of three partly superimposed tracks. **A**, photo of the whole block. The casts are seen from the side and are directed downwards. Two of the tracks only appear as indistinct, flat-bottomed casts. **B**, interpretative drawing of the block, with the three casts indicated by different shades of grey. Cast number 1 is better preserved than 2 and 3. **C**, close up photo of cast 1, showing the well-defined casts of three short, sharp digits being dragged deep down through the sediment. **D**, interpretative drawing of cast 1 with arrows indicating the casts of the digits. Scale bar on knife handle equals 10 cm.

outward rotated digit impressions (Thulborn 1990; Lockley 1991; Lockley *et al.* 1994; Wright 2005). The two previously described sauropod pes tracks (Milàn & Bromley 2005) measured respectively 68 and 69 cm in length and 48 an 45 cm in width, which gives a length/width ratio of approximately 1.5. When this ratio is applied to the new track it gives an estimated length of 46 cm, showing that the track originates from a significantly smaller individual.

Block with superimposed tracks

A large block consisting of natural casts of three partly superimposed tracks was found on the beach in 2005 (Fig. 5). Two of the track casts appear as featureless, flat-bottomed casts approximately 40 and 50 cm in diameter. A third cast of a track is better preserved, showing steep, well-defined trackwalls and the visible side of the cast shows clear casts of two short, sharp digits being dragged through the sediment (Fig. 5B). The outline of the track cast is elliptical, 28 cm long and approximately 40 cm wide. Unfortunately, the block broke up during transportation, destroying most of the preserved features and hindering further measurement. The remains of the block are stored at the visitor centre NaturBornholm.

Interpretation. The two poorly defined casts do not show any features that can easily attribute them to any specific dinosaur group, however, it is possible that they represent sauropod manus tracks. The morphology of the third, well-preserved track resembles the purported thyreophoran manus track described by Milàn & Bromley (2005), especially in its broad, elliptical outline and the short, but sharp digits. This track, however, is significantly larger, 28 cm long, than the track described by Milàn & Bromley (2005) which measured 15.5 cm in length and was 19.5 cm wide.
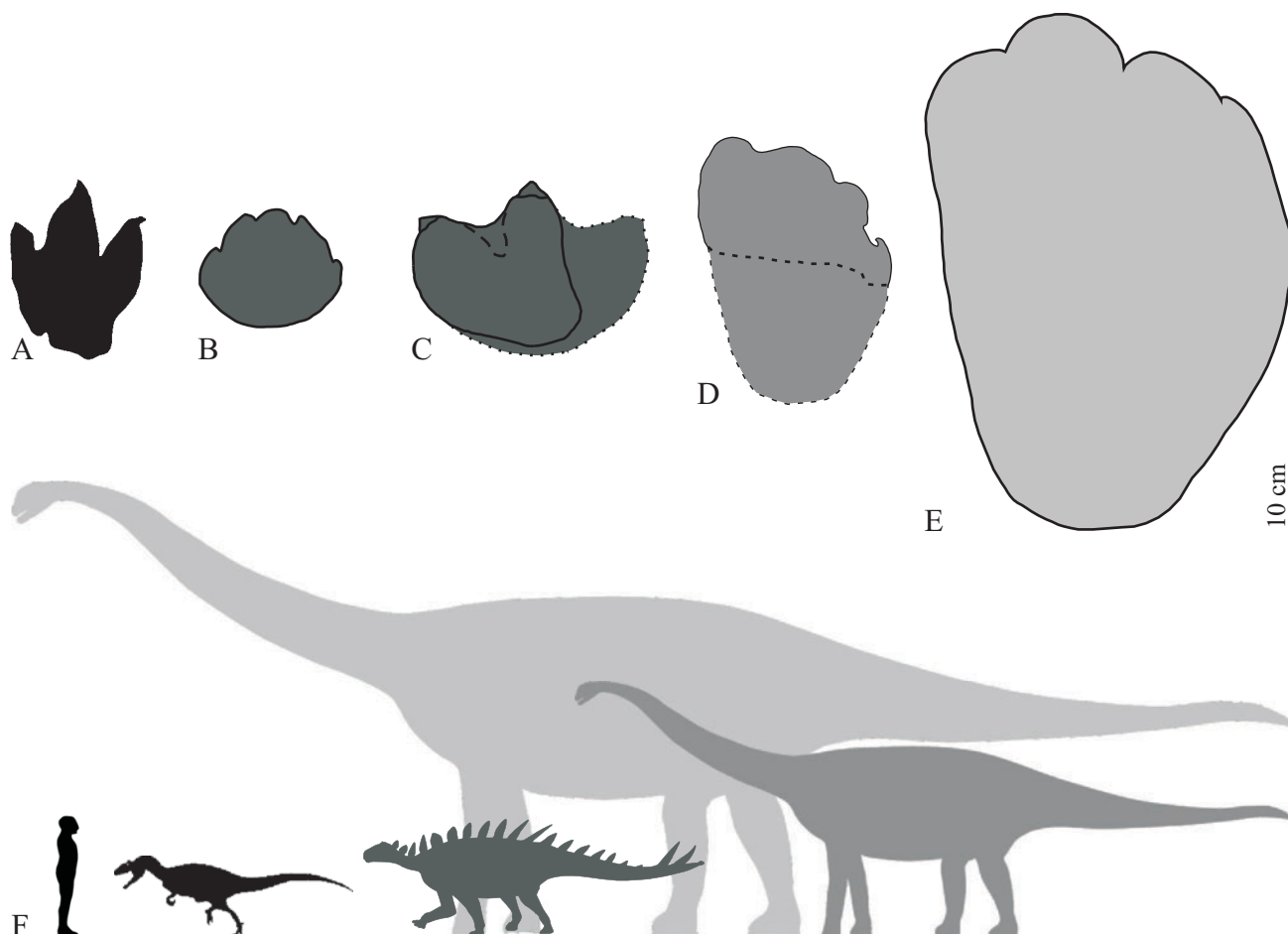
Fig. 6. Schematic representation of the different dinosaur tracks known from the Middle Jurassic Bagå Formation. All tracks reproduced to same scale. **A**, pes track from a medium-sized theropod with a footlength of 25 cm. **B**, manus track from a thyreophoran dinosaur, from Milàn & Bromley (2005). **C**, pes track from a thyreophoran dinosaur. **D**, small sauropod pes track. **E**, large sauropod pes track, from Milàn & Bromley (2005). **F**, silhouettes demonstrating the relative size of the track makers of the tracks with a human silhouette for scale. The Middle Jurassic dinosaur fauna on Bornholm comprised large and small sauropods, thyreophorans, and theropods. The colour of the silhouettes corresponds to the colour of the tracks.

Discussion

The Middle Jurassic is characterized by a worldwide scarcity of dinosaurian body fossils (Romano & Whyte 2003, 2010; Whyte et al. 2007, 2010). In Europe the scarcity of body fossils is especially pronounced and ichnological data thus become an important source of information about the dinosaurian diversity and biogeography during the Middle Jurassic. As an example, the Middle Jurassic Cleveland Basin of the Yorkshire coast has preserved one of the most diverse track assemblages from the Middle Jurassic of Europe, with abundant tracks from theropods, ornithopods, stegosaurians, sauropods, and crocodilians (Romano & Whyte 2003, 2010; Whyte et al. 2006, 2007, 2010). In contrast, skeletal material is only represented by a few scattered, often badly preserved bones (Romano & Whyte 2003; Whyte et al. 2010). Middle Jurassic sauropod tracks are known from Portugal (Santos et al. 1994), sauropod tracks together with tracks from theropods are known from Oxfordshire in England (Day et al. 2004), and theropod tracks and trackways are found on the Isle of Skye, Scotland (Clark et al. 2005). The sauropod and thyreophoran tracks from the Middle Jurassic of Bornholm (Milàn & Bromley 2005) are from a formation where, to date, no skeletal remains have been discovered. The new finds, although fragmentary, are important new information about the Middle Jurassic dinosaur fauna of Bornholm (Fig. 6) and add to our knowledge about the poorly known Middle Jurassic dinosaur distribution in Europe.

As in the case with the first tracks from the Bagå Formation (Milàn & Bromley 2005), the tracks described here are preserved as natural casts in coarse-grained fluvial sandstone. The sediment constituting the casts is horizontally laminated, demonstrating passive infill from suspension of an existing void. None of the original tracking surface is preserved in the new tracks, but Milàn & Bromley (2005) described distorted clay layers between the tracks found in 2004, originating from the original tracking surface, and palynological analysis of the sediment between the tracks confirmed that the tracks originated from the Bagå Formation (Milàn & Bromley 2005).

The track walls on all track casts are steep and well defined, and are at a steep angle to the surrounding sediment where present, showing that the natural casts are casts of the true tracks and not cast of undertracks (sensu Lockley 1991). Undertracks tend to be shallower, less well-defined and with a broader outline than the true tracks (Manning 2004; Milàn & Bromley 2006, 2008). The type of track preservation found on Bornholm is typical of tracks preserved in siliciclastic sediments and is very similar to tracks found in floodplain deposits in the Middle Jurassic of England (Romano & Whyte 2003; Whyte et al. 2007), the Upper Jurassic of Asturias, Spain (Garcia-Ramos et al. 2006; Lockley et al. 2008), the Upper Jurassic Morrison Formation of Utah (e.g. Lockley & Hunt 1995; Platt & Hasiotis 2006) and the Upper Jurassic Lourinhã Formation of Portugal (Mateus & Milàn 2010).

Conclusion

Three new dinosaur tracks are interpreted as tracks from a theropod, a thyreophoran, and a small sauropod. Together with previously described tracks, they are the only evidence of a Middle Jurassic dinosaur fauna of Bornholm that comprised theropods, small and large sauropods and at least one type of thyreophoran dinosaur (Fig. 6). This is important data, as the Middle Jurassic of Europe is characterized by a pronounced scarcity of skeletal material.

All the tracks from the Bagå formation are found as natural casts on the underside of blocks of fluvial sandstone that were dumped on the beach from the nearby Hasle Klinkefabrik's abandoned clay pit, now flooded and named Pyritsøen. A systematic investigation and excavation of the sandstone blocks from the clay pit might expose more tracks that add can further to the record.

Acknowledgements

References

Ahlberg, A. & Siverson, M. 1991: Lower Jurassic dinosaur footprints in Helsingborg, southern Sweden. Geologiska Föreningens i Stockholm Förhandlingar 113, 339–340.

Bonde, N. 2004: An Early Cretaceous (Ryazanian) fauna of "Purbeck-Wealden" type at Robbedale, Bornholm, Denmark. In: Arratia, G. & Tintori, A. (eds): Mesozoic Fishes 3 – systematics, palaeoenvironments and biodiversity, 507–528. München: Verlag Dr. Friedrich Pfeil.

Bonde, N. & Christiansen, P. 2003: New dinosaurs from Denmark. Comptes Rendus Palevol 2, 13–26.

Bölau, E. 1952: Neue Fossilfünde aus dem Rhät Schonens und ihre paläogeographisch-ökologische Auswertung. Geologiska Föreningens i Stockholm Förhandlingar 74, 44–50.

Bölau, E. 1954: The first finds of dinosaurian skeletal remains in the Rhaetic–Liassic of N. W. Scania. Geologiska Föreningens i Stockholm Förhandlingar 76, 501–502.

Christiansen, P. & Bonde, N. 2003: The first dinosaur from Denmark. Neues Jahrbuch für Geologie und Paläontologie Abhandlungen 227, 287–299.

Clark, N.D.L., Ross, D.A. & Booth, P. 2005: Dinosaur tracks from the Kilmalaug Formation (Bathonian, Middle Jurassic) of Score Bay, Isle of Skye, Scotland, UK. Ichnos 12, 93–104.

Day, J.J., Norman, D.B., Gale, A.S., Upchurch, P. & Powell, H.P. 2004: A Middle Jurassic dinosaur Trackway site from Oxfordshire, UK. Palaeontology 47, 319–348.

Farlow, J.O., Gatesy, S.M., Holtz, T.R., Hutchinson, J.R. & Robinson, J-M. 2000: Theropod locomotion. American Zoologist 40, 640–663.

Garcia-Ramos, J.C., Piñuela, L. & Lires, J. 2006: Atlas del Jurássico de Asturias. Ediciones Nobel, Oviedo. 225 pp.

Gierlinski, G. & Ahlberg, A. 1994: Late Triassic and Early Jurassic dinosaur footprints in the Höganäs Formation of southern Sweden. Ichnos 3, 99–105.

Gierlinski, G. & Sabath, K. 2008: Stegosaurian footprints from the Morrison Formation of Utah and their implication for interpreting other ornithischian tracks. Oryctos 8, 29–46.

Gierlinski, G., Menducki, P., Janiszewska, K., Wicik, I. & Boczarowski, A. 2009: A preliminary report on dinosaur track assemblages from the Middle Jurassic of the Imilchil area, Morocco. Geological Quarterly 53, 477–482.

Gravesen, P., Rolle, F. & Surlyk, F. 1982: Lithostratigraphy and sedimentary evolution of the Triassic, Jurassic and Lower Cretaceous of Bornholm, Denmark. Danmarks Geologiske Undersøgelse Serie B 7, 51 pp.

Gry, H. 1969: Megaspores from the Jurassic of the island of Bornholm, Denmark. Meddelelser fra Dansk Geologisk Forening 19, 69–89.

Koppelhus, E.B. & Nielsen, L.H. 1994: Palynostratigraphy and palaeoenvironments of the Lower to Middle Jurassic Bagå Formation of Bornholm, Denmark. Palynology 18, 139–194.

Lindgren, J., Rees, J., Siverson, M. & Cuny, G. 2004: The first Mesozoic mammal from Scandinavia. GFF 126, 325–330.

Lindgren, J., Currie, P.J., Siverson, M., Rees, J., Cederström, P., & Lindgren, F. 2007: The first neoceratopsian dinosaur remains from Europe. Palaeontology 50, 929–937.

Lindgren, J., Currie, P.J., Rees, J., Siverson, M., Lindström, S. & Alwmark, C. 2008: Theropod dinosaur teeth from the lowermost Cretaceous Rabekke Formation on Bornholm, Denmark. Geobios 41, 253–262.

Lockley, M. 1991: Tracking Dinosaurs. 238 pp. New York: Cambridge University Press.

Lockley, M. & Hunt, A.P. 1995: Dinosaur tracks and other fossil footprints of the Western United States. 338 pp. New York: Columbia University Press.

Lockley, M.G. & Hunt, A.P. 1998: A probable stegosaur track from the Morrison Formation of Utah. Modern Geology 23, 331–342.

Lockley, M.G., Farlow, J.O. & Meyer, C.A. 1994: *Brontopodus* and *Parabrontopodus* ichnogen. nov. and the significance of wide- and narrow-gauge sauropod trackways. Gaia 10, 135–146.

Lockley, M.G., Garcia-Ramos, J.C., Lires, J., Piñuela, L. & Avanzini, M. 2008: A review of vertebrate track assemblages from the Late Jurassic of Asturias, Spain with comparative notes on coeval ichnofaunas from the western USA: implications for faunal diversity in association with siliciclastic facies assemblages. Oryctos 8, 53–70.

Manning, P. 2004: A new approach to the analysis and interpretation of tracks: examples from the dinosauria. In: McIlroy, D. (ed.): The application of ichnology to palaeoenviromental and stratigraphic analysis. Geological Society, London, Special Publication 228, 93–123.

Mateus, O. & Milàn, J. 2010: A diverse Upper Jurassic dinosaur ichnofauna from Central-west Portugal. Lethaia 43, 245–257.

Michelsen, O., Nielsen, L.H., Johannessen, P.N., Andsbjerg, J. & Surlyk, F. 2003: Jurassic lithostratigraphy and stratigraphic development onshore and offshore Denmark. In: Ineson, J.R. & Surlyk, F. (eds): The Jurassic of Denmark and Greenland. Geological Survey of Denmark and Greenland Bulletin 1, 147–216.

Milàn, J. 2006: Variations in the morphology of emu (*Dromaius novaehollandiae*) tracks, reflecting differences in walking pattern and substrate consistency: ichnotaxonomical implications. Palaeontology 49, 405–420.

Milàn, J. & Bromley, R.G. 2005: Dinosaur footprints from the Middle Jurassic Bagå Formation, Bornholm, Denmark. Bulletin of the Geological Society of Denmark 52, 7–15.

Milàn, J. & Bromley, R.G. 2006: True tracks, undertracks and eroded tracks, experimental work with tetrapod tracks in laboratory and field. Palaeogeography, Palaeoclimatology, Palaeoecology 231, 253–264.

Milàn, J. & Bromley, R.G. 2008: The impact of sediment consistency on track and undertrack morphology: experiments with emu tracks in layered cement. Ichnos 15, 18–24.

Milàn, J. & Gierlinski, G. 2004: A probable thyreophoran (Dinosauria, Ornithischia) footprint from the Upper Triassic of southern Sweden. Bulletin of the Geological Society of Denmark 51, 71–75.

Milàn, J., Avanzini, M., Clemmensen, L.B, Garciá-Ramos, J.C. & Piñuela, L. 2006: Theropod foot movement recorded from Late Triassic, Early Jurassic and Late Jurassic fossil footprints. New Mexico Museum of Natural History and Science Bulletin 37, 352–364.

Moratalla, J.J., Sanz, J.L. & Jimenez, S. 1988: Multivariate analysis on Lower Cretaceous dinosaur footprints: Discrimination between ornithopods and theropods. Geobios 21, 395–408.

Nielsen, L.H., Petersen, H.I., Dybkjær, K. & Surlyk, F. 2010: Lake-mire deposition, earthquakes and wildfires along a basin margin fault; Rønne Graben, Middle Jurassic, Denmark. Palaeogeography, Palaeoclimatology, Palaeoecology 292, 103–126.

Noe-Nygaard, N. & Surlyk, F. 1988: Washover fan and brackish bay sedimentation in the Berriasian–Valanginian of Bornholm, Denmark. Sedimentology 35, 197–217.

Noe-Nygaard, N., Surlyk, F. & Piasecki, S., 1987: Bivalve mass mortality caused by toxic dinoflagellate blooms in a Berriasian–Valanginian lagoon, Bornholm, Denmark. Palaios 2, 263–273.

Platt, B. & Hasiotis, S.T. 2006: Newly discovered sauropod dinosaur tracks with skin and foot-pad impressions from the Upper Jurassic Morrison Formation, Bighorn Basin, Wyoming, U.S.A. Palaios, 21, 249–261.

Pleijel, C. 1975: Nya dinosauriefotspår från Skånes Rät–Lias. Fauna och Flora 3, 116–120.

Rees, J., Lindgren, J. & Evans, S.E. 2005: Amphibians and small reptiles from the Berriasian Rabekke Formation on Bornholm, Denmark. GFF 127, 233–238.

Romano, M. & Whyte, M.A. 2003: Jurassic dinosaur tracks and trackways of the Cleveland Basin, Yorkshire: preservation, diversity and distribution. Proceedings of the Yorkshire Geological Society 54, 185–215.

Romano, M. & Whyte, M.A. 2010: Crocodilian and other non-dinosaurian tracks and trackways from the Ravenscar Group (Middle Jurassic) of the Cleveland Basin, Yorkshire, UK. New Mexico Museum of Natural History and Science Bulletin 51, 69–81.

Santos, V.F., Lockley, M.G., Meyer, C.A., Carvalho, J. Galopim de Carvalho, A.M. & Moratalla, J.J. 1994: A new sauropod tracksite from the Middle Jurassic of Portugal. Gaia 10, 5–13.

Schwarz-Wings, D., Rees, J. & Lindgren, J. 2009: Lower Cretaceous Mesoeucrocodylians from Scandinavia (Denmark and Sweden). Cretaceous Research 30, 1345–1355.

Surlyk, F., Milàn, J. & Noe-Nygaard, N. 2008: Dinosaur tracks and possible lungfish aestivation burrows in a shallow coastal lake; lowermost Cretaceous, Bornholm, Denmark. Palaeogeography, Palaeoclimatology, Palaeoecology 231, 253–264.

Thulborn, T. 1990: Dinosaur Tracks. 410 p. London: Chapman & Hall.

Whyte, M.A., Romano, M. & Watts, W. 2010: Yorkshire dinoasaurs: a history in two parts. In: Moody, R.T.J., Buffetaut, E., Naish, D. & Martill, D.M. (eds). Dinosaurs and Other Extinct Saurians: A Historical Perspective. Geological Society, London, Special Publication 343, 189–207.

Whyte, M.A., Romano, M. & Elvidge, D.J. 2007: Reconstruction of Middle Jurassic dinosaur- dominated communities from the vertebrate ichnofauna of the Cleveland Basin of Yorkshire, UK. Ichnos 14, 117–129.

Whyte, M.A., Romano, M., Hudson, J.G., & Watts, W. 2006: Discovery of the largest theropod dinosaur tracks known from the Middle Jurassic of Yorkshire. Proceedings of the Yorkshire Geological Society 56, 77–80.

Wright, J.L. 2005: Steps in understanding sauropod biology. In: Curry Rogers, K.A. & Wilson, J.A. (eds): The Sauropods: Evolution and Paleobiology, 252–285. Berkeley: University of California Press.

Bite traces in a turtle carapace fragment from the middle Danian (Lower Paleocene) bryozoan limestone, Faxe, Denmark

JESPER MILÀN, BENT E.K. LINDOW & BODIL W. LAURIDSEN

A fragment of a turtle carapace from the Middle Danian bryozoan limestone at the Faxe quarry, eastern Denmark, is identified as a partial costal plate from the carapace of a chelonioid turtle. The fragment bears traces of three separate acts of predation or scavenging. Two circular bite traces *Nihilichnus nihilicus* Mikuláš *et al.* 2006, 4 mm in diameter, situated 2.5 cm apart, are interpreted as crocodylian. Groups of parallel scrapes, *Machichnus bohemicus* Mikuláš *et al.* 2006, 4–5 mm long and 0.5 mm wide, are interpreted as bite traces from sharks. Small circular traces, ~1 mm in diameter, found either alone or in a row of three, are either from sharks or fish. This is the first record of turtles from the Danian bryozoan limestone exposed in Faxe quarry, and thus represents an important addition to the Danian vertebrate fauna of Denmark.

Jesper Milàn [jesperm@oesm.dk], Geomuseum Faxe/Østsjællands Museum, Østervej 2, DK-3640 Faxe, Denmark. Also Department of Geography and Geology, University of Copenhagen, Øster Voldgade 10, 1350 Copenhagen K, Denmark. Bent E.K. Lindow [lindow@snm.ku.dk], Natural History Museum of Denmark, University of Copenhagen, Øster Voldgade 5–7, DK-1350 Copenhagen K, Denmark. Bodil W. Lauridsen [Bodill@geo.ku.dk], Department of Geography and Geology, University of Copenhagen, Øster Voldgade 10, DK-1350 Copenhagen K, Denmark.

Vertebrate skeletal remains are rare in the Danian bryozoan limestone of eastern Denmark. The described vertebrate fauna comprises 13 species of fish, based on otoliths (Schwarzhans 2003), and around 15 species of sharks (Jan Schultz Adolfssen, personal communication 2010). Marine crocodylians are known from single bones and isolated teeth (Bonde *et al.* 2008). Further indirect evidence of large vertebrates is found in the form of polished quartz pebbles interpreted as gastroliths (Noe-Nygaard 1975).

Sea-turtles are known from a collection of carapace fragments from the Upper Danian København Limestone Formation and Selandian Lellinge Greensand Formation (Dames 1897; Rosenkrantz 1920, 1921, 1923; Karl & Lindow in press). Three peripheral elements from the carapace of a marine turtle of the family Cheloniidae are known from the upper Maastrichtian limestone of the Tor Formation, Stevns Klint (Karl & Lindow 2009). Undescribed turtle remains are also known from the Danian limestone of the Limhamn quarry, southern Sweden (Johan Lindgren, personal communication 2010).

Recently, a carapace fragment was found in the Faxe quarry, in a loose bryozoan bioclastic grainstone, together with abundant shark teeth and coprolites. This study describes this first occurrence of a marine turtle from in the middle Danian bryozoan limestone of Faxe and documents multiple sets of bite traces found on the carapace fragment.

Geological Setting

The large Faxe quarry located in south-eastern Sjælland, Denmark, (Fig. 1) contains well-exposed Lower Paleocene (middle Danian), bryozoan and coral limestone, which was deposited shortly after the mass extinction at the Cretaceous–Tertiary boundary during a relative rise in sea level (Thomsen 1976, 1983, 1995;

Surlyk 1997). The azooxanthellate scleractinian coral *Dendrophyllia* evolved and formed coral mound complexes in the epicontinental sea covering Denmark and southern Sweden (Floris 1980; Bernecker & Weidlich 1990, 2005; Willumsen 1995; Bjerager & Surlyk 2007a,b; Bjerager *et al*. 2010; Lauridsen & Damholt 2011).

The bryozoan mounds of the Danish Basin are skeletal deep-water mounds dominated by delicate bryozoan fragments and carbonate mud. They were formed in an outer-ramp setting, probably at the shelf-slope break of a distally steepened ramp (Surlyk 1997). The mound complex and the bryozoan mounds are situated over the easternmost part of the Ringkøbing-Fyn High and had a palaeolatitude of 45° N (Surlyk 1997).

The mounds are autochtonous and biogenically constructed (Cheetham 1971; Thomsen 1976, 1983; Surlyk 1997). The well preserved mound complex in Faxe comprises three main species of frame-building corals. The diversity of the associated fauna is very high with more than 250 species identified, including 30 non-constructional coral species (Gravesen 2001; Lauridsen & Damholt 2011). The invertebrates provided feeding grounds for a large population of vertebrates.

Material

The specimen was found by amateur geologist Alice Rasmussen in 1994 in the north-eastern corner of the Faxe quarry (Fig. 1). The specimen was collected but not given further attention until 2010, when one of the authors (JM) identified it as a fragment of a turtle carapace. The specimen is now catalogued as Danekræ (DK-627) and is part of the collection of the Natural History Museum of Denmark (MGUH 29293). It is currently on display in Geomuseum Faxe.

Order Testudines Linnaeus, 1758
Superfamily Chelonioidea Baur, 1893
Chelonioidea indet.

Description: The turtle material consists of a single irregularly rhomboid-shaped medial fragment of a costal plate, measuring 39 mm by 26 mm, with an average thickness of 4 mm (Fig. 2A–C). The dorsal surface is smooth and displays two shallow grooves delimiting the borders of the overlying unpreserved dermal scutes (Fig. 2A). The ventral surface is dominated by the sloping medial end of the rib head which is triangular in ventral aspect (Fig. 2B). The ventral surface of the rib slopes laterally, rapidly becoming confluent
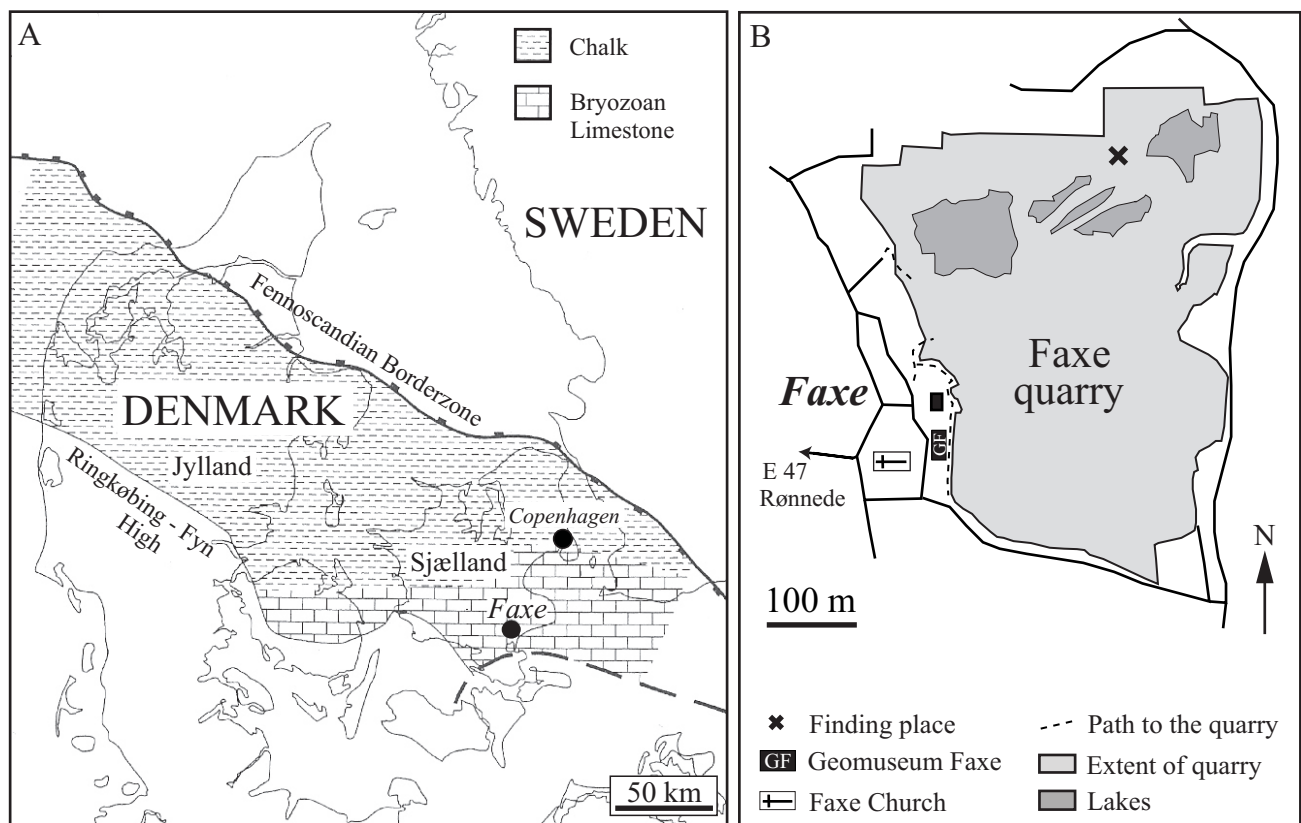
Fig. 1. **A**, Faxe quarry is located in the south-eastern part of the Danish island Sjælland, approximately 70 km south of Copenhagen. Modified from Schnetler *et al*. (2001). **B**, map of Faxe and Faxe quarry, with the finding place indicated.

with the ventral surface of the costal plate. The medial face of the rib end is lightly concave, opposite to the intervertebral region; the plate thins dorsally in this area (Fig. 2B). In addition, the presence of a wide scar for attachment of the medial end of the first rib (1Ra on Fig. 2B) identifies the specimen as the anteriormost costal plate from the left side of the animal (Fig. 3). Within turtles, from *Proganochelys* onwards, the first thoracic rib is the only one which is free and not incorporated into the carapace (Gaffney 1990); rather, it is attached immediately anterior to the medial head of the second thoracic rib (2Ra on Fig. 2B). Overall, the specimen is too fragmentary for a determination more specific than superfamily Chelonioidea, family Cheloniidae or Toxochelyidae. The Dermochelyidae can be ruled out as the ribs in that family are fully separated from the shell plates.

Bite traces

Close examination of the specimen reveals several sets of bite marks which fall into three categories. On the dorsal side, two prominent rounded indentions in the shell are present (Fig. 2D, E); one hole is circular, measures 4 mm in diameter and has penetrated halfway through the bone (Fig. 2D). A second hole also 4 mm in diameter is present at the edge of the bone and has caused the bone to fracture (Fig. 2E). The distance between the two holes is 25 mm. A second type, also on the dorsal side, comprises groups of parallel, elongated scratch marks which have penetrated the surface of the bone; these marks are 3–4 mm long, 0.8 mm wide, and up to 0.5 mm deep (Fig. 2F, G). The third type comprises small rounded pits less than 1 mm in diameter and about 0.5 mm deep, found on the ventral side of the fragment. When seen in high magnification, the fragmented surface of the depressed bone can be seen in the bottom of the pits. The pits occur as individuals in rows of three (Fig. 2H, I).

Discussion

Bite traces or tooth marks in skeletal remains are well known from the zoological literature (e.g., Binford 1981; Brain 1981; Haynes 1980, 1983), and in recent years they have been studied increasingly in fossil material (Deméré & Cerutti 1982; Cigala-Fulgosi 1990; Schwimmer *et al.* 1997, Tanke & Currie 1998; Corral *et al.* 2004; Mikuláš *et al.* 2006; Jacobsen & Bromley 2009; Schwimmer 2010). Bite traces can originate from various behaviors ranging from predation (the deathblow, slaughter and feeding) to subsequent scavenging including the later use of the skeletal parts as a source of calcium. Bite marks in the form of rounded pits, arising from perpendicular impression of teeth not penetrating the bone, have been given the ichnotaxonomic name *Nihilichnus nihilicus* Mikuláš *et al.* 2006. Parallel to sub-parallel scratches less than 1mm wide are named *Machichnus bohemicus* Mikuláš *et al.* 2006, and are interpreted as gnawing traces formed while feeding on the soft tissue on the bone (Mikuláš *et al.* 2006).

The large predators known from the Faxe quarry and adjacent Danian limestone deposits comprise several genera of sharks and the marine crocodylian *Thoracosaurus*. Crocodylian teeth are not serrated and are circular in cross-section, whereas shark teeth are compressed, often serrated, and elliptical in cross section with sharp tips. *Thoracosaurus*, however, is a longirostrine crocodylian with long slender teeth, and it is uncertain if it could feed on turtles, but finds of isolated broader more cone-like crocodilian teeths suggest the presence of other brevirostrine crocodylians in the fauna. A recent study of bite traces from Dwarf Caimans preying on turtles shows that crocodylian bite traces include round puncture holes, *Nihilichnus*, as well as elongated, irregular scratches and large crushed areas from repeated bites to the same areas (Milàn *et al.* 2010). Fossil records of crocodylian-produced *Nihilichnus* in chelonian carapaces include a complete turtle skeleton from the Kimmeridgian of Eichstätt, Germany with abundant *Nihilichnus* and crushing of the carapace (Karl & Tichy 2004). *Nihilichnus* in chelonians has also been described from the Upper Cretaceous Blufftown Formation of Georgia and Alabama, USA (Schwimmer 2010). Here the bites are interpreted as originating from the giant Late Cretaceous crocodylian *Deinosuchus*, and similar traces are found in chelonian carapaces from the Paleocene of the Wannagan Creek quarry in Minnesota (Erickson 1984).

An alternative explanation has been suggested for the origin of *Nihilichnus*, especially in Mesozoic ammonites and nautiloids, as the result of limpet home scars dissolved into the aragonitic shells (Kase *et al.* 1998; Seilacher 1998). However, this interpretation is disputed by Kaufmann (2004) who retains the original interpretation by Kaufmann and Kiesling (1960) as predation by large vertebrates. In the case of bite traces in turtle shells, no alternative hypotheses have been suggested, as many modern crcodylians have a chelonivorous diet.

The large rounded bites traces in the Faxe specimen (Fig. 2D, E) are similar to the crocodylian bite traces interpreted from other fossil examples (Erickson 1984; Karl & Tichy 2004; Schwimmer 2010) and can, together
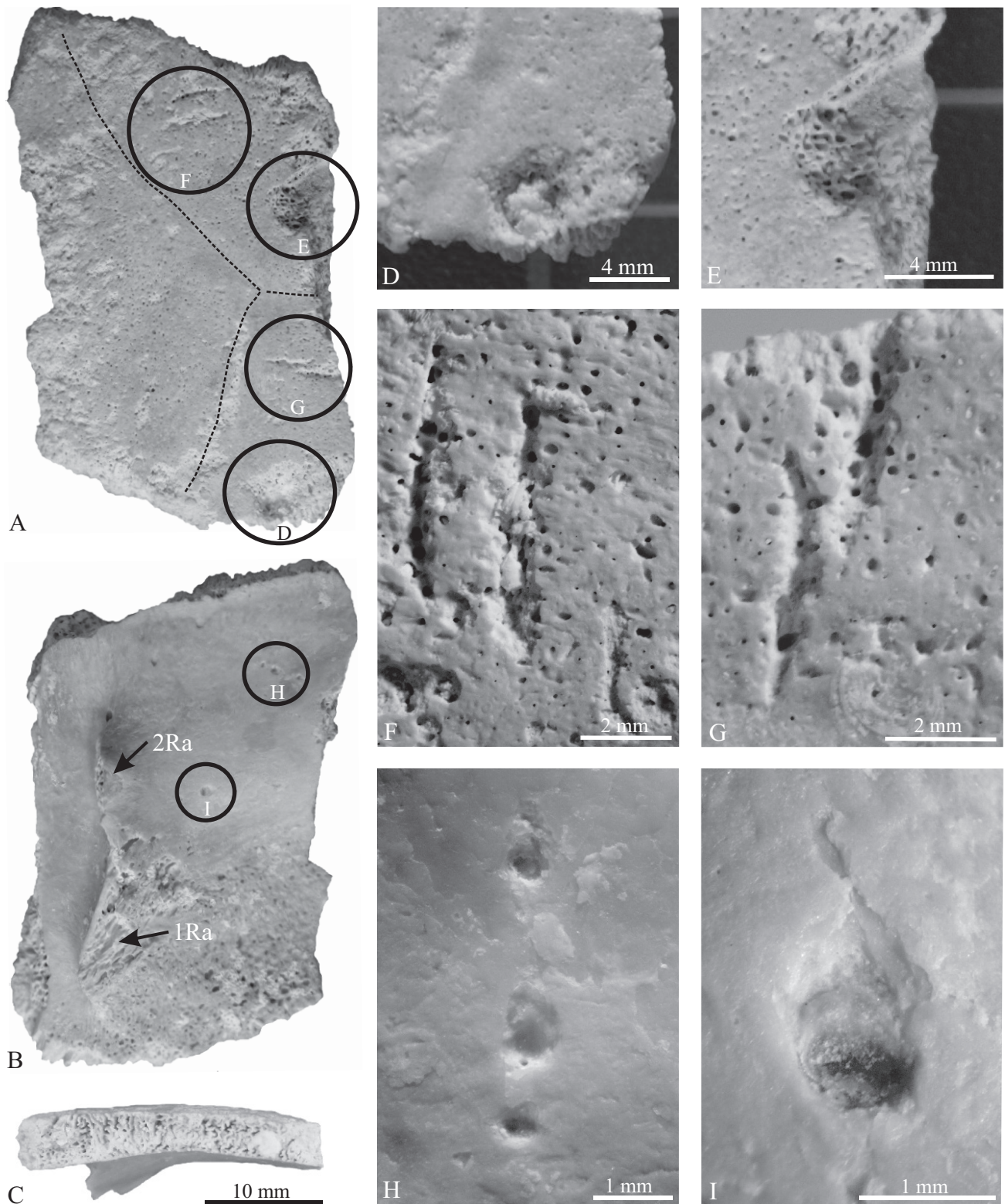
Fig. 2. **A**, dorsal view of the carapace fragment (MGUH 29293). The shallow grooves (indicated by thin broken lines) show that the fragment is a costal plate. **B**, ventral view of the plate with visible attachment scars for the ribs; 1Ra: attachment of 1st thoracic rib; 2Ra: attachment of 2nd thoracic rib. **C**, the costal plate in posterior view, showing the slight curvature of the carapace. A–C are reproduced to the same scale; circled areas refer to D–I. **D**, large bite, *Nihilichnus nihilicus*, that has penetrated halfway through the bone. **E**, large bite which has caused the carapace to fracture. **F**, three small parallel scratches, *Machichnus bohemicus*, which have penetrated the surface of the bone. **G**, two small subparallel *Machichnus bohemicus*; the scratches are morphologically similar to those in F. **H**, row of three small bites, *Nihilichnus nihilicus,* in the ventral side of the carapace fragment. **I**, single small *Nihilichnus nihilicus* in the bone. Note the crushed bone in the bottom of the pit.

with the small round traces (Fig. 2H, I,), confidently be assigned to *Nihilichnus nihilicus* Mikuláš *et al*. 2006. They are likely to be the result of predation by crocodylians, as crocodylian remains are documented from the Faxe quarry (Bonde *et al*. 2008) and the adjacent Limhamn quarry (Troedsson 1923, 1924). The parallel to sub-parallel scratches appear as sharp cuts in the bone surface (Fig. 2F, G) and are morphologically similar to bite traces from sharks recorded in the bones of Pliocene dolphins (Bianucci *et al*. 2010) and marine turtles from the Cretaceous (Schwimmer *et al*. 1997; Shimada & Hooks 2004), and are referred to *Machichnus bohemicus* Mikuláš *et al*. 2006.

On the basis of the ichnological evidence, a scenario for the fate of the turtle is as follows. The large bites, *Nihilichnus nihilicus*, are primary predation marks from a crocodylian crushing the carapace, which was fatal to the turtle. The smaller scratches, *Machichnus bohemicus*, and pits are the result of subsequent cleaning of the carcass by smaller scavengers, most likely small sharks and carnivorous fishes.

Conclusion

A costal plate fragment from a marine turtle carapace is the first record of turtles in the middle Danian bryozoan limestone exposed in the Faxe quarry and in correlative layers elsewhere in Denmark, and thus forms an important addition to the sparse Danian vertebrate record of Denmark. The presence of the attachment scar of the free anteriormost thoracic rib identifies the plate as the anteriormost costal plate from the left side of the animal. Due to the fragmentary nature of the specimen it can only be confidently referred to the superfamily Chelonioidea. The carapace fragment bears evidence of predation by a crocodylian and subsequent gnawing by small scavengers such as sharks and fish.

Acknowledgements
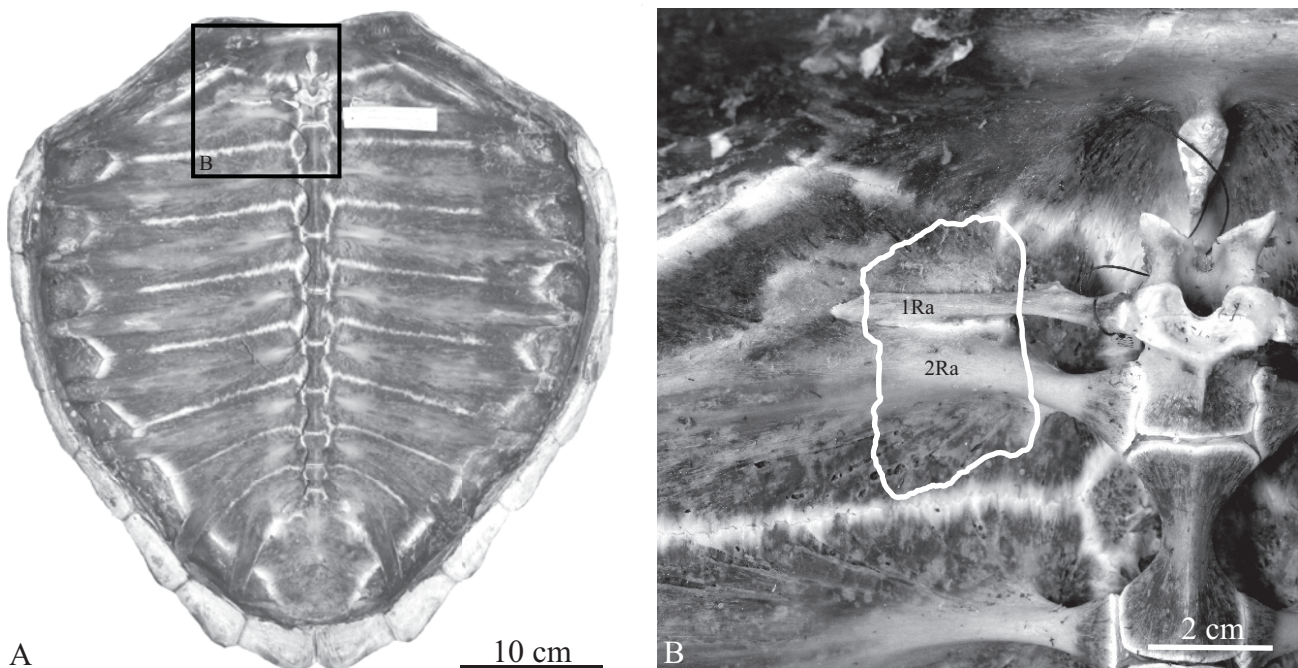
Fig. 3. **A**, ventral view of the carapace from a modern marine turtle *Caretta caretta* of the family Cheloniidae, from the Natural History Museum of Denmark (R2726). **B**, enlarged section showing the position of the fossil specimen, with the corresponding rib attachments indicated.

Dansk sammendrag

Det første kendte stykke af skjoldet fra en havskildpadde er blevet fundet i bryozokalken i Faxe Kalkbrud (Fig.1). Stykket blev fundet af Alice Rasmussen i 1995, men blev først identificeret i 2010. Stykket måler 39 x 16 mm, er 4 mm tykt og er svagt buet. På oversiden af stykket ses en svag fure, der markerer kontakten mellem tre af de overliggende hornplader, der ikke er blevet bevaret (Fig. 2A–C). På undersiden af stykket ses to ribbensfæster, der viser, at det er den forreste rygplade fra skjoldet, da det kun er den forreste rygplade i et skildpaddeskjold, der har to ribbensfæster (Fig. 3). Det er ikke muligt at identificere stykket nærmere end overfamilien Chelonioidea, som omfatter de moderne havskildpadder. Stykket er det første kendte eksemplar af en havskildpadde i det mellemste Danien i Danmark. Derudover viser stykket en dramatisk historie, idet der er tre forskellige typer af bidemærker i det. Den første type består af to cirkulære huller, 4 mm i diameter med en afstand på 25 mm mellem sig (Fig. 2D, E). Disse bidemærker henføres til ichnoslægten *Nihilichnus nihilicus* Mikuláš *et al.* 2006. Et af disse bidemærker er placeret på en brudflade i stykket. Det er sandsynligt at pladen er blevet knust af dette bid (Fig. 2E). Disse huller tolkes som bidemærker fra en krokodille, da disse har tænder med cirkulært tværsnit og hullerne er magen til både fossile og recente eksempler, hvor krokodiller har spist skildpadder. En anden type bidemærker består af parallelle til sub-parallelle furer 4–5 mm lange og 0.5 mm brede, *Machichnus bohemicus* Mikuláš *et al.* 2006, som stammer fra hajer der har raspet kød af skjoldfragmentet (Fig. 2F, G). En sidste type små *Nihilichnus nihilicus* omkring 1 mm i diameter optræder enkeltvis og i en gruppe af tre på en række. Man kan se knusning af knoglevævet i bunden af disse, og de formodes at stamme fra enten hajer eller fisk (Fig. 2H, I). Baseret på bidemærkerne kan følgende forløb for skildpaddens skæbne opstilles: Først er den blevet angrebet af en havkrokodille, der har knust skjoldet og dræbt skildpadden. Dernæst har små hajer og fisk raspet skjoldstykkerne rene for de sidste kødrester, inden det blev begravet i havbunden. Stykket er erklæret for Danekræ (DK-627), da det er det første stykke af en havskildpadde, der er fundet i det mellemste Danien i Danmark, og da det afslører en forhistorisk interaktion mellem rovdyr, byttedyr og ådselsædere.

References

Baur, G. 1893: Notes on the classification and taxonomy of the Testudinata. Proceedings of the American Philosophical Society 31, 210–225.

Bernecker, M. & Weidlich, O. 1990: The Danian (Paleocene) coral limestone of Fakse, Denmark: a model for ancient aphotic, azooxanthellate coral mounds. Facies 22, 103–138.

Bernecker, M. & Weidlich, O. 2005: Azooxanthellate corals in the Late Maastrichtian – Early Paleocene of the Danish basin: bryozoan and coral mounds in a boreal shelf setting. In: Freiwald, A. & Roberts, J.M. (eds), Cold-water Corals and Ecosystems, 3–25. Berlin and Heidelberg: Springer-Verlag.

Bianucci, G., Sorce, B., Storai, T. & Landini, W. 2010: Killing in the Pliocene: shark attack on a dolphin from Italy. Palaeontology 53, 457–470.

Binford, L.R. 1981: Bones - ancient men and modern myths, 320 pp. New York: Academic Press.

Bjerager, M. & Surlyk, F. 2007a: Danian cool-water bryozoan mounds at Stevns Klint, Denmark – A new class of non-cemented skeletal mounds. Journal of Sedimentary Research 77, 634–660.

Bjerager, M. & Surlyk, F. 2007b: Benthic palaeoecology of Danian deep-shelf bryozoan mounds in the Danish Basin. Palaeogeography, Palaeoclimatology, Palaeoecology 250, 184–215.

Bjerager, M., Surlyk, F. Lykke-Andersen, H., Thibault, N. & Stemmerik, L. 2010: Danian cool-water coral reefs in southern Scandinavia localised over seafloor highs. Marine and Petroleum Geology 27, 455–466.

Bonde, N., Andersen, S., Hald, N. & Jakobsen, S.L. 2008: Danekræ – Danmarks bedste fossiler. 224 pp. Copemhagen: Gyldendal.

Brain, C.K. 1981: The hunters or the hunted? An introduction to African cave taphonomy. 365 pp. Chicago: The University of Chicago Press.

Cheetham, A.H. 1971: Functional morphology and biofacies distribution of cheilostome bryozoa in the Danian Stage (Paleocene) of southern Scandinavia. Smithsonian Contributions to Paleobiology 6, 1–87.

Cigala-Fulgosi, F. 1990: Predation (or possible scavenging) by a great white shark on an extinct species of bottlenosed dolphin in the Italian Pliocene. Tertiary Research 12, 17–36.

Corral, J.C., Pereda Suberbiola, X. & Bardet, N. 2004: Marcas de ataque atribuidas a un selacio en una vertebra de mosasaurio del Cretácico Superior de Álava (Region Vasco-Cantábrica). Revista Española de Paleontologia 19, 23–32.

Dames, W. 1897: Ueber Meeresschildkröten aus der oberen Kreide von Kopenhagen. Meddelelser fra Dansk Geologisk Forening 1, 73–74.

Deméré, T.A. & Cerutti, R.A. 1982: A Pliocene shark attack on a cetotheriid whale. Journal of Paleontology 56, 1480–1482.

Erickson, B.R. 1984: Chelonivorous habits of the Paleocene crocodile *Leidysuchus formidabilis*. Scientific Publications of the Science Museum of Minnesota, New Series 5, 1–9.

Floris, S. 1980: The coral banks of the Danian of Denmark. Acta Palaeontologica Polonica 25, 531–540.

Gaffney, E. S. 1990: The comparative osteology of the Triassic turtle *Proganochelys*. Bulletin of the American Museum of Natural History 194, 1–263.

Gravesen, P. 2001: Den geologiske udforskning af Fakse Kalkbrud fra midten af 1700-tallet til nu. Geologisk Tidsskrift 2001, 1–40.

Haynes, G. 1980: Prey bones and predators: potential ecological information from analyzing of bone site. Ossa 7, 75–97.

Haynes, G. 1983: A guide for differentiating mammalian carnivore taxa responsible for gnaw damage to herbivore limb bones. Paleobiology 9, 164–172.

Jacobsen, A.R. & Bromley, R.G. 2009: New ichnotaxa based on tooth impressions in dinosaur and whale bones. Geological Quarterly 53, 373–382.

Karl, H.-V. & Tichy, G. 2004: The structure of fossil teeth of chelonophagous crocodiles (Diapsida: Crocodylia). Studia Geologica Salmanticensia 40, 115–124.

Karl, H.-V. & Lindow, B.E.K. 2009: First evidence of a Late Cretaceous marine turtle (Testudines: Chelonioidea) from Denmark. Studia Geologica Salmanticensia 45, 175–180.

Karl, H.-V. & Lindow, B.E.K. in press: Revision of the Paleocene turtles of Denmark. In: H.-V. Karl (ed.), Studia Palaeocheloniologica IV. Turtle faunal change during the Jurassic-Cretaceous boundary in Germany and the rise of sea turtles. Studia Geologica Salmanticensa.

Kase, T., Johnston, P.A., Seilacher, A. & Boyce, J.B. 1998: Alleged mosasaur bite marks on Late Cretaceous ammonites are limpet (patellogastropoda) home scars. Geology 26, 947–950.

Kaufmann, E.G. 2004: Mosasaur predation on Upper Cretaceous nautiloids and ammonites from the United States Pacific coast. Palaios 19, 96–100.

Kaufmann, E.G. & Kiesling, R.V. 1960: An Upper Cretaceous ammonite bitten by a mosasaur. University of Michigan Contributions from the Museum of Paleontology 15, 193–248.

Lauridsen, B.W. & Damholt, T. 2011: Faxe Kalkbrud – et mylder af liv på frodige koralrev dybt på havets bund. In: Lindow, B.E.K. & Krüger, J. (eds), Geologiske naturperler – enestående brikker til Jordens puslespil, 52-67. Copenhagen: Gyldendal.

Linnaeus, C. v. 1758: Systema Naturae, 10th edition, 824 pp. Stockholmiae.

Mikuláš, R., Cadlecová, E., Fejfar, O. & Dvořák, Z. 2006: Three new ichnogenera of biting and gnaving traces on reptilian and mammalian bones: a case study from the Miocene of the Czech Republic. Ichnos 13, 113–127.

Milàn, J., Kofoed, J. & Bromley, R.G. 2010: Crocodylian – chelonian carnivory: bite traces of Dwarf Caiman, *Paleosuchus palpebrosus*, in Red-eared Slider, *Trachemys scripta*, carapaces. New Mexico Museum of Natural History and Science Bulletin 51, 195–199.

Noe-Nygaard, A. 1975: Erratics from the Danish Maastrichtian and Danian Limestones. Bulletin of the Geological society of Denmark 24, 75–81.

Rosenkrantz, A. 1920: Craniakalk fra Kjøbenhavns Sydhavn. Danmarks Geologiske Undersøgelse Serie II 36, 1–79.

Rosenkrantz, A. 1921: Meddelelse om tertiære Skildpadder fra Danmark. In: Oversigt over Dansk geologisk Forenings Møder og Ekskursioner fra Januar til December 1921. Meddelelser fra Dansk Geologisk Forening 6 (1), 2–3.

Rosenkrantz, A. 1923: En Trionyx fra Craniakalk-blokke i København. Meddelelser fra Dansk Geologisk Forening 6 (19), 3–14.

Schnetler, K.I., Lozouet, P. & Pacaud, J.-M. 2001: Revision of the gastropod family Scissurellidae from the Middle Danian (Paleocene) of Denmark. Bulletin of the Geological Society of Denmark 48, 79–90.

Schwarzhans, W. 2003: Fish otoliths from the Paleocene of Denmark. Geological Survey of Denmark and Greenland Bulletin 2, 1–94.

Schwimmer, D.R. 2010: Bite marks of the giant crocodylian *Deinosuchus* on Late Cretaceous (Campanian) bones. New Mexico Museum of Natural History and Science Bulletin 51, 183–190.

Schwimmer, D.R., Stewart, J.D. & Williams, G.D. 1997: Scavenging by sharks of the genus *Squalicorax* in the Late Cretaceous of North America. Palaios 12, 71–83.

Seilacher, A. 1998: Mosasaurs, limpets or diagenesis: how *Placenticeras* shells got punctured. Mitteilungen aus dem Museum für Naturkunde in Berlin – Geowissenschaftliche Reihe 1, 93–102.

Shimada, K. & Hooks, G.E. 2004: Shark-bitten protostegid turtles from the Upper Cretaceous Mooreville Chalk, Alabama. Journal of Paleontology 78, 205–210.

Surlyk, F. 1997: A cool-water carbonate ramp with bryozoan mounds: Late Cretaceous – Danian of the Danish Basin. In: James, N.P. & Clarke, J.A.D. (eds):, Cool-water Carbonates. Society for Sedimentary Geology Special Publication 56, 293–307.

Tanke, D.H. & Currie, P.J. 1998: Head-biting behavior in theropod dinosaurs: Paleopathological evidence. Gaia 15, 167–184.

Thomsen, E. 1976: Depositional environment and development of Danian bryozoan biomicrite mounds (Karlby Klint, Denmark). Sedimentology 23, 485–509.

Thomsen, E. 1983: Relation between currents and the growth of Palaeocene reef-mounds. Lethaia 16, 165–184.

Thomsen, E. 1995: Kalk og kridt i den danske undergrund. In: Nielsen, O.B. (ed.), Danmarks geologi fra Kridt til i dag. Århus Geokompendier 1, 31–67. University of Århus.

Troedsson, G.T. 1923: Om krokodilfyndan i Skånes yngsta Krita. GFF 45, 549–567.

Troedsson, G.T. 1924: On crocodilian remains from the Danian of Sweden. Lunds Universitets Årsskrift 20, 1–75.

Willumsen, M.E. 1995: Early lithification in Danian azooxanthellate scleractinian lithoherms, Faxe Quarry, Denmark. Beiträge zur Paläontologie 20, 123–131.

The emplacement and crystallization of the U–Th–REE-rich agpaitic and hyperagpaitic lujavrites at Kvanefjeld, Ilímaussaq alkaline complex, South Greenland*

HENNING SØRENSEN, JOHN C. BAILEY & JOHN ROSE-HANSEN

The U–Th–REE deposit located at the Kvanefjeld plateau in the north-west corner of the Ilímaussaq alkaline complex, South Greenland, consists of lujavrites which are melanocratic agpaitic nepheline syenites. The fine-grained lujavrites of the Kvanefjeld plateau can be divided into a northern and a southern part with an intermediate zone between them. The northern part is situated along the north contact of the Ilímaussaq complex and continues east of the Kvanefjeld plateau as a lujavrite belt along the contact. This part has relatively 'low' contents of U, Th, and REE, and hyperagpaitic mineralogy is restricted to its highest-lying parts. The fine-grained lujavrites of the intermediate and southern part of the Kvanefjeld plateau occur between and below huge masses of country rocks which we show are practically *in situ* remnants of the roof of the lujavrite magma chamber. These lujavrites have high contents of U, Th, and REE, and hyperagpaitic varieties with naujakasite, steenstrupine and villiaumite are widespread.

We present a model for the formation of the fine-grained lujavrites of the Kvanefjeld plateau. In this model, an off-shoot from the large lujavrite magma body in the central part of the complex intruded into a fracture zone along the north contact of the Ilímaussaq complex and was forcefully emplaced from north-west to south-east. The intruding lujavrite magma was bounded to the west, north, and at its roof by strong volcanic country rocks, and to the south by the weaker, earlier rocks of the complex. The magma stored in the fracture crystallized, squeezing volatile and residual elements upwards. A subsequent violent explosion opened up fractures in the weaker southern rocks, and the residual volatile-enriched magma was squeezed into fractures in augite syenite, naujaite, and also in the overlying volcanic roof rocks. The removal of the volatile-rich lujavrite magma in the upper part of the fracture-bounded magma chamber made room for the rise of volatile-poor magma from the lower part of the magma chamber, and these lujavrites crystallized to form the northern continuous lujavrite belt.

Transfer and accumulation of volatile and residual elements in a lujavrite magma crystallizing below an impervious cover played a key role in the formation of the Kvanefjeld U–Th–REE deposit, as it also did in the crystallization of the lujavrite magma body in the central part of the Ilímaussaq complex.

Henning Sørensen [kimik@compaqnet.dk], John C. Bailey [johnb@geo.ku.dk], John Rose-Hansen [rose-hansen@dadlnet.dk], Department of Geography and Geology (IGG), University of Copenhagen, Øster Voldgade 10, DK-1350 Copenhagen K, Denmark.

*) Contribution to the Mineralogy of Ilímaussaq no. 136

The Kvanefjeld plateau at the north-western corner of the Ilímaussaq[*] alkaline complex, South Greenland, has been a focus of economic interest since the discovery of its uranium–thorium deposit in 1956. Exploration was carried out by Danish Government institutions: the Geological Survey of Greenland, the Institute of Petrology of the University of Copenhagen, and the Atomic Energy Commission. The deposit was drilled in 1958, 1962, 1969 and 1977 with a total core length of 10,722 m. Core logs are described in internal reports by Sørensen *et al.* (1971), Nyegaard *et al.* (1977) and Nyegaard (1979).

The plateau was topographically mapped in 1957 and 1964, and geological mapping was carried out from 1964 to 1969 (Sørensen *et al.* 1969, 1974).

From 1978 to 1980, a 960 m long tunnel was driven through the Kvanefjeld lujavrites at an elevation of 470–512 m above sea level (a.s.l.), about 150 m below the surface of the plateau. Its geology is described in an internal report (Nyegaard 1980). The purpose was to procure material for ore beneficiation experiments, which were carried out at Risø National Laboratory, Denmark, and are documented in many reports (Kalvig 1983). The activities run by the Danish Government were closed in 1984 when nuclear energy was removed from the Danish agenda and uranium exploration was banned by the Greenland authorities.

In 2002, it was decided to close the research reactor at Risø and to clean the area of all radioactive materials. Because there was a great risk that the drill cores would be part of this decommissioning activity, we examined the cores once more to secure material of crucial geological importance. Representative samples from all cores are stored at the Department of Geography and Geology, University of Copenhagen.

Although the Danish exploration of the Kvanefjeld deposit was closed in 1984, scientific examination of the huge amount of sampled material has continued to this day. The present paper presents our interpretation of the emplacement and petrology of this unique mineral occurrence.

Geological setting

The Ilímaussaq complex (Fig. 1) is a late member of the Mid-Proterozoic Gardar province of South Greenland and dates to around 1160 Ma (see reviews by Larsen & Sørensen 1987; Markl *et al.* 2001; Sørensen 2006). It was intruded into basement granitoids and uncomform-

ably overlying sandstones and lavas which form part of the Gardar supracrustals.

The complex is the type locality for agpaitic nepheline syenites (Ussing 1912), i.e. peralkaline nepheline syenites with complex Zr–Ti silicate minerals such as eudialyte and rinkite (the chemical compositions of the minerals mentioned in the text are given in Table 1). The term hyperagpaitic was introduced to characterize certain mineral associations in special pegmatites and veins from the Lovozero and Khibina complexes of the Kola Peninsula, Russia (Khomyakov 1995). These mineral associations represent a more highly evolved stage than in the common agpaitic rocks and are distinguished by a great variety of Na-rich minerals some of which are soluble in water. In the Ilímaussaq complex, hyperagpaitic mineral associations occur not only in pegmatites and veins but also in highly evolved lujavrites and in fenitized roof rocks (Sørensen 1997; Khomyakov *et al.* 2001; Sørensen & Larsen 2001; Andersen & Sørensen 2005).

The exposed part of the complex was emplaced in four main intrusive phases (Sørensen 2006). Phase 1 formed a mildly alkaline augite syenite shell, while phase 2 formed peralkaline quartz syenite and alkali

Table 1. Minerals mentioned in the text

Mineral	*Chemical formula*
aegirine	$NaFeSi_2O_6$
albite	$NaAlSi_3O_8$
analcime	$NaAlSi_2O_6 \cdot H_2O$
arfvedsonite	$Na_3(Fe^{2+},Mg)_4Fe^{3+}Si_8O_{22}(OH)_2$
britholite	$(Ce,Ca)_5(SiO_4,PO_4)_3(OH,F)$
eudialyte	$Na_{15}Ca_6Fe_3Zr_3Si_{26}O_{73}(O,OH,H_2O)_3(Cl,OH)_2$
microcline	$KAlSi_3O_8$
monazite	$(Ce,La,Nd,Th)PO_4$
natrolite	$Na_2Si_3Al_2O_{10} \cdot 2H_2O$
naujakasite	$Na_6(Fe,Mn)Al_4Si_8O_{26}$
nepheline	$(Na,K)AlSiO_4$
neptunite	$KNa_2Li(Fe,Mg,Mn)_2Ti_2Si_8O_{24}$
rhabdophane	$(Ce,La,Nd)PO_4 \cdot H_2O$
rinkite	$(Na,Ca)_3(Ca,Ce)_4(Ti,Nb)(Si_2O_7)_2(O,F)_4$
Sodalite	$Na_4Si_3Al_3O_{12}Cl$
sphalerite	ZnS
steenstrupine	$Na_{14}(Ce,Th,U)_6Mn_2Fe_2Zr(PO_4)_7Si_{12}O_{36}(OH)_2 \cdot 3H_2O$
ussingite	$NaAlSi_3O_8NaOH$
villiaumite	NaF
vitusite	$Na_3(Ce,La,Nd)(PO_4)_2$
vuonnemite	$Na_5TiNb_3(Si_2O_7)_3O_2F_2 \cdot 2Na_3PO_4$

---

[*] old Greenlandic orthography is used for the established name of the geological complex; modern Greenlandic orthography is used for all place names.

granite sheets beneath the roof. Phase 3 formed a roof series which crystallized from the roof downwards in the succession pulaskite, foyaite, sodalite foyaite and the volumetrically dominant naujaite; the assumed simultaneously produced floor cumulates are not exposed. Phase 4 formed the exposed floor cumulates, kakortokites, followed upwards by varieties of aegirine lujavrite and arfvedsonite lujavrite. The lujavrites thus form a sandwich horizon between the roof series and the kakortokites (Ussing 1912; Ferguson 1964; Rose-Hansen & Sørensen 2002).

The Kvanefjeld plateau measures close to 2.1 x 0.9 km (Figs 1, 2) and comprises the westernmost part of a 4.5 km long belt of lujavrites that stretches south-west from the foothills of the Ilimmaasaq mountain (Fig. 1). The north and west margins of the plateau coincide with the north and west contacts of the complex. To the north-east the Kvanefjeld lujavrites are continuous with the lujavrites beneath Steenstrup Fjeld (Figs. 1, 3). The east margin of the plateau is the escarpment just east of the small peak of Kvanefjeld mountain (Fig. 3). The south-east margin is the steep slope towards the Narsaq Elv valley. In the western part of this slope,

the lujavrites of the plateau are underlain by augite syenite and below that by naujaite. The eastern part of the valley slope consists from the top downwards of country rocks, medium- to coarse-grained lujavrite (M-C lujavrite), fine-grained lujavrite, and in the river valley naujaite (Fig. 4).

The adjacent country rocks are Gardar supracrustals - lavas, agglomerates and sandstones - which are intruded by dykes and sheets of gabbro and trachyte. These rocks form the NE–SW trending ridges that dominate the topography of the southern part of the plateau and are prominent in many of its drill cores, but they play a minor role in the northernmost part of the plateau and the area below Steenstrup Fjeld which are dominated by lujavrites (Figs. 1, 2; Sørensen et al. 1969, 1974; Nyegaard 1979).

The basaltic country rocks adjacent to the lujavrites below Steenstrup Fjeld and Ilimmaasaq mountain and in the ridges of gabbro and other roof rocks in the southern part of the Kvanefjeld plateau are strongly sheared. The vertical shear planes are oriented NE–SW, i.e. parallel to the contact of the complex. The shear zones in the ridges of roof rocks are intruded
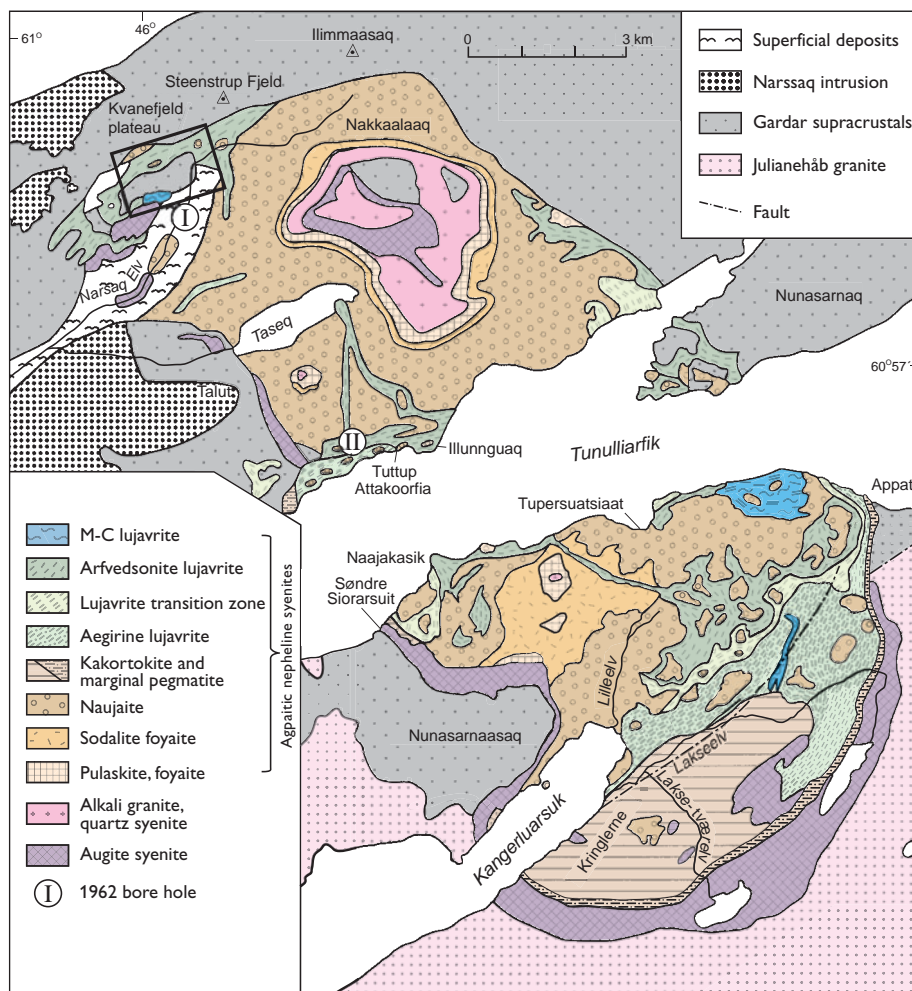
Fig. 1. Simplified geological map of the Ilímaussaq complex mainly based on Ferguson (1964) and Andersen et al. (1988). The frame in the upper left corner indicates the area shown in Fig. 2. Ringed numbers I and II are boreholes from 1962 mentioned in the text (Rose-Hansen & Sørensen 2002). All place names are given in modern Greenlandic orthography.

by fine-grained lujavrites (Sørensen *et al.* 1969, 1974).

Sørensen *et al.* (1974) divided the Kvanefjeld plateau into a southern central part, a northernmost part and a north-eastern part. We distinguish here a narrow northern part that is continuous with the lujavrites in the foothills of Steenstrup Fjeld and Ilímmaasaq mountain, a southern part dominated by the ridges of country rocks, and an intermediate zone between these two parts.

On the Kvanefjeld plateau and its south slope, lujavrites are exposed from 650 to 325 m a.s.l. (Sørensen *et al.* 1969) and in the steep foothills of Steenstrup Fjeld and Ilímmaasaq mountain from 800 to 400 m a.s.l. (Ferguson 1964; Sørensen 2006). Fine-grained lujavrites occur in most of the drill cores on the Kvanefjeld plateau, down to 195 m a.s.l. in core 37 terminating in naujaite, and down to 271 m a.s.l. in core 38 terminating in lujavrite. A borehole placed at a low stratigraphical position in the Kvanefjeld area and drilled to 500 m ended in lujavrite (GMEL 2008, p. 36).

In the northern part of the Kvanefjeld plateau, the lujavrites are separated from the country rocks by naujaite and a marginal pegmatite (Fig. 2) which are sheared and altered. Short apophyses of naujaite with the characteristic poikilitic texture intrude the basalts and there are small basaltic xenoliths in a narrow contact-near zone in the naujaite (Steenfelt 1972).

Naujaite xenoliths measuring tens of metres are seen on the surface and in drill cores from the plateau, the Steenstrup Fjeld area and at depth in the tunnel. Large augite syenite, alkali syenite and anorthosite xenoliths are restricted to the south-western part of the plateau where they dominate outcrops. Nielsen and Steenfelt (1979) noted the identical orientation of structures in some neighbouring augite syenite xenoliths.

Small (centimetre- to decimetre-sized) xenoliths of volcanic country rocks and naujaite are common in outcrops and cores. Xenoliths of pulaskite, foyaite and sodalite foyaite are found on the Kvanefjeld plateau and along the north contact of the complex from Kvanefjeld to Ilímmaasaq where some xenoliths consist of pulaskite and sheared basalt that may represent samples of the original apicalcontact of the complex. At Kvanefjeld, the transition from pulaskite to naujaite takes place over 5 m in one large roof series xenolith (Steenfelt 1972; Sørensen *et al.* 1974). In core 44 from the Steenstrup Fjeld area, centimetre- to decimetre-sized xenoliths change from foyaite through sodalite foyaite to naujaite with increasing depth and thus, despite fragmentation, reproduce the downward sequence of the roof series.
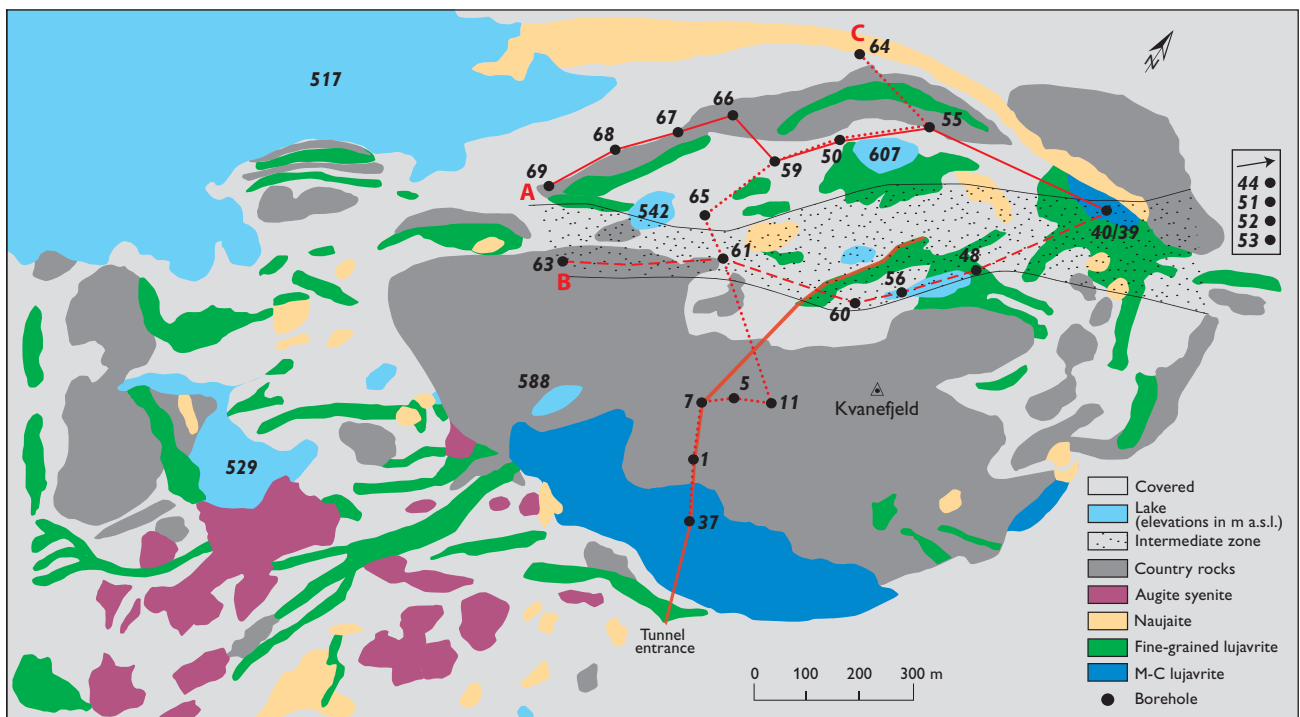
Fig. 2. Simplified geological map of the Kvanefjeld plateau based on Sørensen *et al.* (1974). Boreholes (drill cores) are shown as black dots with numbers. The kinked red lines A, B and C show the three constellations of drill cores depicted in Fig. 6. The location of all boreholes mentioned in the present paper is shown in Fig. 5. The position of the tunnel (thick red line) is shown projected onto the surface. The intermediate zone between the northern and southern parts of the Kvanefjeld plateau is discussed in the text.

Geological relations of the fine-grained lujavrites of the Kvanefjeld plateau

The Kvanefjeld plateau contains several varieties of fine-grained lujavrite including aegirine-, arfvedsonite-, naujakasite- and brown aegirine ('acmite') lujavrites. Because of the complexity of their distribution they are all grouped together as fine-grained lujavrite on the published geological map of the Kvanefjeld plateau (Sørensen *et al.* 1969, 1974). The M-C lujavrite in the southern part of the plateau represents a younger intrusive phase (Figs 2, 4) (Sørensen *et al.* 1969) and is not the subject of this paper.

Geological mapping of the northern part of the plateau showed a regular distribution of the different lujavrite types (Sørensen *et al.* 1974). The lujavrites in contact with the volcanic country rocks in the sidewall, and with the roof in cores 64 and 70, are rich in aegirine and grade inwards and downwards into arfvedsonite lujavrites. Aegirine lujavrite is found in contact with the naujaitic wall rocks, and aegirine commonly occurs in the contact between arfvedsonite lujavrite and naujaite xenoliths. The development of aegirine thus seems to take place near contacts.

The aegirine-rich lujavrites are succeeded inwards by arfvedsonite lujavrites and these again by lujavrites rich in brown aegirine (acmite in earlier literature), in the following called brown lujavrites, and by naujakasite lujavrites. Macroscopically, the northern arfvedsonite lujavrites are characterized by vertical sequences extending for around 100 m in drill cores and consisting of alternations of lujavrite with spheroidal texture and lujavrite with brown aegirine patches and schlieren (*cf.* Sørensen *et al.* 2003). It appears that there is a gradual transition from the lujavrites of the northern part of the plateau into those of the intermediate zone, often in the form of alternating bands of the different rocks. Rare cases of naujakasite lujavrite

intruding other lujavrites have been noted, and there are at least two generations of naujakasite lujavrite. Exposures and the drill cores available to us are insufficient to decide whether the relations between these lujavrites and the lujavrites covered by gabbro in the southern part of the plateau are gradational or not.

Villiaumite is common in the cores at the Kvanefjeld plateau but, due to dissolution by groundwater, the cores lack villiaumite within 50 m of the surface and the mineral is uncommon down to the 100 m level. Villiaumite is rare elsewhere in the Ilímaussaq complex (Sørensen *et al.* 1974; Rose-Hansen & Sørensen 2002).

Naujakasite lujavrite

Naujakasite lujavrite occurs at several levels in the cores. It is the predominant lujavrite in the tunnel and has been observed in 28 of our 66 cores, although many of our cores are too shallow to reach the naujakasite lujavrite sequences (Fig. 5).

Naujakasite lujavrite typically occurs as the uppermost part of arfvedsonite lujavrite sequences. With the exception of cores 35, 50 and 56, which are located on naujakasite lujavrite exposures, and thin horizons in arfvedsonite lujavrite, naujakasite lujavrite in all cores examined by us underlies xenoliths of naujaite, augite syenite or country rocks. The highest-lying naujakasite lujavrites are in contact with the rocks of the roof of the lujavrite magma. At 580 to about 550 m a.s.l., naujakasite lujavrite underlies naujaite xenoliths, and at about 500 m a.s.l. it underlies augite syenite xenoliths. In eleven cores, there is a thin naujakasite-free zone between xenoliths and the underlying naujakasite lujavrite.

The majority of upper boundaries of naujakasite lujavrite horizons lie at 570 ± 10 m, 550 ± 10 m and 510 ± 10 m, a few at higher and lower elevations. Thin sheets of arfvedsonite lujavrite and naujakasite lujavrite intersect xenoliths of country rocks and naujaite at these el-
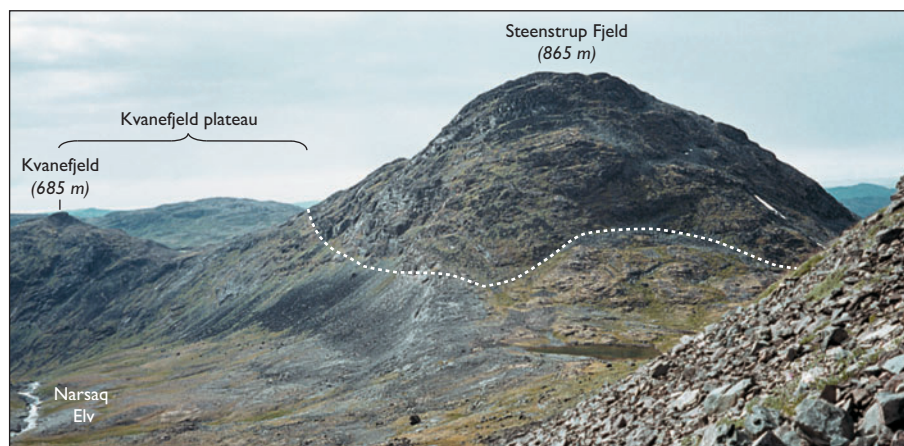
Fig. 3. The Kvanefjeld plateau seen between Steenstrup Fjeld to the right and Kvanefjeld to the left, looking WSW from the foothill of the Ilimmaasaq mountain. The sharp contact between the volcanic country rocks (right) and the scree-covered lujavrites is marked by a dashed white line.

evations, an indication of prominent near-horizontal fracture systems. Five cores terminate in naujakasite lujavrite. The longest naujakasite lujavrite intersection in cores is 95 m and the lowest-lying naujakasite lujavrite horizon is at 420 m a.s.l. Only exceptionally are naujakasite lujavrite horizons found at the same elevation in adjacent cores, though the elevation of their upper boundaries may vary in a regular way.

The 960 m long tunnel presents a horizontal N–S section through the plateau about 150 m below its surface (Figs. 2, 4). From its opening in the south slope of the plateau and northwards, the tunnel intersects augite syenite intruded by arfvedsonite lujavrite, a sheet of M-C lujavrite, and, measured from the opening, at 220–460 m, 585–640 m, 680–740 m and 755–880 m, four sections of naujakasite lujavrite which are separated from each other by sections of country rocks, naujaite and arfvedsonite lujavrite (Nyegaard 1980). The tunnel terminates in volcanic country rocks about 200 m from the position of the north contact, assuming that the contact plane is vertical. Thus naujakasite lujavrite dominates a more than 600 m wide horizon about 150 m below the surface of the plateau.

Of the many boreholes in the area above the tunnel, only boreholes 1 and 7 are intersected by the tunnel. In core 1, 20 m of naujakasite lujavrite forms the upper part of an arfvedsonite lujavrite sequence that terminates the core at 442 m a.s.l. (Fig. 6). In core 7, 95 m of naujakasite lujavrite terminate the core at 490 m a.s.l. (Fig. 6). There are three 10 m thick horizons of arfved-

sonite lujavrite in the naujakasite lujavrite. Boreholes 1 and 7 are located about 125 m from each other. The upper boundary of the naujakasite lujavrite lies at 500 m a.s.l. in core 1, and at 585 m a.s.l. in core 7. This large difference of 85 m shows that the naujakasite lujavrite sections intersected by the tunnel cannot be assembled into one unbroken horizon. This impression is strengthened by the observation that cores 43 and 63, located about 200 m and 350 m west of the tunnel, intersect naujakasite lujavrite from 520 to 500 m a.s.l. in core 43 and from 500 to 430 m a.s.l in core 63, that is thicknesses of 20 and 70 m. Core 33 located 100 m west of core 7 has two horizons of naujakasite lujavrite at 570 to 560 and 518 to 505 m a.s.l., and in core 42, 50 m north of core 5, a 170 m long sequence of volcanic country rocks is intruded by naujakasite lujavrite from 610 to 555 and 515 to 495 m a.s.l. The few other long cores in this part of the plateau do not intersect naujakasite lujavrite.

Naujakasite lujavrite is absent in most cores from the north Kvanefjeld–Steenstrup Fjeld lujavrite belt, but it has been observed in outcrops and in cores 39, 50, 69 and 70. In core 50 it occurs as a thin zone in the uppermost part of an exposure of arfvedsonite lujavrite (Fig. 6), and in cores 39, 69 and 70 it occurs beneath country rock xenoliths in arfvedsonite lujavrite.

Borehole 35 is the most south-westerly borehole on the Kvanefjeld plateau, and here naujakasite lujavrite veins intrude the closely packed augite syenite and naujaite xenoliths. These veins have xenoliths of au-
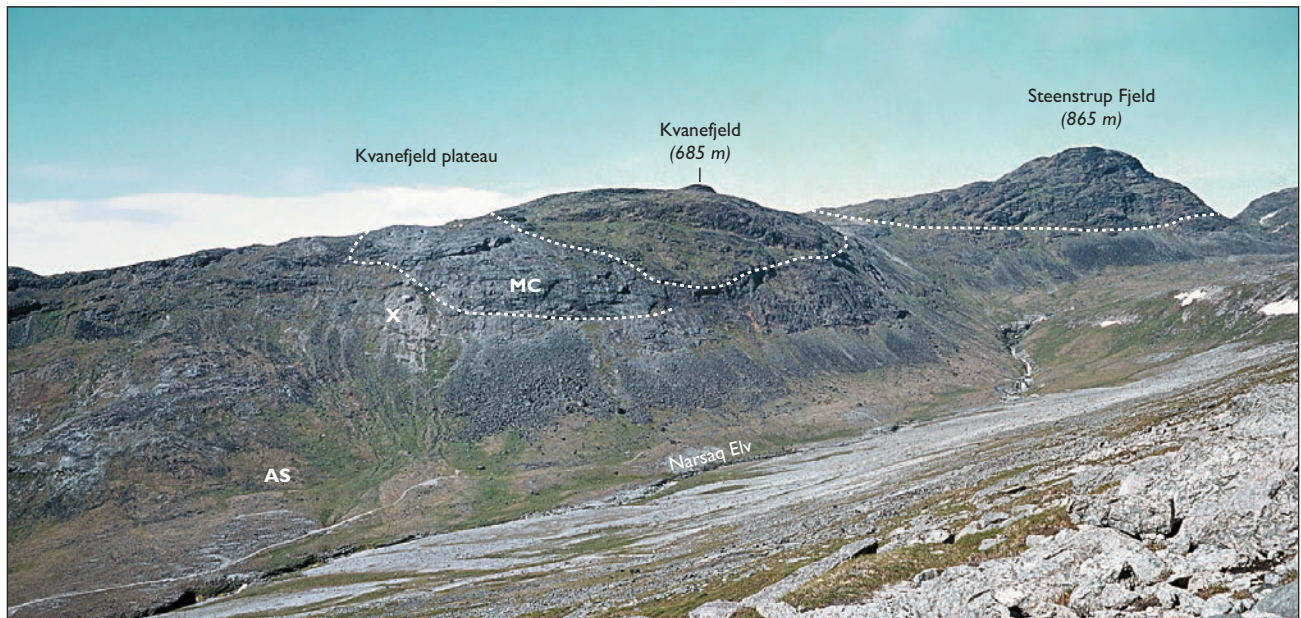
Fig. 4. Kvanefjeld with a small peak at 685 m in the centre and Steenstrup Fjeld to the right, viewed from the south. The sharp contact between the volcanic country rocks and the underlying lujavrites is marked by a dashed white line. In the centre of the photo, the medium- to coarse-grained lujavrite (MC) sheet underlying the volcanic rocks is also indicated. The brownish rock at the foot of the Kvanefjeld plateau to the left is augite syenite (AS). The light-coloured rock low in the river valley is naujaite. The photo is from 1974 before the tunnel was made. The entrance of the later tunnel is indicated with a white ×.

gite syenite, naujaite, foyaite and volcanic roof rocks. Parts of the south slope of the plateau are covered with veritable naujakasite gravel.

Steenstrup Fjeld lujavrites

The Steenstrup Fjeld lujavrites are continuous with the Kvanefjeld lujavrites (Figs. 1, 3, 4). The lujavrites in the footwalls of Steenstrup Fjeld and Ilimmaasaq mountain were not included in the detailed mapping of the Kvanefjeld plateau. A reconnaissance examination of the area and four boreholes (44, 51, 52, 53; Figs. 2, 6) showed that, similar to the northern part of the Kvanefjeld plateau, arfvedsonite lujavrite and brown lujavrite dominate this lujavrite area. The former is

weakly radioactive (0.1–0.2 milliroentgen per hour (mr/h), similar to the northern arfvedsonite lujavrites of the plateau), whereas the brown lujavrite, in places naujakasite-bearing, is moderately radioactive (0.4-0.5 mr/h similar to the brown lujavrites of the plateau). Two samples of the brown lujavrite were analysed and contain 340 ppm U, 866 ppm Th, and 616 ppm U, 1560 ppm Th. The south contact of the lujavrites has been eroded but field relations indicate that naujaite formed the south wall (Fig. 1).

The arfvedsonite lujavrite next to the volcanic country rocks in the north contact is rich in aegirine and aegirine-bearing M-C lujavrite veins. A separate large body of aegirine lujavrite is enclosed in and intruded by the arfvedsonite lujavrite. Its lamination is near vertical and parallel to the lamination of the
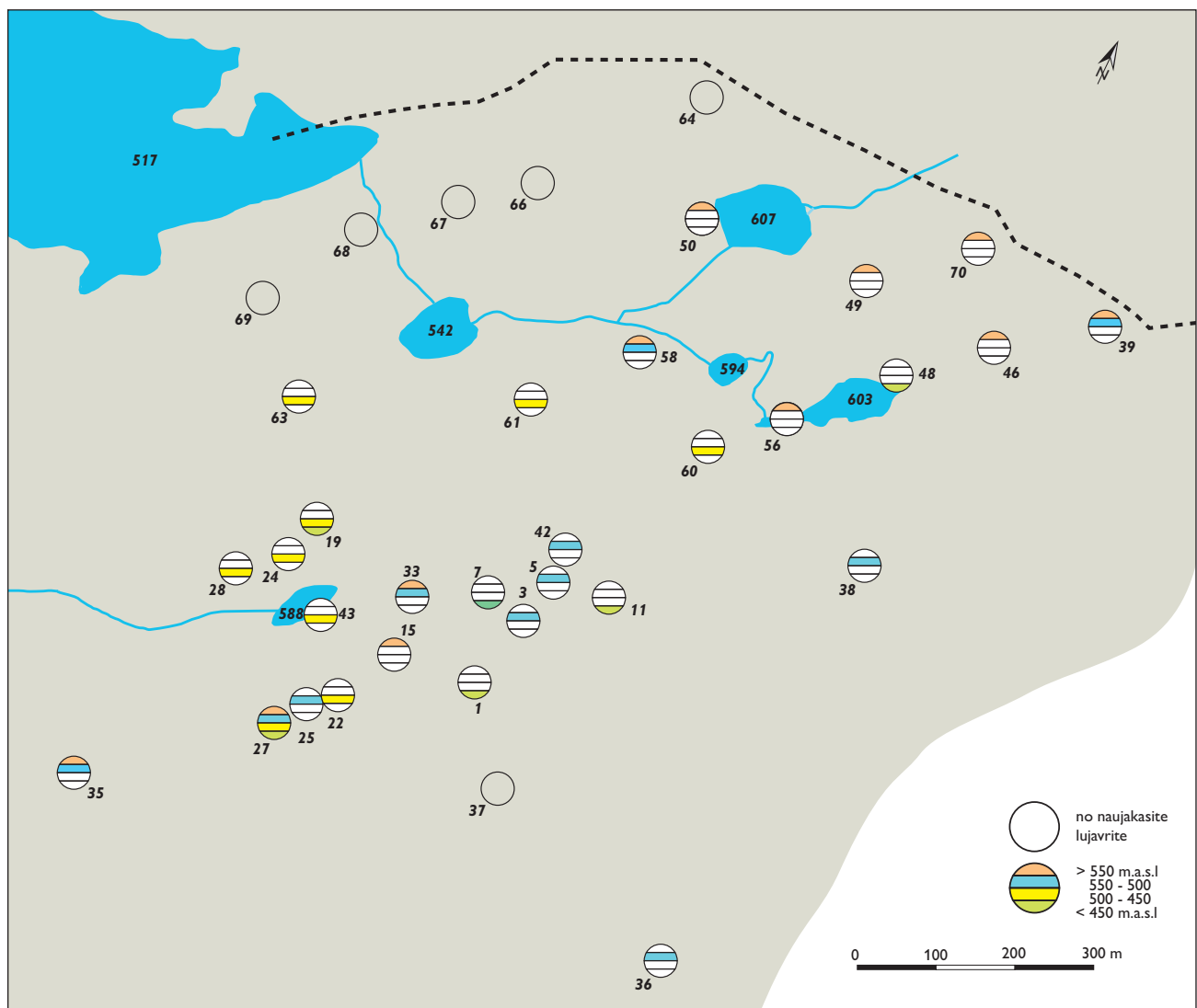
Fig. 5. Sketch map of the Kvanefjeld plateau showing the elevation of the upper boundary of the horizons of naujakasite lujavrite in the drill cores. The elevation is generally highest in the north-east and is lower and irregular in other parts of the plateau; see text for discussion. Compare with Fig. 2. The figure also shows the location of all the boreholes on the Kvanefjeld plateau mentioned in the text. The dashed line marks the north-eastern boundary of the Ilìmaussaq complex.
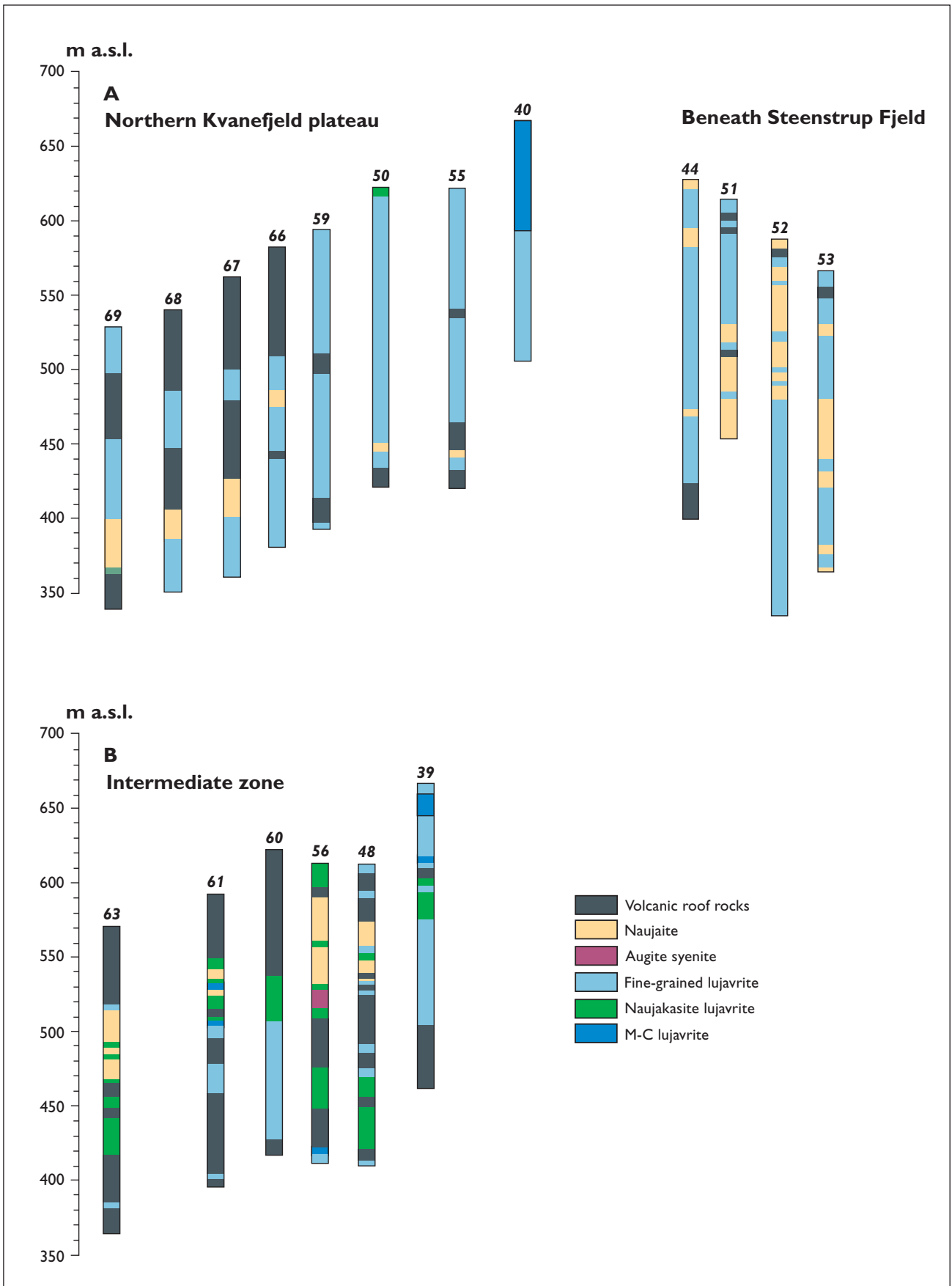
enclosing arfvedsonite lujavrite and to shear zones in the adjacent country rocks. Some sections of the cores consist of layered and /or spheroidal lujavrites. Large naujaite xenoliths are found in the upper parts of the two northerly cores (44 and 52), and in the lower part of the southerly cores (51 and 53; Fig. 6). Villiaumite is present in large parts of the lujavrites and also in naujaite. Naujakasite was not observed in the four cores. Small xenoliths of volcanic country rocks are widespread; xenoliths of pulaskite, foyaite, sodalite foyaite and augite syenite are found up to 770 m a.s.l. in the footwall of Ilimmaasaq mountain.

The area has been re-examined by Greenland Minerals and Energy Ltd. (GMEL) who found a 250 m wide zone of mineralized lujavrite at a higher level than represented by our four boreholes (GMEL 2008, p. 26).
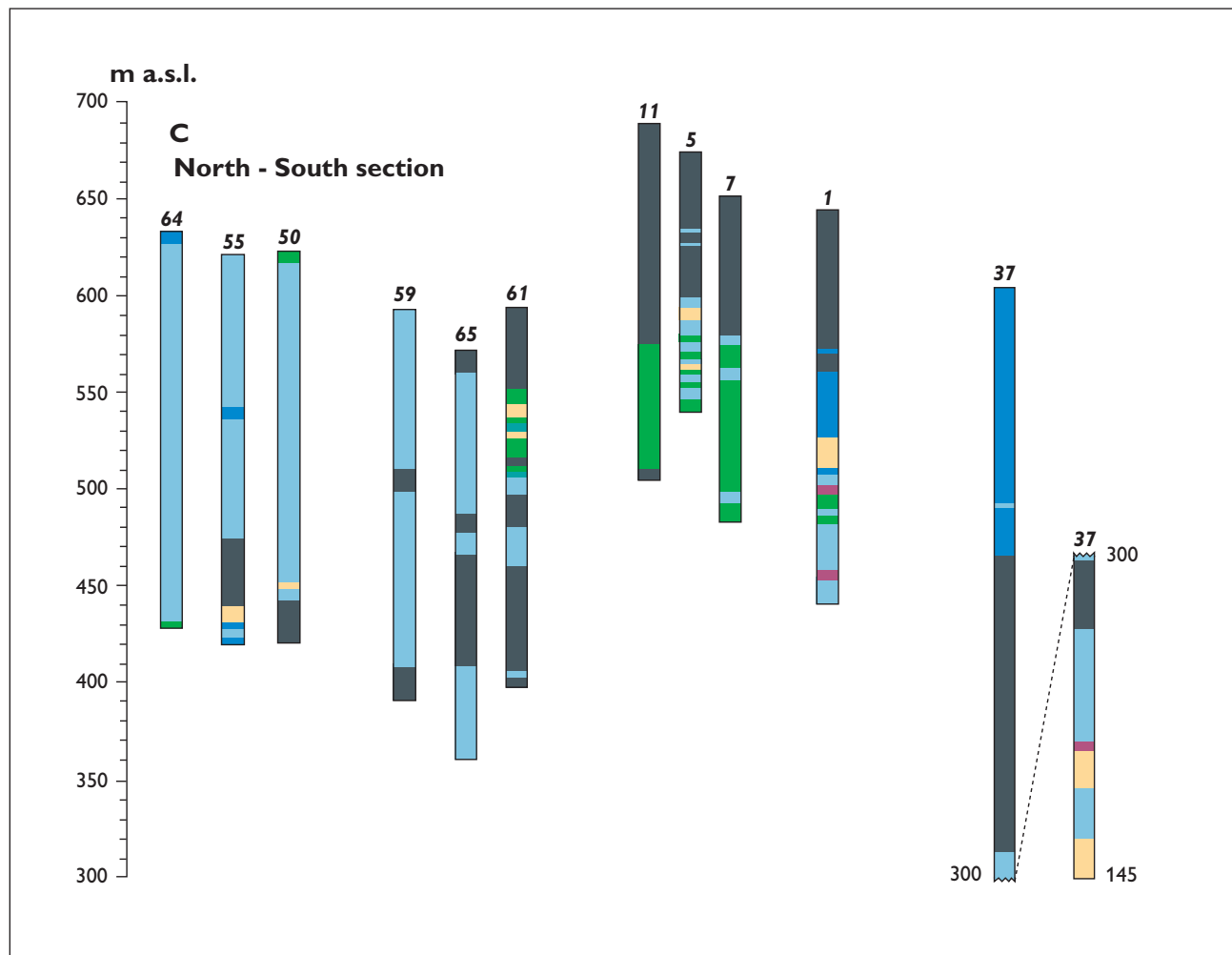
Fig. 6. Constellations of drill core logs. Facing page: **A**. Logs from the northernmost part of the Kvanefjeld plateau and the Steenstrup Fjeld area. With the exception of core 50, these cores do not contain naujakasite lujavrite. Note the sloping boundaries of xenoliths in cores 66-67-68-69 and of naujaite in cores 67-68-69. Also note that the number of roof rock xenoliths decreases from core 69 (west) to core 40 (east). **B**. Logs of cores from the southern part of the Kvanefjeld plateau where lujavrites crystallized under a tight cover of roof rocks and naujakasite lujavrite is frequent. Note the irregular location of naujakasite lujavrite in these cores, the possible arch-form of the elevation of the lower boundaries of roof xenoliths in cores 60-61-62-63, and that the roof xenoliths have been removed by erosion in cores 56-48-39. This page: **C**. A north-south section through the plateau. Cores 64-55-50-59-65 belong to the northern part of the plateau where naujakasite lujavrite is nearly absent. Cores 61-11-5-7-1 are from the central and southern part of the plateau where lujavrites crystallized under a tight cover and naujakasite lujavrite is frequent. Cores 1 and 7 intersect the tunnel at 500 m a.s.l. The lower boundary of the roof xenoliths in cores 11-5-7 forms an upwards-convex form and these cores have particularly thick naujakasite lujavrite sequences. Core 37 is the southernmost deep drill-hole that was sited in M-C lujavrite. Vertical scale, metres above sea level; horizontally, the cores are arranged with approximately correct distances between them. The location of the three sections A, B and C is shown in Fig. 2.

The M-C lujavrite

A large body of medium- to coarse-grained, unlaminated lujavrite, described as M-C lujavrite (Sørensen *et al*. 1969), is exposed in the south part of the Kvanefjeld plateau (Figs. 2, 4). It is at least 700 m long, roughly 200 m across and up to 160 m thick. It continues from the surface of the plateau at 610–620 m down through the tunnel at *c*. 480 m a.s.l. and is still present in some cores at 400 m a.s.l. It forms a cylinder- or sheet-like intrusion plunging towards the east. The M-C lujavrite intersects and encloses all other rocks and intersects the structures of the pre-existing intrusion breccia and its matrix of fine-grained lujavrite. It sends apophyses and pegmatitic and hydrothermal veins into the adjacent rocks which are strongly deformed, even folded, and are recrystallized and metasomatized up to 200 m from the contact of the body (Sørensen *et al*. 1969, 1974). In the contact aureole, gabbro and basalt with shear zones invaded by fine-grained arfvedsonite lujavrite are folded and recrystallized close to the M-C lujavrite. The result is a lujavrite-looking rock which, however, is a contact metamorphosed rock that cannot be distinguished from altered lujavrite in thin section. The arfvedsonite and feldspar are partly or wholly converted to aegirine and zeolites, respectively. These rocks are the U- and Th-richest rocks of the plateau with up to 15 vol. % steenstrupine that occurs in clusters of small crystals or as large crystals that may contain abundant inclusions and show a sub-poikilitic texture. The metasomatized rocks have up to 0.1% U and 0.5% Th and were the target for the first phase of uranium exploration.

Petrography of the lujavrites of the Kvanefjeld plateau

Away from the north contact, the aegirine lujavrite is moderately laminated and consists of nepheline wrapped by aegirine needles, microcline laths, pale yellow platy eudialyte and occasional albite laths. There is a small amount of sodalite. All felsic phases are partly altered to analcime, which also occurs interstitially. Aegirine can be surrounded by sub-poikilitic arfvedsonite and is occasionally altered to brown aegirine. Accessory minerals include vitusite, neptunite and sphalerite.

The Kvanefjeld plateau arfvedsonite lujavrites are strongly to moderately laminated, cumulate rocks. Subhedral crystals of nepheline and occasional sodalite are wrapped by smaller albite laths and/or microcline plates and stout prismatic arfvedsonite crystals. Nepheline and sodalite contain randomly
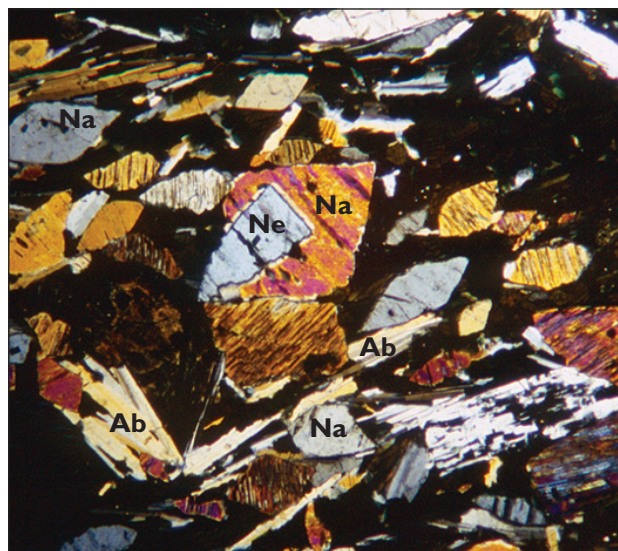
Fig. 7. Microphoto (crossed polarizers) of naujakasite lujavrite from core 7, depth 112.20 m. Note the parallel orientation of the lozenge-shaped naujakasite crystals (Na) and the feldspar laths (Ab). In the centre, a nepheline crystal (Ne) is partially overgrown by naujakasite. Black: arfvedsonite and analcime). Width of photo 5 mm.

oriented inclusions of arfvedsonite and feldspars. The albite laths are occasionally bent and broken. The microcline shows the tiled pattern of penetration twinning typical of agpaitic rocks (Ussing 1893; Sørensen 1962; Borutskii & Semenov 1969; Smith & McLaren 1983). Small platy, dusty eudialyte crystals are occasionally preserved and may reach *c*. 5 vol % but are usually altered to fine-grained mixtures of monazite splinters and other secondary products. Steenstrupine is widespread in the lujavrites of the southern and intermediate zones and may make up 10–15 vol. % of the rocks. Minor accessories include vitusite, britholite, white mica (?Li-mica), sphalerite, galena and monazite-rhabdophane pseudomorphs after vitusite. Ussingite occurs in millimetre-sized patches in a few thin sections of arfvedsonite lujavrite from the northern Kvanefjeld plateau where it replaces feldspars (Makovicky *et al*. 1980).

The distribution and varieties of steenstrupine overlap in naujakasite lujavrite and in the preceding and succeeding arfvedsonite lujavrite. The freshest steenstrupine is cream-coloured and metamict. Crystals are often zoned in shades of brown and variably altered to a fine-grained mixture of minerals. Small steenstrupine crystals tend to concentrate in the margins of naujakasite crystals (Buchwald & Sørensen 1961; Sørensen 1962; Wollenberg 1971; Sørensen *et al*. 1974; Makovicky *et al*. 1980; Khomyakov *et al*. 2001; Khomyakov & Sørensen 2001). Pseudomorphs after steenstrupine consist of monazite, neptunite and micron-sized thorite, but only of analcime and minute

needles of arfvedsonite and aegirine in the ultimate alteration product.

Petrographically, when arfvedsonite lujavrite grades into naujakasite lujavrite, naujakasite appears to take over the role of nepheline. Grains of naujakasite can overgrow nepheline and there are examples of naujakasite with small, corroded nepheline cores (Fig. 7) (Khomyakov *et al.* 2001).

At all contents of naujakasite, the least altered rocks contain no well-defined interstitial material. Instead, there are isolated pools and patches of dusty natrolite or analcime.

Naujakasite lujavrite is overlain by arfvedsonite lujavrites in several drill cores. As the amount of naujakasite decreases, nepheline again becomes abundant. The arfvedsonite lujavrite overlying naujakasite

Table 2. Uranium and thorium in fine-grained lujavrites of the Kvanefjeld plateau

Tunnel	Distance from opening, m		Rock type*	U, ppm	Th, ppm	Th/U
	220–450		Njk lujavrite	296–603	402–1392	1.1–2.9
	585–640		Njk lujavrite	322–379	776–1126	2.2–2.4
	690–730		Njk lujavrite	192–330	245–876	2.3–2.4
	755–880		Njk lujavrite	298–543	654–1291	1.4–2.9
Boreholes	Depth in core, m	Zone				
No 1	147.60	S	Njk lujavrite	342	815	2.4
	156.06		Njk lujavrite	343	1100	3.2
	159.60		Arf lujavrite	470	1130	2.4
	178.50		Arf lujavrite	34	1340	3.8
No 5	82.52	S	Arf lujavrite	447	2495	5.6
	105.70		Arf lujavrite	271	613	2.3
	115.68		Arf lujavrite	464	1276	2.8
	124.40		Njk lujavrite	646	1671	2.6
No 7	81.05	S	Njk lujavrite	433	1352	3.1
	85.10		Njk lujavrite	483	1542	3.2
	91.50		Njk lujavrite	736	2165	2.9
	94.53		Njk lujavrite	825	3310	4.0
	106.50		Njk lujavrite	852	2875	3.4
	129.85		Njk lujavrite	639	1420	2.3
	145.70		Njk lujavrite	291	547	1.9
	161.10		Njk lujavrite	268	538	2.0
No 11	121.05	S	Njk lujavrite	531	1420	2.7
	130.25		Njk lujavrite	570	1185	2.1
	135.15		Njk lujavrite	263	790	3.0
	149.00		Njk lujavrite	462	650	1.4
	149.10		Njk lujavrite	410	700	1.7
	151.53		Njk lujavrite	403	1407	3.5
No 37	44.35	S	Arf lujavrite	317	743	2.3
No 38	382.50	S	Arf lujavrite	211	294	1.4
No 48	170	I	Njk lujavrite	376	874	2.3
No 49	74	I	Njk lujavrite	369	764	2.1
	120		Arf lujavrite	417	780	1.9
No 50	71	N	Arf lujavrite	280	360	1.3
No 55	40	N	Arf lujavrite	316	533	1.7
No 59	60	N	Arf lujavrite	243	619	2.6
No 60	101	N	Njk lujavrite	375	960	2.6
No 64	10	N	Ae lujavrite	106	186	1.8
No 70	140	N	Arf lujavrite	300	365	1.2

*) Ae= aegirine; Arf= arfvedsonite; Njk= naujakasite.
S = Southern Zone, I = Intermediate Zone, N = Northern Zone.

lujavrite is, in most cases, moderately to intensely zeolitized.

Solution cavities in the lujavrites are thought to indicate the former presence of villiaumite. This is clear for cavities where relict villiaumite is still present, but cavities may result from the former presence of other water-soluble minerals such as natrosilite (Sørensen 1982). There are occasional diffuse bands, as well as sharply defined veins, rich in villiaumite or relict cavities. In some villiaumite-bearing lujavrites, zeolites are totally or largely absent and only villiaumite occupies interstitial areas. Villiaumite is occasionally seen in metasomatized naujaite xenoliths (e.g. Nyegaard 1980). The interstitial distribution of villiaumite suggests it is a late magmatic mineral, and the occurrence of marginal zones of zeolites around cores of villiaumite imply that it is the last magmatic mineral to crystallize. In some rocks villiaumite forms large interstitial pools with poikilitic outer margins.

Geochemistry

For the fine-grained lujavrites of the Kvanefjeld plateau, the most comprehensive geochemical survey has been carried out for U and Th (examples in Table 2). This has been supported by analyses of characteristic elements from drill core samples in northern Kvanefjeld (Kunzendorf *et al.* 1982) and by major and trace element analyses of the main lujavrite types (Table 3). The U and Th contents were determined by gamma-spectrometry as described by Løvborg *et al.* (1968, 1971, 1972, 1980). Major and trace element analyses were performed by X-ray fluorescence analysis, following the methods described in Kystol and Larsen (1999) and Bailey *et al.* (2006).

From the north contact to the central and southern parts of the plateau, the U contents of the lujavrites increase from 130–140 to 310–320 ppm U, Th from 90–200 to 360–390 ppm, and Th/U ratios from *c*. 1 to *c*. 2 (Nyegaard 1979).

Sheets of fine-grained steenstrupine arfvedsonite lujavrite accompanied by mineralizations containing steenstrupine, Li-mica, sphalerite, Be-minerals and monazite occur in fractures in the volcanic country rocks. These lujavrites have 400–800 ppm U and Th/U ratios of 2–4 (and up to 8) (Sørensen *et. al.* (1974, p. 35).

In the tunnel, the two innermost naujakasite lujavrite sequences have U contents varying from 192 to 543 ppm, Th from 245 to 1291 ppm and Th/U ratios from 1.4 to 2.9 (Table 2). In the two outermost naujakasite lujavrite sequences, U varies from 296 to 603 ppm, Th from 402 to 1392 ppm and Th/U from 1.4 to 2.4 (Nyegaard 1980). The average values for

Table 3 Chemical analyses of fine-grained lujavrites from the Kvanefjeld plateau

	1	2	3
Core	55	55	48
Depth(m)	162.59	69.60	163.00
Major elements (wt%)			
SiO_2	51.22	48.25	50.02
TiO_2	0.24	0.25	0.22
ZrO_2	0.75	0.45	0.16
Al_2O_3	12.06	12.30	13.12
Fe_2O_3	5.44	7.03	4.27
FeO	8.80	7.72	9.40
MnO	0.56	0.54	0.70
MgO	0.06	0.02	0.03
CaO	0.26	0.14	0.19
Na_2O	9.90	14.31	12.41
K_2O	3.31	3.41	3.28
P_2O_5	0.73	0.58	0.48
H_2O^+	3.41	1.78	1.94
H_2O^-	0.09	0.09	0.07
F	0.04	1.04	0.48
Cl	0.09	0.37	0.18
S	0.15	0.16	0.21
others	1.57	1.00	1.68
sum	98.59	99.44	98.29
A.I.	1.65	2.21	1.83
FeO*	13.69	14.04	13.24
ns	7.48	11.92	10.35
Zr/U	58.6	17.0	3.2
Trace elements (ppm)			
Nb	480	275	428
Y	595	671	929
Th	76	89	970
U	95	196	358
Ba	75	29	32
La	3210	2060	2490
Ce	3900	2350	3460
Nd	937	529	899
Li	741	792	882
Be	48	39	61
Sr	46	30	33
Rb	557	936	971
Zn	2680	1430	2450
Pb	466	332	346
Ga	101	115	131
As	1.6	8.3	6.8
Br	<0.5	1.9	2.9
Mo	1.1	12	18
Ge	2.0	1.9	1.8
Tl	2.5	3.4	3.1
Cs	12	8.6	30
Sn	248	514	317

1. arfvedsonite lujavrite, 2 villiaumite-arfvedsonite lujavrite, 3 naujakasite lujavrite. A.I., agpaitic index; FeO*, total iron as FeO; ns, normative sodium disilicate.

the four naujakasite lujavrite sequences from the opening inward are: U 419, 348, 304 and 440 ppm; Th 726, 911, 597 and 1051 ppm; Th/U 1.2, 2.6, 1.9 and 2.4. Thus, in the two innermost sequences, U contents are relatively constant and lower than in the two outermost sequences, whereas Th contents are more variable. This recalls the relations observed in drill cores where U contents vary very little with elevation in long sequences of naujakasite lujavrite but decrease abruptly when approaching the overlying xenolith. Th contents and Th/U ratios are more variable and generally increase abruptly at the top of the naujakasite lujavrite sequences.

U contents, however, increase upwards in the 200 m long cores near the north contact that are dominated by arfvedsonite lujavrite and locally by aegirine lujavrite. In sequences where arfvedsonite lujavrites are overlain by naujakasite lujavrites, U contents generally increase upwards in arfvedsonite lujavrite but remain more or less constant in the naujakasite lujavrite. Th contents and Th/U ratios may be more or less parallel to the U contents in the arfvedsonite lujavrite, but generally increase upwards in the naujakasite lujavrite sequences, as mentioned above. There are also cases where U contents decrease upwards, or first increase and then decrease. Th and Th/U may follow the same pattern or increase upwards.

The general increase in U and Th contents towards the higher levels in lujavrites coincides with an upward decrease in Zr contents in the lower part of the lujavrite sequence (Kunzendorf *et al.* 1982). The combination of relatively low U-Th and high Zr is characteristic for arfvedsonite lujavrite containing eudialyte, whereas high U-Th combined with low Zr is characteristic for naujakasite lujavrite where eudialyte is absent but steenstrupine is significantly present (Andersen *et al.* 1981a; Kunzendorf *et al.* 1982).

The highest U content recorded by us is 1.70 wt% U that was found in a hydrothermal mineralization in the contact between the arfvedsonite lujavrite and the overlying roof of volcanic rocks in the foothill of the Ilimmaasaq mountain in the easternmost part of the lujavrite belt (Rose-Hansen *et al.* 1977).

Multi-element analyses of three lujavrite samples (Table 3) are consistent with these variations in U-Th versus Zr. The most striking difference between the arfvedsonite lujavrite and naujakasite lujavrite is the high Na_2O in the latter which is responsible for the high agpaitic index and normative *ns* (sodium disilicate) (*cf.* Sørensen 1997; Khomyakov *et al.* 2001). The mineral chemistry of naujakasite translates to *ns* = 12 wt. %. Naujakasite lujavrite is also characterized by a high content of MnO (Table 3).

Fluorine and Na_2O contents increase from the arfvedsonite lujavrite to naujakasite lujavrite (Table 3)

and are clearly linked to the presence of villiaumite. Increased levels of villiaumite lead to an increased agpaitic index and *ns* (an increase of 4 wt. % villiaumite increases *ns* by *c.* 6 wt %). The abundance of villiaumite in both arfvedsonite lujavrite and naujakasite lujavrite is erratic, despite its well-established interstitial setting.

The content of P_2O_5 reflects the presence of REE phosphates and REE silicophosphates such as vitusite, monazite, and especially steenstrupine. The abundance of REE + Y varies from around 9,000 to 15,000 ppm.

In general, the fine-grained lujavrites at the Kvanefjeld plateau have high contents of many residual elements (U, Th, REE, Y, P, F, Li, Be, Rb, Cs, Sn, Zn, Pb, Mo, As, Tl, Ga).

Discussion

Lujavrite thickness

In the northernmost part of the Kvanefjeld plateau, a narrow zone of arfvedsonite lujavrite is delineated by our 200 m long drill cores (Fig. 6a, c). Most of our boreholes in the southern part of the complex are too shallow to estimate the thickness of the lujavrites underlying the large roof rock xenoliths. Thus, we have only an incomplete knowledge of the architecture of these lujavrites, i.e. how much space there is between xenoliths and how these are oriented. There are indications of more than 100 m thick lujavrite sequences but no definitive information about their lateral extent.

According to GMEL (2008, 2009), the lujavrite forms thick sub-horizontal layers that are continuous for hundreds of metres. Their sections indicate that the thick layers are split up into several thin layers towards the southwest.

Emplacement of the fine-grained Kvanefjeld lujavrites and relations to earlier rocks

The fine-grained lujavrites of the central part of the Ilímaussaq complex are sandwiched between naujaite and kakortokite and were emplaced after these rocks had solidified. At the time of the formation of the central sandwich lujavrites, the upper part of the complex consisted of a huge naujaite dome draped over by a package of sodalite foyaite, foyaite and pulaskite from the third intrusive phase, augite syenite from the first phase and alkali granite from the second phase, and at the apical part of the dome at Nakkaalaaq by remnants of the roof of volcanic rocks (Fig. 1).

Protrusions from the lujavrite sandwich horizon transgress the naujaite and are in direct contact with the country rocks along parts of the east and west contacts of the complex (Fig. 1). We interpret the NE–SW-oriented lujavrite belt from Ilimmaasaq mountain to the Kvanefjeld plateau in the northwest corner of the complex as a protrusion along the north contact of the complex.

In the north wall of the Narsaq Elv valley, naujaite is in contact with the country rocks from about 1000 m a.s.l. below Ilimmaasaq mountain to 800 m a.s.l. From 800 to 600 m a.s.l., the lujavrite belt forms the contact without disturbing its regular course, i.e. the emplacement of the lujavrite was controlled by the wall of country rocks in the north contact of the naujaite. The basaltic country rocks are strongly sheared parallel to the contact, an indication that the lujavrite was emplaced through a fracture system along the north contact of the complex.

The lujavrite belt sends a south-directed 'finger' into the naujaite south of Steenstrup Fjeld, and three lujavrite 'fingers' penetrate the southwest contact of the complex (Fig. 1), indicating a forceful SW-directed emplacement of the lujavrite magma.

At 600 m a.s.l. the lujavrite belt becomes the northernmost part of the Kvanefjeld plateau and is separated from the country rocks by a narrow zone of naujaite and marginal pegmatite that forms a bulge on the north contact of the complex (Figs 1, 2). Naujaite apophyses intrude the country rocks proving that the naujaite is located in its place of consolidation. The logical explanation of the isolated occurrence is that this naujaite is the contact facies of a larger naujaite body that occupied the area before the emplacement of the lujavrite. The bulge was separated from the main naujaite body when the lujavrite magma intruded into fractures in the shear zone along the north contact and engulfed the naujaite adjacent to the shear zone. The occurrence of large naujaite xenoliths on the Kvanefjeld plateau and in the Steenstrup Fjeld area, and in drill cores from these two areas, proves that a large body of naujaite occupied the Kvanefjeld area when the lujavrite was emplaced.
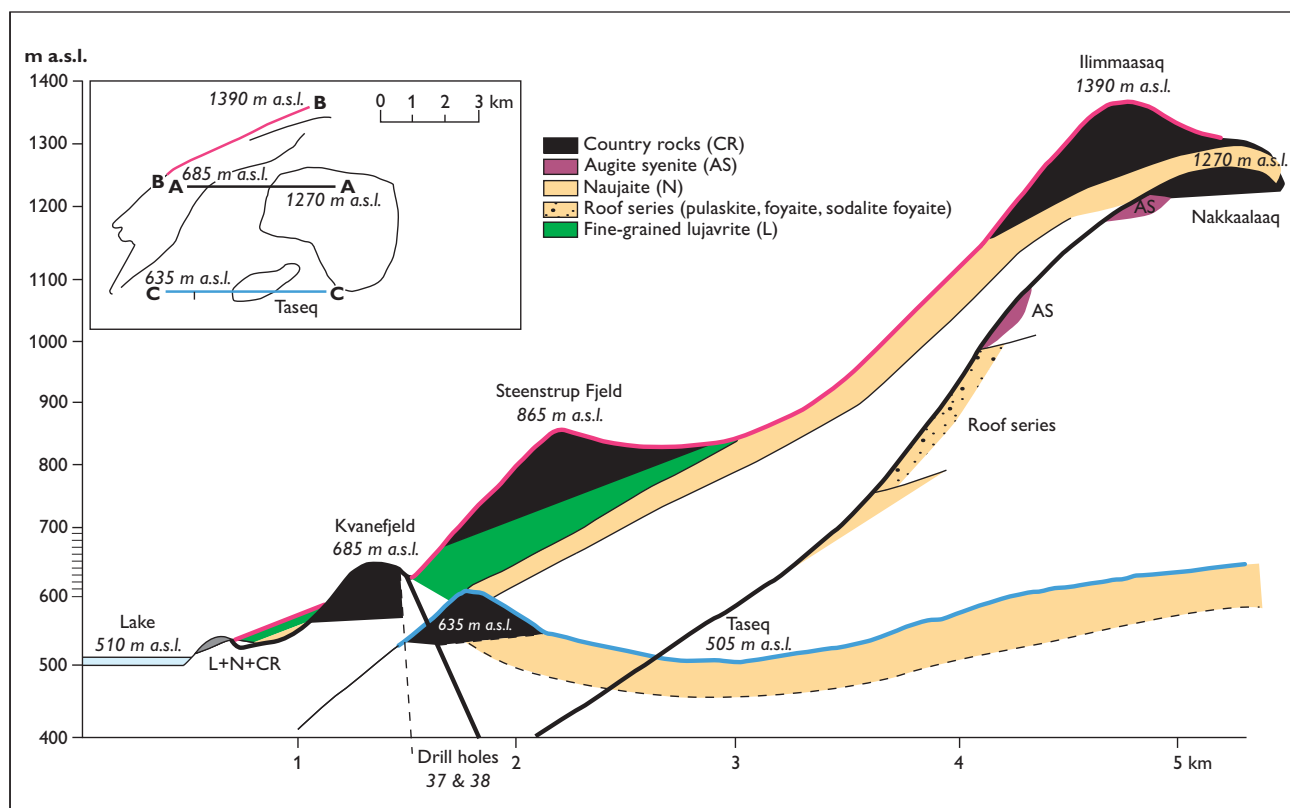
Fig. 8. Three vertical cross sections of the Narsaq Elv valley based on the geological map of Ferguson (1964). The black section (AA) runs from the roof remnant at 1270 m in the Nakkaalaaq mountain over the Kvanefjeld peak (685 m) to lake 510 m (517 m in Fig. 2) at the northern contact of the Ilímaussaq complex. This section intersects the volcanic roof rocks, augite syenite (alkali granite is omitted), and the roof series dominated by sodalite foyaite and naujaite. The red section (BB) runs from the Ilimmaasaq mountain (1390 m) over Steenstrup Fjeld (865 m) to lake 510 m at the northern contact of the complex and shows the contact between the volcanic country rocks and naujaite, and from 800 m a.s.l. between a lujavrite and the country rocks. The blue section (CC) passes through the Taseq lake (505 m) and the peak 635 m. The blue and red sections show the contact between naujaite and the volcanic country rocks (*cf.* Fig.9).

At the Kvanefjeld plateau, naujaite xenoliths are generally separated from the country rocks by lujavrite, but direct contact exists in a number of cores in the northernmost part of the plateau. One would expect to find sodalite foyaite, foyaite and pulaskite between the naujaite and the overlying country rocks and this is actually the case in core 48. The occurrence of pulaskite, foyaite and sodalite foyaite is, however, restricted to the apical part of the naujaite, whereas naujaite is in direct contact with the country rocks at the lateral contacts (Sørensen 2006).

Xenoliths of sodalite foyaite, foyaite and pulaskite in the lujavrites in the northernmost parts of the Kvanefjeld plateau and the Steenstrup Fjeld area show that the lujavrite magma at least locally penetrated the apical part of the naujaite and came into contact with the overlying rocks. These xenoliths are interpreted as remnants of a westward plunging extension of the package of earlier rocks that overlies the naujaite at Nakkaalaaq (Sørensen 2006). The slope of the package is almost identical with the slopes of the north and west contacts of the naujaite against the country rocks (Figs. 8, 9).

The augite syenite xenoliths in the south-western part of the Kvanefjeld plateau are intersected by deformation zones and intruded by lujavrite (Fig. 2). The observation of Nielsen and Steenfelt (1979) that an identical orientation of structures is seen in neighbouring augite syenite xenoliths, and the fact that augite syenite is in direct contact with the volcanic country rocks in the valley and Narsaq Elv river bed south of the Kvanefjeld plateau, show that most parts of the augite syenite have preserved their original position. The augite syenite in the river bed is intruded by naujaite and lujavrite (Ferguson 1964; Sørensen 2006). In this part of the complex, the lowest-lying contact between naujaite and the volcanic roof rocks is located in the Narsaq Elv bed, indicating that the augite syenite in the valley and the south-west slope of Kvanefjeld plateau formed an obstacle to the advance of the naujaite magma.

The two deepest boreholes, nos. 37 and 38 located in the southern part of the plateau, intersect gabbro and other roof rocks from respectively 560 to 260 and 670 to 330 m a.s.l. and roof rocks dominate a few of the shallow boreholes. The 960 m long tunnel intersects masses of roof rocks at 200-215, 450-588, 730-755 and 880-960 m from its opening. The locations of large masses of roof rocks at these deep levels may be parts of vertical screens of pre-naujaitic rocks that resisted successive attacks from intruding naujaitic and lujavritic magmas. They are intersected by thin sheets of augite syenite, more rarely by naujaite, but thicker sheets of arfvedsonite and naujakasite lujavrite have many small xenoliths of naujaite, suggesting that fissures in the screens were first invaded by naujaite and later by lujavrite.

The country rocks in the west contact of the complex are basalts intersected by a swarm of gabbroic dykes and, less than 1 km away, by the Dyrnæs-Narsaq intrusion consisting of gabbro, syenite and granite which is older than the Ilímaussaq complex (Allaart 1973). The massive gabbroic dykes, and perhaps also recrystallization caused by heat and emanations from

Fig. 9. Panorama of the Narsaq Elv valley looking upstream (north-east). The Ilimmaasaq mountain lies at the eastern end of the red section of Fig. 8. The blue section in Fig. 8 passes through peak 635 m and Kvanefjeld at 685 m, and the black section runs from highest part of the Nakkaalaaq mountain across the light grey slope of naujaite to Kvanefjeld. The dark walls on both sides of the Narsaq Elv valley are the volcanic rocks of the west contact of the Ilímaussaq complex.

The emplacement and crystallization of the lujavrites at Kvanefjeld, Ilímaussaq · 83

the consolidating Dyrnæs-Narsaq complex, may have fortified the volcanic country rocks. The large roof xenoliths in the southern part of Kvanefjeld plateau consist of these resistant country rocks. The elevation of their underside is almost the same as that of the volcanic rocks in contact with the naujaite on the south side of the Narsaq Elv valley and fits exactly the extrapolation of the course of the contact between naujaite and the overlying volcanic roof rocks located north and south of Kvanefjeld plateau (Figs. 8, 9). This supports the view of Sørensen *et al.* (1974) that the large xenoliths of roof rocks that cover most of the southern part of Kvanefjeld plateau have retained their original position and are *in situ* remnants of the roof of the lujavrite magma.

Very few large country rock xenoliths are exposed in the northern part and the intermediate zone of the Kvanefjeld plateau, but up to 50 m thick xenoliths of the volcanic roof are common in the cores from these parts of the plateau. In our opinion, these xenoliths and the above-mentioned naujaite xenoliths are fragments of the rocks that constituted the roof of the intruding lujavrite magma.

The Steenstrup Fjeld lujavrites are continuous with the lujavrite of the northern Kvanefjeld plateau but their relation to the lujavrite in the south Kvanefjeld area is not visible because the rocks have been eroded between the Steenstrup Fjeld area and the escarpment that forms the south-east margin of Kvanefjeld plateau (Fig. 3). Thin veins of lujavrite in fractures in the large roof xenolith that forms the escarpment may, however, be an incipient penetration of lujavrite magma.

Larsen (1977) demonstrated that the lava sequences in the Kvanefjeld xenoliths are located 300–400 m lower than identical lavas in the undisturbed lava sequence outside the complex. This would support the idea that a foundering of large masses of roof rocks took place in connection with the emplacement of the lujavrite. Against this idea speaks, firstly, that the the volcanic roof rocks and naujaite of the Kvanefjeld plateau are located at the same elevation as the same rocks on the south side of the Narsaq Elv valley, and, secondly, that the regular course of the contact between naujaite and the country rocks (Figs. 8, 9) suggests that displacement of the lava sequences took place before emplacement of the naujaite. Fault activity was most probably the cause of major displacement of the country rocks before emplacement of the Ilímaussaq complex (Sørensen 2006).

Nielsen & Steenfelt (1979) pointed out that pulaskite belongs to a higher stratigraphic level in the complex than naujaite. Therefore, the occurrence of pulaskite xenoliths at Kvanefjeld at the same level as the naujaite and marginal pegmatite of the contact should indicate that the pulaskite xenoliths have foundered in the lujavrite melt. Sørensen (2006) argued that the occurrence of the whole suite of the roof series rocks from pulaskite to sodalite foyaite in one xenolith means that the roof series here was very thin and that the pulaskite xenoliths may therefore be more or less in their original position.

Naujakasite lujavrite

Naujakasite ($Na_6(Fe,Mn)Al_4Si_8O_{26}$) is a unique mineral. It is composed of common elements and is a rock-forming mineral in the Ilímaussaq complex where it constitutes up to 80 % of the naujakasite lujavrite. However, the Ilímaussaq complex is the only place in the world where it has been found. This must mean that its stability field is very restricted or unique. Khomyakov *et al.* (2001) conclude that naujakasite is formed in hyperagpaitic magmas rich in Fe and Mn and with a high Na/K ratio, and emphasize the frequent occurrence beneath large xenoliths of naujaite, augite syenite and volcanic country rocks, i.e. places where volatiles could accumulate. Andersen & Sørensen (2005) consider that an uncommon combination of low oxygen fugacity and high water activity stabilises naujakasite in highly sodic liquids.

Naujakasite lujavrite forms the upper part of arfvedsonite lujavrite sequences beneath large xenoliths of naujaite, augite syenite and volcanic country rocks, but there is commonly a thin naujakasite-free zone of arfvedsonite lujavrite between the xenolith and the underlying naujakasite lujavrite. The alternation of layers with and without naujakasite shows that the stability field of naujakasite is narrow, whereas the large masses of naujakasite lujavrite indicate that the stability field can be attained in large masses of magma at the same time.

Naujakasite lujavrite occurs at several levels in the south Kvanefjeld area and the intermediate zone (Figs. 5, 6C). The highest-lying naujakasite lujavrites have most probably been in contact with the rocks which formed the roof over the lujavrite magma and at lower elevations with naujaite and augite syenite xenoliths.

Naujakasite lujavrite is absent in most cores from the contact-near Kvanefjeld-Steenstrup Fjeld lujavrite belt and has only been observed in three cores (39, 50 and 70). These lujavrites are situated at a higher elevation than all other lujavrite cores of the plateau. The U contents increase upwards in the arfvedsonite lujavrites in these cores, and the specific conditions required to stabilize naujakasite were only met in their upper parts. Gamma-spectrometric logging shows that in arfvedsonite lujavrite sequences crystallizing close to the roof of the magma, U contents generally increase upwards, often paralleled by Th contents,

but remain more or less constant throughout the naujakasite lujavrites (Sørensen *et al.* 1971; Nyegaard *et al.* 1977). This can be explained by the narrow stability field of naujakasite. Some of these sequences terminate upwards in a naujakasite-free arfvedsonite lujavrite which generally has lower U contents and higher Th contents than the underlying rock. The upwards decrease in U could in fact be a downward increase, if the conditions for crystallization of naujakasite were established some time after the lujavrite magma came in contact with the overlying xenolith.

Outside the Kvanefjeld plateau, naujakasite lujavrite occurs in the uppermost part of the arfvedsonite lujavrites south of Tupersuatsiaat bay on the south coast of Tunulliarfik Fjord (Fig. 1; Bondam & Sørensen 1958; Petersen & Andersen 1975; Khomyakov *et al.* 2001) and in the uppermost part of the lujavrites underlying the naujaite south, east and west of Tupersuatsiaat (Danø & Sørensen 1959). Naujakasite lujavrite also occurs as dykes in the naujaite north of the Taseq lake (Engell 1973). This emphasizes that the presence of a lid of strong country rocks which prevents volatile and residual elements from escaping is a pre-condition for crystallization of naujakasite and steenstrupine in lujavrite magmas and for the formation of the Kvanefjeld type of U–Th–REE deposits.

The importance of this condition is demonstrated by the upward increasing contents of U, REE and Y in the upper parts of six of the drill holes located 6 km south of Kvanefjeld (GMEL 2011). These drill holes intersect the dome of the central arfvedsonite lujavrite body. This dome passes westwards into a depression of the upper surface of the lujavrite above the site of borehole II on the north coast of Tunulliarfik (Fig. 1). The uppermost 70 m of the lujavrite here are rich in steenstrupine and have up to 1200 ppm U and 5500 ppm Th (Sørensen 1962; Rose-Hansen & Sørensen 2002).

Magmatic evolution of the fine-grained Kvanefjeld lujavrites

The 4.5 km long lujavrite belt from Ilimmaasaq mountain to the Kvanefjeld plateau separates naujaite, the dominating agpaitic rock of the upper part of the Ilímaussaq complex, from its supracrustal country rocks along a NE–SW oriented part of the north contact and in the north-western corner of the complex. It is interpreted to be an offshoot from the sandwich horizon lujavrite magma in the central part of the complex. On the Kvanefjeld plateau, a northern and a southern lujavrite facies may be distinguished. The northern facies forms a continuous belt from the foothills of Ilimmaasaq mountain in the east to the west contact of the complex (Fig. 1) and

is dominated by ordinary arfvedsonite and aegirine lujavrites. The southern facies occurs in the southern part of the Kvanefjeld plateau and in the intermediate zone where hyperagpaitic lujavrite varieties containing naujakasite, villiaumite and steenstrupine are widespread.

Nyegaard (1979) concluded that the lujavrites located near the north contact and in the Steenstrup Fjeld area were formed by a single pulse of relatively volatile-poor magma of deep origin, whereas the lujavrites in the central part of the plateau were formed by several pulses of lujavrite magma from a relatively high level in the central lujavrite magma chamber. We have observed no major discontinuities but cannot exclude their existence between the exposed lujavrites and those covered by roof xenoliths, i.e. caused by vertical screens of country rocks. Gradational vertical relations are, however, observed in drill cores.

The general stratigraphy of the lujavrite sandwich in the central part of the complex was assembled over several studies (Ferguson 1964; Andersen *et al.* 1981a, b; Bohse & Andersen 1981; Sørensen 2006; Sørensen *et al.* 2006). The lowermost part consists of aegirine lujavrite which is overlain by a sequence of alternating aegirine and arfvedsonite lujavrite followed by the main mass of arfvedsonite lujavrite. It is interesting that the sequence of crystallization of the main lujavrite sandwich is largely repeated at Kvanefjeld. A large xenolith of aegirine lujavrite in the gully between the Ilimmaasaq mountain and Steenstrup Fjeld is proof of the former existence of aegirine lujavrite at this place. Aegirine is common in the contact-near arfvedsonite lujavrites and in arfvedsonite lujavrite in contact with naujaite xenoliths. The marginal lujavrites along the north contact have layered sequences and horizons of spheroidal lujavrites, and similar rocks are seen to lie immediately above the aegirine lujavrite on the north coast of Tunulliarfik and at Appat south of Tunulliarfik (Sørensen *et al.* 2003; Sørensen 2006) , i.e. the Kvanefjeld magma appears to stem from the lower part of the arfvedsonite lujavrite sandwich.

The Kvanefjeld lujavrites follow the Zr-U-Y geochemical trend found among lujavrites in the southern Ilímaussaq complex but evolve to even lower values of Zr, Zr/U and Zr/Y and higher values of U and Y, especially in the naujakasite lujavrite (Andersen *et al.* 1981a). These trends were attributed to fractionation of eudialyte. The Kvanefjeld lujavrites were thought to have undergone more prolonged fractionation in an isolated magma chamber, an evolution that eventually led to naujakasite lujavrite, the most fractionated of the Kvanefjeld lujavrites.

Andersen *et al.* (1981a) also noted that the Zr-U data from kakortokites plot along well-defined correlation lines whereas the Zr-U data from the Kvanefjeld lujavrites tend to plot in fields or clusters. They attributed this to the changing character of the analysed rocks.

Thus, the kakortokites represent well-layered cumulate rocks which resulted from efficient density sorting of cumulus minerals into black, red and white layers. In contrast, in the overlying lujavrites, the decreased vertical interval for crystal settling and the mush-like character of the magmas led to poor separation of cumulus phases from the magma. Overall, the combination of rapid fractionation and the appearance of poorly sorted partial cumulates led to the samples plotting in fields or clusters on geochemical diagrams.

Kunzendorf *et al.* (1982) considered that the Kvanefjeld lujavrites crystallized from bottom to top and that fractionation of eudialyte crystals by gravity settling gave rise to increasing U and Th contents in the highest levels, as had been documented by Nyegaard *et al.* (1977). Fractionation of eudialyte took place in the early aegirine lujavrite stage of the central sandwich lujavrites (Andersen *et al.* 1981a, b). Enrichment in eudialyte has been demonstrated in the light-coloured layers in micro-layered arfvedsonite lujavrites on the north coast of Tunulliarfik, but the much thicker dark-coloured layers are poor in eudialyte and there is no general fractionation of eudialyte upwards in the lujavrite sequence (Bailey *et al.* 2006). Our petrographic studies indicate that the fractionation effect of eudialyte was minimal or non-existent after the early arfvedsonite lujavrite and that there are no signs of crystal fractionation in the scale needed to explain the exceptionally high contents of F, P, Na, REE, Th, U etc. in the Kvanefjeld lujavrites.

Larsen & Sørensen (1987) and Sørensen & Larsen (1987) emphasized that the kakortokite-lujavrite suite behaved as a multiply saturated (anchieutectic) system with feldspars, nepheline, aegirine, arfvedsonite, eudialyte and occasionally sodalite as liquidus phases. Crystallization took place in a stagnant bottom layer of the magma and released residual liquids to the overlying magma, which would crystallize the liquidus assemblage releasing volatile and residual elements to the overlying magma, and so on. This resulted in the rather constant composition of rocks and minerals in the kakortokites (*cf.* Sørensen & Larsen 1987 and Pfaff *et al.* 2008) and in the sandwich of arfvedsonite lujavrites (Rose-Hansen & Sørensen 2002). The rock-forming minerals incorporate traces of residual volatile elements, e.g. H_2O and F in arfvedsonite and U in eudialyte, and the U content of eudialyte shows a weak increase upwards in the layered sequence (Bohse *et al.* 1974). The accessory minerals britholite, vitusite, and monazite occur in so small amounts that U, Th, REE and P would steadily be squeezed out and move upwards as long as the system was closed. Thus liquid fractionation, rather than crystal fractionation, was involved in the formation of the Kvanefjeld deposit.

According to Greenland Minerals and Energy Ltd., the mass of the indicated and inferred U–REE–Zn multielement occurrence at Kvanefjeld is 457 million tons. The volume of 457 million tons of lujavrite is about 0.16 billion cubic kilometres, corresponding to a body measuring 1000×1000×160 m, which is the right order of magnitude. The uranium resource is 283 M lbs U_3O_8 (i.e. about 110,000 t of U) at a cut-off grade of 150 ppm and an average grade of 280 ppm U_3O_8 or 240 ppm U (GMEL 2011). The lowermost arfvedsonite lujavrites of the central sandwich lujavrite body have 40–100 ppm U (Rose-Hansen & Sørensen 2002). If we assume that the uranium content of the original lujavrite magma was 50 ppm, 100,000 tons of uranium corresponds to the total quantity of U in 2.2 billion tons or 0.8 cubic kilometres of original arfvedsonite lujavrite magma. The Kvanefjeld-Ilimmaasaq lujavrite belt is about 4.5 km long and its dyke (northern) facies is about 300 m wide. A volume of 0.8 cubic kilometres of lujavrite magma emplaced in a fracture of this size would be about 500 m deep, corresponding to a derivation at a low level in the lujavrite sandwich horizon. The figure for the uranium resource includes the U contained in the arfvedsonite M-C lujavrite and its contact aureole estimated to 14,420 t by Sørensen *et al.* (1974).

Comparison of the mass of the Kvanefjeld ore body with that of the assumed original lujavrite magma indicates that the formation of the ore body requires crystallization of about 80% of the original lujavrite magma.

Comparison with the central arfvedsonite lujavrite body

Twelve boreholes located approximately 6 km south and south-east of Kvanefjeld (GMEL, 2011) provide new information about the main mass of the central sandwich of arfvedsonite lujavrite. Six of these boreholes intersect the marginal part and six the central part of the dome-shaped contact between the naujaite and the underlying lujavrite which is exposed in the north wall of Tunulliarfik (Fig. 10). The lujavrites of the marginal cores and the lower part of the central cores display the uniform contents of U, REE and Y which we, as discussed above, ascribe to the anchieutectic crystallization of the sandwich arfvedsonite lujavrite magma and the continuous release of incompatible elements to the overlying magma. The contents of U, REE and Y in the marginal facies are similar to those in the lower part of the sandwich lujavrite sequence. In the upper 100–200 m of the six central cores, the contents of U, REE and Y increase upwards until 20–50 m from the roof of the magma chamber from where the contents decrease upwards. (In some cores, the LREE contents continue to increase upwards).

The higher contents of U, REE and Y in the upper than in the lower central lujavrites may be explained as

follows. When the ascending central lujavrite magma met the impervious roof of the magma chamber, the release of volatile and residual elements to the overlying magma was prevented. The elevated contents of residual and volatile elements in the lujavrite magma stored under the roof caused a lowering of its liquidus temperature and its density. Eventually, the magma crystallized from the roof downwards and from its base upwards, the uppermost 30–50 m of lujavrites displaying a downward increase in U contents and the lower part an upwards increase resulting in the formation of steenstrupine lujavrite. The upper part may be termed an 'upper border group' of lujavrite.

The average U content of the central lujavrites is higher than that of the Kvanefjeld lujavrites. This can be related to the much larger volume of lujavrite magma in the central part of the intrusion and suggests that this sequence of arfvedsonite lujavrites consolidated beneath a roof that prevented volatiles from escaping during the major part of crystallization. This view is strengthened by the presence of an upper border group, i.e. a contact facies of this part of the lujavrite body. Further evidence of the importance of a volatile phase is found in sheets and dykes of steenstrupine arfvedsonite lujavrite and naujakasite lujavrite and widespread albite veins rich in Be minerals intersecting the overlying naujaite, indicating fracturing of the naujaite roof at a late stage in the consolidation of the main arfvedsonite lujavrite intrusion (Engell *et al.* 1971; Engell 1973).

The emplacement mechanism of the Kvanefjeld lujavrites

The Kvanefjeld plateau is the broadest part of the Kvanefjeld - Ilimmaasaq lujavrite belt. The contact between the country rocks and the lujavrites in the foothills of the Steenstrup Fjeldand Ilimmaasaq mountains and in the northern part of the Kvanefjeld plateau is NE–SW oriented, vertical, unbroken and practically straight. The widening of the lujavrite belt was therefore towards the south. The lujavrites there have higher contents of U, Th and REE than those in the narrower part of the belt east of the plateau. It is therefore of interest to know the cause of the widening. Three explanations may be proposed:

1. The intruding lujavrite spread out when it encountered the solid mass of volcanic rocks, gabbro, naujaite, etc. which then occupied the Kvanefjeld area. It invaded fractures in these rocks, engulfing xenoliths of these, and penetrated the western contact forming the three lujavrite fingers that petered out after about 1 km (Fig. 1). There are, however, no indications of spreading in the lujavrites in the Steenstrup Fjeld area and it is difficult to see how the evolved lujavrites in the south Kvanefjeld area could be formed from the less evolved magma disseminated in small volumes across the plateau.

2. Our favoured explanation is that the intruding Kvanefjeld lujavrite magma was forcefully injected in a fracture system along the north contact of the complex from Ilimmaasaq mountain to the northwestern corner of the complex (Figs. 3, 4). The magma was bounded to the north and west and at its roof by the dyke-enforced country rocks which arrested its advance. The southwest and south walls of the confined magma consisted of augite syenite, naujaite and overlying roof rocks. The multiply saturated lujavrite magma stored in the fracture crystallized from the bottom upwards, squeezing residual and volatile components upwards. Pressure would rise in the upper part of the magma. We imagine that when the pressure exceeded the strength of the weakest confining rocks, i.e. naujaite and augite syenite in the west and southwest walls, a violent explosion opened fractures in these rocks. The north wall and the roof of the fracture did not yield and reflected the north-directed pressure waves to reinforce the south-directed pressure, squeezing the volatile-rich

Fig. 10. The north wall of Tunulliarfik showing the dome shape of the central lujavrite (dark grey, the upper boundary marked with a dashed white line) and the lujavrite off-shoots in the overlying naujaite (at arrows). Note the horizons of naujaite rafts (white) in the dark lujavrite.

magma into fractures in not only naujaite and augite syenite but also in the overlying volcanic roof rocks where it consolidated as sheets of steenstrupine arfvedsonite lujavrite accompanied by mineralizations of steenstrupine, Li-mica, sphalerite, Be-minerals and monazite formed from the released volatile phase. Xenoliths of pulaskite, foyaite and sodalite foyaite in the lujavrites indicate that the apical part of the Ilímaussaq complex was penetrated by the lujavrite magma. The violence of the process is demonstrated by a) the widening of the plateau towards the south, b) the three NE–SW oriented lujavrite fingers that penetrated the south-west wall in prolongation of the fracture system through which the lujavrite was emplaced (Fig. 1), c) the small xenoliths of roof and wall rocks, especially volcanic rocks and naujaite, that are widely distributed in the lujavrites, d) the occurrence of xenoliths of higher-lying rocks such as pulaskite and sodalite foyaite in lujavrite veins that infiltrate the low-lying deformed masses of augite syenite, syenite and anorthosite in a very intricate way (Nielsen & Steenfelt 1979; Sørensen 2006) and e) the strong deformation and recrystallization of country rocks adjacent to near-horizontal fractures in these in the depth interval 650 to 450 m a.s.l. in almost all drill cores from the southern part of the plateau; such a mineralised fracture was described by Sørensen *et al.* (1974, p. 35), and the adjacent roof rocks are strongly sheared, deformed and recrystallized but they are perfectly fresh a few metres from the fracture. The explosive squeezing-out of the volatile-rich lujavrite magma that occupied the upper part of the fracture made room for volatile-poor magma from the lower part of the fracture, which crystallized to form the lujavrites in the north Kvanefjeld–Ilimmaasaq lujavrite belt.

3. A third cause of widening of the lujavrite belt and the elevated contents of U, Th, REE, etc. could be that this is the place where the lujavrite magma ascended from the underlying sandwich lujavrite magma.

Some evidence may be gleaned from the central arfvedsonite lujavrite body. Boreholes in the naujaite areas 3–7 km south and south-east of Kvanefjeld (Fig. 1) show that the naujaite is underlain by alternating lujavrite and naujaite horizons (GMEL 2008, 2011). A similar relationship between naujaite and the underlying sandwich lujavrite can be seen in the north wall of the Tunulliarfik fjord (Figs. 1, 10), and supports the view of Ussing (1912) and subsequent authors that the sandwich horizon lujavrite underlies naujaite in the whole complex. This view is strengthened by the occurrence of lujavrite dykes and sheets intersecting the naujaite north of the Taseq lake (Engell 1973), the Narsaq Elv bed and drill core I (Fig. 1) (Rose-Hansen & Sørensen 2002). In the north wall of Tunulliarfik, it

is clearly seen that such veins are offshoots from the sandwich horizon (Figs. 1, 10).

In the cross sections of the complex provided by the north and south coasts of Tunulliarfik, the upper surface of the lujavrite shows swells and depressions (Sørensen 2006). The Kvanefjeld – Steenstrup – Ilimmaasaq lujavrite belt may be a swell, the Narsaq Elv valley a depression and the Taseq area a swell.

Without knowing the distribution of rocks beneath the Kvanefjeld plateau it is impossible to decide whether the lujavrite magma was introduced along the north contact, from below the plateau, or both. In the first case, one would expect that the evolved lujavrites in horizontal fractures in the roof rocks are underlain by naujaite, in the last case by lujavrites or lujavrites with horizontal rafts of naujaite. Our deepest borehole (37) terminates with 30 m naujaite at 173 m a.s.l., which could support the first view.

The Kvanefjeld U-Th-REE deposit

It is a general observation that U, Th and REE are concentrated in the upper parts of the youngest components of igneous complexes. This is also the case in the Ilímaussaq complex where the uppermost part of the youngest phase, the lujavrite sandwich horizon, has higher contents of U, Th, LREE, Li, Be and Zn than the lower part, the kakortokites. These are rich in eudialyte and have high contents of Zr, Hf, HREE, Nb, Ba and Sr (Bailey *et al.* 1981).

Sørensen *et al.* (1974) distinguished six types of U–Th mineralization in drill cores 1–43 at Kvanefjeld: (1) arfvedsonite lujavrite with interstitial steenstrupine crystals, monazite, U-bearing pigmentation and pseudomorphs after eudialyte. The steenstrupine crystals are generally unaltered; (2) naujakasite lujavrite with interstitial steenstrupine crystals which may be enclosed in naujakasite and are generally more altered than in type 1; (3) lujavrites in which analcime replaces the felsic minerals and naujakasite. The steenstrupine is commonly poikilitic and strongly altered; (4) the contact metasomatic mineralization around the M-C lujavrite intrusion in the south Kvanefjeld area, which has the highest recorded contents of U and Th on the plateau; (5) similar but much smaller mineralizations associated with the aegirine– rich M-C lujavrite near the north contact; and (6) mineralization in zones of deformation in xenoliths enclosed in the lujavrite.

The chemical composition of the arfvedsonite lujavrites in the central sandwich horizon is rather monotonous, both horizontally and vertically. There is, however some variation in contents of U, Th, and REE due to xenoliths of country rocks and naujaite with low contents of these elements or to intersecting

steenstrupine-bearing pegmatites and hydrothermal veins. It is therefore difficult to give precise values for average contents, but 100 ppm U, 100 ppm Th and 8,000 ppm REE are characteristic values for the main mass of arfvedsonite lujavrites. Higher contents are found in the Kvanefjeld area, in the highest-lying exposed lujavrites south of Tupersuatsiaat and on the north coast of Tunulliarfik.

In the earlier agpaitic rocks of the complex, REE are mainly held in eudialyte (Bailey *et al.* 2001), but the copious crystallization of eudialyte in kakortokite and early lujavrites led to decreased contents of Zr so that eudialyte became a minor mineral in the early arfvedsonite lujavrite of Kvanefjeld and is absent in the subsequent Kvanefjeld lujavrites. During differentiation of the agpaitic rocks, P_2O_5 contents rose from *c.* 0.01 wt. % to 0.19 wt. % in the average arfvedsonite lujavrite with even higher levels in Kvanefjeld lujavrites (0.25–0.31 wt. %, Table 3). The association of REE, Na and P became dominant in the Kvanefjeld lujavrites and led to complex REE mineral assemblages. These include apatite (Rønsbo 2008) and monazite/rhabdophane; other phosphates where Si may replace P (vitusite, Pekov *et al.* 1997); silicophosphates where P replaces Si (steenstrupine, britholite); and silicates containing independent phosphate molecules (vuonnemite) (Makovicky & Karup-Møller 1981; Rønsbo *et al.* 1983; Kalsbeek *et al.* 1990).

North of Tunulliarfik, a major part of the exposed rocks of the complex consists of naujaite, but since Ussing (1912) it has been the general opinion that the naujaite is underlain by arfvedsonite lujavrite. This led Sørensen (in IAEA 1980, p. 158) to suggest that the speculative resources in the Kvanefjeld area could amount to 600,000 t U at 150 ppm U, in addition to the 43,000 t reasonably assured and estimated additional resources known at that time. Sørensen (1992) argued that multi-element mining would be the way to exploit the rare elements of the arfvedsonite lujavrite.

Conclusions

The lujavrites along the northwestern margin of the Ilímaussaq complex constitute a 5 km long elongate intrusion of which the Kvanefjeld plateau is the western part. The intrusion was formed by consolidation of an off-shoot from the sandwich horizon of arfvedsonite lujavrite magma in the central Ilímaussaq magma chamber. Field relations suggest that the off-shoot was emplaced through a fracture zone along parts of the north contact of the complex, but we cannot exclude the possibility that there were other routes.

Two facies of fine-grained arfvedsonite lujavrites may be distinguished in the U–Th–REE deposit at Kvanefjeld. One facies comprises the continuous lujavrite belt in the northern part of the Kvanefjeld plateau which extends to the north-east below Steenstrup Fjeld. These lujavrites have contents of U, Th and REE that are lower than in most other lujavrites of the Kvanefjeld plateau, but slightly higher than in the arfvedsonite lujavrite sandwich in the central part of the complex. The second lujavrite facies comprises the fine-grained arfvedsonite lujavrites in the southern part of the Kvanefjeld plateau which consolidated under a strong roof of gabbro-reinforced volcanic rocks that make up most of the surface of this area and are interpreted as *in situ* remnants of the original roof of the lujavrite magma. In the intermediate zone and in the northern Kvanefjeld plateau the roof has been fragmented into separate large xenoliths.

The high contents of U, Th and REE in the lujavrite facies in the southern part of the Kvanefjeld plateau, and the evidence of a violent emplacement process, indicate that volatiles and residual elements assembled at the top of the crystallizing off-shoot magma pool leading to increasing pressure and an explosion that squeezed the volatile-rich magma into fractures in the western and southern sidewalls of the magma chamber where it consolidated as steenstrupine-rich arfvedsonite lujavrite.

The violent expulsion of the volatile-rich magma made room for magma with lower contents of volatile and residual elements which streamed in from below and crystallized in the feeder system through which the magma was emplaced.

The formation of the Kvanefjeld type of U–Th–REE deposit requires slow, uninterrupted crystallization of a large volume of an agpaitic magma enriched in residual and volatile elements below a tight cover. This is a rarely met combination of conditions which explains why the Ilímaussaq complex is the only known occurrence of large masses of hyperagpaitic rocks and that naujakasite and rock-forming steenstrupine are only known from this complex.

References

Allaart, J.H. 1973: Geological map of Greenland 1:100 000, Julianehåb 60 V.2 Nord. Descriptive text, 41 pp. Copenhagen: Geological Survey of Greenland (also Meddelelser om Grønland 192, 4).

Andersen, S., Bailey, J.C. & Bohse, H. 1981a: Zr-Y-U stratigraphy of the kakortokite-lujavrite sequence, southern Ilímaussaq intrusion. Rapport Grønlands Geologiske Undersøgelse 103, 69–76.

Andersen, S., Bohse, H. & Steenfelt, A. 1981b: A geological section through the southern part of the Ilímaussaq intrusion. Rapport Grønlands Geologiske Undersøgelse 103, 39–42.

Andersen, S., Bohse, H. & Steenfelt, A. 1988: The southern part of the Ilímaussaq complex, South Greenland. Special map sheet 1:20,000. Copenhagen: Grønlands Geologiske Undersøgelse.

Andersen, T. & Sørensen, H. 2005: Stability of naujakasite in hyperagpaitic melts, and the petrology of naujakasite lujavrite in the Ilímaussaq alkaline complex, South Greenland. Mineralogical Magazine 69, 125–136.

Bailey, J.C., Rose-Hansen, J., Løvborg, L. & Sørensen, H. 1981: Evolution of Th and U whole-rock contents in the Ilímaussaq intrusion. Rapport Grønlands Geologiske Undersøgelse 103, 87–98.

Bailey, J.C., Gwozdz, R., Rose-Hansen, J. & Sørensen, H. 2001: Geochemical overview of the Ilímaussaq alkaline complex, South Greenland. Geology of Greenland Survey Bulletin 190, 35–53.

Bailey, J.C., Sørensen, H., Andersen, T., Kogarko, L.N. & Rose-Hansen, J. 2006: On the origin of microrhythmic layering in arfvedsonite lujavrite from the Ilímaussaq alkaline complex, South Greenland. Lithos 91, 301-318.

Bohse, H. & Andersen, S. 1981: Review of the stratigraphic divisions of the kakortokite and lujavrite in southern Ilímaussaq. Rapport Grønlands Geologiske Undersøgelse 103, 53–62.

Bohse, H., Rose-Hansen, J., Sørensen, H., Steenfelt, A., Løvborg, L., & Kunzendorf, H. 1974: On the behaviour of uranium during crystallization of magmas - with special emphasis on alkaline magmas. In: Formation of uranium ore deposits, 49-60. Vienna: International Atomic Energy Agency.

Bondam, J. & Sørensen, H. 1958: Uraniferous nepheline syenites and related rocks in the Ilimaussaq area, Julianehaab District, southwest Greenland. Proceedings 2nd UN International Conference on the Peaceful Uses of Atomic Energy 2, 555–559.

Borutskii, B.E. & Semenov, E.I. 1969: Feldspars from the Ilímaussaq alkaline massif. Trudy Mineralogicheskogo Muzeya im A.E. Fersman 19, 3–11 (in Russian).

Buchwald, V.F. & Sørensen, H. 1961: An autoradiographic examination of rocks and minerals from the Ilímaussaq batholith, South West Greenland. Bulletin Grønlands Geologiske Undersøgelse 28, 35 pp.

Danø, M & Sørensen, H. 1959: An examination of some rare minerals from the nepheline syenites of South West Greenland. Bulletin Grønlands Geologiske Undersøgelse 2035 pp. (also Meddelelser om Grønland 162, 5).

Engell, J. 1973: A closed system crystal-fractionation model for the agpaitic Ilímaussaq intrusion, South Greenland, with special reference to the lujavrites. Bulletin of the Geological Society of Denmark 22, 334–362.

Engell, J., Hansen [Rose-Hansen], J., Jensen, M., Kunzendorf, H.& Løvborg, L. 1971: Beryllium mineralization in the Ilímaussaq intrusion, South Greenland, with description of a field beryllometer and chemical methods. Rapport Grønlands Geologiske Undersøgelse 33, 40 pp.

Ferguson, J. 1964: Geology of the Ilímaussaq alkaline intrusion, South Greenland. Description of map and structure. Bulletin Grønlands Geologiske Undersøgelse 39, 82 pp. (also Meddelelser om Grønland 172, 4).

GMEL 2008 (Greenland Minerals and Energy Ltd. Perth, Australia): Annual Report 2008, 115 pp. http://www.ggg.gl/Investor/Annual-Reports.htm

GMEL 2009 (Greenland Minerals and Energy Ltd, Perth Australia): Annual report 2009, 37+69 pp. http://www.ggg.gl/Investor/Annual-Reports.htm

GMEL 2011 (Greenland Minerals and Energy Ltd, Perth Australia): Greenland Minerals confirms a substantial new multi-element deposit (REEs, U, Zn) with big drill intercepts. Company Announcement, Thursday February 17th, 2011. http://www.ggg.gl/userfiles/file/ASX/Greenland_Confirms_New_Discovery.pdf

IAEA 1980: International Fuel Cycle Evaluation. Report of Working Group 1: Fuel and Heavy Water Availability. Vienna, International Atomic Energy Agency, 314 pp.

Kalsbeek, N., Larsen, S. & Rønsbo, J.G. 1990: Crystal structures of rare earth element rich apatite analogues. Zeitschrift für Kristallographie 191, 249–263.

Kalvig, P. 1983: Preliminary mining assessment of the uranium resource at Kvanefjeld, the Ilímaussaq intrusion, South Greenland. Unpublished report, Risø National Laboratory, Roskilde, Denmark, 109 pp + appendices (in GEUS archives, GEUS Report File 20566).

Khomyakov, A.P. 1995: Mineralogy of hyperagpaitic alkaline rocks, 223 pp. Oxford: Clarendon.

Khomyakov, A.P. & Sørensen, H. 2001: Zoning in steenstrupine-(Ce) from the Ilímaussaq alkaline complex, South Greenland: a review and discussion. Geology of Greenland Survey Bulletin 190, 109–118.

Khomyakov, A.P., Sørensen, H., Petersen, O.V. & Bailey, J.C. 2001: Naujakasite from the Ilímaussaq alkaline complex, South Greenland, and the Lovozero alkaline complex, Kola Peninsula, Russia: a comparison. Geology of Greenland Survey Bulletin 190, 95–108.

Kunzendorf, H., Nyegaard, P. & Nielsen, B.L. 1982: Distribution of characteristic elements in the radioactive rocks of the northern part of Kvanefjeld, Ilímaussaq intrusion, South Greenland. Rapport Grønlands Geologiske Undersøgelse 109, 32 pp.

Kystol, J. & Larsen, L.M. 1999: Analytical procedures in the Rock Geochemical Laboratory of the Geological Survey of Denmark and Greenland. Geology of Greenland Survey Bulletin 184, 59–62.

Larsen, J.G. 1977: Petrology of the late lavas of the Eriksfjord Formation, Gardar province, South Greenland. Bulletin Grønlands Geologiske Undersøgelse 125, 31 pp.

Larsen, L.M. & Sørensen, H. 1987: The Ilímaussaq intrusion – progressive crystallization and formation of layering in an agpaitic magma. In: Fitton, J.G. & Upton, B.G.J. (eds): Alkaline igneous rocks. Geological Society of London, Special Publication 30, 473–488.

Løvborg, L., Kunzendorf, H. & Hansen [Rose-Hansen], J. 1968: Use of field gamma-spectrometry in the exploration of uranium and thorium deposits in South Greenland. In: Nuclear techniques and mineral resources, 197–211. Vienna: International Atomic Energy Agency.

Løvborg, L., Wollenberg, H., Sørensen, P. & Hansen, [Rose-Hansen], J. 1971: Field determination of uranium and thorium by gamma-ray spectrometry, exemplified by measurements in the Ilímaussaq alkaline intrusion, South Greenland. Economic Geology 66, 368–384.

Løvborg. L., Wollenberg, H., Rose-Hansen, J. & Nielsen, B.L. 1972: Drill-core scanning for radioelements by gamma-ray spectrometry. Geophysics 37, 675–693.

Løvborg, L., Nyegaard, P., Christiansen, E.M & Nielsen, B.L. 1980: Borehole logging for uranium by gamma-ray spectrometry. Geophysics 45, 1077–1090.

Makovicky, E. & Karup-Møller, S. 1981: Crystalline steenstrupine from Tunugdliarfik in the Ilímaussaq alkaline intrusion, South Greenland. Neues Jahrbuch für Mineralogie Abhandlungen 140, 3, 300–330.

Makovicky, M., Makovicky, E., Nielsen, B.L., Karup-Møller, S. & Sørensen, E. 1980: Mineralogical, radiographic and uranium leaching studies on the uranium ore from Kvanefjeld, Ilímaussaq complex, South Greenland. Risø-R-416, 186 pp. Risø National Laboratory, Roskilde, Denmark.

Markl, G., Marks, M., Schwinn, G. & Sommer, H. 2001. Phase equilibrium constraints on intensive crystallization parameters of the Ilímaussaq complex, South Greenland. Journal of Petrology 42, 2231–2258.

Nielsen, B.L. & Steenfelt, A. 1979: Intrusive events at Kvanefjeld in the Ilímaussaq igneous complex. Bulletin of the Geological Society of Denmark 27, 143–155.

Nyegaard, P. 1979: Evaluation of the uranium deposit at Kvanefjeld. Unpublished report, Grønlands Geologiske Undersøgelse, København, 39 pp.

Nyegaard, P. 1980: Geologisk arbejde i Kvanefjeld tunnelen 1979/1980. Uranudvindingsprojektet, 19 pp. + figs + tables. Unpublished report, Grønlands Geologiske Undersøgelse, København.

Nyegaard, P., Nielsen, B.L., Løvborg, L. & Sørensen, P. 1977: Kvanefjeld uranium project. Drilling programme 1977, 46 pp. + figs + tables. Unpublished report, Geological Survey of Greenland, Copenhagen.

Pekov, V., Chukanov, N.V., Rønsbo, J. & Sørensen, H. 1997: Erikite – a pseudomorph after vitusite. Neues Jahrbuch für Mineralogie Monatshefte 1997, 97–112.

Petersen, O.V. & Andersen, S. 1975: The crystal habit of naujakasite with a note on some new occurrences. Bulletin Grønlands Geologiske Undersøgelse 116, 5–9.

Petersen, O.V., Khomyakov, A.P. & Sørensen, H. 2001: Natrophosphate from the Ilímaussaq alkaline complex, South Greenland. Geology of Greenland Survey Bulletin 190, 139–141.

Pfaff, K., Krumrei, T., Marks, M., Wenzel, T., Rudolf, T. & Markl, G. 2008: Chemical and physical evolution of the 'lower layered sequence' from the nepheline syenitic Ilímaussaq intrusion, South Greenland: Implications for the origin of magmatic layering in peralkaline felsic liquids. Lithos 106, 280-296.

Rønsbo, J.G. 2008: Apatite in the Ilímaussaq alkaline complex: Occurrence, zonation and compositional variation. Lithos 106, 71–82.

Rønsbo, J.G., Leonardsen, E.S., Petersen, O.V. & Johnsen, O. 1983: Second occurrence of vuonnemite: the Ilímaussaq alkaline intrusion, South West Greenland. Neues Jahrbuch für Mineralogie Monatshefte 10, 451–460.

Rose-Hansen, J. & Sørensen, H. 2002: Geology of the lujavrites from the Ilímaussaq alkaline complex, South Greenland, with information from seven boreholes. Meddelelser om Grønland, Geoscience 40, 58 pp.

Rose-Hansen, J., Karup-Møller, S., Sørensen, E., & Sørensen, H. 1977: Uranium-rich albitites from the northern contact of the Ilímaussaq alkaline intrusion. In: Rose-Hansen, J. & Sørensen, H. (compilers): Current research in the Ilímaussaq region, South Greenland. Rapport Grønlands Geologiske Undersøgelse 85, 68 only.

Smith, K.L. & McLaren, A.C. 1983: TEM investigation of a microcline from a nepheline syenite. Physics and Chemistry of Minerals 10, 69–76.

Sørensen, E. 1982: Water-soluble substances in Kvanefjeld lujavrite. 4 pp. Unpublished report, Risø National Laboratory, Roskilde, Denmark.

Sørensen, H. 1962: On the occurrence of steenstrupine in the Ilímaussaq massif, Southwest Greenland. Bulletin Grønlands Geologiske Undersøgelse 32, 251 pp. (also Meddelelser om Grønland 167, 1).

Sørensen, H. 1992: Agpaitic nepheline syenites: a potential source of rare elements. Applied Geochemistry 7, 417–427.

Sørensen, H. 1997: The agpaitic rocks – an overview. Mineralogical Magazine 61, 485–498.

Sørensen, H. 2006: The Ilímaussaq alkaline complex, South Greenland – an overview of 200 years of research and an outlook. Meddelelser om Grønland, Geoscience 45, 70 pp.

Sørensen, H. & Larsen, L.M. 1987: Layering in the Ilímaussaq alkaline intrusion, South Greenland. In: Parson, I. (ed): Origins of Igneous layering. NATO Advanced Science Institute, Series C. Mathematical and Physical Sciences , 1–28. Dordrecht: Reidel Publishing Company.

Sørensen, H. & Larsen, L.M. 2001: The hyper-agpaitic stage in the evolution of the Ilímaussaq alkaline intrusion, South Greenland. Geology of Greenland Survey Bulletin 190, 83–94.

Sørensen, H., Hansen [Rose-Hansen], J. & Bondesen, E. 1969: Preliminary account of the geology of the Kvanefjeld area of the Ilímaussaq intrusion, South Greenland. Rapport Grønlands Geologiske Undersøgelse 18, 40 pp.

Sørensen, H., Rose-Hansen, J. & Nielsen, B.L. 1971: Geologisk beskrivelse af uranforekomsterne på Kvanefjeldsplateauet, Sydgrønland. Unpublished GGU internal report.

Sørensen, H., Rose-Hansen, J., Nielsen, B.L., Løvborg, L., Sørensen, E. & Lundgaard, T. 1974: The uranium deposit at Kvanefjeld, the Ilímaussaq intrusion, South Greenland. Geology, reserves and beneficiation. Rapport Grønlands Geologiske Undersøgelse 60, 54 pp.

Sørensen, H., Bailey, J.C., Kogarko, L.N., Rose-Hansen, J. & Karup-Møller, S. 2003: Spheroidal structures in arfvedsonite lujavrite, Ilímaussaq alkaline complex, South Greenland – an example of macro-scale liquid immiscibility. Lithos 70, 1–20.

Sørensen, H., Bohse, H. & Bailey, J.C. 2006: The origin and mode of emplacement of lujavrites from the Ilímaussaq alkaline complex, South Greenland. Lithos 91, 286–300.

Steenfelt, A. 1972: Beskrivelse af pulaskit, heterogen foyait, sodalitfoyait, naujait og kakortokit på Kvanefjeldsplateauet, Ilímaussaq. Unpublished cand. scient thesis, Institute of Petrology, University of Copenhagen, 52 pp + appendices.

Ussing, N.V. 1893: Alkalifeldspaterne i de Sydgrønlandske Nefelinsyeniter og beslægtede Bjærgarter. Meddelelser om Grønland 14, 1–106.

Ussing, N.V. 1912: Geology of the country around Julianehaab, Greenland. Meddelelser om Grønland 38, 1–376.

Wollenberg, H. 1971: Fission track radiography of uranium and thorium in radioactive minerals. Risø Report 228, 40 pp.

Remains of *Saurichthys* (Pisces, Actinopterygii) from the Early Triassic Wordie Creek Formation of East Greenland

ILJA KOGAN

Previously undescribed specimens of *Saurichthys* from the basal part of the Early Triassic Wordie Creek Formation (Griesbachian) of East Greenland demonstrate a remarkably complete squamation especially in the anterior trunk portion. Scales of the mid-lateral row are high and those of the mid-dorsal and mid-ventral rows broad and conspicuous by having a pronounced longitudinal keel on their inner surface; additional dorso-lateral and ventro-lateral scale rows are present. This pattern resembles that of *Saurichthys dayi* from the Early Triassic of Alberta and British Columbia. Differences in fin morphology suggest, however, that the Greenland form is probably not conspecific. A second Early Triassic species of *Saurichthys* occurring in East Greenland probably comes from a higher stratigraphic level (late Griesbachian to early Dienerian) with a different ichthyofaunal composition.

Key words: Saurichthys, East Greenland, Wordie Creek Formation, stratigraphy.

I. Kogan [i.kogan@gmx.de], Freiberg University of Mining and Technology, Geological Institute, Bernhard-von-Cotta str. 2, 09599 Freiberg, Germany.

Numerous fossil fishes from the Early Triassic of East Greenland have been collected in the course of several Danish palaeontological expeditions in the 1930s. First remains of *Saurichthys* Agassiz, 1834 were discovered by Eigil Nielsen in 1932 and only briefly mentioned in his subsequent publications (Nielsen 1935, 1936, 1961). The fourteen specimens reported in Nielsen (1961) are stored in The Natural History Museum of Denmark, Copenhagen (Geological Museum – MGUH numbers) and have never been described in detail, except for two skulls (MGUH-VP-992 and -994) that were published by Mutter *et al*. (2008) who referred to them as *Saurichthys* cf. *ornatus*.

Already Nielsen (1936) suggested the possible presence of more than one saurichthyid species in his collection because of differences in size and proportions. A preliminary survey of the material indicates that the occurrence of different morphotypes probably corresponds to two distinct stratigraphic levels. At least the specimens MGUH-VP-988, -997 and -1000 are referable to a single morphotype based on their peculiar squamation. They are described in the following account.

Material and methods

The three specimens described below have been collected by E. Nielsen during the 1930s in the Kap Stosch area at the north coast of Hold with Hope, East Greenland (Fig. 1). Nielsen (1935) distinguished six subsequent vertebrate-bearing levels, i.e. five "fish zones" and one "tetrapod zone", in his study area. Of the 14 *Saurichthys* specimens enumerated in Nielsen (1961), five were referred to his fish zone 2 and nine to his fish zone 5. According to the labels, specimens MGUH-VP-1000 and -997 were found in 1933 at the so-called Østlokaliteten and Vestlokaliteten, respectively. These localities are mentioned in Nielsen (1935: fig. 19) and belong to his fish zone 2 (Nielsen 1935: 100 ff.). Both localities are situated in the Neviatiakdal area and placed in the former *Otoceras* beds. This level corresponds to the interval from *Hypophiceras martini* to *Metophiceras subdemissum* zone (lowermost upper Griesbachian) in the stratigraphic scheme of Bjerager *et al*. (2006) and occurs near the base of the Wordie Creek Formation only few metres above the presumed Permian-Triassic boundary. No detailed information is given on the specimen MGUH-VP-988.

All specimens are preserved as concretions in laminated mudstones deposited under marine conditions during a period of local sea-level rise (Bjerager *et al.* 2006).

The fossils were studied under a WILD binocular microscope and photographed with a NIKON D 80 digital camera with a 35-70 mm zoom lens. Drawings were made by means of a camera lucida as well as on the basis of photographs. To enhance contrasts, specimen MGUH-VP-988 B was examined and photographed immersed in alcohol.

The use of open nomenclature follows Bengston (1988).

Fig. 1. Map of East Greenland showing the outcrop areas of the Early Triassic Wordie Creek Formation and the assumed find locality of *Saurichthys* aff. *dayi* on the north coast of Hold With Hope. Modified from Bjerager et al. (2006).

Systematic palaeontology

Subclass: Actinopterygii Cope, 1887
Order: Saurichthyiformes Aldinger, 1937
Family: Saurichthyidae Owen, 1860
[sensu Stensiö 1925]
Genus: *Saurichthys* Agassiz, 1834
Type species: *Saurichthys apicalis* Agassiz, 1834

Saurichthys aff. *dayi* (Raymond, 1925)

Referred material: MGUH-VP-1000 (anterior trunk portion and incomplete skull), MGUH-VP-997 (trunk fragment), MGUH-VP-988 A, B (trunk fragment with dorsal and anal fins in part and counterpart); possibly also MGUH-VP-990 (fragmentary skull) and MGUH-VP-996 (caudal peduncle).

Description

Specimen MGUH-VP-1000 (Fig. 2) is an incomplete skull with the anterior body portion preserved in a concretion. Most dermal bones of the skull are weathered away and only the right mandible and the right opercular are preserved in lateral view. The preserved portion of the mandible is 124 mm long and the tip of the snout is missing. Delicate subvertical striae can be recognized on the dentary. Some teeth are preserved on both jaws, the largest of them being ca. 4 mm high by 2.5 mm wide.

The opercular is considerably higher than long (28 mm high, 17 mm long) and ornamented with concentric ridges of ganoin parallel to its margins. The cleithrum has the shape of an inverted 'T' whose anterior and posterior branches are nearly equal in length.

The pectoral fin is fan-shaped and consists of at least 18 unsegmented lepidotrichia.

The postcranial body fragment shows 18 mid-lateral scales. They are very high (ca. 25 mm in height to 5 mm in length along the lateral line) and roughly rectangular in shape, and the lateral line sensory canal divides them into a somewhat smaller upper (dorsal) part and a larger lower (ventral) part. The scales are inclined anteroventrally and ornamented with a combination of ridges and tubercles of ganoin. In the lower parts, subvertical and somewhat sigmoidal ridges predominate and tubercles are restricted to the margins of the scale. The pattern is similar in the upper parts of the anteriormost scales, whereas farther back the ornament is composed of tubercles arranged in subhorizontal rows.

Further scales are present on the body but neither their number nor their exact shape can be determined due to the preservation. It seems, however, that the
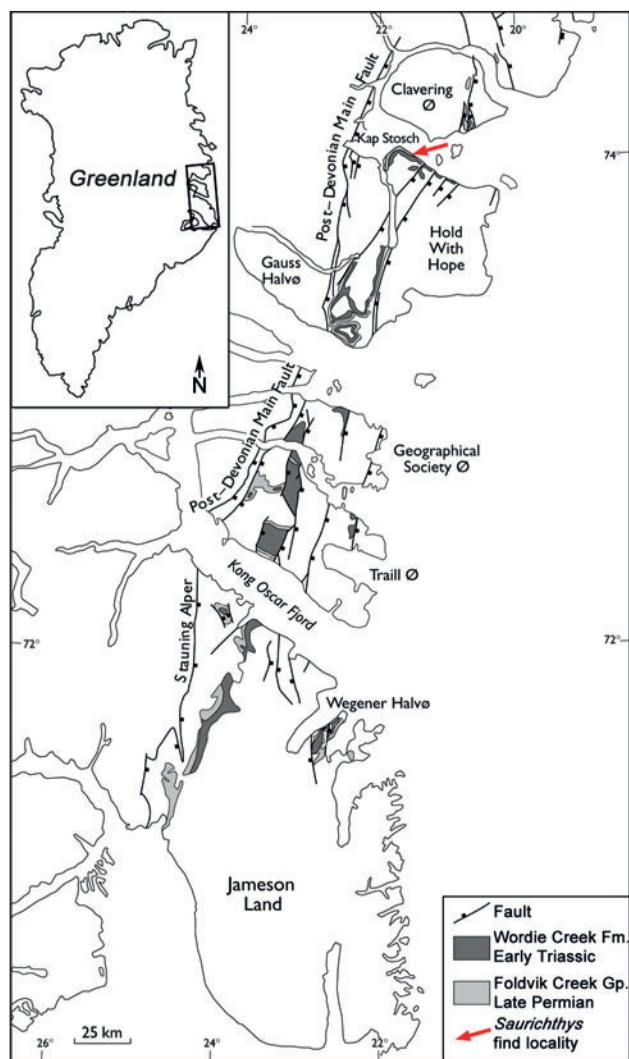
anterior scales of the mid-dorsal row are oval and very small, increasing in size posteriorly.

Specimen MGUH-VP-997 (Fig. 3) represents a cast of a body fragment presumably between the skull and the pelvic fins. Remnants of 8 mid-lateral scales are visible. They show the same proportions as described for specimen MGUH-VP-1000, but it can be seen that the sigmoidal subvertical ridges that constitute the ornamentation of their lower parts are mainly composed of fused tubercles. The upper parts of the scales are ornamented with distinct tubercles arranged in curved, subhorizontal rows.

Three rows of scales can be distinguished between the mid-lateral and the mid-ventral scale row. The scales correspond to the mid-lateral scales in number. The long axis of all of these ventrolateral scales is anteroventrally directed, opposing the anterodorsal axis of the mid-lateral scales. Scales of the uppermost ventrolateral row are bigger and rectangular in shape (ca. 8 to 4 mm), the remaining scales are 3-5 mm long and oval to triangular. All of them are ornamented with tubercles.

The mid-ventral scales are preserved only as impressions of their outside. They are cordiform to V-shaped, pointing posteriorly, 5 mm wide and 7 mm long. They also roughly correspond in number to the mid-lateral scales. The ornamentation is composed of tubercles arranged in longitudinal rows.

The portion dorsally to the mid-lateral scales is insufficiently preserved. Several scales of different size are present, which could possibly reflect the pattern in the ventral part.

Specimen MGUH-VP-988 A and B (Fig. 4) represents the region of the dorsal and anal fin in part and counterpart. About 20 mid-lateral scales are preserved anteriorly to the fins; compared to the mid-lateral scales of more anterior body segments, documented by specimens MGUH-VP-1000 and -997 (apparently belonging to individuals of comparable size) they are less high (about 20 mm) and slightly more rhombic than rectangular in outline. Their length, however, is still between 4 and 5 mm, and the ornamentation follows the pattern described above. Comparatively larger areas of the lower part of the scales, near their anterior and ventral margins, are covered with tubercles. The scales of the mid-dorsal and mid-ventral rows are only half as numerous as the mid-lateral ones; further scale rows seem not to be present.

Scales of the mid-ventral and mid-dorsal rows have the same shape in front of the dorsal and anal fins. They are rounded, 10-11 mm broad and 11-12 mm long. On the inside, a prominent longitudinal keel runs

Fig. 2. *Saurichthys* aff. *dayi*, incomplete skull and anterior body portion. Specimen MGUH-VP-1000.

along the midline, passing from one scale to another. The anterior edge of every scale is pointed and fits into a groove on the inside of the preceding one. The surface of the scales presents a V-shaped outline and an ornament of tubercles arranged in longitudinal rows.

The dorsal fin is supported by at least 8 endoskeletal radials divided in elongated proximal axonosts and square-shaped distal baseosts. The fin consists of at least 28 lepidotrichia, the longest of which are segmented no less than 5 times. Basal and fringing fulcra are present on its anterior margin, whose fragmentary preservation precludes from more exact description of these elements. The anal fin is supported by at least 10 endoskeletal radials, and about 40 segmented lepidotrichia can be counted, the posteriormost of which are very thin. Three or four basal fulcra can be recognized in front of it. The anterior margin bears fringing fulcra. Taking into account that in all known saurichthyids the dorsal and anal fins are highly symmetrical, the structures of both might be much more similar than they appear due to the state of preservation.

Four mid-ventral and four mid-dorsal scales are preserved behind the anal and dorsal fin. Their shape is the same as in front of the fins, but both rows are set closer to each other, forming the beginning of the narrow caudal peduncle. Remnants of smaller scales should belong to the mid-lateral row which would have decreased in height in the caudal part.

Part of the vertebral column is exposed in specimen MGUH-VP-988 B (Fig. 4B, C, 5). Ossified dorsal and ventral elements (pairs of neural and haemal arches, respectively) are placed dorsolaterally and ventrally to the notochord, which has partly been calcified. The neural arches consist of an enlarged, rounded basal part narrowing dorsally, and short anterodorsal articulation processes (praezygapophyses). Conspicuous posterodorsally ascending neural spines emerge from the neural arches anterior to the dorsal fin. They are cylindrical proximally but become slightly flattened distally. It is not clear if separate postzygapophyses were also developed to articulate with the praezygapophyses of the following neural arch. The haemal arches are of roughly rectangular shape and are separated from each other by round foramina. They seem to correspond to the neural arches in number. Presence of haemal spines is indicated by a couple of elongated elements apparently associated with the haemal arches (Fig. 4C). The vertebrae are more numerous than the mid-lateral scales in the corresponding body portion.

Specimens MGUH-VP-990 and -996 are attributed to the same species only tentatively. MGUH-VP-996

Fig. 3. *Saurichthys* aff. *dayi*, fragment probably from the abdominal region as preserved in specimen MGUH-VP-997. Anterior to the left.
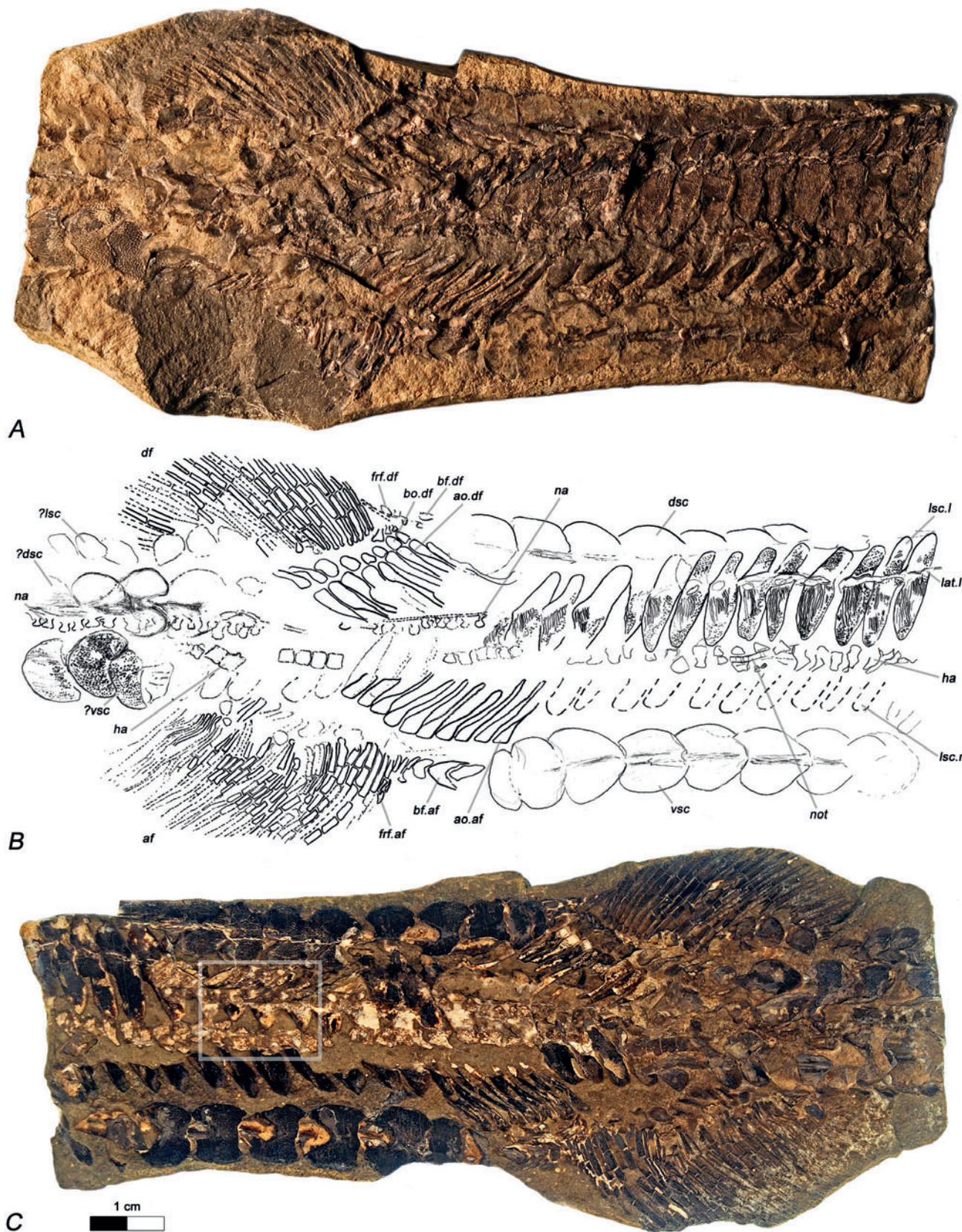
Fig. 4. *Saurichthys* aff. *dayi*, posterior body portion with the opposed dorsal and anal fins. **A**, specimen MGUH-VP-988 A (anterior to the right); **C**, its counterpart MGUH-VP-988 B (anterior to the left); **B**, sketch compiled after both parts (anterior to the right). Abbreviations: *af* anal fin, *df* dorsal fin, *ao* axonosts, *bo* baseosts, *bf* basal fulcra, *frf* fringing fulcra, *dsc* mid-dorsal scale row, *vsc* mid-ventral scale row, *lsc* mid-lateral scales, *lsc.l* left mid-lateral scale row, *lsc.r* right mid-lateral scale row, *lat.l* lateral line, *na* neural arches, *ha* haemal arches, *not* notochord. The box in **C** indicates the frame of Fig. 5.
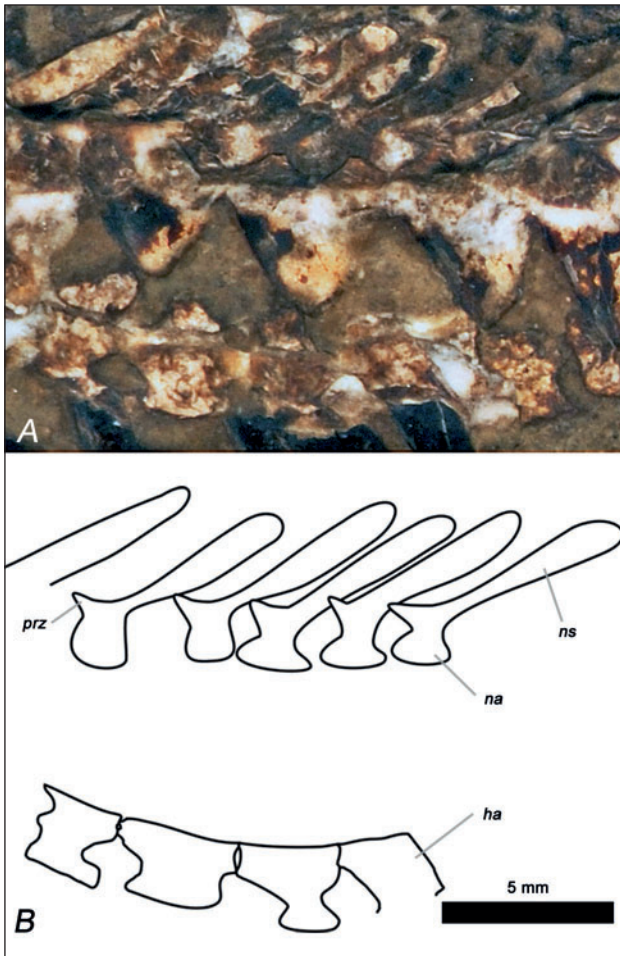
Fig. 5. **A**, *Saurichthys* aff. *dayi*, detail of the vertebral column as preserved in specimen MGUH-VP-988 B; **B**, interpretative sketch of A. Abbreviations: *na* neural arch, *ha* haemal arch, *prz* praezygapophysis, *ns* neural spine. Anterior to the left. Position of picture is shown in Fig. 4C.

is the fragment of a caudal peduncle, showing a part of a dorsal or anal fin and several V-shaped scales ornamented with tubercles. MGUH-VP-990 is a fragmentary skull with rather short, rounded opercular, resembling that of MGUH-VP-1000. Both specimens probably also come from Nielsen's (1935) fish zone 2, as suggested by their finding localities: MGUH-VP-996 was collected at Østlokaliteten, and MGUH-VP-990 at River 13 which is also located in the Neviatiakdal area.

Remarks

If the assumption of their provenience is correct, the specimens here referred to *Saurichthys* aff. *dayi* are the five *Saurichthys* specimens listed by Nielsen (1961) for fish zone 2. Accordingly, the remaining nine specimens must be those collected from fish zone 5; indeed, this is in agreement with their find-

ing localities that, as far as indicated on the labels, correspond to outcrops of fish zone 5 mentioned in Nielsen (1935). This is also the case for MGUH-VP-992 and -994 described by Mutter *et al.* (2008) as *Saurichthys* cf. *ornatus*. The opercular bone as preserved in specimens MGUH-VP-991 and -992 is posterodorsally expanded, resembling the opercular of *Saurichthys ornatus*, and the skull fragment MGUH-VP-999 closely resembles MGUH-VP-994 in general shape. Therefore, the specimens MGUH-VP-991, -992, -994 and -999 can preliminarily be referred to *Saurichthys* cf. *ornatus*; remaining fossils lack diagnostic features. In summary, the distribution of distinguishable specimens suggests that *Saurichthys* aff. *dayi* most probably comes from fish zone 2, whereas *Saurichthys* cf. *ornatus* occurs in fish zone 5.

Already Nielsen (1935) observed differences in the fossil assemblages of fish zones 2 and 5. For instance, *Bobasatrania* that by far dominates the assemblage of fish zone 2 is nearly absent in zone 5, which in contrast is dominated by *Pteronisculus* and parasemionotids (rare in zone 2) and coelacanths (Nielsen, 1961). According to the stratigraphic scheme of Bjerager *et al.* (2006), zone 5 can be placed in the late Griesbachian to possibly early Dienerian, whereas zone 2 is clearly Griesbachian. Whatever the reasons for a faunal change, it is not surprising to find different species of *Saurichthys* in short stratigraphic succession, as was demonstrated e.g. by Rieppel (1992) for the Monte San Giorgio area.

Discussion and conclusions

The new Greenland saurichthyid most closely resembles *Saurichthys dayi* (Raymond, 1925) from the Early Triassic (Griesbachian–Smithian or Spathian) of Alberta and British Columbia, as described and depicted by Mutter *et al.* (2008). Characteristics of this species are very high, somewhat rhomboidal mid-lateral scales and V-shaped to oval, broad mid-dorsal and mid-ventral scales; these are ornamented with longitudinal rows of tubercles and have a conspicuous longitudinal keel on their inside which takes part in the scale-to-scale articulation within each row (Mutter *et al.* 2008: fig. 11). This pattern is best seen in the specimen MGUH-VP-988. The mid-lateral scales also strongly resemble those depicted by Mutter *et al.* (2008).

High mid-lateral scales have also been reported by Stensiö (1925) for *Saurichthys wimani* (Woodward, 1912) and *Saurichthys elongatus* Stensiö, 1925 from the Smithian of Spitzbergen, and by Lehman (1952) for the Dienerian *Saurichthys madagascariensis* Piveteau, 1944-45. However, the two aforementioned forms differ from

the Greenland material in having small mid-dorsal and mid-ventral scales (Stensiö 1925). *Saurichthys madagascariensis*, in turn, has mid-dorsal and mid-ventral scales of comparable shape (but ornamented with striae rather than with tubercles), but Rieppel (1980) judged the high scales to be the ventro-lateral ones, suggesting that the lateral line is supported by a series of smaller, square-shaped to rounded scales. According to Rieppel's (1980) description, there are no smaller scales between the high lateral scales and the mid-ventral scale row, in contrast to what is seen in the Greenland material.

The existence of additional ventrolateral and/or dorsolateral scale rows in *Saurichthys dayi* could not be ruled out by Raymond (1925), neither by Schaeffer & Mangus (1976) who even questioned the validity of the species, nor by Mutter *et al*. (2008) who described additional material. However, Mutter *et al*. (2008) reported on anterior flanks entirely covered by scales. In the Greenland form, ventrolateral and dorsolateral scales seem to be absent in the region behind the pelvic fins, as indicated by the specimen MGUH-VP-988.

Nevertheless, belonging of the present material to *Saurichthys dayi* seems improbable because this latter species has all fin rays unsegmented (Schaeffer & Mangus 1976; Mutter *et al*. 2008). The strong segmentation of dorsal and anal fin in MGUH-VP-988 represents, for the moment, the only diagnostic feature distinguishing the new form from *Saurichthys dayi*.

It is therefore probable that the material described constitutes a new species of *Saurichthys*. The incompleteness of the specimens and the fact that material of *Saurichthys dayi* could not be examined, however, prevents from establishing a new taxon. According to Mutter *et al*. (2008), further saurichthyid fossils from Greenland should exist in collections. If so, they have to be incorporated into a more detailed study, which should also include the re-investigation of the forms from North America and Spitzbergen.

Acknowledgements

References

Agassiz, L. 1834: Abgerissene Bemerkungen über fossile Fische. Neues Jahrbuch für Mineralogie, Geognosie, Geologie und Petrefaktenkunde 1834, 379–390.

Aldinger, H. 1937: Permische Ganoidfische aus Ostgrönland. Meddelelser om Grønland 102(3), 1–392.

Bengston, P. 1988: Open nomenclature. Palaeontology 31(1), 223–227.

Bjerager, M., Seidler, L., Stemmerik, L. & Surlyk, F. 2006: Ammonoid stratigraphy and sedimentary evolution across the Permian-Triassic boundary in East Greenland. Geological Magazine 143(5), 635–656.

Cope, E.D. 1887: Geology and Palæontology. Zittel's manual on Palæontology. American Naturalist 22(11), 1014–1019.

Lehman, J.-P. 1952: Etude complémentaire des Poissons de l'Eotrias de Madagascar. Kungliga Svenska Vetenskapsakademiens Handlingar Serie 4, vol. 2(6), 1–201.

Mutter, R.J., Cartanyà, J. & Basaraba, S.A.U. 2008: New evidence of *Saurichthys* from the Lower Triassic with an evaluation of early saurichthyid diversity. In: Arratia, G., Schultze, H.-P., & Wilson, M.V.H. (eds), Mesozoic Fishes 4 – Homology and Phylogeny. Verlag Dr. Friedrich Pfeil, München, 103–127.

Nielsen, E. 1935: The Permian and Eotriassic Vertebrate-bearing Beds at Godthaab Gulf (East Greenland). Meddelelser om Grønland 98(1), 1–111.

Nielsen, E. 1936: Some few preliminary Remarks on Triassic Fishes from East Greenland. Meddelelser om Grønland 112(3), 1–55.

Nielsen, E. 1961: On the Eotriassic Fish Faunas of Central East Greenland. In: Raasch, G.O. (ed.), Geology of the Arctic. Volume 1. Toronto University Press, Toronto, 255–257.

Owen, R. 1860: Palaeontology or A systematic summary of extinct animals and their geological relations. A. and C. Black, Edinburgh, 420 pp.

Piveteau, J. 1944–1945: Paléontologie de Madagascar. XXV – Les Poissons du Trias inférieur. La famille des Saurichthyidés. Annales de Paléontologie 31, 79–89.

Raymond, P.E. 1925: Two new fossil fishes from Alberta. American Journal of Science Series 5, vol. 10(60), 551–555.

Rieppel, O. 1980: Additional specimens of *Saurichthys madagascariensis* PIVETEAU, from the Eotrias of Madagascar. Neues Jahrbuch für Geologie und Paläontologie, Monatshefte 1, 43–51.

Rieppel, O. 1992: A new species of the genus *Saurichthys* (Pisces: Actinopterygii) from the Middle Triassic of Monte San Giorgio (Switzerland), with comments on the phylogenetic interrelationships of the genus. Palaeontographica Abt. A 221, 63–94.

Schaeffer, B. & Mangus, M. 1976: An Early Triassic fish assemblage from British Columbia. Bulletin of the American Museum of Natural History 156(5), 515–564.

Stensiö, E.A. 1925: Triassic fishes from Spitzbergen. Kungliga Svenska Vetenskapsakademiens Handlingar Serie 3, vol. 2(1), 1–261.

Woodward, A.S. 1912: Notes on some Fish-remains from the Lower Trias of Spitzbergen. Bulletin of the Geological Institution of the University of Uppsala 11, 291–297.

Bio- and chemostratigraphic assessment of carbon isotope records across the Triassic–Jurassic boundary at Csővár quarry (Hungary) and Kendlbachgraben (Austria) and implications for global correlations

CHRISTOPH KORTE & HEINZ W. KOZUR

Carbon isotope trends are useful for stratigraphic correlation, especially for time intervals when major perturbations of the global carbon cycle occurred. Such perturbations have been documented for the Triassic–Jurassic (T–J) boundary, and several successions from this time interval are characterized by (1) an initial negative excursion, followed by (2) a pronounced positive excursion and a subsequent (3) main negative carbon isotope excursion. These features, however, are not present in all T–J boundary sections, or the stratigraphic position of the positive or the main negative excursion has variable locations. In the present study, we analysed carbon isotopes in bulk carbonate from the pelagic Csővár quarry section in Hungary and from the intra-platform basin to shallow subtidal marine Kendlbachgraben section in Austria. Both T–J boundary successions are biostratigraphically well controlled enabling – with particular focus on the bio- and chemostratigraphy of other T–J boundary sections – correlation of the carbon isotope trends. This evaluation shows that the apex of the initial negative δ13C excursion occurred slightly, but distinctly, below the mass extinction event and represents an excellent stratigraphic correlation tool.

Key words: Triassic–Jurassic boundary, chemostratigraphy, carbon isotopes, biostratigraphy, Csővár, Kendlbachgraben.

Christoph Korte (ck@geo.ku.dk), Department of Geography and Geology, University of Copenhagen, Øster Voldgade 10, DK-1350 Copenhagen K, Denmark. Heinz W. Kozur (kozurh@helka.iif.hu), Rézsü u. 83, H-1029 Budapest, Hungary.

At the Triassic–Jurassic (T–J) transition, major environmental changes took place on Earth resulting in a major mass extinction event and distinct perturbations of oceanic and atmospheric geochemistry (e.g. Weems 1992; Hallam & Wignall 1997; Pálfy *et al.* 2001; Cohen & Coe 2002, 2007; Hesselbo *et al.* 2002; Pálfy 2003; Tanner *et al.* 2004; McElwain & Punyasena 2007; Hautmann *et al.* 2008; Kiessling *et al.* 2009; Kiessling 2010; Bonis 2010; Ruhl 2010; Ruhl *et al.* 2010a). Particularly large amplitude carbon isotope excursions have been reported for marine carbonate and organic matter across the T–J boundary (e.g. McRoberts *et al.* 1997; McElwain *et al.* 1999; Pálfy *et al.* 2001; Ward *et al.* 2001; Hesselbo *et al.* 2002; Guex *et al.* 2004; Galli *et al.* 2005; Lucas *et al.* 2007), and additional distinctive shifts have been also reported for the time span before and after the T–J boundary (Cleveland *et al.* 2008; Schaller

et al. 2011; Ruhl & Kürschner 2011; Korte & Hesselbo 2011; Mette *et al.* unpublished manuscript).

Recent studies have shown that the geometry of the δ13C trend across the T–J boundary is similar in many instances, consisting of: (1) an 'initial' negative excursion, followed by (2) a pronounced positive excursion, and (3) a 'main' negative excursion (Hesselbo *et al.* 2002; Ward *et al.* 2007; Kuerschner *et al.* 2007; Williford *et al.* 2007; McRoberts *et al.* 2007; Ruhl *et al.* 2009). A similar trend is also reported for terrestrial sediments (Hesselbo *et al.* 2002; Pieńkowski *et al.* 2011; Steinthorsdottir *et al.* 2011). These features were reported for bulk organic carbon as well as for well preserved low-Mg-calcite oysters which are resistant to diagenetic alteration (Korte *et al.* 2009). However, the 'main' negative excursion is not observed in all marine sections (e.g. see Pálfy *et al.* 2007; Galli *et al.*

2007; van de Schootbrugge *et al.* 2008; Götz *et al.* 2009), suggesting that local effects might have influenced the seawater $\delta^{13}C$ in some cases. The initial negative excursion, on the other hand, which is present in nearly all carbon isotope records of the discussed time interval, is large in magnitude (~ 5 ‰) for total organic carbon (TOC) in the Northern Alps sections (Kuhjoch and Hochalpengraben), but this magnitude is even larger (~8.5 ‰) when analysing specific biomarkers (Ruhl *et al.* 2011). This suggests that the carbon cycle was even more perturbed than previously thought.

The occurrence and the geometric similarities of the carbon isotope sequence in several localities of the Tethys and the region of western Pangaea argue for a secular $\delta^{13}C$ signal. Such large-scale parallel fluctuations are generally caused by perturbations in the Earth's carbon cycle (e.g. Kump & Arthur 1999, see also Beerling & Berner 2002), thus enabling the use of these carbon isotope excursions for stratigraphic correlation as demonstrated for many stage boundaries including the Permian–Triassic boundary (e.g. Kraus *et al.* 2009; Korte & Kozur 2010), the Cenomanian–Turonian boundary (e.g. Sageman *et al.* 2006), and for the base of the Eocene (e.g. Magioncalda *et al.*, 2004). $\delta^{13}C$ fluctuations across the T–J boundary have been used for chemostratigraphic correlation (e.g. McRoberts *et al.* 2007). In some cases, however, it is difficult to compare the organic and carbonate $\delta^{13}C$ excursions because shifts in bulk organic carbon isotopes can be caused by changes in the photosynthetic fractionation within plants due to modification of CO_{2aq}, influencing the growth rate of organisms (e.g. Kump & Arthur 1999). In addition, it has to be taken into account that the sources for carbonate and organic carbon isotopes might have been decoupled in the earliest Jurassic (Clémence *et al.* 2010). Because of all these factors it cannot be assumed that a simple one-to-one phase correlation can be expected for $\delta^{13}C_{org}$ and $\delta^{13}C_{carb}$, although it can be assumed that shifts go in the same directions.

Here we present new bulk carbonate $\delta^{13}C$ values for the T–J boundary sections at Csővár ('Csővár quarry', Cserhát Mts., Hungary) and Kendlbachgraben (Northern Alps, Austria) and make comparisons to carbon isotope results of bulk organic matter and pristine oyster-shells from the literature. The goal of the present study is to use the Csővár quarry conodont biostratigraphy and carbon isotopes to correlate to bio- and chemostratigraphical results from other sections. This correlation enables definition of a general carbon isotope trend of at least the initial negative excursion in high resolution and provides evidence for its outstanding correlation potential for a well-dated stratigraphic level somewhat below the T–J boundary.

Sampling localities

Csővár

Bulk rock carbonate samples originate from the Csővár quarry (also named Pokol-völgy quarry), northern Hungary (Fig. 1). This succession belongs to the Transdanubian Range Unit, representing – according to Haas *et al.* (1997) – the most internal part of the Transdanubian Range segment of the Tethys shelf. It comprises two limestone formations. The Tuvalian to Rhaetian Csővár Limestone Formation (Balogh 1981) consists of dark, bituminous limestones, partly graded (often with transported shallow water fossils and clasts from adjacent reefs), cherty limestones, and marls (all basinal to toe-of-slope sediments). The uppermost Rhaetian, Hettangian and Sinemurian Várhegy Cherty Limestone Formation consists of bedded, light-yellowish to light-brownish micritic limestones and cherty limestones (Kozur & Mock 1991; Kozur 1993). These two formations are regarded by other workers as a single formation (Csővár Limestone Formation *s.l.*) (e.g. Haas *et al.* 1997; Haas & Tardy-Filácz 2004). The investigated part of the succession comprises the Rhaetian and Hettangian stages and the *Misikella posthernsteini*, *Misikella ultima* and *Neohindeodella detrei* conodont zones (Fig. 2). The rich occurrence of Nassellaria-dominated radiolarians indicates deep water, but in some beds transported shallow-water reef fossils from adjacent reefs dominate (including corals, Kozur & Mostler 1973; Haas *et al.* 1997; Haas & Tardy-Filácz 2004). Especially striking is a thick bed at the top of the Csővár Limestone Formation *ss*. It contains numerous transported shallow-water fossils, among them also corals that were transported from adjacent reefs. Transported lithoclasts are also common. It seems that this bed indicates a sea-level drop that exposed the reefs and brought the new reef margin closer to the deposition area of the Csővár section. The maximum of this sea-level drop coincides with the extinction event of the Triassic faunal elements. Immediately above these beds a sequence of marls, marly limestones, and silty shales begins, into which no shallow-water macrofossils and lithoclasts were transported. This is interpreted to indicate a sudden sea-level rise. Compared with the underlying beds, these marly, partly silty beds are very poor in fossils. Moreover, the carbonate production apparently decreased for a short interval (about 2 m in the section) and terrigenous input consists not only of clay, but also silt. This coupling of sea-level drop and immediately following sea-level rise confirms the scenario of an extinction event caused by cooling and contemporaneous sea-level drop, followed by warming (Schoene *et al.* 2010). This is also indicated by the extinction mode

of conodonts. *Misikella ultima* disappeared first; this species was dominant before the extinction and occurs only in equatorial, very warm water environments. During the slightly younger main extinction event the warm water genus *Misikella* disappeared, whereas *Neohindeodella* continued, a genus which occurs both in warmer and cooler water.

The Csővár quarry beds (and the entire Tuvalian to Sinemurian basinal to toe-of-slope succession) were for a considerable period assigned to the lower Carnian. A latest Triassic age for the Csővár quarry locality was first reported by Kozur & Mostler (1973) and confirmed by Detre *et al.* (1986). Subsequently, Kozur & Mock (1991) recorded *M. ultima* and *N. detrei* from this quarry and defined the late Rhaetian *M. ultima* and *N. detrei* zones (Fig. 3), although for the latter zone it was not clear whether it extended into the Jurassic. A Hettangian age for the upper part of the *N. detrei* Zone was demonstrated by Kozur (1993) using radiolarians.

Fig. 1. Location maps, modified after Delecat (2005) and Bonis *et al.* (2009) for Kendlbachgraben (47° 41′ 15″ N / 13° 21′ 3″ E; Krystyn *et al.* 2005), as well as for the Csővár quarry (47° 49′ 09″ N / 19° 18′ 24″ E), including the location of the Castle Hill section at Csővár which was investigated by Pálfy *et al.* (2001, 2007).
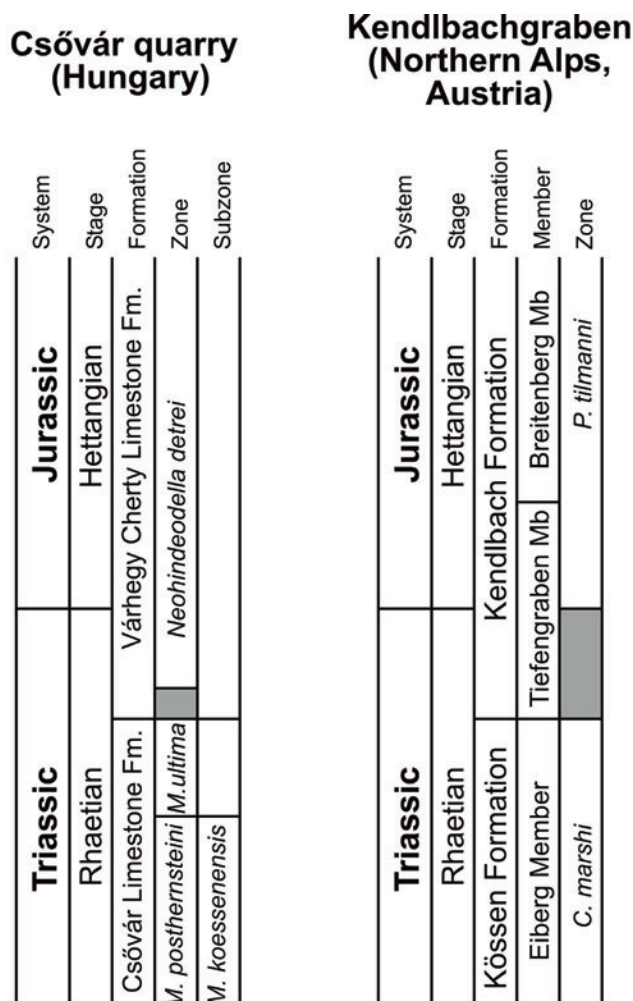
Fig. 2. Lithostratigraphic units and biostratigraphy of the investigated sections after Kozur & Mock (1991) and Kozur (1993) for Csővár and after Golebiowski (1990) and Kuerschner *et al.* (2007) for Kendlbachgraben.

Carbonates of the Csővár quarry are rich in conodonts; reworking of these (even in distal calciturbites) has not occurred, and the first appearance datum (FAD) and last occurrence datum (LOD) are easy to locate, well known, and possible to correlate with the isotope trends. Previously published isotope data are sparse (five [87]Sr/[86]Sr ratios for conodonts (Korte *et al.* 2003) and only six δ^{13}C data for bulk carbonates (Korte *et al.* 2005)) and are restricted to the *M. posthernsteini* and *M. ultima* zones, and based on this sparse δ^{13}C dataset it was impossible to define an accurate carbon isotope trend.

Bulk carbonate δ^{13}C data across the T–J boundary exist from the Castle Hill (Vár-hegy) section at Csővár (Pálfy *et al.* 2001, 2007; Götz *et al.* 2009), a locality that is situated about 200 m north-east of the Csővár quarry (Fig. 1). A bed-by-bed correlation between the Castle Hill section and Csővár quarry is difficult because in the Castle Hill T–J boundary succession fewer conodonts can be found, and sedimentological complications (slump structures) occur. Calciturbites occur in both sections, but they only indicate transport of contemporaneous shallow-water deposits and slope material from the reef and reef slope into the basin; they do not contain any older conodonts. The slump structures in the Castle Hill T–J boundary succession may have resulted in somewhat older material being admixed into the succession. H.W. Kozur and R. Mock also investigated the conodont succession of the Castle Hill T–J boundary succession. As some reworked older conodonts were found, these data were not published and only the conodont data from the quarry section were published in Kozur & Mock (1991). As the aim of this work is exact dating of the initial negative excursion, we have restricted our investigations to the quarry section.

Kendlbachgraben

Bulk carbonate samples from the Kendlbachgraben section at the Lake Wolfgang (Austria) were investigated for isotopic composition (Fig. 4). The sediments were deposited in an intraplatform basin (Eiberg Basin) (Kuerschner *et al.* 2007). The succession comprises the Eiberg Member (higher part of the Kössen Formation) and the Tiefengraben and Breitenberg Members of the Kendlbach Formation. The *C. marshi* and the *P. tilmanni* ammonoid zones are present (Figs 2, 4). The marls of the lower Tiefengraben Member (Fig. 4) have earlier been named Grenzmergel (e.g. Hallam & Goodfellow 1990).

From the Kendlbachgraben locality, the Kössen and Kendlbachgraben Formations have been intensely studied biostratigraphically (e.g. Suess & Mojsisovics

1868; Morbey 1975; Krystyn 1980). Subsequently, Golebiowski & Braunstein (1988) have presented detailed biostratigraphic fossil ranges in comparison to those of the Tiefengraben section; the latter locality is situated approximately 3 km north of the Kendlbachgraben section (Fig. 1). For Kendlbachgraben, δ^{13}C was analysed in bulk carbonate by Hallam & Goodfellow (1990), but Morante & Hallam (1996) suggested that the ^{13}C-depleted data of these authors, at least for the mudstones, are most probably diagenetically altered because a distinct positive δ^{13}C excursion occurred coevally for bulk organics. A similar positive trend in the mudstones was reported for the same section

Table 1. Analytical data. Samples are numbered by their relative height in metres in the sections in Figs 3 and 4.

Csővár			Kendlbachgraben		
m	δ^{13}C	δ^{18}O	m	δ^{13}C	δ^{18}O
-12.3	2.20	-1.51	-355	3.00	-1.27
-11.6	2.95	-2.75	-337	2.73	-1.73
-11.1	2.26	-0.79	-311	3.05	-1.36
-11.0	2.13	-0.64	-283	2.94	-1.25
-10.8	2.00	-0.44	-275	2.88	-1.37
-10.5	2.24	-0.97	-244	2.87	-1.90
-10.4	2.12	-0.64	-211	2.88	-2.65
-10.0	2.12	-1.20	-177	2.79	-2.02
-9.7	2.05	-0.71	-145	2.67	-1.44
-9.1	2.46	-0.34	-118	2.41	-1.71
-8.8	2.26	-1.38	-93	2.59	-2.68
-8.2	2.44	-0.86	-76	2.42	-2.25
-6.0	2.81	0.29	-73	2.40	-1.99
-2.0	1.52	-6.67	-56	2.27	-3.81
-1.5	1.88	-9.68	-54	2.61	-2.31
-1.2	1.36	-1.74	-49	2.56	-2.09
-0.9	1.75	-3.58	-22	2.51	-2.14
-0.6	1.44	-5.76	-6	2.29	-1.21
-0.3	2.26	-4.74	-5	2.32	-0.79
0.0	2.17	-5.13	-1	1.80	-1.99
0.1	2.43	0.20	305	2.81	-1.17
0.2	1.68	-4.09	305	2.84	-1.29
0.4	2.26	-3.04	318	2.81	-0.76
0.7	2.03	-13.06	318	2.87	-1.10
0.9	2.31	-1.82			
1.0	2.06	-2.48			
1.1	2.45	-1.88			
1.4	2.65	-2.05			
1.7	2.72	-1.83			
2.0	2.79	-1.64			
5.0	2.39	-1.66			
5.6	3.50	-1.41			
6.3	3.01	-5.19			

by Ruhl *et al.* (2009), for the Tiefengraben section by Kuerschner *et al.* (2007), and for other sections in the Northern Alps (Ruhl *et al.* 2009).

Material and methods

Bulk rock carbonate from both sections was analysed for stable isotopes. Samples of 2 to 5 mg of fine-grained bulk carbonates – drilled from fresh surfaces – were analysed for $\delta^{13}C$ and $\delta^{18}O$ at the Department of Earth Sciences at the University of Oxford using the VG Isogas Prism II mass spectrometer with an online VG Isocarb common acid bath preparation system. The samples reacted in the instrument with purified phosphoric acid (H_3PO_4) at 90°C. Calibration to the V-PDB standard via NBS-19 is made daily using the Oxford in-house (NOCZ) Carrara Marble standard. Reproducibility of replicated standards was better than 0.1‰ for both carbon and oxygen isotopes. $\delta^{13}C$ and $\delta^{18}O$ values (Table 1) have been reported in delta notation relative to the Vienna Pee Dee Belemnite (V-PDB) international scale.

Biostratigraphy was investigated in the field and by the determination of conodonts (acetic acid treatment). The positions of the analysed samples are shown in Figs 3 and 4.
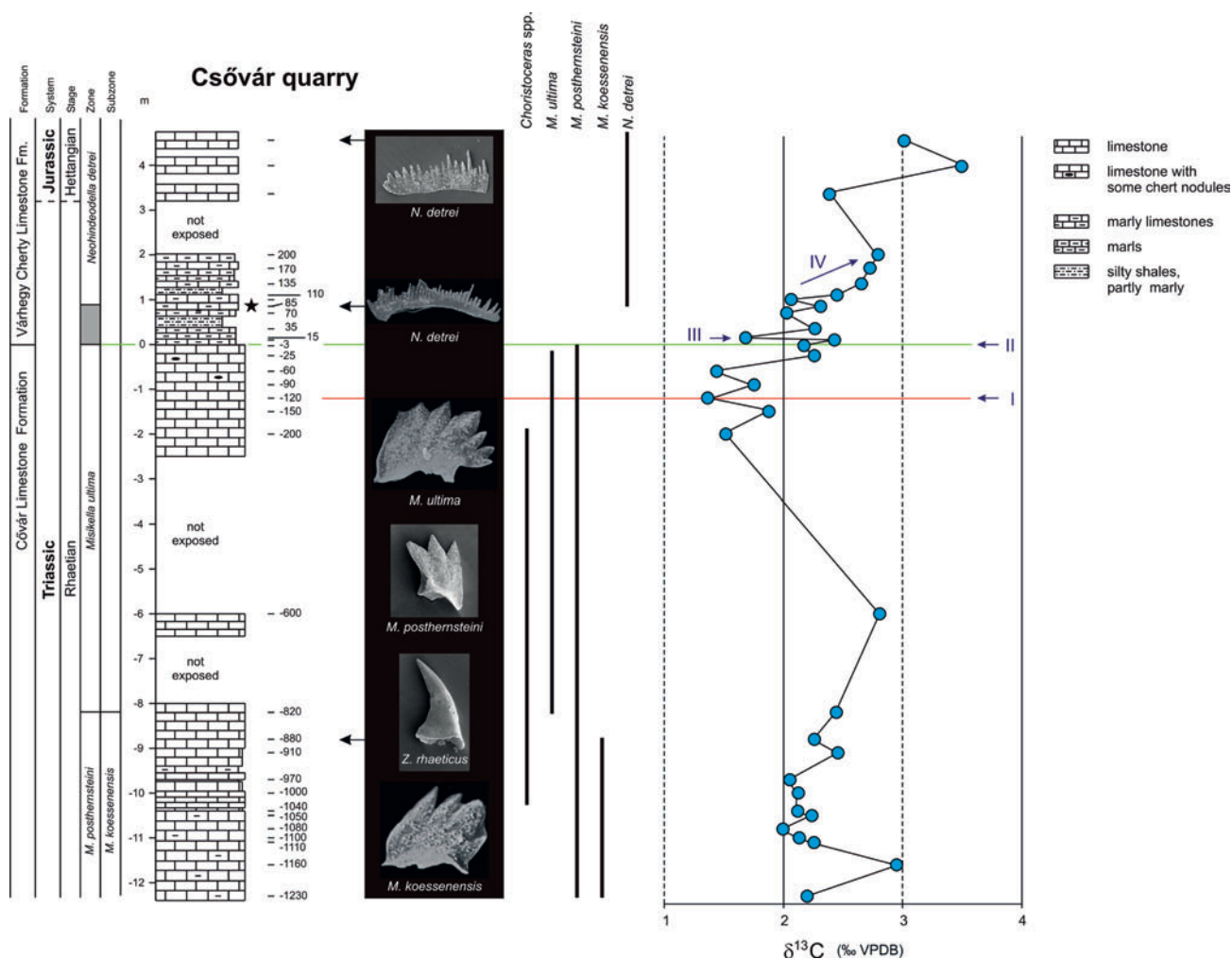
Fig. 3. Csővár quarry section, showing biostratigraphy, sample locations and carbon isotope values for bulk carbonates. The stratigraphically most important late Rhaetian and basal Hettangian conodonts are shown. Star: level of the transitional ammonoid form (see text and Fig. 5); Red line: apex of the initial negative carbon isotope excursion; Green line: LOD of Triassic *Misikella* conodonts; Grey shadow: 'pre-*planorbis* Beds' without definitive Triassic and Jurassic faunas; (I) minimum of the initial negative $\delta^{13}C$ excursion; (II) LOD of *Misikella* and other Triassic conodonts and beginning of the 'grey zone' ('pre-*planorbis* Beds'); (III) second negative $\delta^{13}C$ excursion in the basal part of the 'grey zone' ('pre-*planorbis* Beds'); (IV) a positive carbon isotope excursion.

Results

Biostratigraphy

The new conodont biostratigraphic investigations at Csővár quarry confirm the results of Kozur & Mock (1991) and Kozur (2003a, b). Most of the quarry section belongs to the late Rhaetian *M. ultima* conodont Zone (Fig. 3). Triassic conodonts remain common and diverse up to the top of this biozone and only *Norigondolella steinbergensis* (Mosher) disappears earlier. Ammonoids in the *M. ultima* Zone are rare and mostly represented by different *Choristoceras* species. *Choristoceras* is absent in the uppermost metre of the *M. ultima* Zone, but the remaining fauna remains abundant and diverse below the 'pre-*planorbis* Beds' for both pelagic faunal elements (especially badly preserved radiolarians of the late Rhaetian *Globolaxtorium tozeri* Zone) and transported shallow-water elements from adjacent reefs.

A major facies change occurs in the uppermost Csővár quarry section. The very fossil-rich, dark, bituminous, partly cherty limestones, which are often distinctly laminated especially in the upper part, are overlain with a sharp boundary by poorly fossiliferous, marly-silty beds with some marly limestone intercalations ('Pre-*planorbis* Beds'; grey zone in Fig. 3). An unconformity is not present at this level; the water remains deep, but a sea-level drop is indicated for the uppermost bed of the *M. ultima* Zone (see above). A
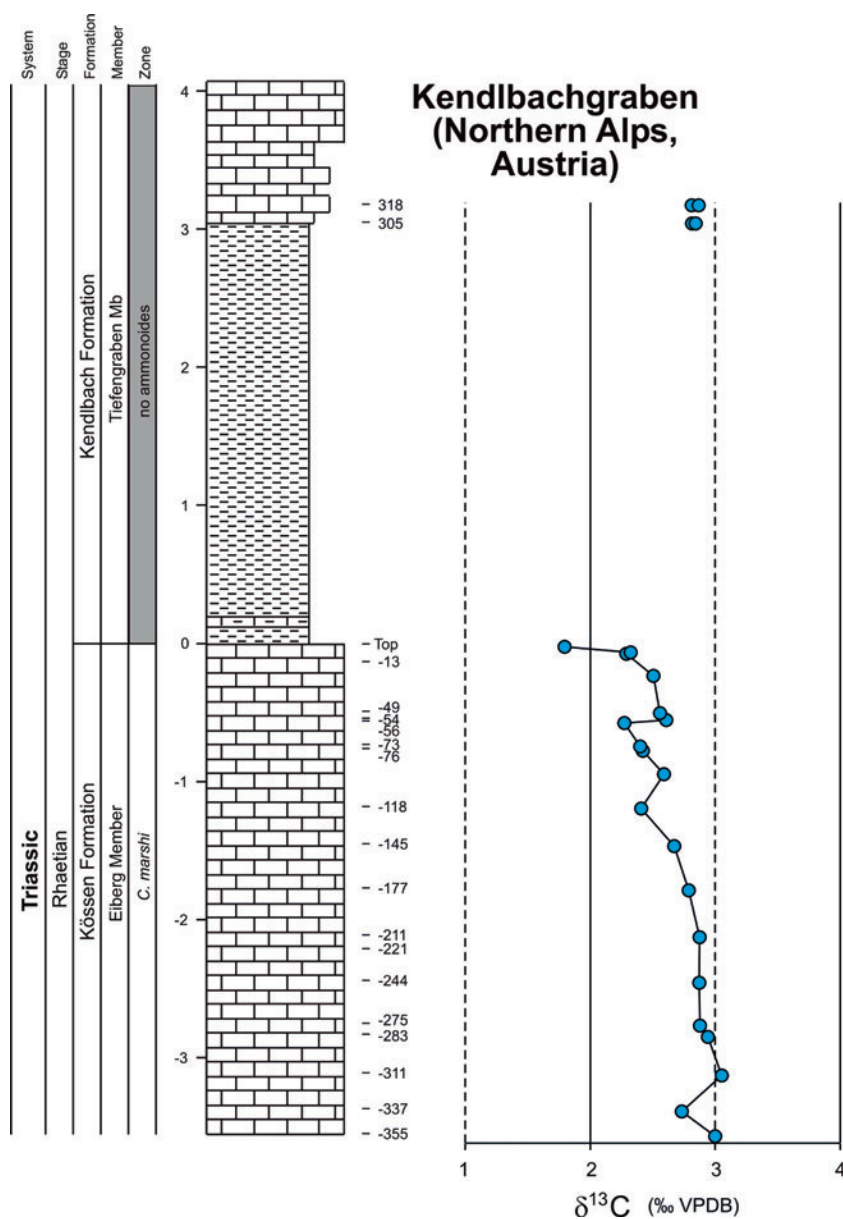
Fig. 4. Stratigraphic section for Kendlbachgraben, showing sample locations and carbon isotope values for bulk carbonates (see also the caption to Fig. 3).

distinct mass extinction of Triassic faunal elements (e.g., the rich *Misikella* conodont fauna), somewhat postdating the disappearance of the *Choristoceras* ammonoid fauna, occurs at the facies boundary. The sediments above the sharp lithological facies change are named the 'pre-*planorbis* Beds' of the basal Várhegy Cherty Limestone Formation; a very poor conodont fauna of the *N. detrei* Zone occurs in these deposits consisting of only very few representatives of the index species. This taxon, *N. detrei* (Kozur & Mock), is somewhat more common in the overlying micritic limestones (Fig. 3) where it continues to be found up to beds with poorly preserved earliest Jurassic radiolarians and Psiloceratids indet. (Kozur 1993; Götz *et al.* 2009). This occurrence of *N. detrei* represents the youngest (early Hettangian) conodont fauna of the world (Kozur 2003a, b).

A single ammonoid specimen has been recovered from a marly limestone intercalation about 0.9 m above the base of the 'pre-*planorbis* Beds' of the Csövár quarry section (Fig. 3: star, Fig. 5). This ammonoid was determined by Prof. Jean Guex (Lausanne) as a transitional form between the Triassic *Rhacophyllites* and the Hettangian *Psiloceras*, confirming the transitional Rhaetian–Hettangian character of these beds. In the 'pre-*planorbis* Beds' and time-equivalents between the last *Misikella* and the FAD of *Psiloceras spelae* (Guex), ammonoids are virtually absent world-wide (e.g. in New York Canyon (USA) a short ammonoid-free interval is present between the uppermost Triassic *Choristoceras crickmayi* zone and lowermost Jurassic *Psiloceras tilmanni* zone ammonoid faunas). Hence, the discovery of this Rhaetian–Hettangian transition ammonoid emphasizes the importance of this locality for biostratigraphy.

Carbon isotopes

Bulk carbonate carbon isotope values from the Csővár quarry (Fig. 3) vary between 2 and 3 ‰ in the *Misikella koessenensis* subzone of the *M. posthernsteini* zone, and are about 2 ‰ at its top. The values increase to 2.8 ‰ from the lower to the middle *M. ultima* Zone followed by a decrease to values of about 1.5 ‰ about 1 m below the top of the *M. ultima* Zone. By using biostratigraphy as a correlative baseline, we conclude that these low $\delta^{13}C$ values in the upper *ultima* zone (Fig. 6) represent the initial negative carbon isotope excursion at the T–J boundary (cf. Hesselbo *et al.* 2002). In the Csővár quarry section it is a multiple signal (Fig. 3) consisting of three small negative shifts situated between 2 m and 0.6 m below the top of the *M. ultima* zone (around I in Fig. 3), separated by slight, short recoveries. After a distinct recovery to about 2.4 ‰ (II in Fig. 3), a fourth weaker negative signal occurs 0.15 m above the top of the *M. ultima* zone (III in Fig. 3) within the basal 'pre-*planorbis* Beds'. This negative shift 0.15 m above the top of the *M. ultima* zone could be interpreted as the last signal of the initial negative shift at the T–J boundary. Instead, we suggest that this represents an additional traceable smaller negative excursion that is also observable at the same stratigraphic level at Lavernock Point, St. Audrie's Bay, Tiefengraben and New York Canyon (Fig. 6). This additional negative carbon isotope excursion is separated from the initial negative shift (cf. Hesselbo *et al.* 2002; Ruhl *et al.* 2009) by a distinct $\delta^{13}C$ recovery (just below the green line in Figs 3 and 6). Above this additional negative shift the curve increases to values of 3.5 ‰ in the *N. detrei* zone (IV in Fig. 3), representing the positive $\delta^{13}C$ excursion at the T–J boundary *sensu* Hesselbo *et al.* (2002).
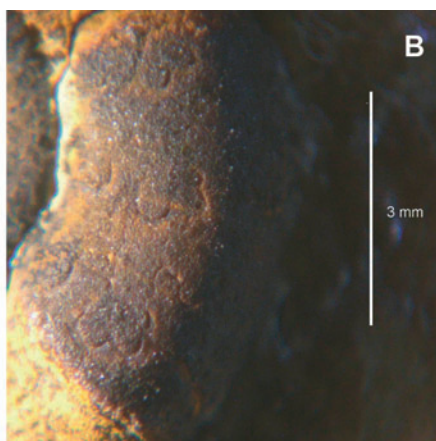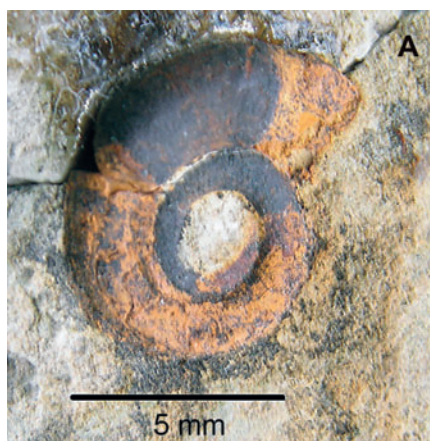
Fig. 5. Transitional form between the Triassic earliest Hettangian *Rhacophyllites* and the early Hettangian *Psiloceras* (det. Prof. Jean Guex, Lausanne), 0.9 m above the base of the 'pre-*planorbis* Beds' (= 0.9 m above the LOD of *M. posthernsteini* Kozur & Mock). This form has not been described previously. The level from which the ammonoid has been derived (above the last Triassic conodonts = above the LOD of *Misikella*, and below *Psiloceras tilmanni* (Lange) and *P. spelae* (Guex), in general has no ammonoids. a) entire specimen, b) detail with suture line. This specimen documents that real Jurassic ammonoids were not yet present after Triassic forms had disappeared.

The carbon isotope curve from the Kendlbachgraben section decreases gradually from about 3 ‰ to 1.8 ‰ in the *Choristoceras marshi* zone and the lowest value is situated at the top of the Kössen beds (Fig. 4). For the overlying Kendlbach Formation no data were obtained for the mudstones and δ¹³C values of nearly 3 ‰ are obtained from the base of the overlying limestones (see also Morante & Hallam 1996).

Discussion

To be able to utilize the T–J boundary carbon isotope trends for stratigraphic correlation it is necessary to constrain the δ¹³C fluctuations biostratigraphically. For this purpose, the Csővár quarry is important because of the presence of the well known FAD and LOD of conodonts. The importance of the carbon isotope trend from the Csővár quarry becomes clear when it is compared to bulk organic and pristine oyster-shell data

from the literature (Fig. 6). The initial δ¹³C minimum at Csővár quarry is about 1 m (between 0.6 to 2 m) below the top of the *ultima* zone. This result is similar to that for the Csővár Castle Hill section (see Pálfy *et al.* 2001, 2007; Haas & Tardy-Filácz 2004; Götz *et al.* 2009; Haas *et al.* 2010), but we note that the data by Pálfy *et al.* (2001, 2007) vary between – 4 and + 2 ‰ in their T–J boundary interval, whereas the T–J boundary interval data of the present study (~ 'grey zone') are between +1.5 and +2.5 ‰ (Fig. 3). At St Audrie's Bay, the initial negative carbon isotope excursion in the Lilstock Formation is about 1 m below the LOD of *M. posthernsteini* discovered in another nearby section (Fig. 6; see also Swift 1989, 1995; Hesselbo *et al.* 2002). The carbon isotope values from the New York Canyon (Ferguson Hill) section (Nevada, USA) are also important. Ranges for ammonites (Guex *et al.* 2004, Lucas *et al.* 2007) and conodonts (Orchard *et al.* 2007) from this locality are well established. Several δ¹³C fluctuations and a distinct initial negative excursion are observed in the carbon isotope values of this locality (Guex *et*
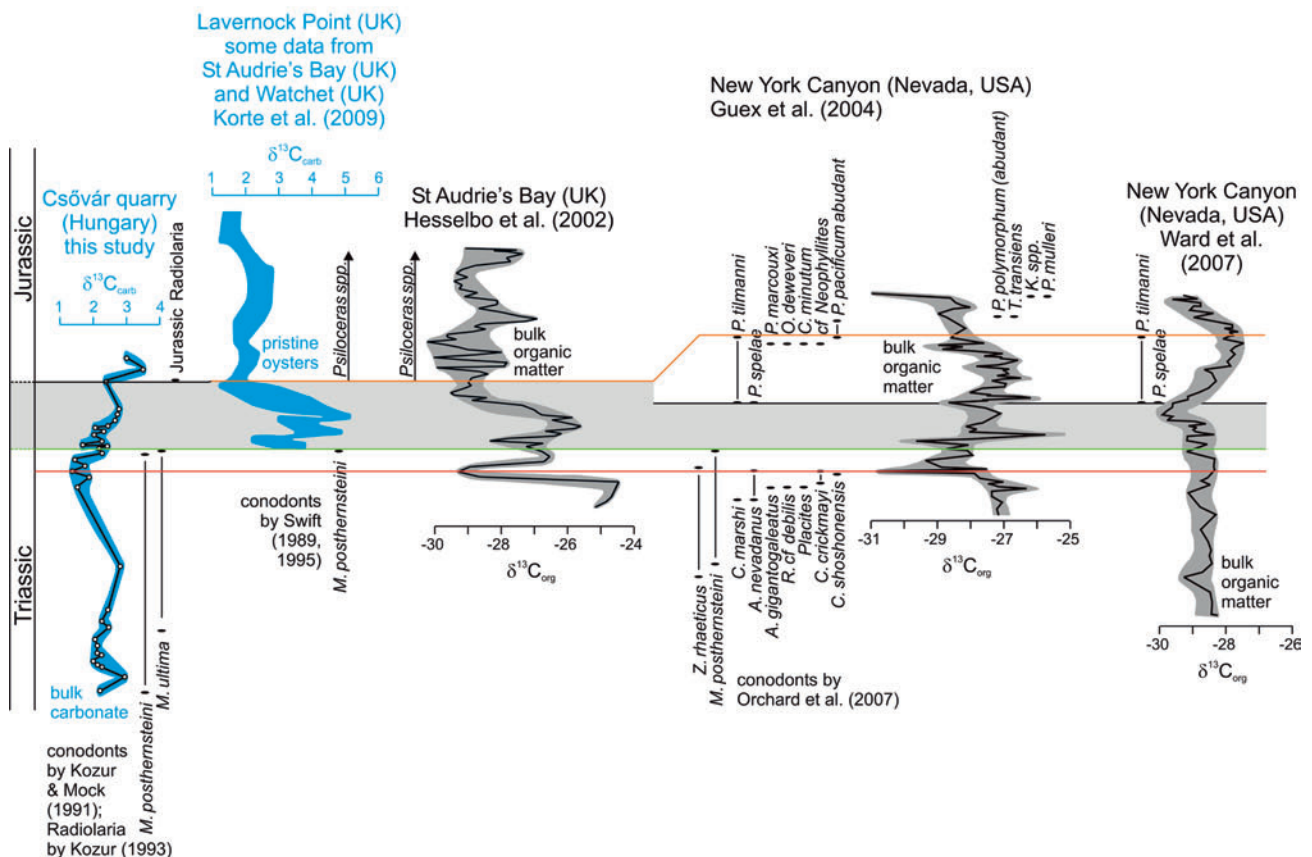
▲▶Fig. 6: Carbon isotope trends of bulk carbonates, pristine oysters and bulk organics for different T–J boundary sections, for comparison. Grey shadow: Interval without definitive Triassic and Jurassic faunas. Red line: apex of the initial negative carbon isotope excursion. Green line: LOD of Triassic *Misikella* conodonts. Orange line: FAD of moderately advanced *Psiloceras*, such as *Psiloceras planorbis* (Sowerby), *Psiloceras pacificum* (Guex). The correlation documents the chemostratigraphic correlation potential of the initial negative carbon isotope excursion. (Figure developed after McRoberts *et al.* 2007).

al. 2004; see Fig. 6). A different carbon isotope feature is reported by Ward *et al.* (2007) for the same section: a distinct initial negative shift is not recorded and a positive excursion occurs stratigraphically higher (Fig. 6; see also Guex *et al.* 2004). However, the first negative carbon isotope excursion at the New York Canyon recorded by Guex *et al.* (2004) is about 2 to 2.5 m below the LOD of *M. posthernsteini* (see Orchard *et al.* 2007 for conodont distribution) and this characteristic, as well as its shape and magnitude, is very similar to the initial negative carbon isotope excursion at St Audrie's Bay (Hesselbo *et al.* 2002).

Accepting that the negative New York Canyon excursion about 2 m below LOD of *M. posthernsteini* recorded by Guex *et al.* (2004, see also Lucas *et al.* 2007) is a reliable isotope signature, then we have a correlateable, uniform, conodont-controlled stratigraphic level for the initial T–J boundary δ13C minimum at three different regions in Hungary, England and Nevada. These δ13C minima are all distinctly (0.6 to 2.5 m) below the disappearance of the genus *Misikella*, marked by the red line in Fig. 6. At this point it is necessary to explain the distribution of the genus *Misikella*. *Misikella* occurred only at low latitudes; *M. ultima* was restricted to equatorial regions, whereas *M. posthernsteini* was distributed somewhat farther to the north (up to the Rhaetian palaeolatitudes of England and Nevada) compared to *M. ultima*. In equatorial regions (e.g. Hungary), *M. posthernsteini* and *M. ultima* became extinct almost contemporaneously. Therefore, the LOD of *M. ultima* and *M. posthernsteini* in Hungary and in the Alps corresponds to the LOD of *M. posthernsteini* in England and Nevada and defines the disappearance of the latest Triassic-type conodont faunas. At the Kennecott Point section (Queen Charlotte Islands, Canada), *Misikella* does not occur because this locality was situated even farther to the north than England and Nevada in T–J times, but here the disappearance of *Norigondolella* corresponds approximately to the LOD of *Misikella* and this is about 2–3 m below the first appearance of Jurassic radiolarians (M. Orchard, personal communication 2010).
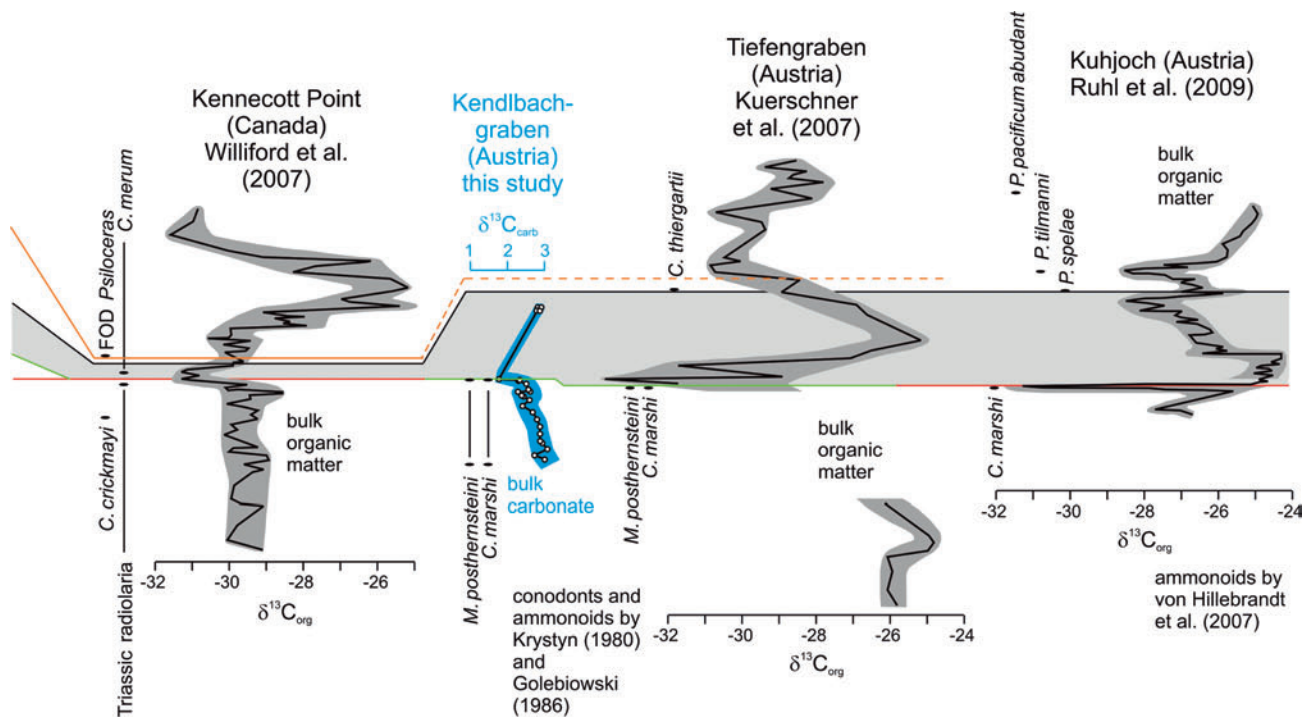
A different feature is visible for the Alpine Kendl-bachgraben and Tiefengraben sections (Fig. 6). Here the disappearance of *M. posthernsteini* and of *Choristoceras marshi* (Hauer) are contemporaneous (Fig. 6; see also Kuerschner *et al.* 2007) whereas in other sections *C. marshi* disappears distinctly before the LOD of *M. posthernsteini* and *M. ultima*. The contemporaneous disappearance of *C. marshi* and *Misikella* at the boundary between the Kössen and Kendlbach formations at a negative carbon isotope shift indicates either a short stratigraphic gap immediately before the 'pre-*planorbis* Beds', or a major condensation of the sequence. In all low-latitude sections towards the north as far as New York Canyon and St Audrie's Bay, the initial negative excursion lies distinctly below the LOD of *Misikella*. This observation is confirmed by von Hillebrandt *et al.* (2007) who pointed out that the equivalent of the uppermost Kössen Formation Bed T, of around 20 cm thickness in the GSSP Kuhjoch section, Austria, is absent at Kendlbachgraben and Tiefengraben due to non-deposition.

No conodonts exist for the uppermost Kössen Formation at the Kuhjoch section (Fig. 6). Therefore, it is not biostratigraphically clear whether a gap is present in the Kuhjoch section above bed T of the topmost Kössen Formation, as observed at Kendlbachgraben and Tiefengraben. However, the negative δ13C peak in the Kuhjoch section is situated at the boundary between the Kössen Formation and the Kendlbach Formation (Tiefengraben Member), immediately above a limestone unit, similar to the relationships observed at Kendlbachgraben and Tiefengraben. The stratigraphic position of this δ13C negative peak at Kendlbachgraben and Tiefengraben corresponds most likely to the negative shift in the basal part of the 'pre-*planorbis* Beds' in the Csővár quarry section and not to that of the upper *M. ultima* Zone. On the other hand, the LOD of *C. marshi* at the level of the negative excursion in the Northern Alps sections indicates that this negative shift corresponds to the initial negative shift. In both cases, a short gap must be present at Kendlbachgraben and Tiefengraben, arguing for a condensation or a non-sedimentation level in the basal part of the 'pre-*planorbis* Beds'. An additional correlation marker for the initial negative shift is a peak in prasinophytes that can be observed in the Alpine sections and Csővár at the level of the upper part of the initial negative excursion in the basal Kendlbach Formation of the Eiberg Basin in the Northern Alps and in the uppermost Csővár Limestone Formation in Hungary (Bonis *et al.* 2009, 2010; Götz *et al.* 2009; Bonis 2010; Ruhl *et al.* 2010b). In addition to the stratigraphic importance of the prasinophyte maximum during the (upper part of the) initial negative excursion, these fossils have also a palaeoecological importance. These 'disaster species'

can be often found close to levels of mass extinctions. Otherwise, they either prefer brackish to freshwater conditions or low water temperatures (e.g. Prauss 2007; Bonis 2010). Bonis *et al.* (2010) favoured brackish conditions because no glaciations are known close to the T–J boundary. However, shorter cooling events will not lead to glaciations, and cooler water temperatures at low latitudes can also be present in times without high latitude glaciations. Moreover, in partly restricted basins such as the Eiberg Basin, brackish conditions can easily be established. However, at Csővár, open sea marine conditions prevailed at the level of the initial negative excursion and the prasinophyte acme. Here, somewhat lower water temperatures are favoured because brackish conditions can be excluded by the stenohaline marine fauna. Furthermore, the mode of the mass extinction instead indicates rapid cooling as the cause (see above). Such short periods of cooler temperatures are characteristic of large scale volcanism, such as the Central Atlantic Magmatic Province (CAMP) plateau basalts at the T–J boundary (Courtillot & Renne 2003). Also in the uppermost Permian, mass extinction events occur that are related to both global warming and global cooling events (Korte & Kozur 2011; Kozur & Weems 2011). Kozur & Weems (2005) have used conchostracans to show that the CAMP volcanism was not restricted to the Jurassic, but that the first lava flow in the Newark Supergroup belongs to the upper Rhaetian because it is immediately under- and overlain by late Rhaetian conchostracan faunas. Cirilli *et al.* (2009) have also reached similar conclusions by evaluation of sporomorphs. Thus, the main extinction event of marine uppermost Triassic low latitude faunas is apparently related to the onset of plateau basalt volcanism within the CAMP, just as the main extinction event within the uppermost Permian of marine low latitude faunas is contemporaneous with the onset of plateau basalt effusion above the tuffs within the Siberian Trap (Renne & Basu 1991; Korte *et al.* 2010; Kozur & Weems 2010, 2011). The latest Permian low latitude marine main extinction event was suggested to be caused by global cooling, whereas the earlier continental and high latitude marine extinction horizon within the uppermost Permian was caused, in contrast, by global warming (Kozur & Weems 2011). Such different phases of short-lasting global cooling and longer-lasting global warming may also be present within the uppermost Triassic and affected the biota (Schoene *et al.*, 2010).

As a consequence of the above discussion, an essential correlation horizon around the low latitude T–J boundary is the LOD of *Misikella* (*M. posthernsteini, M. ultima*) and this is clearly seen in the uncondensed sections at Csővár and New York Canyon to occur above the disappearance of Triassic ammonoid species of

Choristoceras (*C. marshi*, *C. crickmayi*) (Fig. 6). The initial δ¹³C minimum is coeval with the disappearance of *C. marshi* and *C. crickmayi*. Note that *C. crickmayi* may occur stratigraphically somewhat higher up than *C. marshi*, but this phenomenon might be a LOD of the latter species in Nevada because *C. crickmayi* is a typical North America form, but *C. marshi* is not.

The initial T–J boundary δ¹³C minimum is synchronous; its position occurs near the LOD of *C. crickmayi* (and at or somewhat above the LOD of *C. marshi*) and somewhat below the disappearance of genus *Misikella*.

A second time line is the base of the 'grey zone' (green line in Fig. 6) at the LOD of *Misikella*, and this is somewhat above the initial δ¹³C minimum. In the 'grey zone', faunas are not definitively Triassic or Jurassic. Significantly, the transitional form between the Triassic ammonoid *Rhacophyllites* and the Hettangian ammonoid *Psiloceras* was found in this horizon at the Csővár quarry section. Both the red and the green time lines contrast for the Alpine localities because, for Kendlbachgraben, Tiefengraben and Kuhjoch, the base of the 'grey zone' starts already at the initial δ¹³C minimum, and even somewhat lower and somewhat below the δ¹³C minimum at Tiefengraben. We also note that in Kössen intraplatform basins the disappearance of *Misikella* occurs at the top of the Koessen limestone (see Golebiowski & Braunstein 1988) and there the 'pre-*planorbis* Beds' ('grey zone') begin at the initial δ¹³C minimum. At Csővár, in England, and in New York Canyon, the 'pre-*planorbis* Beds' begin somewhat later, at the LOD of *Misikella* above the initial δ¹³C minimum. Alternatively, and more probably, they begin at the same level but there is a short gap below the 'pre-*planorbis* Beds' in the Kendlbachgraben and Tiefengraben sections (see above), and perhaps also in the Kuhjoch section (no conodonts are known from this section).

The top of the 'grey zone' is diachronous and therefore not a timeline. The 'grey zone' ends with the first ammonite indicative of a Jurassic age, but we note that the first *Psiloceras* from the New York Canyon (Nevada) and Kuhjoch sections (Austria) are older than *P. planorbis*. The FAD of *Psiloceras* spp. at Ferguson Hill (see Guex *et al.* 2003, 2004; Lucas *et al.* 2007; Ward *et al.* 2007) is defined by the appearance of *P. tilmanni* (Lange) and *P. spelae* whereas at the Kuhjoch section it is defined by the FOD of *P. spelae tirolicum* Hillebandt & Krystyn (von Hillebandt *et al.* 2007; von Hillebandt & Krystyn 2009). The FAD of this latter subspecies may postdate the FAD of *P. spelae* in Nevada by up to 100 000 years (Ruhl 2010). In ammonoid-free marine sections and in continental sections, the FAD of the sporomorph *Cerebropollenites thiergartii* (Schulz) may be used as a proxy for correlation with the base of the *P. tilmanni* Zone, because this species begins only somewhat ear-

lier in the Kuhjoch section (von Hillebrandt *et al.* 2007; Bonis *et al.* 2009, 2010; Bonis 2010), and Kuerschner *et al.* (2007) used the FAD of *C. thiergartii* for definition of the base of the Jurassic. Jurassic radiolarians seem to appear somewhat before the oldest *Psiloceras* (Williford *et al.* 2007).

The first *Psiloceras* in England belongs to the younger *P. planorbis*-group, rather than to *P. tilmanni* or *P. spelae.* The appearance of *Psiloceras* spp. *(Psiloceras planorbis* group*)* in England is in accordance with *P. marcouxi*, *P. pacificum*, *P. polymorphum* in Nevada and therefore a further timeline can be constructed (orange line in Fig. 6). The orange timeline is an important baseline for further considerations.

For the 'grey zone' a main positive carbon isotope excursion was reported by Hesselbo et al. (2002) followed by the main negative excursion just below the orange time line, and this general trend has been confirmed by Kuerschner et al. (2007), Korte et al. (2009) and Ruhl et al. (2009) as well as in the present study of pelagic carbonates in the Csővár quarry section (Figs 3 and 6). Albeit not as pronounced as in other sections, this general positive excursion is also recognizable in the New York Canyon dataset (Guex et al. 2004, 2006) (Fig. 6). For St Audries's Bay (Hesselbo et al. 2002), Lavernock Point (Korte et al. 2009), New York Canyon (Guex et al. 2004) and Tiefengraben, the first negative peak of the main negative excursion is slightly below the orange line; for the other sections not enough data exist to delineate a trend in this stratigraphic level. Contrasting features (Fig. 6) are reported for both the New York Canyon Ferguson Hill section (Ward et al. 2007) and for Kennecott Point (Williford et al. 2007). At these localities, a negative excursion occurs in the middle of the 'grey zone' and a distinct positive excursion is reported at or above the orange time-line; this distinct positive excursion at Ferguson Hill and Kennecott Point is at that level in which the first negative peak of the main negative excursion occurs in other sections (Fig. 6). A late Hettangian age for the positive carbon (Fig. 6) (and sulphur) isotope excursion(s) by Williford et al. (2007, 2009) for Kennecott Point is also suggested by further biostratigraphic evaluations by Guex et al. (2011). The main negative excursion in the Kuhjoch section begins considerably below the FAD of *P. spelae* and ends within the *P. tilmanni* Zone and cannot be correlated with any other section. In all other sections most of the main negative excursion lies much higher, mainly above the *P. tilmanni* Zone. Hence, the main negative excursion in the Kuhjoch section does not occur at the same time as the main negative excursion in St Audrie's Bay and other sections.

Conclusions

Integrated biostratigraphy (conodonts and ammonoids) and carbon isotope stratigraphy for the T–J boundary sections at Csővár quarry (Hungary) and comparison with fossil distribution and δ¹³C trends of coeval localities (St Audrie's Bay, Lavernock Point, New York Canyon, Kennecott Point, Tiefengraben, Kuhjoch), allows a succession of stratigraphic markers to be defined. The apex of the initial negative carbon isotope excursion occurs approximately at the LOD of *C. crickmayi* and *C. marshi* (possibly somewhat above the latter), and slightly below (0.6 to 2 m) the disappearance of the genus *Misikella*. The positive excursion culminated in the 'grey zone', in which neither definitive Triassic nor definitive Jurassic faunas occur. The first negative peak of the main negative isotope excursion is most probably slightly below the timeline defined by the first appearance of *Psiloceras* spp. (*Psiloceras planorbis* group) in England and *P. marcouxi*, *P. pacificum*, *P. polymorphum* in Nevada. Therefore, the combined bio- and event chronology in ascending order is as follows:

1. *C. crickmayi* and *C. marshi* (the latter perhaps somewhat earlier) disappear contemporaneously with the occurrence of the initial negative δ¹³C excursion minimum.
2. LOD of *Misikella* and other Triassic conodonts and beginning of the 'grey zone' ('pre-*planorbis* Beds').
3. A second negative δ¹³C excursion (maybe a last minimum of the initial negative excursion) in the basal part of the 'grey zone' ('pre-*planorbis* Beds') insignificantly above the LOD of *Misikella* and other Triassic conodonts (at Csővár quarry section 0.15 m above the LOD of *Misikella*).
4. A positive δ¹³C excursion (weak at Csővár and Kuhjoch sections, not well defined at New York Canyon (one high value by Guex *et al.* 2004).
5. FAD of primitive *Psiloceras* (*P. spelae*, *P. tilmanni*).
6. FAD of moderately advanced *Psiloceras* (such as *P. marcouxi*, *P. pacificum*, *P. planorbis*).
7. The main negative δ¹³C excursion, beginning somewhat below event 6, but most of it lies above event 6. This excursion is not identical with main negative excursion at the Kuhjoch section.

Acknowledgements

References

Balogh, K. 1981: Correlation of the Hungarian Triassic. Acta Geologica Academiae Scientiarum Hungaricae 24(1), 3–48.

Beerling, D.J. & Berner, R.A. 2002: Biogeochemical constraints on the Triassic–Jurassic boundary carbon cycle event. Global Biogeochemical Cycles 16(3), 1036, doi:10.1029/2001GB001637.

Bonis, N.R. 2010: Palaeoenvironmental changes and vegetation history during the Triassic–Jurassic transition. Laboratory of Palaeobotany and Palynology Contribution Series 29, 1–216.

Bonis, N.R., Kürschner, W.M. & Krystyn, L. 2009: A detailed palynological study of the Triassic–Jurassic transition in key sections of the Eiberg Basin (Northern Calcareous Alps, Austria). Review of Palaeobotany and Palynology 156, 376–400, doi:10.1016/j.revpalbo.2009.04.003.

Bonis, N.R., Ruhl, M. & Kürschner, W.M. 2010: Climate change driven black shale deposition during the end-Triassic in the western Tethys. Palaeogeography, Palaeoclimatology, Palaeoecology 290, 151–159, doi:10.1016/j.palaeo.2009.06.016.

Cirilli, S., Marzoli, A., Tanner, L., Bertrand, H., Buratti, N., Jourdan, F., Bellieni, G., Kontak, D. & Renne, P.R. 2009: Latest Triassic onset of the Central Atlantic Magmatic Province (CAMP) volcanism in the Fundy Basin (Nova Scotia): New stratigraphic constraints. Earth and Planetary Science Letters 286, 514–525, doi:10.1016/j.epsl.2009.07.021.

Clémence M.-E., Bartolini A., Gardin S., Paris G., Beaumont V. & Page K.N. 2010: Early Hettangian benthic–planktonic coupling at Doniford (SW England): Palaeoenvironmental implications for the aftermath of the end-Triassic crisis. Palaeogeography, Palaeoclimatology, Palaeoecology 295, 102–115, doi:10.1016/j.palaeo.2010.05.021.

Cleveland, D.M., Nordt, L.C., Dworkin, S.I., & Atchley, S.C. 2008: Pedogenic carbonate isotopes as evidence for extreme climatic events preceding the Triassic–Jurassic boundary: Implications for the biotic crisis? Geological Society of America Bulletin 120, 1408-1415, doi:10.1130/B26332.1.

Cohen, A.S. & Coe, A.L. 2002: New geochemical evidence for the onset of volcanism in the Central Atlantic magmatic province and environmental change at the Triassic-Jurassic boundary. Geology 30, 267–270, doi:10.1130/0091-7613(2002)030<0267:NGEFTO>2.0.CO;2.

Cohen, A.S. & Coe, A.L. 2007: The impact of the Central Atlantic Magmatic Province on climate and on the Sr- and Os-isotope evolution of seawater. Palaeogeography, Palaeoclimatology, Palaeoecology 244, 374–390, doi:10.1016/j.palaeo.2006.06.036.

Courtillot, V.E. & Renne, P.R. 2003: On the ages of flood basalt events. Comptes Rendus Geoscience 335, 113–140, doi:10.1016/S1631-0713(03)00006-3.

Delecat, S. 2005: Porifera-microbialites of the Lower Liassic (Northern Calcareous Alps) – Re-settlement strategies on submarine mounds of dead Rhaetian reefs by ancestral benthic communities. Ph.D. thesis, Univ. Göttingen, http://webdoc.sub.gwdg.de/diss/2005/delecat/

Detre, C.S., Dosztály, L. & Herman, V. 1986: Uj kicsavarodott Ammonoidea-lelet a hazai triászból. Asványgyüjtö Figyelö 3, 24–27.

Galli, M. T., Jadoul, F., Bernasconi, S. M. & Weissert, H. 2005: Anomalies in global carbon cycling and extinction at the Triassic/Jurassic boundary: evidence from a marine C-isotope record. Palaeogeography, Palaeoclimatology, Palaeoecology 216, 203–214, doi:10.1016/j.palaeo.2004.11.009.

Galli, M.T., Jadoul, F., Bernasconi, S.M. Cirilli, S. & Weissert, H. 2007: Stratigraphy and palaeoenvironmental analysis of the Triassic–Jurassic transition in the western Southern Alps (Northern Italy). Palaeogeography, Palaeoclimatology, Palaeoecology 244, 52–70, doi:10.1016/j.palaeo.2006.06.023.

Golebiowski, R. 1990: Facial and faunistic changes from Triassic to Jurassic in the Northern Calcareous Alps (Austria). Les Cahiers de I'Universite Catholique de Lyon série Sciences 3, 175–184.

Golebiowski, R. & Braunstein, R.E. 1988: A Triassic/Jurassic boundary section in the Northern Calcareous Alps (Austria). Berichte der Geologischen Bundesanstalt 15, 39–46.

Götz, A.E., Ruckwied, K., Pálfy, J. & Haas, J. 2009: Palynological evidence of synchronous changes within the terrestrial and marine realm at the Triassic/Jurassic boundary (Csővár section, Hungary). Review of Palaeobotany and Palynology 156, 401–409, doi:10.1016/j.revpalbo.2009.04.002.

Guex, J., Bartolini, A., Atudorei, V. & Taylor, D. 2003: Two negative $\delta^{13}C_{org}$ excursions near the Triassic-Jurassic boundary in the New York Canyon area (Gabbs Valley Range, Nevada). Bulletin de Géologie Lausanne 360, 1–4.

Guex, J., Bartolini, A., Atudorei, V. & Taylor, D. 2004: High-resolution ammonite and carbon isotope stratigraphy across the Triassic–Jurassic boundary at New York Canyon (Nevada). Earth and Planetary Science Letters 225, 29–41, doi:10.1016/j.epsl.2004.06.006.

Guex, J., Taylor, D.G., Rakus, M., Bartolini, A., Atudorei, V., Carter, E.S. & Lucas, S. 2006: Proposal of the Muller Canyon section (New York Canyon area, Nevada, USA) as stratotype for the Triassic–Jurassic boundary. Volumina Jurassica 4, 283–285.

Guex J., Bartolini A., Spangenberg J., Schoene B., Atudorei, V. & Schaltegger U. 2011: The age of the major $\delta^{13}C_{org}$ and $\delta^{34}S$ Hettangian excursions at Kennecott Point (Queen Charlotte Islands, Canada). Geophysical Research Abstracts 13, EGU2011-1696.

Haas, J. & Tardy-Filácz, E. 2004: Facies changes in the Triassic–Jurassic boundary interval in an intraplatform basin succession at Csővár (Transdanubian Range, Hungary). Sedimentary Geology 168, 19–48, doi:10.1016/j.sedgeo.2004.03.002.

Haas, J., Tardi-Filácz, E., Oravecz-Scheffer, A., Góczán, F. & Dosztály, L. 1997: Stratigraphy and sedimentology of an Upper Triassic toe-of-slope and basin succession at Csővár–1, North Hungary. Acta Geologica Hungarica 40, 11–177.

Haas, J., Götz, A. E. & Pálfy, J. 2010: Late Triassic to Early Jurassic palaeogeography and eustatic history in the NW Tethyan realm: New insights from sedimentary and organic facies of the Csővár Basin (Hungary). Palaeogeography, Palaeoclimatology, Palaeoecology 291, 456–468, doi:10.1016/j.palaeo.2010.03.014.

Hallam, A. & Goodfellow, W.D. 1990: Facies and geochemical evidence bearing on the end-Triassic disappearance of the Alpine reef ecosystem. Historical Biology 4, 131–138.

Hallam A. & Wignall P.B. 1997: Mass extinctions and their aftermath, 320 pp. Oxford University Press, Oxford.

Hautmann, M., Benton, M.J., & Tomasŏvých A. 2008: Catastrophic ocean acidification at the Triassic–Jurassic boundary. Neues Jahrbuch für Geologie und Paläontologie - Abhandlungen 249, 119–127, doi:10.1127/0077-7749/2008/0249-0119.

Hesselbo, S.P., Robinson, S.A., Surlyk, F. & Piasecki, S. 2002: Terrestrial and marine extinction at the Triassic–Jurassic boundary synchronized with major carbon-cycle perturbation: A link to initiation of massive volcanism? Geology 30, 251–254, doi:10.1130/0091-7613(2002)030<0251:TAMEAT>2.0.CO;2.

Kiessling, W. 2010: Reef expansion during the Triassic: Spread of photosymbiosis balancing climatic cooling. Palaeogeography, Palaeoclimatology, Palaeoecology 290, 11–19, doi:10.1016/j.palaeo.2009.03.020.

Kiessling, W., Roniewicz, E., Villier, L., Léonide, P. & Struck, U. 2009: An early Hettangian coral reef in southern France: Implications for the end-Triassic reef crisis. Palaios 24, 657–671, doi:10.2110/palo.2009.p09-030r.

Korte, C. & Hesselbo, S.P., 2011: Shallow-marine carbon- and oxygen-isotope and elemental records indicate icehouse-greenhouse cycles during the Early Jurassic. Paleoceanography, doi:10.1029/2011PA002160, in press.

Korte, C. & Kozur, H.W. 2010: Carbon isotope stratigraphy across the Permian–Triassic boundary: A review. Journal of Asian Earth Sciences 39, 215–235, doi:10.1016/j.jseaes.2010.01.005.

Korte, C. & Kozur, H.W. 2011: Temperature changes across the Permian–Triassic boundary and observations pertaining to some geological/geochemical features around this level. In: Bhargava, O.N. (ed.): Facets of Phanerozoic (Collection of papers in honour of Prof. S.B. Bhatia), Memoir of the Geological Society of India 78, 100–139.

Korte, C., Kozur, H.W., Bruckschen, P. & Veizer, J. 2003: Strontium isotope evolution of Late Permian and Triassic seawater. Geochimica et Cosmochimica Acta 67, 47–62, doi:10.1016/S0016-7037(02)01035-9.

Korte, C., Kozur, H.W. & Veizer, J. 2005: $\delta^{13}C$ and $\delta^{18}O$ values of Triassic brachiopods and carbonate rocks as proxies for coeval seawater and palaeotemperature. Palaeogeography, Palaeoclimatology, Palaeoecology 226, 287–306, doi:10.1016/j.palaeo.2005.05.018.

Korte, C., Hesselbo, S.P., Jenkyns, H.C., Rickaby, R.E.M. & Spötl, C. 2009: Palaeoenvironmental significance of carbon- and oxygen-isotope stratigraphy of marine Triassic–Jurassic boundary sections in SW Britain. Journal of the Geological Society, London 166, 431–445, doi:10.1144/0016-76492007-177.

Korte, C., Pande, P., Kalia, P., Kozur, H.W., Joachimski M.M. & Oberhänsli, H. 2010: Massive volcanism at the Permian–Triassic boundary and its impact on the isotopic composition of the ocean and atmosphere. Journal of Asian Earth Sciences 37, 293–311, doi:10.1016/j.jseaes.2009.08.012.

Kozur, H. 1993: First evidence of Liassic in the vicinity of Csővár (Hungary), and its paleogeographic and paleotectonic significance. Jahrbuch der Geologischen Bundesanstalt 136(1), 89–98.

Kozur, H.W. 2003a: Integrated ammonoid, conodont and radiolarian zonation of the Triassic and some remarks to stage/substage subdivision and the numeric age of the Triassic stages. Albertiana 28, 57–83.

Kozur, H.W. 2003b: Integrated ammonoid, conodont and radiolarian zonation of the Triassic. Hallesches Jahrbuch für Geowissenschaften B 25, 49–79.

Kozur, H. & Mock, R. 1991: New Middle Carnian and Rhaetian conodonts from Hungary and the Alps. Stratigraphic importance and tectonic implications for the Buda Mountains and

adjacent areas. Jahrbuch der Geologischen Bundesanstalt 134(2), 271–297.

Kozur, H. & Mostler, H. 1973: Mikrofauna und Stratigraphie im Raume Csövár, Ungarn. Verhandlungen der Geologischen Bundesanstalt 1973(2), 291–325.

Kozur, H.W. & Weems, R.E. 2005: Conchostracan evidence for a late Rhaetian to early Hettangian age for the CAMP volcanic event in the Newark Supergroup, and a Sevatian (late Norian) age for the immediately underlying beds. Hallesches Jahrbuch für Geowissenschaften B 27, 21–51.

Kozur, H.W. & Weems, R.E. 2010: The biostratigraphic importance of conchostracans in the continental Triassic of the northern hemisphere. In: Lucas, S.G. (ed.), The Triassic timescale. Geological Society, London, Special Publication 334, 315–417, doi:10.1144/SP334.13

Kozur, H.W. & Weems, R.E. 2011: Detailed correlation and age of continental late Changhsingian and earliest Triassic beds: Implications for the role of the Siberian Trap in the Permian–Triassic biotic crisis. Palaeogeography, Palaeoclimatology, Palaeoecology 308, 22–40, doi:10.1016/j.palaeo.2011.02.020.

Kraus, S.H., Siegert, S., Mette, W., Struck, U. & Korte, C. 2009: Stratigraphic significance of carbon isotope variations in the shallow-marine Seis/Siusi Permian–Triassic boundary section (Southern Alps, Italy). Fossil Record 12, 197–205, doi: 10.1002/mmng.200900007.

Krystyn, L. 1980: Triassic Conodont Localities of the Salzkammergut Region. Abhandlungen der Geologischen Bundesanstalt 35, 61–98.

Krystyn, L., Böhm, F., Kuerschner, W.M. & Delecat, S. 2005: The Triassic–Jurassic boundary in the Northern Calcareous Alps. In: Pálfy, J. & Ozsvárt, P. (eds), Program, Abstracts and Field Guide. 5th Field Workshop of IGCP 458 Project (Tata and Hallein, September 2005), A1–A39.

Kuerschner, W.M., Bonis, N.R. & Krystyn, L. 2007: Carbon isotope stratigraphy and palynostratigraphy of the Triassic–Jurassic transition in the Tiefengraben section – Northern Calcareous Alps (Austria). Palaeogeography, Palaeoclimatology, Palaeoecology 244, 257–280, doi:10.1016/j.palaeo.2006.06.031.

Kump, L.R. & Arthur, M.A. 1999: Interpreting carbon-isotope excursions: Carbonates and organic matter. Chemical Geology 161, 181–198, doi:10.1016/S0009-2541(99)00086-8.

Lucas, S.G., Taylor, D.G., Guex, J., Tanner, L.H. & Krainer, K. 2007: The proposed Global Stratotype Section and Point for the base of the Jurassic System in the New York Canyon area, Nevada, USA. In: Lucas, S.G. & Spielmann, J.A. (eds), Triassic of the American West. New Mexico Museum of Natural History and Science Bulletin 40, 139–161.

Magioncalda, R., Dupuis, C., Smith T., Steurbaut, E. & Gingerich, P.D. 2004: Paleocene–Eocene carbon isotope excursion in organic carbon and pedogenic carbonate: Direct comparison in a continental stratigraphic section. Geology 32, 553–556, doi: 10.1130/G20476.1.

McElwain, J.C., & Punyasena S.W. 2007: Mass extinction events and the plant fossil record. Trends in Ecology and Evolution 22, 548–557, doi:10.1016/j.tree.2007.09.003.

McElwain, J.C., Beerling D.J. & Woodward F.I. 1999: Fossil plants and global warming at the Triassic–Jurassic boundary. Science 285, 1386–1390, doi:10.1126/science.285.5432.1386.

McRoberts, C.A., Furrer, H. & Jones, D.S. 1997: Palaeoenvironmental interpretation of a Triassic-Jurassic boundary section from Western Austria based on palaeoecological and geochemical data. Palaeogeography, Palaeoclimatology, Palaeoecology 136, 79–95, doi:10.1016/S0031-0182(97)00074-6.

McRoberts, C.A., Ward, P.D. & Hesselbo, S.P. 2007: A proposal for the base Hettangian stage (=base Jurassic System) GSSP at New York Canyon (Nevada, USA) using carbon isotopes. International Subcommission on Jurassic Stratigraphy Newsletter 34 (1), 43–49.

Mette, W., Elsler, A. & Korte, C. unpublished manuscript: Palaeoenvironmental and stratigraphical changes in the Late Triassic (Rhaetian) of the Northern Calcareous Alps: clues from stable isotopes and microfossils.

Morante, R. & Hallam, A. 1996: Organic carbon isotopic record across the Triassic–Jurassic boundary in Austria and its bearing on the cause of the mass extinction. Geology 24, 391–394, doi:10.1130/0091-7613(1996)024<0391:OCIRAT>2.3.CO;2.

Morbey, S.J., 1975: The palynostratigraphy of the Rhaetian stage, Upper Triassic in the Kendelbachgraben, Austria. Palaeontographica, Abteilung B 152, 1–75.

Orchard, M.J., Carter, E.S., Lucas, S.G., & Taylor, D.G. 2007: Rhaetian (Upper Triassic) conodonts and radiolarians from New York Canyon, Nevada, USA. Albertiana 35, 59–65.

Pálfy, J. 2003: Volcanism of the Central Atlantic Magmatic Province as a potential driving force in the end-Triassic mass extinction. In: Hames, W.E., McHone, J.G., Renne, P.R. & Ruppel, C. (eds), The Central Atlantic Magmatic Province: Insights from Fragments of Pangea. Geophysical Monograph, American Geophysical Union 136, 255–267.

Pálfy, J., Demény, A., Haas, J., Hetényi, M., Orchard, M.J. & Vető, I. 2001: Carbon isotope anomaly and other geochemical changes at the Triassic-Jurassic boundary from a marine section in Hungary. Geology 29, 1047–1050, doi:10.1130/0091-7613(2001)029<1047:CIAAOG>2.0.CO;2.

Pálfy, J. Demény, A., Haas, J., Carter, E.S., Görög, A., Halász, D. Oravecz-Scheffer, A., Hetényi, M., Márton, E., Orchard, M.J., Ozsvárt, P., Vető, I. & Zajzon, N. 2007: Triassic–Jurassic boundary events inferred from integrated stratigraphy of the Csővár section, Hungary. Palaeogeography, Palaeoclimatology, Palaeoecology 244, 11–33, doi:10.1016/j.palaeo.2006.06.021.

Pieńkowski, G., Niedźwiedzki, G. & Waksmundzka, M. 2011: Sedimentological, palynological and geochemical studies of the terrestrial Triassic–Jurassic boundary in northwestern Poland. Geological Magazine, doi:10.1017/S0016756811000914, in press.

Prauss, M.L. 2007: Availability of reduced nitrogen chemospecies in photic-zone waters as the ultimate cause for fossil prasinophyte prosperity. Palaios 22, 489–499, doi:10.2110/palo.2005.p05-095r.

Renne, P.R. & Basu, A.R. 1991: Rapid eruption of the Siberian Traps flood basalts at the Permo–Triassic boundary. Science 253, 176–179.

Ruhl, M. 2010: Carbon cycle changes during the Triassic–Jurassic transition. Laboratory of Palaeobotany and Palynology Contribution Series 28, 1–151.

Ruhl, M. & Kürschner, W.M. 2011: Multiple phases of carbon cycle disturbance from large igneous province formation at the Triassic–Jurassic transition. Geology 39: 431–434. doi:10.1130/G31680.1

Ruhl, M., Kürschner, W.M. & Krystyn, L. 2009: Triassic–Jurassic organic carbon isotope stratigraphy of key sections in the western Tethys realm (Austria). Earth and Planetary Science Letters 281, 169–187, doi:10.1016/j.epsl.2009.02.020.

Ruhl, M., Deenen, M.H.L., Abels, H.A., Bonis, N.R., Krijgsman, W. & Kürschner, W.M. 2010a: Astronomical constraints on the duration of the early Jurassic Hettangian stage and recovery rates following the end-Triassic mass extinction (St

Audrie's Bay/East Quantoxhead, UK). Earth and Planetary Science Letters 295, 262–276, doi:10.1016/j.epsl.2010.04.008.

Ruhl, M., Veld, H. & Kürschner, W.M. 2010b: Sedimentary organic matter characterization of the Triassic–Jurassic boundary GSSP at Kuhjoch (Austria). Earth and Planetary Science Letters 292, 17–26, doi:10.1016/j.epsl.2009.12.046.

Ruhl, M., Bonis, N.R., Reichart, G.-J., Sinninghe Damsté, J.S., Kürschner, W.M. 2011: Atmospheric carbon injection linked to end-Triassic mass extinction. Science 333, 430–434, doi:10.1126/science.1204255.

Sageman, B.B., Meyers, S.R. & Arthur, M.A. 2006: Orbital time scale and new C-isotope record for Cenomanian-Turonian boundary stratotype. Geology 34, 125–128, doi: 10.1130/G22074.1.

Schaller, M.F., Wright, J.D., & Kent, D.V. 2011: Atmospheric PCO_2 perturbations associated with the Central Atlantic Magmatic Province. Science 331: 1404–1409. doi:10.1126/science.1199011

Schoene, B., Guex, J., Bartolini, A., Schaltegger, U. & Blackburn, T.J. 2010: Correlating the end-Triassic mass extinction and flood basalt volcanism at the 100 ka level. Geology 38, 387–390; doi:10.1130/G30683.1.

Steinthorsdottir, M., Jeram, A. J., & McElwain, J. C. 2011: Extremely elevated CO_2 concentrations at the Triassic/Jurassic boundary. Palaeogeography, Palaeoclimatology, Palaeoecology 308, 418–432, doi:10.1016/j.palaeo.2011.05.050.

Suess, E. & Mojsisovics, E. 1868: Studien über die Gliederung der Trias und Jurabildungen in den östlichen Kalkalpen. Nr. II. Die Gebirgsgruppe des Osterhornes. Jahrbuch der Kaiserlich-Königlichen Geologischen Reichsanstalt 18, 167–200.

Swift, A. 1989: Fist records of conodonts from the late Triassic of Britain. Palaeontology 32, 325–333.

Swift, A. 1995: Conodonts from the late Permian and late Triassic of Britain. Monograph of the Palaeontological Society, 80 pp., London.

Tanner, L.H., Lucas, S.G. & Chapman, M.G. 2004: Assessing the record and causes of Late Triassic extinctions. Earth-Science Reviews 65, 103–139, doi:10.1016/S0012-8252(03)00082-5.

van de Schootbrugge, B., Payne, J.L., Tomasovych, A., Pross, J., Fiebig, J., Benbrahim, M., Föllmi, K.B. & Quan, T.M. 2008: Carbon cycle perturbation and stabilization in the wake of the Triassic–Jurassic boundary mass-extinction event. Geochemistry, Geophysics, Geosystems 9(4), 16 pp, Q04028, doi:10.1029/2007GC001914.

von Hillebrandt, A. & Krystyn, L. 2009: On the oldest Jurassic ammonites of Europe (Northern Calcareous Alps, Austria) and their global significance. Neues Jahrbuch für Geologie und Paläontologie, Abhandlungen 253(2–3), 163–195.

von Hillebrandt, A., Krystyn, L. & Kuerschner, W.M. 2007: A candidate GSSP for the base of the Jurassic in the Northern Calcareous Alps (Kuhjoch section, Karwendel Mountains, Tyrol, Austria). International Subcommission on Jurassic Stratigraphy Newsletter 34 (1), 2–20.

Ward, P.D., Haggart, J.W., Carter, E.S., Wilbur, D., Tipper, H.W. & Evans, T. 2001: Sudden productivity collapse associated with the Triassic–Jurassic boundary mass extinction. Science 292, 1148–1151, doi:10.1126/science.1058574.

Ward, P.D., Garrison, G.H., Williford, K.H., Kring, D.A., Goodwin, D., Beattie, M.J. & McRoberts, C.A. 2007: The organic carbon isotopic and paleontological record across the Triassic–Jurassic boundary at the candidate GSSP section at Ferguson Hill, Muller Canyon, Nevada, USA. Palaeogeography, Palaeoclimatology, Palaeoecology 244, 281–289, doi:10.1016/j.palaeo.2006.06.042.

Weems, R.E. 1992: The "terminal Triassic catastrophic extinction event" in perspective: a review of Carboniferous through Early Jurassic terrestrial vertebrate extinction patterns. Palaeogeography, Palaeoclimatology, Palaeoecology 94, 1–29, doi:10.1016/0031-0182(92)90111-H.

Williford, K.H., Ward, P.D., Garrison, G.H. & Buick, R. 2007: An extended organic carbon-isotope record across the Triassic–Jurassic boundary in the Queen Charlotte Islands, British Columbia, Canada. Palaeogeography, Palaeoclimatology, Palaeoecology 244, 290–296, doi:10.1016/j.palaeo.2006.06.032.

Williford, K.H., Foriel, J., Ward, P.D., & Steig E.J. 2009: Major perturbation in sulfur cycling at the Triassic-Jurassic boundary. Geology 37, 835–838; doi: 10.1130/G30054A.1

Instructions to authors

The Bulletin publishes articles normally not exceeding 16 printed pages, notes not longer than 4 pages, and short contributions of maximum 1 printed page. Longer articles may be published at the discretion of the editor, but it is advisable to consult the editor before submitting long manuscripts. Short contributions may be comments on previously published articles, presentation of current scientific activities, short scientific notes, or book reviews.

Manuscripts with complete sets of illustrations, tables, captions, etc., should be submitted electronically to the chief editor (lml@geus.dk). The **main text** with references and figure captions should be either in Word or pdf format, **figures** should be in either pdf, jpeg, or tiff format, and **tables** should be in Word text format, i.e. written in lines with tab spacing between table columns. "Word tables" are discouraged because they are not re-formatted easily. Consult the editor before submitting other formats.

Manuscripts will be reviewed by two referees; suggestions of referees are welcome. Articles will be published approximately in the order in which they are accepted for publication. The final decision on whether or not a manuscript will be accepted for publication rests with the chief editor, acting on the advice of the scientific editors.

Manuscript

Language – Manuscripts should be in English. Authors who are not proficient in English should ask an English-speaking colleague for assistance before submission of the manuscript.

Title – Titles should be short and concise, with emphasis on words useful for indexing and information retrieval. An abbreviated title to be used as running head must also be submitted.

Abstract – An abstract in English must accompany all papers. It should be short (no longer than 250 words), factual, and stress new information and conclusions rather than describing the contents of the manuscript. Conclude the abstract with a list of key words.

Main text – Use 1.5 or double spacing throughout, and leave wide margins. Italics should be used only in generic and species names and in some Latin abbreviations (*e.g. c., et al., ibid., op. cit*).

Spelling – Geological units named after localities in Greenland, formal lithostratigraphical units and intrusions named after localities in Greenland remain unchanged even if the eponymous locality names have since been changed in accordance with modern Greenlandic orthography.

References to figures, tables and papers – References to figures and tables in the text should have the form: Fig. 1, Figs 1–3, Table 3 or as (Smith 1969, fig. 3) when the reference is to a figure in a cited paper.

References to papers are given in the form Smith (1969) or (Smith 1969). Combined citations by different authors are separated by a semicolon; two or more papers by same author(s) are separated by commas. Citations are mentioned chronologically and then alphabetically. Use '*et al.*' for three or more authors, e.g. Smith *et al.* (1985).

Reference list

Use the following style:

Smith, A.A. 1989: Geology of the Bulbjerg Formation. Bulletin of the Geological Society of Denmark 38, 119–144. [Note that name of journal is given in full].

Smith, A.A., Jensen, B.B. & MacStuff, C.C. 1987: Sandstones of Denmark, 2nd edition, 533 pp. New York: Springer Verlag. [For more than 10 authors, use first author followed by *et al.*].

Smith, A.A., Jensen, B.B. & MacStuff, C.C. 1992: Characterization of Archean volcanic rocks. In: Hansen, D.D. *et al.* (eds): Geology of Greenland. Geological Survey of Denmark and Greenland Bulletin 40, 1397–1438. [More than three editors – therefore *et al.* form is used].

Sorting – Danish letters æ, ø and å (aa) are treated as ae, o and a (aa), respectively.

References are sorted by:

1: Alphabetically by the first author's surname

2: Papers by one author: two or more papers are arranged chronologically

3: Papers by two authors: alphabetically after second author's name. Two or more papers by the same two authors: chronologically.

4: Papers by three or more authors: chronologically. Papers from the same year are arranged alphabetically after second, third, etc.author's name.

Authors themselves are responsible for the accuracy and completeness of their references. If incorrect references are found, the manuscript will be returned to the author for complete rechecking. The reference list must include all, and only, the references cited in the paper (including figures, tables etc).

Illustrations

May be prepared in either black and white or colour. There is no colour charge. Horizontal illustrations are much to be preferred. Size of smallest letters in illustrations should not be less than 5.5 pt. Remember scale.

All figures (including photographs) should be submitted in electronic form ready for direct reproduction, i.e. having the dimensions of the final figure with a standard resolution of 300 dpi for photographs. Preferred formats are pdf, tiff and jpg.

Size – The width of figures must be 82 mm, 125 mm or 171 mm. Maximum height is 223 mm.

Captions – Captions to figures, tables and plates must be delivered on separate pages.

Proofs

Proofs – Authors receive page proofs of the article after technical set-up. The cost of any alterations against the final manuscript will be charged to the author.

Content, vol. 59